October **2015**

Journal of Metallomics and Nanotechnologies

http://web2.mendelu.cz/af_239_nanotech/J_Met_Nano/ volume 2 issue 3

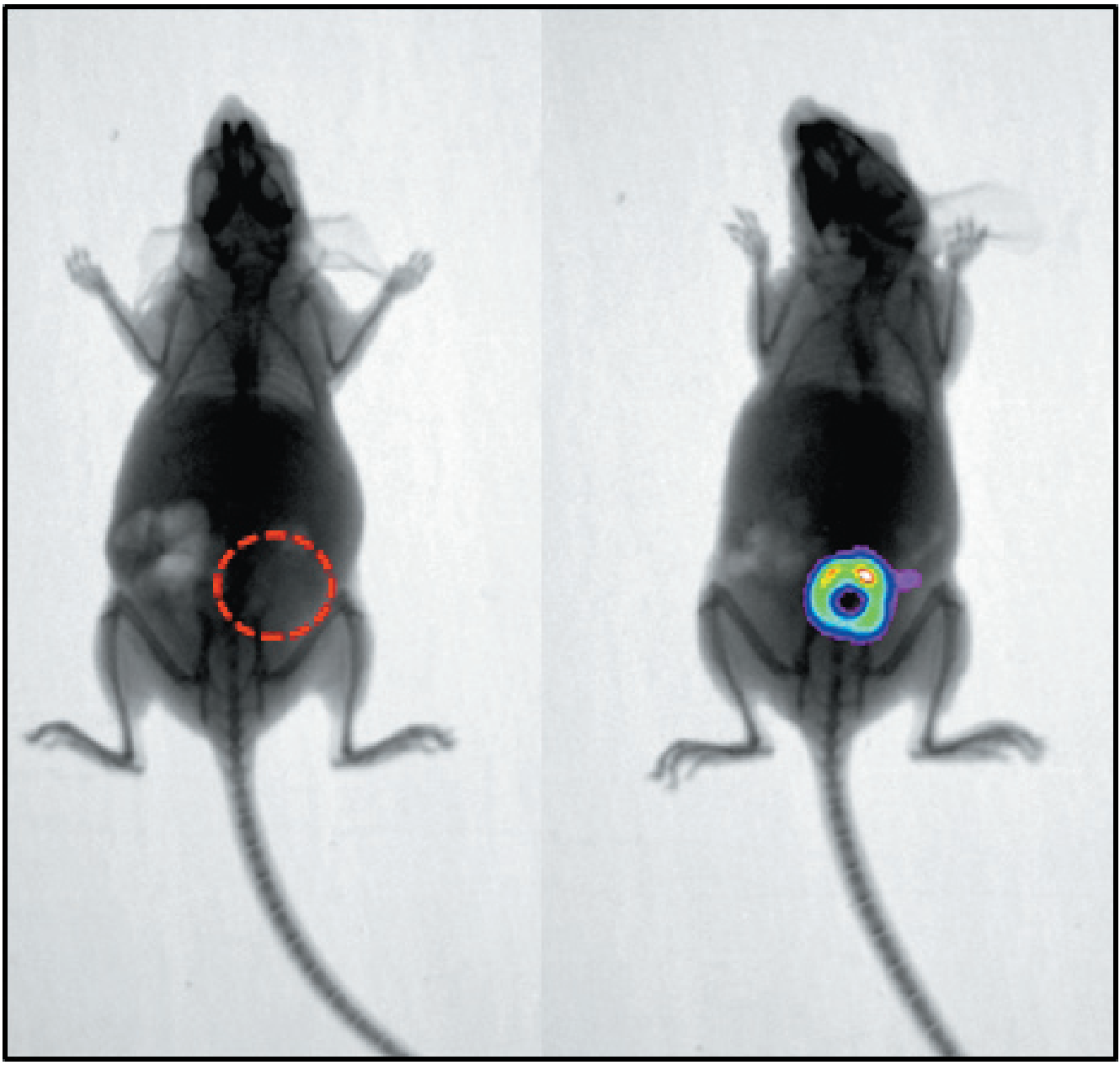

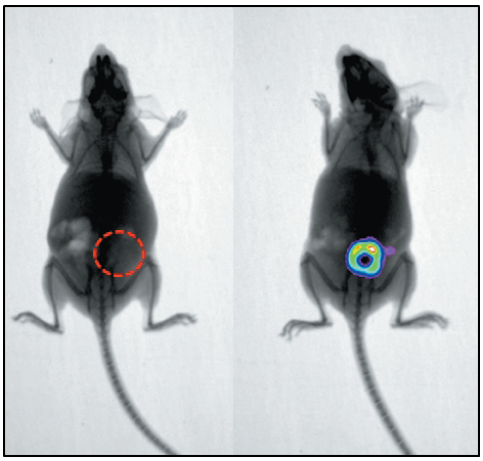

The journal of Metallomics and Nanotechnologies is exclusively in ellectronic form and is published quarterly. The thematic conent is focused on nano--biochemistry, nanotechnology, biomedicine and nanomedicine. The journal is published without regional mutations in Czech, Slovak and English language. Publisher: Laboratory of metallomics and nanotechnologies, Mendel University in Brno, Zemedelska 1, 613 00 Brno, Czech Republic.

The Journal of Metallomics and Nanotechnologies is a new educational and scientific journal which is associated with emerging metallomics and nanotechnologies as a new field of research. This journal is freely available and distributable via website with minimal advertising support. The objective of articles, which is comming quarterly, is application of nano-scale techniques for biologic, chemical and biotechnological research or specific nanobiotechnologic applications.

Cover:

Left part – X-ray *in vivo* image of nude *nu/nu* mouse inoculated by breast carcinoma cells. The mouse was injected (i. v. injection) by fluorescent cleavable probe monitoring the activity of matrix metalloproteinases (MPPsense) and the fluorescence at 700 nm was detected 6 hours after injection. Right part – a merged X-ray and fluorescence image.
(Photo was captured in Laboratory of Applied nanobiotechnology, author: Marketa Vaculovicova).

Indexing & Abstracting Services

This licence allows users to download and share the article for non-commercial purposes, so long as the article is reproduced in the whole without changes, and the original authorship is acknowledged.

Journal of Metallomics and Nanotechnologies
Publisher: Mendel University in Brno, **Chief editor**: Ondrej Zitka, **Edition**: Third 2015
Number of pages: 116, based electronically, ISSN 2336-3940

Dear readers,

the third issue of „Journal of Metallomics and Nanotechnologies“ in 2015 is dedicated to a biophysical characterization of nanomaterials or bio-nanomaterials, especially by optical methods. Another part of this issue is focused on research in area of nanotechnology and biotechnology. The Laboratory of metallomics and nanotechnologies is the iniciator of the Visegrad Metallomic Scientific Network also known as V4MSNet which connects researchers from Czech Republic, Slovak Republic, Poland and Hungary. Main aim of the project was to establish functional consortia for further research on European level. This was mainly secured by organization of the conference, which was finally held in Brno. The events were visited by many students, who were the direct target group. Information transfer and spreading of knowledge have enhanced the level of education in this field and it should help to increase student´s interest in the field of Metallomics. Project partners are ready and willing to give the chance to young students and scientists within the future projects of consortia. Countries of V4 are therefore considered to play a crucial role in future development of Metallomics in Europe.

The last coming number of the volume in 2015 will be open for all the contributors in the main area of the Journal of Metallomics and Nanotechnologies. The papers preferred for this issue should be focused on novel nanotechnology in electrochemically focused analysis.

Ondřej Zítka
Editor in Chief

Editorial Board of the Journal of Metallomics and Nanotechnologies:

Chief Editor: Ondrej Zitka, Mendel University in Brno, Czech Republic
Assistant Manager Editor: Michal Horak, Mendel University in Brno, Czech Republic
Assistant Manager Editor: Sylvie Skalickova, Mendel University in Brno, Czech Republic

Expert editorial board:
David Hynek, Central European Institute of Technology, Czech Republic
Carlos Fernandez, Robert Gordon University, United Kingdom
Elena María Planells del Pozo, University of Granada, Spain
Gabriella Emri, University of Debrecen, Hungary
Jan Labuda, Slovak Technical University in Bratislava, Slovakia
Jaromir Hubalek, University of Technology in Brno, Czech Republic
Jitka Petrlova, Lund University, Sweden
Kledi Xhaxhiu, University of Tirana, Albania
Libuse Trnkova, Masaryk University, Czech Republic
Marie Stiborova, Charles University in Prague, Czech Republic
Marketa Vaculovicova, Central European Institute of Technology, Czech Republic
Marta Kepinska, Wroclaw Medical University, Poland
Martin Pumera, Nanyang Technological University, Singapore
Michal Masarik, Masaryk University, Czech Republic
Milan Antonijevic, University of Belgrade, Serbia
Miroslav Pohanka, University of Defence, Czech Republic
Naser A. Anjum, University of Aveiro, Portugal
Pavel Kopel, Mendel University in Brno, Czech Republic
Rene Kizek, Mendel University in Brno, Czech Republic
Tomas Eckschlager, Charles University in Prague, Czech Republic
Sarmistha Raychaudhuri, University of Calcutta, India
Vojtech Adam, Mendel University in Brno, Czech Republic

The authors declare they have no potential conflicts of interests concerning drugs, products, services or another research outputs in this study.

The Editorial Board declares that the manuscript met the ICMJE „uniform requirements“ for biomedical papers.

Open Access content means the content is free of cost, and no restrictions are applied on its Licensing and Copyrights. Open Access Journals provide free of charge scholarly content. The literature is available for reading, downloading, and editing. The benefit of open access is that the content can be reused for a novel cause/research/experiment.

Special issue for V4 projekt

Editioral material

Article

Regular issue

Review

Article

EDITORIAL MATERIAL

Laboratory of Metallomics and Nanotechnologies – an initiator of the Metallomics Scientific Network formation

Vlastimil Sochor[1*], Marketa Vaculovicova[1], Vojtech Adam[1], Rene Kizek[1]

[1] Department of Chemistry and Biochemistry, Faculty of Agronomy, Mendel University in Brno, Zemedelska 1, CZ-613 00 Brno, Czech Republic, Emails: sochor@node.mendelu.cz (V.S.); marketa.ryvolova@seznam.cz (M.V.); vojtech.adam@mendelu.cz (V.A.); kizek@sci.muni.cz (R.K.)

* Author to whom correspondence should be addressed; E-Mail: sochor@mendelu.cz; Tel.: +420-5-4513-3350; Fax: +420-5-4521-2044.

Received:18.9.2015 / Accepted:24.9.2015 / Published:1.10.2015

The researchers from Laboratory of Metallomics and Nanotechnologies at Department of Chemistry and Biochemistry of Mendel University in Brno were, in connection to their research priorities, interested in the idea to create a cooperating partner network joining the excellent central European laboratories focused on the metallomic research. The effort in this area was supported by the project Metallomic Scientific Network of The International Visegrad Fund, which is devoted to both creation and support of the close collaboration between citizens and institutions in the Visegrad Group countries as well as the cooperation of these countries with other states and regions.

Keywords: metallomics; networking; International Visegrad Fund

1. Introduction

The main goal of the project Metallomic Scientific Network was to create the metallomic network joining the partners, which will collaborate on the common projects in the long-term horizon. Laboratory of Metallomics and Nanotechnologies sees the perspective area of its research in metallomics – the progressive scientific field focused on rapid and noninvasive methods of determination, localization and treatment of cancer. The newly formed network enables the Laboratory of Metallomics and Nanotechnologies and the project partners to utilize the scientific potential, diversify the research tasks and contribute to their solution. The obtained results are available to all partners, which contribute to the project. The viability of the Network is confirmed by the former successful collaboration between Laboratory of Metallomics and Nanotechnologies and the Faculty of Pharmacy of the Wroclaw Medical University on the metallothionein research. The results of this research focused on determination of human and rabbit metallothionein by Brdicka reaction and mass spectrometry were published in FEBS Journal. Furthermore, the cooperation on the investigation of the metallothionein´s influence on the zinc bioavailability could have the essential impact on the understanding of mechanisms regulating the life processes at the molecular level.

2. The main outcomes of the project

The organization necessities connected to the formation of the Metallomic Scientific Network were discussed at several video-discussion at which each partner introduced himself, his scientific stuff as well as the results obtained in his laboratory. Even though Laboratory of Metallomics and Nanotechnologies cooperated with all partners individually in the past, the video-discussion was the first contact between each other. The following video-discussions were focused not only on the scientific topics but also on the arrangement on two personal

meetings of the partners at Metallomics and Technology Conference in Brno and Workshop in Debrecen.

2.1 Conference of Metallomics Technology

Metallomics Technology Conference was held from 14th to 18th June 2015 at the premises of Mendel University in Brno. The conference dealt with the latest trends and strategies in the metallomic research.

The conference was organized under patronage of rector of Mendel University Prof. RNDr. Ladislav Havel, PhD. During the first day of the conference, the invited lectures by Prof. Hajo Haase from the Technical University of Berlin on the effect of zinc on the immunity cell functions and by Prof. Juan Hidalgo from the Autonomous University of Barcelona on the effects of metallothionein in neuroinfection were presented. In the second lecture session, scientists from Masaryk University and from Laboratory Metallomics and Nanotechnologies from Mendel University in Brno presented their lectures devoted to metallothionein. The first day of the conference was finished with a guided tour of the premises of the hosting laboratory

Figure 1: Lecture by Associate Professor Vojtech Adam of Mendel University in Brno on the role of metallothionein in cancer [1].

During the second day, the project partners presented the results connected to the project topic achieved by their departments, and discussed the possibilities for future cooperation in research projects. During the third day of the conference, the participants visited the Department of Pathophysiology, Masaryk University, where, among other things, they were acquainted with the results of the joint research of prostate cancer obtained through the ongoing collaboration of Masaryk University and Mendel University in Brno. The fourth day of the conference was, within the framework of so-called Round table, was devoted to the determination of major joint research interests in relation to the creation of the metallomics scientific network. This aims to not only at close cooperation between the scientific institutions of the Visegrad Group but also at the transfer of expertise and exchange of information related to monitored metallomics issues.

Figure 2: „Round table“ of principal investigator and project partners of Metallomic Scientific Network [1].

2.2 Workshop in Debreceen

Workshop was organized by Dermatology Department of the Medical Faculty Debrecen University was devoted to the possibilities of metallomics application in skin cancer therapy and was held from 1st to 3rd July 2015.

Among the most important outcomes belong, besides the existence of the mentioned network, three-day workshop as a bridge the gaps between the specialists and fields of science as diverse as inorganic chemists, biochemists and clinicians. The seminars were focused on Metallotionein and skin cancer presented by Vojtech Adam, Electrophoresis and electrochemistry of metallomics presented by Marta Kepinska and Jan Labuda. The project ideas of

Clinical characteristic and treatment of skin cancers were introduced by Gabriela Emri followed by contributions about Photodynamic therapy in the management of skin cancers and Photodynamic therapy in the management of skin cancers. During the workshop the visit of histopathology laboratory was done. Here could the participants see various histopathological samples connected to skin cancer. The last day was the round table organized and the visitors could discuss about metallomics and cancer.

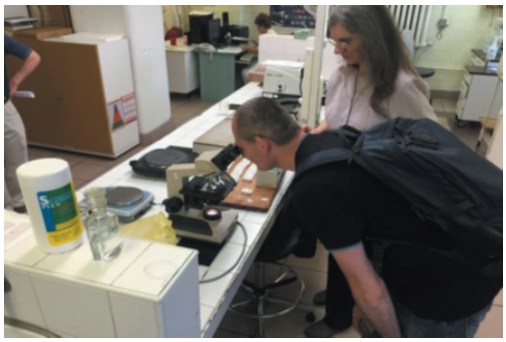

Figure 3: Workshop Metallomics and Skin Cancer at University of Debrecen – prof. René Kizek, PhD (LMaN) and Dr. Gabriella Emri (UD) [2].

2.3 Videoconference of Metallomics and Analytical Methods

In August 25th and 26th a videoconference entitled The Metallomics and Analytical Methods was realized. This videoconference was focused on advances in metallomics as well as progress in the field of analytical techniques in connection to this rapidly developing scientific field and its application in cancer therapy. This two-day session was hosted by associate professor Vojtech Adam PhD, the head of the Department of Chemistry and Biochemistry, vice-rector of Mendel University in Brno and the main researcher of the whole project Metallomic Scientific Network.

Figure 4: Lecture by Associate Professor Kledi Xhaxhiu of University of Tirana, Albania [3]

3. Other outcomes of Metallomic Scientific Network

Under the project of Metallomic Scientific Network were arranged other outcomes of the project include five webseminars [3-7], one seminar [8], three videoconferences [9-11] and one workshop [2]. All these actions were focused on metallomics in connection with cancer and metallothionein imaging. Here, we are reported the summarization of past events in a comprehensive table (Tab. 1). The overview of the combined work of researchers of Visegrad group is given the book of abstracts of Metallomics Technology Conference 2015: Recent Advances and Strategies [12-33], or in the book of abstracts of Metallomics Technology Conference 2015: Metallomics and analytical method [32,34-43]. The electronic version of these books of abstracts is downloadable from websites of the project

http://web2.mendelu.cz/af_239_nanotech/V4dp.php?ip=138.

Videoseminars

Date	Authors	Title	Venue
24.4.2015	Adam V, Kizek R	**Metallomics - What is it? (Part I)**	Mendel University in Brno, LMaN, Zemedelska 1, 613 00 Brno, Czech Republic
15.5.2015	Adam V, Kizek R	**Metallomics - What is it? (Part II)**	Mendel University in Brno, LMaN, Zemedelska 1, 613 00 Brno, Czech Republic
5.6.2015	Guran R, Zitka O, Adam V	**MALDI Imaging of MT in tissue slices of tumors**	Mendel University in Brno, LMaN, Zemedelska 1, 613 00 Brno, Czech Republic
14.8.2015	Guran R, Zitka O, Adam V	**MALDI Imaging of MT in tissue slices of chicken embryos**	Mendel University in Brno, LMaN, Zemedelska 1, 613 00 Brno, Czech Republic
21.8.2015	Xhaxhiu K, Adam V	**Particle size distribution analyses**	Mendel University in Brno, LMaN, Zemedelska 1, 613 00 Brno, Czech Republic

Seminar

Date	Authors	Title	Venue
31.7.2015	Adam V, Kizek R	**Metallomics and skin cancer —DEBRECEN meeting summary**	Mendel University in Brno, LMaN, Zemedelska 1, 613 00 Brno, Czech Republic

Videoconferences

Date	Authors	Title	Venue
19.8.2015	Adam V, Moulick A, Kominkova M, Emri G	**Metallomic and melanoma cancer**	Mendel University in Brno, LMaN, Zemedelska 1, 613 00 Brno, Czech Republic
10.4.2015	Adam V, Richtera L, Hynek D, Labuda J	**Metallomic and cancer**	Mendel University in Brno, LMaN, Zemedelska 1, 613 00 Brno, Czech Republic
25.-26.8.2015	-	**Metallomics Technology Conference 2015:Metallomics and analytical methods**	Mendel University in Brno, LMaN, Zemedelska 1, 613 00 Brno, Czech Republic

Conference

Date	Title	Venue
14.-18.6.2015	**Metallomics Technology Conference 2015: Recent Advances and Strategies**	Mendel University in Brno, LMaN, Zemedelska 1, 613 00 Brno, Czech Republic

Workshop

Date	Title	Venue
1.-3.7.2015	**Metallomics and skin cancer**	. University of Debrecen, Egyetem tér 1, 4032 Debrecen, Hungary

Articles

Date	Authors	Title	ISSN
30.9.2015	Emri, G	**Immunohistochemical detection of metallothionein**	2336-3940
30.9.2015	Guran, R	**Maldi-tof msi and electrochemical detection of metallothionein in chicken liver after cadminum exposure**	2336-3940
1.10.2015	Kepinska, M	**Capillary electrophoresis of metallothionein**	2336-3940
	Sochor, V	**Laboratory of metallomics and nanotechnologies —an initiator of the metallomics scientific network formation**	2336-3940
30.9.2015	Xhaxhiu, K	**Synthetic birnessites and buserites as heavy metal cation traps and environmental remedies**	2336-3940

Proceedings

Authors	Title
Adam, V., Kizek, R.	**Metallomics Technology Conference 2015:Metallomics and analytical methods,**
Adam, V., Kizek, R.	**Metallomics Technology Conference 2015: Recent Advances and Strategies**

Table 1: Summarization of other outcomes of Metallomic Scientific Network.

It is obvious, the role of metallothionein is discussed in all presented contributions as an important metal-binding protein in the field of metallomics. In recent decade, the role of metallothionein was clarified in the connection with higher oxidative stress and cancer. Many studies have reported higher expression of MT-I and its mRNA in various human cancers; such as breast, kidney, lung, nasopharynx, ovary, prostate, salivary gland, testes, urinary bladder, cervical, endometrial, skin carcinoma, melanoma, acute lymphoblastic leukemia (ALL), and pancreatic cancers. Or the increased expression of MT I and II could be correlated to higher tumor grade/stage, chemotherapy/radiation resistance, and poor prognosis [44]. Due to metallothionein importance, various methods for studying this metalloprotein have been developed. We can mention electrochemical detection by Brdicka´s reaction, PCR, capillary electrophoresis and last but not least MALDI imaging, which seems to be a novel, perspective method to studying the metallothionein levels in tumor tissues.

3.1 Published papers

For the above mentioned topic follows articles which are focused on the problematic of metallothionein and cancer, were published in the Journal of Metallomics and Nanotechnologies to give a comprehensive view on all this problematics: Immunohistochemical detection of metallothionein by Emri et al [45], MALDI-TOF MSI and electrochemical detection of metallothionein in chicken liver after cadminum exposure by Guran et al [46], Capillary electrophoresis of metallothionein by Kepinska et al [47], Synthetic birnessites and buserites as heavy metal cation traps and environmental remedies by Xhaxhiu et al [48]. All the articles are published in this volume of the journal.

3. Conclusion

The finalization of the Metallomic Scientific Network project on August 31st 2015 is a symbolic start of a new period of collaboration within the metallomic research of V4 countries on only in terms of ongoing exchange of the experiences but also in in terms of preparation of new projects, which will be based of the newly developed collaboration.

Acknowledgement

The financial support from Metallomic Scientific Network V4MSNet (project 11440027) is greatly acknowledged.

Conflicts of Interest

The authors declare no conflict of interest.

The authors declare they have no potential conflicts of interests concerning drugs, products, services or another research outputs in this study. The Editorial Board declares that the manuscript met the ICMJE „uniform reguirements“ for biomedical papers.

References

1. Metallomics technology conference 2015: Recent advances and strategies; Mendel University in Brno, LMaN, Zemedelska 1, 613 00 Brno, Czech Republic, 14. - 16. 6. 2015, 2015.
2. Emri, G.; Adam, V. Metallomics and skin cancer University of Debrecen, Egyetem tér 1, 4032 Debrecen, Hungary, 01/03-07-2015.
3. Xhaxhiu, K.; Adam, V. Particle size distribution analyses; Mendel University in Brno, LMaN, Zemedelska 1, 613 00 Brno, Czech Republic, 21-08-2015.
4. Adam, V.; Kizek, R. Metallomics - what is it? – part ii; Mendel University in Brno, LMaN, Zemedelska 1, 613 00 Brno, Czech Republic, 15_05_2015.
5. Adam, V.; Kizek, R. Metallomics - what is it? – part i; Mendel University in Brno, LMaN, Zemědělská 1, 613 00 Brno, Czech Republic, 24-04-2015.
6. Guran, R.; Zitka, O.; Adam, V. Maldi imaging of mt in tissue slices of tumors; Mendel University in Brno, LMaN, Zemedelska 1, 613 00 Brno, Czech Republic, 05_06_2015.
7. Guran, R.; Zitka, O.; Adam, V. Maldi imaging of mt in tissue slices of chicken embryos; Mendel University in Brno, LMaN, Zemedelska 1, 613 00 Brno, Czech Republic, 14-08-2015.
8. Adam, V.; Kizek, R. Metallomics and skin cancer – debrecen meeting summary; Mendel University in Brno, LMaN, Zemedelska 1, 613 00 Brno, Czech Republic, 31-07-2015.
9. Adam, V.; Moulick, A.; Kominkova, M.; Emri, G. Metallomic and melanoma cancer; Mendel University in Brno, LMaN, Zemedelska 1, 613 00 Brno, Czech Republic, 19-08-2015.
10. Adam, V.; Richtera, L.; Hynek, D.; Labuda, J. Metallomic and metallothionein; Mendel University in Brno, LMaN, Zemedelska 1, 613 00 Brno, Czech Republic, 05-06-2015.
11. Adam, V.; Zitka, O.; Emri, G.; Vaculovicova, M.; Kepinska, M. Metallomic and cancer; Mendel University in Brno, LMaN, Zemedelska 1, 613 00 Brno, Czech Republic, 10-04-2015.

12. Merlos Rodrigo, M.A.; Skalickova, S.; Zitka, O.; Adam, V.; Kizek, R. In Metal nanoparticles in soils and cells, Metallomics Technology Conference 2015: Recent Advances and Strategies, Department of Chemistry and Biochemistry, Faculty of Agronomy, Mendel University in Brno, 14. – 18. 6. , 2015; Adam, V.; Kizek, R., Eds. Mendel University in Brno, Zemědělská 1, 613 00 Brno: Department of Chemistry and Biochemistry, Faculty of Agronomy, Mendel University in Brno, pp 18-20.ISBN 978-80-7509-309-7; ISBN 978-80-7509-314-1 (on-line)
13. Adam, V.; Kizek, R. In Electrochemistry of metallothioneins, Metallomics Technology Conference 2015: Recent Advances and Strategies, Department of Chemistry and Biochemistry, Faculty of Agronomy, Mendel University in Brno, 14. – 18. 6. , 2015; Adam, V.; Kizek, R., Eds. Mendel University in Brno, Zemědělská 1, 613 00 Brno: Department of Chemistry and Biochemistry, Faculty of Agronomy, Mendel University in Brno, pp 14-15.ISBN 978-80-7509-309-7
14. Emri, G.; Emri, E. In Immunohistochemical detection of metallothioneins, Metallomics Technology Conference 2015: Recent Advances and Strategies, Department of Chemistry and Biochemistry, Faculty of Agronomy, Mendel University in Brno, 14. – 18. 6. , 2015; Adam, V.; Kizek, R., Eds. Mendel University in Brno, Zemědělská 1, 613 00 Brno: Department of Chemistry and Biochemistry, Faculty of Agronomy, Mendel University in Brno, pp 21-22.ISBN 978-80-7509-309-7; ISBN 978-80-7509-314-1 (on-line)
15. Haase, H. In Zinc signals and the control of immune cell functions, Metallomics Technology Conference 2015: Recent Advances and Strategies, Department of Chemistry and Biochemistry, Faculty of Agronomy, Mendel University in Brno, 14. – 18. 6. , 2015; Adam, V.; Kizek, R., Eds. Mendel University in Brno, Zemědělská 1, 613 00 Brno: Department of Chemistry and Biochemistry, Faculty of Agronomy, Mendel University in Brno, p 8.ISBN 978-80-7509-309-7 ISBN 978-80-7509-314-1 (on-line)
16. Gumulec, J.; Raudenska, M.; Adam, V.; Kizek, R.; Masarik, M. In Metallothionein – immunohistochemical cancer biomarker: A meta-analysis, Metallomics Technology Conference 2015: Recent Advances and Strategies, Department of Chemistry and Biochemistry, Faculty of Agronomy, Mendel University in Brno, 14. – 18. 6. , 2015; Adam, V.; Kizek, R., Eds. Mendel University in Brno, Zemědělská 1, 613 00 Brno: Department of Chemistry and Biochemistry, Faculty of Agronomy, Mendel University in Brno, p 13.ISBN 978-80-7509-309-7; ISBN 978-80-7509-314-1 (on-line)
17. Hidalgo, J. In Metallothionein and neuroinflammation, Metallomics Technology Conference 2015: Recent Advances and Strategies, Department of Chemistry and Biochemistry, Faculty of Agronomy, Mendel University in Brno, 14. - 18. 6. , 2015; Adam, V.; Kizek, R., Eds. Mendel University in Brno, Zemědělská 1, 613 00 Brno: Department of Chemistry and Biochemistry, Faculty of Agronomy, Mendel University in Brno. ISBN 978-80-7509-309-7; ISBN 978-80-7509-314-1 (on-line)
18. Hlavata, L.; Striesova, I.; Ignat, T.; Kizek, R.; J., L. In DNA based biosensor for an evaluation of damage to DNA by quantum dots, Metallomics Technology Conference 2015: Recent Advances and Strategies, Department of Chemistry and Biochemistry, Faculty of Agronomy, Mendel University in Brno, 14. – 18. 6. , 2015; Adam, V.; Kizek, R., Eds. Mendel University in Brno, Zemědělská 1, 613 00 Brno: Department of Chemistry and Biochemistry, Faculty of Agronomy, Mendel University in Brno, pp 25-26.ISBN 978-80-7509-309-7; ISBN 978-80-7509-314-1 (on-line)
19. Holubova, M.; Axmanova, M.; Gumulec, J.; Raudenska, M.; Sztalmachova, M.; Adam, V.; Kizek, R.; Masarik, M. In Pathways in zinc resistance, Metallomics Technology Conference 2015: Recent Advances and Strategies, Department of Chemistry and Biochemistry, Faculty of Agronomy, Mendel University in Brno, 14. – 18. 6. , 2015; Adam, V.; Kizek, R., Eds. Mendel University in Brno, Zemědělská 1, 613 00 Brno: Department of Chemistry and Biochemistry, Faculty of Agronomy, Mendel University in Brno, p 12.ISBN 978-80-7509-309-7; ISBN 978-80-7509-314-1 (on-line)
20. Holubova, M.; Sztalmachova, M.; Hudcova, K.; Balvan, J.; Gumulec, J.; Adam, V.; Masarik, M. In Zinc resistant prostate cancer cell lines and methods for their analysis – workshop, Metallomics Technology Conference 2015: Recent Advances and Strategie, Department of Chemistry and Biochemistry, Faculty of Agronomy, Mendel University in Brno, 14. – 18. 6. , 2015; Adam, V.; Kizek, R., Eds. Mendel University in Brno, Zemědělská 1, 613 00 Brno: Department of Chemistry and Biochemistry, Faculty of Agronomy, Mendel University in Brno, pp 72-78.ISBN 978-80-7509-309-7; ISBN 978-80-7509-314-1 (on-line)
21. Chudobova, D.; Richtera, L.; Cihalova, K.; Kremplova, M.; Milnerowitz, H.; Labuda, J.; Milosavljevic, V.; Kopel, P.; Adam, V.; Kizek, R. In The composites of graphene oxide with metal or semimetal nanoparticles and their effect on pathogenic microorganisms, Metallomics Technology Conference 2015: Recent Advances and Strategies, Department of Chemistry and Biochemistry, Faculty of Agronomy, Mendel University in Brno, 14. – 18. 6. , 2015; Adam, V.; Kizek, R., Eds. Mendel University in Brno, Zemědělská 1, 613 00 Brno: Department of Chemistry and Biochemistry, Faculty of Agronomy, Mendel University in Brno, pp 27-31.ISBN 978-80-7509-309-7; ISBN 978-80-7509-314-1 (on-line)
22. Kensova, R.; Richtera, L.; Kremplova, M.; Bizon, A.; Emri, G.; Hynek, D.; Kizek, R. In Study of the interaction of graphene oxide with chromate anion using aas, Metallomics Technology Conference 2015: Recent Advances and Strategies, Department of Chemistry and Biochemistry, Faculty of Agronomy, Mendel University in Brno, 14. – 18. 6. , 2015; Adam, V.; Kizek, R., Eds. Mendel University in Brno, Zemědělská 1, 613 00 Brno: Department of Chemistry and Biochemistry, Faculty of Agronomy, Mendel University in Brno, pp 50-53.ISBN 978-80-7509-309-7; ISBN 978-80-

7509-314-1 (on-line)
23. Kepinska, M.; Milnerowicz, H. In Capillary electrophoresis of metallothionein, Metallomics Technology Conference 2015: Recent Advances and Strategies, Department of Chemistry and Biochemistry, Faculty of Agronomy, Mendel University in Brno, 14. – 18. 6. , 2015; Adam, V.; Kizek, R., Eds. Mendel University in Brno, Zemědělská 1, 613 00 Brno: Department of Chemistry and Biochemistry, Faculty of Agronomy, Mendel University in Brno, pp 23-24.ISBN 978-80-7509-309-7; ISBN 978-80-7509-314-1 (on-line)
24. Kopel, P.; Kremplova, M.; Wawrzak, D.; Chudobova, D.; Cihalova, K.; Milnerowicz, H.; Adam, V.; Kizek, R. In Biological activity and molecular structures of bis(benzimidazoles) and trithiocyanurate complexes, Metallomics Technology Conference 2015: Recent Advances and Strategies, Department of Chemistry and Biochemistry, Faculty of Agronomy, Mendel University in Brno, 14. – 18. 6. , 2015; Adam, V.; Kizek, R., Eds. Mendel University in Brno, Zemědělská 1, 613 00 Brno: Department of Chemistry and Biochemistry, Faculty of Agronomy, Mendel University in Brno, pp 54-58.ISBN 978-80-7509-309-7; ISBN 978-80-7509-314-1 (on-line)
25. Krejcova, L.; Michalek, P.; Kopel, P.; Bizon, A.; Emri, G.; Hynek, D.; Adam, V.; Kizek, R. In Magnetic beads based isolation and electrochemical detection of specific influenza sequences labeled by quantum dots, Metallomics Technology Conference 2015: Recent Advances and Strategies, Department of Chemistry and Biochemistry, Faculty of Agronomy, Mendel University in Brno, 14. – 18. 6. , 2015; Adam, V.; Kizek, R., Eds. Mendel University in Brno, Zemědělská 1, 613 00 Brno: Department of Chemistry and Biochemistry, Faculty of Agronomy, Mendel University in Brno, pp 36-39.ISBN 978-80-7509-309-7; ISBN 978-80-7509-314-1 (on-line)
26. Kremplova, M.; Richtera, L.; Kensova, R.; Hynek, D.; Milnerowitz, H.; Labuda, J.; Kizek, R. In The study of interaction of graphene oxide with selenite anion using dpv, Metallomics Technology Conference 2015: Recent Advances and Strategies, Department of Chemistry and Biochemistry, Faculty of Agronomy, Mendel University in Brno, 14. – 18. 6. , 2015; Adam, V.; Kizek, R., Eds. Mendel University in Brno, Zemědělská 1, 613 00 Brno: Department of Chemistry and Biochemistry, Faculty of Agronomy, Mendel University in Brno, pp 45-49.ISBN 978-80-7509-309-7; ISBN 978-80-7509-314-1 (on-line)
27. Kremplova, M.; Richtera, L.; Kopel, P.; Kensova, R.; Kepinska, M.; Emri, G.; Milosavljevic, V.; Hynek, D.; Adam, V.; Kizek, R. In Influence of oxidation stage and exfoliation extent of carbon-based materials on electrochemical detection of as(iii), Metallomics Technology Conference 2015: Recent Advances and Strategies, Department of Chemistry and Biochemistry, Faculty of Agronomy, Mendel University in Brno, 14. – 18. 6. , 2015; Adam, V.; Kizek, R., Eds. Mendel University in Brno, Zemědělská 1, 613 00 Brno: Department of Chemistry and Biochemistry, Faculty of Agronomy, Mendel University in Brno, pp 40-44.ISBN 978-80-7509-309-7; ISBN 978-80-7509-314-1 (on-line)
28. Masarik, M.; Gumulec, J.; Raudenska, M.; Sztalmachova, M.; Exschlager, T.; V., A.; Kizek, R. In Metallothionein in cancer development, Metallomics Technology Conference 2015: Recent Advances and Strategies, Department of Chemistry and Biochemistry, Faculty of Agronomy, Mendel University in Brno, 14. – 18. 6. , 2015; Adam, V.; Kizek, R., Eds. Mendel University in Brno, Zemědělská 1, 613 00 Brno: Department of Chemistry and Biochemistry, Faculty of Agronomy, Mendel University in Brno, p 11.ISBN 978-80-7509-309-7; ISBN 978-80-7509-314-1 (on-line)
29. Nejdl, L.; Habova, M.; Kudr, J.; Ruttkay-Nedecky, B.; Bizon, A.; Pospisilova, L.; Adam, A.; Kizek, R. In Automatic electrochemical determination of soil contaminated by heavy metal ions (cd(ii) and pb(ii)), Metallomics Technology Conference 2015: Recent Advances and Strategie, Department of Chemistry and Biochemistry, Faculty of Agronomy, Mendel University in Brno, 14. – 18. 6. , 2015; Adam, V.; Kizek, R., Eds. Mendel University in Brno, Zemědělská 1, 613 00 Brno: Department of Chemistry and Biochemistry, Faculty of Agronomy, Mendel University in Brno, pp 59-62.ISBN 978-80-7509-309-7; ISBN 978-80-7509-314-1 (on-line)
30. Nejdl, L.; Richtera, T.; R., K.; Kudr, J.; Ruttkaynedecky, B.; Kynicky, J.; Emri, B.; Adam, V.; Kizek, R. In Uv tuning of cadmium telluride quantum dots (cdte) – assessed by spectroscopy and electrochemistry, Metallomics Technology Conference 2015: Recent Advances and Strategies, Department of Chemistry and Biochemistry, Faculty of Agronomy, Mendel University in Brno, 14. - 18. 6. , 2015; Adam, V.; Kizek, R., Eds. Mendel University in Brno, Zemědělská 1, 613 00 Brno: Department of Chemistry and Biochemistry, Faculty of Agronomy, Mendel University in Brno, pp 63-67.ISBN 978-80-7509-309-7; ISBN 978-80-7509-314-1 (on-line)
31. Ruttkay-Nedecky, B.; Nejdl, L.; Vaculovicova, M.; Adam, V.; Kizek, R. In Metalothionein and its role in metabolism of free radicals, Metallomics Technology Conference 2015: Recent Advances and Strategies, Department of Chemistry and Biochemistry, Faculty of Agronomy, Mendel University in Brno, 14. – 18. 6. , 2015; Adam, V.; Kizek, R., Eds. Mendel University in Brno, Zemědělská 1, 613 00 Brno: Department of Chemistry and Biochemistry, Faculty of Agronomy, Mendel University in Brno, pp 16-17.ISBN 978-80-7509-309-7; ISBN 978-80-7509-314-1 (on-line)
32. Vaculovicova, M.; Stanisavljevic, M.; Krizkova, S.; Kepinska, M.; Bizon, A.; Kizek, R.; Adam, V. In Quantum dots in fluorescence resonance energy transfer-based nanosensors and their application, Metallomics Technology Conference 2015: Recent Advances and Strategie, Department of Chemistry and Biochemistry, Faculty of Agronomy, Mendel University in Brno, 14. – 18. 6. , 2015; Adam, V.; Kizek, R., Eds. Mendel University in Brno, Zemědělská 1, 613 00 Brno: Department of Chemistry and Biochemistry, Faculty of Agronomy, Mendel University in Brno, pp 68-71.ISBN 978-80-7509-309-7; ISBN 978-80-7509-314-1 (on-line)
33. Nguyen, H.V.; Richtera, L.; Hynek, D.; Bizon, A.; Emri, G.; Adam, V.; Kizek, R. In Electrochemical

detection of cr(iii) ion using activated glassy carbon electrode, Metallomics Technology Conference 2015: Recent Advances and Strategies, Department of Chemistry and Biochemistry, Faculty of Agronomy, Mendel University in Brno, 14. – 18. 6. , 2015; Adam, V.; Kizek, R., Eds. Mendel University in Brno, Zemědělská 1, 613 00 Brno: Department of Chemistry and Biochemistry, Faculty of Agronomy, Mendel University in Brno, pp 32-35.ISBN 978-80-7509-309-7; ISBN 978-80-7509-314-1 (on-line)

34. Zitka, O.; Guran, R.; Kizek, R.; Adam, V. In Maldi new technology, Metallomics Technology Conference 2015:Metallomics and analytical methods, Department of Chemistry and Biochemistry, Faculty of Agronomy, Mendel University in Brno, 25. - 26. 8. 2015, 2015; Adam, V.; Kizek, R., Eds. Mendel University in Brno, Zemědělská 1, 613 00 Brno: Department of Chemistry and Biochemistry, Faculty of Agronomy, Mendel University in Brno, pp 16-19.ISBN 978-80-7509-326-4 (on-line)
35. Kominkova, M.; Merlos, M.A.; Michalek, P.; Kizek, R. In Phytochelatin analysis in animal, Metallomics Technology Conference 2015:Metallomics and analytical methods, Department of Chemistry and Biochemistry, Faculty of Agronomy, Mendel University in Brno, 25. - 26. 8. 2015, 2015; Adam, V.; Kizek, R., Eds. Mendel University in Brno, Zemědělská 1, 613 00 Brno: Department of Chemistry and Biochemistry, Faculty of Agronomy, Mendel University in Brno, pp 20-23.ISBN 978-80-7509-326-4 (on-line)
36. Hynek, H.; Kizek, R. In Electrochemistry in metallomics, Metallomics Technology Conference 2015:Metallomics and analytical methods, Department of Chemistry and Biochemistry, Faculty of Agronomy, Mendel University in Brno, 25. - 26. 8. 2015, 2015; Adam, V.; Kizek, R., Eds. Mendel University in Brno, Zemědělská 1, 613 00 Brno: Department of Chemistry and Biochemistry, Faculty of Agronomy, Mendel University in Brno, pp 24-27.ISBN 978-80-7509-326-4 (on-line)
37. Krizkova, S.; Adam, V.; Kizek, R. In Metallothionein and cancer, Metallomics Technology Conference 2015:Metallomics and analytical methods, Department of Chemistry and Biochemistry, Faculty of Agronomy, Mendel University in Brno, 25. - 26. 8. 2015, 2015; Adam, V.; Kizek, R., Eds. Mendel University in Brno, Zemědělská 1, 613 00 Brno: Department of Chemistry and Biochemistry, Faculty of Agronomy, Mendel University in Brno, pp 35-37.978-80-7509-326-4 (on-line)
38. Guran, R.; Zitka, O.; Kizek, R.; Adam, V. In Mass spectrometry and chromatography and metallomics, Metallomics Technology Conference 2015:Metallomics and analytical methods, Department of Chemistry and Biochemistry, Faculty of Agronomy, Mendel University in Brno, 25. - 26. 8. 2015, 2015; Adam, V.; Kizek, R., Eds. Mendel University in Brno, Zemědělská 1, 613 00 Brno: Department of Chemistry and Biochemistry, Faculty of Agronomy, Mendel University in Brno, pp 38-41.ISBN 978-80-7509-326-4 (on-line)
39. Xhaxhiu, K. In Synthetic birnessites and buserites as heavy metal cation traps and environmental remedies, Metallomics Technology Conference 2015:Metallomics and analytical methods, Department of Chemistry and Biochemistry, Faculty of Agronomy, Mendel University in Brno, 25. - 26. 8. 2015, 2015; Adam, V.; Kizek, R., Eds. Mendel University in Brno, Zemědělská 1, 613 00 Brno: Department of Chemistry and Biochemistry, Faculty of Agronomy, Mendel University in Brno, pp 62-72.ISBN 978-80-7509-326-4 (on-line)
40. Xhaxhiu, K.; Keçi, E.; Zitka, O.; Kizek, R. In The inhibition the rate of six essential oils upon two bacterial colonies (staphylococcus aureus and escherichia coli), Metallomics Technology Conference 2015:Metallomics and analytical methods, Department of Chemistry and Biochemistry, Faculty of Agronomy, Mendel University in Brno, 25. - 26. 8. 2015, 2015; Adam, V.; Kizek, R., Eds. Mendel University in Brno, Zemědělská 1, 613 00 Brno: Department of Chemistry and Biochemistry, Faculty of Agronomy, Mendel University in Brno, pp 28-34.ISBN 978-80-7509-326-4 (on-line)
41. Emri, G.; Emri, E.; Beke, L.; Boros, G.; Hegedűs, C.; Janka, E.; Gellén, E.; Méhes, G.; Remenyik, E. In Immunohistochemical detection of metallothionein, Metallomics Technology Conference 2015:Metallomics and analytical methods, Department of Chemistry and Biochemistry, Faculty of Agronomy, Mendel University in Brno, 25. - 26. 8. 2015, 2015; Adam, V.; Kizek, R., Eds. Mendel University in Brno, Zemědělská 1, 613 00 Brno: Department of Chemistry and Biochemistry, Faculty of Agronomy, Mendel University in Brno, pp 51-61.ISBN 978-80-7509-326-4 (on-line)
42. Xhaxhiu, K.; Keçi, E.; Zitka, O.; Kizek, R. In The inhibitory effect of six essential oils toward candida albicans, Metallomics Technology Conference 2015:Metallomics and analytical methods, Department of Chemistry and Biochemistry, Faculty of Agronomy, Mendel University in Brno, 25. - 26. 8. 2015, 2015; Adam, V.; Kizek, R., Eds. Mendel University in Brno, Zemědělská 1, 613 00 Brno: Department of Chemistry and Biochemistry, Faculty of Agronomy, Mendel University in Brno, pp 7-12.ISBN 978-80-7509-326-4 (on-line)
43. Vaculovicova, M.; Adam, A.; Kizek, R. In Metallomics and new analytical methods, Metallomics Technology Conference 2015:Metallomics and analytical methods, Department of Chemistry and Biochemistry, Faculty of Agronomy, Mendel University in Brno, 25. - 26. 8. 2015, 2015; Adam, V.; Kizek, R., Eds. Mendel University in Brno, Zemědělská 1, 613 00 Brno: Department of Chemistry and Biochemistry, Faculty of Agronomy, Mendel University in Brno, pp 13-1551-.ISBN 978-80-7509-326-4 (on-line)
44. Krizkova, S.; Fabrik, I.; Adam, V.; Hrabeta, P.; Eckschlager, T.; Kizek, R. Metallothionein - a promising tool for cancer diagnostics. Bratislava Medical Journal-Bratislavske Lekarske Listy 2009, 110, 93-97.0006-9248
45. Emri, G.; Emri, E.; Beke, L.; Boros, G.; Hegedűs, C.; Janka, E.; Gellén, E.; Méhes, G.; Remenyik, E. Immunohistochemical detection of metallothionein. J. Metallomics Nanotech. 2015,

in press.2336-3940
46. Guran, R.; Blazkova, I.; Kensova, R.; Zitka, O.; Kizek, R.; Adam, V. Maldi-tof msi and electrochemical detection of metallothionein in chicken liver after cadminum exposure. J. Metallomics Nanotech. 2015, in press.2336-3940
47. Kepinska, M.; Milnerowicz, H. Capillary electrophoresis of metallothionein J. Metallomics Nanotech. 2015, in press.2336-3940
48. Xhaxhiu, K. Synthetic birnessites and buserites as heavy metal cation traps and environmental remedies J. Metallomics Nanotech. 2015, in press.2336-3940

The article is freely distributed under license Creative Commons (BY-NC-ND). But you must include the author and the document can not be modified and used for commercial purposes.

Capillary electrophoresis of metallothionein

Marta Kepinska* and Halina Milnerowicz

Department of Biomedical and Environmental Analysis, Faculty of Pharmacy, Wroclaw Medical University, Borowska 211, Wrocław 50-556, Poland

* Author to whom correspondence should be addressed; E-Mail: zalewska.m@gmail.com; Tel.: +48-71-7840173; Fax: +48-71-7840172.

Received:31.7.2015 / Accepted:11.8.2015 / Published: 1.10.2015

Mammalian metallothioneins (MTs) are a group of low molecular weight (6-7 kDa) proteins. They consist of a single polypeptide chain of 61-68 amino acid residues, including 20 cysteinyl residues. In the human, there are four isoforms: MT-1, MT-2, MT-3, MT-4. Heterogeneity of isoforms results also from post-translational acetylation and/or variations in metal compositions. MTs are involved in the metabolism of heavy metals and constitute an intracellular reservoir of trace elements. Furthermore, they neutralize electrophilic compounds, have a protective function against DNA damage and an ability to inhibit apoptosis. Due to the characteristics, such as low molecular weight and unique primary structure, elaborating the isolation, separation and determination conditions of MTs analysis poses many problems, especially in achieving a satisfactory sensitivity and specificity. In addition to traditional analytical techniques, such as gel electrophoresis, liquid chromatography, and size exclusion chromatography, capillary electrophoresis (CE) has proven to be a powerful separation technique for MT analysis. Numerous studies devoted to the optimization of CE conditions as capillary surface, electrolyte background or modifiers or kind of detectors. Coupling CE with mass spectrometry creates a powerful analytical tool for the characterization of MT.

Keywords: capillary electrophoresis; metallothionein

1. Introduction

Metallothionein (MT) was first isolated in 1957 from the horse kidney by Margoshes and Vallee [1], subsequently MT presence was demonstrated in other animals, in higher plants, eukaryotic microorganisms, and in some prokaryotes [2]. Mammalian MT belongs to a group of low molecular weight proteins (6000-7000 Da) with 30% content of cysteine. A characteristic feature of all MTs is a tripeptide sequence Cys--Xaa-Cys, where Xaa is an aminoacid other than cysteine [3]. The sulfhydryl groups of cysteine form with metals closely packed spatial structure in which metals are within the molecule [2,4]. It serves as the reservoir of metals for the body (mainly Zn and Cu) which are the part of many enzymes and proteins involved in the removal of DNA damage, replication or transcription. MT protects the cells against the toxicity of heavy metals (Cd, Pb, Hg) by binding them. MT is composed of two domains: α and β linked by lysine dimer. Domain α (C-terminal) is more stable and is able to bind four atoms of Zn or Cd, or five or six atoms of Cu. Beta domain (N terminal) is more reactive, it can bind tri- Zn or Cd, or six atoms of Cu [4].

Slight differences in amino acid composition, hydrophobicity and isoelectric point allowed to separate the four major isoforms: MT-1, MT-2, MT-3 (also known as, growth inhibitory factor GIF), and MT-4. Despite the mutual similarity of MT-1 and MT-2, their roles and presence in tissues differ significantly [5]. While MT-2 isoform in humans is encoded by a single gene MT-2A, MT-1 consists of multiple subtypes encoded by a gene set of MT-1 (MT-1A, 1B-MT, MT-1E, MT-1F, MT-1G, 1H and MT-MT-1X), which determine the micro-heterogeneity of the protein (Figure 1).

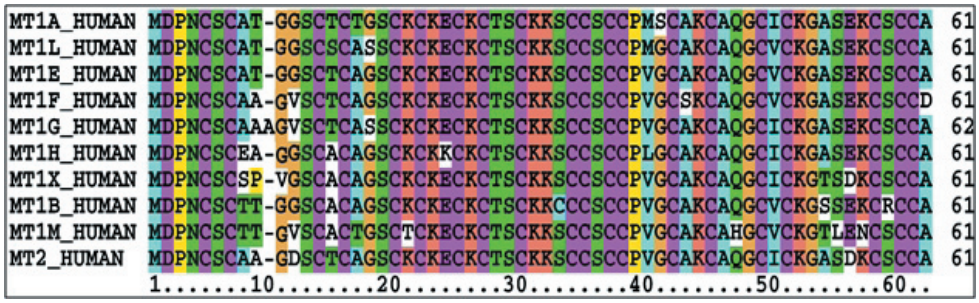

Figure 1: Comparison of the amino acid sequences of MT 1/2 human isoforms using the ClustalX program 2.0.11 [6].

ISOFORM	OCCURRENCE
MT-1/MT-2	Nucleated cells of peripheral tissues, interstitial fluids, blood plasma. Particularly high levels in the liver and kidneys. Also present in the cells of the CNS serving as nourishing and supporting cells (glia, astrocytes, cells of the choroid plexus and tires).
MT-3	Neurons (in the brain mainly in cells of the neocortex, hippocampus, cells of the olfactory bulb and dentate gyrus), renal tubular cells, male reproductive tract.
MT-4	Squamous cells (mouth, esophagus, stomach, appendages, skin, feet, hands).

Table 1: Places of expression of particular isoforms of human MT [Based on 11].

MT-1 and MT-2 genes expression have been demonstrated in many tissues: in the parenchymal cells of the kidney, liver, lung, intestines, pancreas [7], in cells of the sweat glands of the skin, in germ cells, and in epithelial cells of the thymus [8]. Izofom MT-3 is a protein mainly present in brain tissue [9]. The expression of MT-4 is limited to squamous skin and upper gastrointestinal [10]. Sites of presence of particular isoforms of human MT are listed in Table 1 [11].

MT cysteine residues also play a critical role in the removal of free radicals. MT has antitumor activity as it neutralizes toxic electrophiles, reactive oxygen and nitrogen species. MT is also capable of inhibiting apoptosis and developing resistance to radiotherapy and chemotherapy. Higher expression of this protein has been observed in many tumor tissues: lung, kidney, pancreas, bladder, urinary tract. Lower concentration levels have been observed in gastrointestinal tumors tract, including liver cancer or colon cancer.

To identify MT, sensitive and selective analysis techniques are applied. Low molecular weight of protein, and the heterogeneity of the biological material to be analyzed (serum, erythrocyte lysate, urine, different tissues), also causes a variety of methods used for its quantitative determination.

Electrochemical methods such as differential pulse and cathodic stripping voltammetry, saturation analysis methods based on Cd,

Ag and Hg, spectrophotometric methods as well as chromatographic and electrophoretic techniques are used [12]. Among immunological techniques used in MT analyses are: enzyme-linked immunosorbent assay, immunofluorescence assay and radioimmunoassay. These methods are highly sensitive and can detect even small amounts of MT in tested material [13,14]. One of the most widely used techniques in the analysis of proteins including MT is two-dimensional polyacrylamide gel electrophoresis or capillary electrophoresis (CE) often coupled with mass spectrometry (MS). CE allows analysis of both MT as MT in complexes with metals. As the determination of various isoforms is concerned, there must be very sophisticated detection system connected with separation one.

Today, medicine has a lot of interest in research on this protein, and thanks to modern analytical methods with high sensitivity and specificity, the determination of MT concentrations in the biological material is possible, wherein its amount in relation to other proteins is small.

2. Capillary electrophoresis

Electrophoresis was developed by Swedish chemist Arne Tiselius in the 30s of the twentieth century, in order to test serum proteins. For this achievement he obtained the Nobel Prize. The basis of this analytical method is the ability to move of charged species, placed in an electric field to the corresponding pole of the power source.

CE is one of the methods of electrophoresis, which is characterized by high efficiency, substantially higher than the efficiency achieved by high-performance liquid chromatography (HPLC). In CE, capillaries made of synthetic quartz not absorbing ultraviolet radiation are used. The capillaries are immersed in a suitable buffer solution and when cross potential gradient is applied, hydrated cations are attracted toward the cathode, causing a flow in the whole volume of liquid. This phenomenon is known as electroosmotic flow (EOF). In CE, this effect is responsible for the movement of all particles (cationic, anionic or neutral) along the capillary toward the detector. EOF in capillaries filled with a buffer is formed by the ionization of silane groups (SiOH) on the inner surface of the walls at pH above 4. Cations accumulate near the negatively charged surfaces and form electrical double layer - the potential is formed. Applying a voltage across the capillary initiates EOF, whose speed is typically about one order of magnitude greater than the flow rate of solute. So the total migration rate of the substance (μ total) is μsubst + μEOF. As the result of EOF, all substances are transferred into the cathodic end of the capillary, where they pass through the chamber of the detector. Most commonly used detectors are UV-VIS, diode-array detector, fluorescent, electrochemical and mass spectrometer [12,15].

2.1 Types of capillary electrophoresis

There are several methods of separation of different substances by capillary electrophoresis.

Capillary zone electrophoresis (CZE) is the simplest from CE methods. Separation of substances occurs within the capillary filled with a buffer solution of appropriate pH and ionic strength. Upon application of the electric field substances are transferred toward the cathode end of the capillary in a strong flow - EOF. The particles reach the detector in order of decreasing total mobility, which depends on the size and charge of individual substances. CZE cannot be used for the separation of neutral substances. The main means influencing EOF include electric field, pH, ionic strength, composition and additives of electrolyte, as well as capillary wall coating and separation temperature [12].

Micellar electrokinetic capillary chromatography (MECC) is used for distribution of both ions and neutral compounds. It uses the addition to buffer of surfactant solution which forms micelles with a hydrophobic inside and positively or negatively charged surface. The micelles divide neutral substances according to their partition coefficient. More hydrophobic substances arrange inside the micelles, and hydrophilic in buffer solution [16]. Then micelles migrate towards the detector, complexes with a positive charge appear first, then a neutral and at the

end negative ones. The most commonly used surface-active agent is sodium dodecyl sulfate (SDS), which exhibits the best resolution [17]. The MECC basis for separation of substances is their division between the hydrophilic aqueous electrolyte environment and the hydrophobic interior of the negatively charged SDS micelles. Separation is based on differences in hydrophobicity and charge. Separation achieved by MECC is generally lower than in other CE techniques. However, MECC has much higher efficiency of separation and reproducibility of peaks migration times and their surfaces.

Capillary gel electrophoresis is used for separation polymers, proteins and DNA sequencing. The capillary tube is filled with a polyacrylamide or agarose gel. The sample is applied electrokinetically to the capillary, and prior to the analysis it is necessary to remove impurities from sample. Separation of analyte particles takes place under the influence of differences in particle size and speed of their passage through crosslinked gel bed. The larger particles migrate slower through the gel [15,18].

Capillary isoelectric focusing is a technique with a high degree of proteins separation and other amphoteric compounds. The analysis is carried out in a capillary, wherein pH gradient is formed using ampholytes carrier. The isoelectric point values are typically in the range from 3 to 10. Upon application of an electric field, components of the sample migrate and become embedded in such places of capillary, which correspond to their pI. After termination of the separation, all components are analyzed by a detector through which they pass under the pressure applied to the anode end of the capillary [15].

Capillary isotachophoresis is characterized by the use of two different buffering sets, leading buffer with a higher mobility than the mobility of the sample and buffer ending with a lower mobility. In them, the particles of analyte migrate depending on their electrophoretic mobility, to form a chain of adjacent zones, moving at the same speed between the two solutions. This method uses capillaries with inner diameters 500 μm, and the primary detection system is conductometry [18].

Anhydrous capillary electrophoresis is a method that has better solubility and stability for hydrophobic molecules. Separation takes place in a medium consisting of organic solvents in place of aqueous buffer. Acetonitrile or methanol are usually used. The viscosity and dielectric constant of the solvent affect the mobility of analyzed ions and the level of electroosmotic flow [19, 20].

Capillary electrochromatography is a method that combines the advantages of HPLC and CE. It is characterized by a strong EOF with flat profile and a higher selectivity than other CE methods. Separation of charged analytes is carried out on the basis of their electrophoretic migration and adsorption chromatography of neutral particles [19].

3. The use of capillary electrophoresis in metallothionein analysis

For the separation of MT isoforms, different CE techniques in combination with appropriate detectors are used. It provides a wide range of possibilities to optimize the degree of resolution by selecting the pH, temperature, buffer, electrolyte and the type of capillary.

3.1 Types of capillaries

Two types of capillaries have been used: uncoated or coated capillary. The use of uncoated capillaries gives advantages in terms of their stability and the shorter time of analysis, while the use of surface-modified capillaries increases the resolution of MT isoforms separation [21].

3.1.1 Uncoated capillaries

As a result of using uncoated capillaries often occurs undesirable phenomenon of adsorption of proteins on the inner wall of the capillary tube. The reason is that the silane groups at pH 3 or more are ionized. This can be avoided by: (1) the addition of SDS or methanol that limits the proteins ability to interact with the wall; (2) analysis of MTs at low pH but it has limitations because MTs are unstable at pH below 3 and they dissociate metals; (3) the use of buffers of high ionic strength. These buffers generate current which causes excessive heating of the sample and the quantitative loss of resolution.

Therefore, effective cooling of the capillaries is essential; (4) increase or decrease the length of the capillary diameter. As a result, the electrical resistance is reduced and there is an increase of dissipation of excessive heat, what reduces the current flow and heating effects [22].

At low pH MTs are unstable. They dissociate metals and the level of apolipoprotein arise. The release of metal causes a reduction in UV absorbance and MTs sample more concentrated should be used for their determination. Separation of MTs complexes with Cd and Zn in the pH range of 3-5 is not reproducible due to the partial dissociation of the metal. Often, in the electropherogram it is difficult to distinguish the peaks of MT-1 and MT-2 from each other. There is no such problem with MT-3, because it is highly charged, migrates faster and it is completely separated from the MT-1 and MT-2 in neutral and low pH. In order to improve resolution of MT-1 and MT-2 isoforms, ions of surfactants with the electrolyte are added to samples of MT. Use of MECC technique enables the separation of all MT isoforms, which is not possible using only phosphate buffer. The best MECC recommended conditions include using of a 50 cm x 75 µm uncoated capillary, 300 mM borate buffer pH 8.4 containing 85 mM SDS. Furthermore MECC at 10 kV gives a better separation by changing pH from 8.4 to 10.4 or SDS concentration from 60 to 120 mM, when compared with the use of higher voltage [17,21].

3.1.2 Modified capillaries

The inner surface of a fused silica capillary is modified or coated with various substances or ligands in order to eliminate EOF and interaction of proteins with walls. This affects its charge, hydrophobicity and surface chemistry. Neutral capillaries are used for the separation and qualitative assessment of proteins, among others MT isoforms. They enable to use a wide range of different electrolytes and buffers. Both low and neutral pH can be used for analysis by changing the polarity. Good resolution is observed in organic buffers and phosphate. Capillaries coated with amino groups give better results for the separation of proteins positively charged (at pH below the pI of the protein), because the wall has a positive charge. However, some of capillaries are not suitable for use in pH below 3.5. MT isoforms with pI 4-4.5 and charge from 1 to 13 at neutral pH, should not be separated in capillaries coated with amino groups in neutral or alkaline pH. However, using high ionic strength and phosphate buffer at pH above 8 as the electrolyte, a good separation of all MTs is obtained [22].

3.2 Sample preparation for metallothionein analysis

Quantitative determination of MT isoforms in tissues requires adequate sample preparation technique. Radioimmunoassays and some analytical techniques do not require sample purification. They can be used directly to MT measurements. In contrast, samples for chromatography and electrophoresis should be wholly or partially purified. Purification always reduces the amount of tested substance in the sample, so finding optimal solution is desired. MTs in relation to other proteins are heat-stable and they can be purified by heat treatment at the temperature of 60°C for 10 min. or to 100°C for 1 min. The temperature and heating time are depending on the size of the sample [23].

Another method of sample purification is to acidification of tissue fragments prior to analysis, MTs are difficult to denaturize at a low pH, but they lose metals. They are also stable in 50% aqueous solutions of a mixture of solvents: ethanol, acetone and acetonitrile. Many other proteins in these solutions are deposited on the vessel walls.

These procedures cause significant dilution of samples, and from analytical point of view, the use of concentrated samples is required. Therefore, the most used technique for MTs preparation from tissue is by a two-stage solvent extraction having a concentration of 50% and 80-90%. It gives partially clean and concentrated extract, which is analyzed using CZE. In this technique is important to choose a suitable solvent. Using of a mixture of acetonitrile-ethanol as a solvent gives a reproducible and highly efficient procedure. The purification yield can be increased by adding 0.5 mM of sodium chloride to the homogenisation buffer 100 mM Tris-HCl pH 8.0 [22,24].

3.3 The choice of buffer and electrolyte

Increasing the resolution of MT isoforms is achieved by appropriate selection of buffers and electrolytes. Their selection should be guided by three main factors: UV absorbance, conductivity and pH buffering capacity. The most, sodium phosphate is used, because it has a very low absorbance in the UV wavelength range and has very good pH buffer capacity. The phosphate buffer gets a higher degree of resolution than the borate buffer, but generates a higher current because it has a higher ionic strength. Therefore, when using a sodium phosphate is recommended to use narrower (25 and 50 μm) and longer capillaries (50-100 cm). Borate buffer has low conductivity, lower ionic strength and resolution of phosphate buffer. However, the resolution is increased by using higher concentrations of buffer [21]. Good separation of MT is achieved with organic compounds for example: 2-amino-2-hydroxymethyl-propan-1,3--diol (Tris) and mixed buffer, eg. Tris-borate. Virtanen et al. presented a systematic study of the impact of buffer composition, concentration and pH as well as temperature and voltage on separation of MT isoforms [25]. Later, the same author introduced CE method using Tris-tricine buffer containing methanol as a background electrolyte [26]. The advantage of using bipolar organic buffers is their low conductivity and low ionic strength. When using UV detection below 220-230 nm, the absorption of some organic buffers is limited by their high concentrations [27]. From buffers discussed above, the best MT separation was obtained in uncoated capillaries in a phosphate buffer with high ionic strength and low pH [22].

3.4 Methods of metallothionein detection

Identification of separated MT isoforms from tissue extracts and in purified MT samples using CE is not so difficult in comparison with a further detection, especially because of the limited amount of material that can be obtained from tissues. The choice of method for determining MT isoforms in CE depends on the required degree of reproducibility, sensitivity and specifics. The techniques of detection which are used in the analysis of MT isoforms are UV detection, diode array detector and mass spectrometers.

3.4.1 Detection of metallothionein by UV and diode array detector

The absorbance detection is highly universal especially in the deep UV range of spectra, its sensitivity is dependent on the optical pathlength, which is given by the capillary diameter. MT absorbance detection is mostly carried out at 200 nm employing the light absorption by the peptide bond [12]. MT does not disclose the absorbance at 280 nm, as it does not contain aromatic amino acids. The most common method of MT isoforms identification is the use of diode-array detector. Simultaneous monitoring of spectra at different wavelengths: 200, 214, and 254 nm can be done to see: apoproteins at absorbance at 200 nm, Zn-MT - at 214 nm, Cd-MT - at 254 nm. Another problem is the type of buffer used. Organic buffers as HEPES, Tricine strongly absorbs UV light below 230 nm. This limits the use of lower wavelength. In contrast, buffers as phosphate and sodium borate do not absorb UV light and are suitable for the determination in wavelength lower than 230 nm. A mixture of alkaline borate and SDS shows a good separation and repeatability of migration times.

3.4.2 Metallothionein detection with mass spectrometry

A very good method for determining isoforms of MT is to use MS. The device separates the beam of charged particles according to a weight value of the particle charge by means of electric and magnetic fields. There are many types of mass spectrometers differing in the type and direction of fields, shape their area of operation and the distribution of the intensities.

With MS, monomers and polymers of MT isoforms can be identified. The spectrometer analyzes very small sample volumes, making it possible to obtain more detailed information about the fraction obtained after separation on CE, compared with UV or DAD detection. Furthermore, the combination of MS with various techniques for CE gained a lot of important

information on MT. CZE-MS shows the molecular structure of MT and inductively coupled plasma (ICP)-MS binding of MT with metal. The application of CE-ICP-MS has made significant progress in MT analysis in last few decades. The metals complexes of two major MT isoforms, MT-1 and MT-2, were separated and elements present in isoforms were selectively detected by CE-ICP-MS coupled via various interface designs [28,29].

4. Conclusions

MTs are considered as medical or environmental pollution biomarkers therefore methods of their effective determination are needed. The present paper shows advantages of capillary electrophoresis as a tool for MT determination. Despite many years of research on MT and the use of CE in its analysis, there is still lack of method that allows the simultaneous analysis of all isoforms of MT directly in the tissues.

Acknowledgments

Financial support from Wroclaw Medical University Pbmn 178 and Metallomic Scientific Network V4MSNet (project 11440027) is greatly acknowledged.

Conflicts of Interest

The authors declare they have no potential conflicts of interests concerning drugs, products, services or another research outputs in this study. The Editorial Board declares that the manuscript met the ICMJE „uniform reguirements“ for biomedical papers.

References

1. Margoshes, M.; Vallee, B.L. A cadmium protein from equine kidney cortex. J. Am. Chem. Soc. 1957,79, 4813-4814.
2. Klaassen, C.D.; Liu, J.; Chaudhuri, S. Metallothionein: an intracellular protein to protect against cadmium toxicity. Ann. Rev. Pharmacol. Toxicol. 1999, 39, 267-94.
3. Dabrio, M.; Rodriquez, A.R.; Bordin, G.; Bebianno, M.J.; Ley M.D.; Sestakova, I.; Vasak, M.; Nordberg, M. Recent developments in quantification methods for metallothionein. J. Inorg. Biochem. 2002, 88, 123-134.
4. Klaassen, C.D.; Liu, J. Role of metallothionein in cadmium-induced hepatotoxicity and nephrotoxicity. Drug Metab. Rev. 1997, 29, 79-102.
5. Zalewska, M.; Trefon, J.; Milnerowicz, H. The role of metallothionein interactions with other proteins. Proteomics. 2014, 14, 1343-56. Review.
6. Thompson, J.; Higgins, D.; Gibson, T. CLUSTALW: improving the sensitivity of progressive multiple sequence alignment through sequence weighting, position specific gap penalties and weight matrix choice. Nuc. Acids Res. 1994, 22, 4673-4680.
7. Lynes, M.A.; Borghesi, L.A.; Youn, J.; Olson, E.A. Immunomodulatory activities of extracellular metallothionein. I. Metallothionein effects on antibody production. Toxicology 1993, 85,161-177.
8. Vandenoord, J.J.; Deley, M. Distribution of metallothionein in normal and pathological human skin. Arch. Dermatol. Res. 1994, 286, 62-68.
9. Uchida, Y.; Takio, K.; Titani, K.; Ihara, Y.; Tomonaga, M. The growth inhibitory factor that is deficient in the Alzheimer‘s disease brain is a 68 amino acid metallothionein-like protein. Neuron 1991, 7, 337-47.
10. Quaife, C.J.; Findley, S.D.; Erickson, J.C. Induction of a new metallothionein isoforms (MT-IV) occurs during differentiation of stratified epithelia. Biochemistry 1994 ,33, 7250-7259.
11. Ryvolova, M.; Krizkowa, S.; Adam, V.; Becklova, M.; Trnkova, L.; Hubalek, J.; Kizek, R. Analytical methods for metallothionein detection. Curr. Anal. Chem. 2011, 7, 243-261.
12. Ryvolova, M.; Adam, V.; Kizek, R. Analysis of metallothionein by capillary electrophoresis. J Chromatogr A 2012, 1226, 31-42. Review.
13. Milnerowicz, H.; Bizoń, A. Determination of metallothionein in biological fluids using enzyme-linked immunoassay with commercial antibody. Acta Biochim Pol. 2010, 57, 99-104.
14. Krizkova, S.; Ryvolova, M.; Masarik, M.; Zitka, O.; Adam, V.; Hubalek, J.; Eckschlager, T.; Kizek, R. Modern bioanalysis of proteins by electrophoretic techniques. Methods Mol Biol. 2014, 1129, 381-396.
15. Zalewska, M.; Bizoń, A.; Milnerowicz, H. Comparison of capillary electrophoretic techniques for analysis and characterization of metallothioneins. J Sep Sci. 2011, 34, 3061-3069.
16. Sieradzka, E.; Witt, K.; Milnerowicz, H. The application of capillary electrophoresis techniques in toxicological analysis. Biomed Chromatogr. 2014, 28, 1507-1513. Review.
17. Beattie, J.H.; Richards, M.P. Analysis of metallothionein isoforms by capillary electrophoresis: optimization of protein separation conditions using micellar electrokinetic capillary chromatography. J Chromatogr A. 1995, 700, 95-103
18. Bo, T.; Pawliszyn, J. Characterization of phospholipid-protein interactions by capillary isoelectric focusing with whole-column imaging detection. Anal Biochem. 2006, 350, 91-98.
19. Riekkola, M.L.; Jonsson, J.A.; Smith, R.M. Terminology for analytical capillary electromigration. Pure Appl. Chem. 2004, 76, 443-451
20. Ding S.; Qi. L.; Tian K. Novel and simple nonaqueous capillary electrophoresis separation

and determination bioactive triterpens in Chinese herbs. J. Pharm. Biomed. Anal. 2006, 40, 35-41.
21. Richards, M.P.; Beattie, J.H. Comparison of different techniques for the analysis of metallothionein isoforms by capillary electrophoresis. J. Chromatogr. B. 1995, 669, 27-37.
22. Beattie, J.H. Strategies for the qualitative and quantitative analysis of metallothionein isoforms by capillary electrophoresis. Talanta 1998, 46, 255-270.
23. Li, Y.; Yang, H.; Liu, N.; Luo, J.; Wang, Q.; Wang, L. Cadmium accumulation and metallothionein biosynthesis in cadmium-treated freshwater mussel Anodonta woodiana. PLoS One 2015, 10, e0117037.
24. Kubo, K.; Sakita, Y.; Minami, T. Effect of heat treatment on metallothionein isoforms using capillary zone electrophoresis. Analusis 2000, 28, 366-369.
25. Virtanen, V.; Bordin, G.; Rodriguez, A.R. Separation of metallothionein isoforms with capillary zone electrophoresis using an uncoated capillary column—effects of pH, temperature, voltage, buffer concentration and buffer composition. J Chromatogr A 1996, 734, 391-400.
26. Virtanen, V.; Bordin, G. Tricine buffer for metallothionein isoform separation by capillary zone electrophoresis. Anal Chim Acta 1999, 402, 59-66.
27. Virtanen, V.; Bordin, G. Isoform separation of metallothioneins by capillary zone electrophoresis with Tris–tricine buffer in the presence or absence of methanol. Anal. Chem. A. 1998, 372, 231-239.
28. Guo, X.; Chan, H.M.; Guevremont, R.; Siu, K.W. Analysis of metallothioneins by means of capillary electrophoresis coupled to electrospray mass spectrometry with sheathless interfacing. Rapid Commun Mass Spectrom. 1999, 13, 500-507.
29. Tomalová, I.; Foltynová, P.; Kanický, V.; Preisler, J. MALDI MS and ICP MS detection of a single CE separation record: a tool for metalloproteomics. Anal Chem. 2014, 7, 647-654.

The article is freely distributed under license Creative Commons (BY-NC-ND). But you must include the author and the document can not be modified and used for commercial purposes.

Synthetic birnessites and buserites as heavy metal cation traps and environmental remedies

Kledi Xhaxhiu [1],*

[1] Department of Chemistry, Faculty of Natural Sciences, Blv. "Zog I" No.2/1, 1001, Tirana Albania; E-Mail: kledi.xhaxhiu@unitir.edu.al

* Author to whom correspondence should be addressed; E-Mail: kledi.xhaxhiu@unitir.edu.al; Tel.: +35542229590 (ext. 123); Fax: +35542231120.
Received:7.8.2015 / Accepted:1.9.2015 / Published:1.10.2015

Microporous Na-birnessite-type manganese oxides are synthesized by oxidation of $Mn(OH)_2$ with $K_2S_2O_8$ in strong alkaline environment. Subsequent ion-exchange reactions in aqueous solutions containing Sr, Ba promote their incorporation into the layered structural frameworks, which upon further hydration lead to the respective layered Buserites. Chemical composition and surface structure are assessed by X-ray powder diffraction, nitrogen- and argon- sorptiometry. Na-birnessites and Sr-buserites display good crystallinity. Ba-buserites consist mainly of nanocrystals. Their N_2 adsorption/desorption isotherms of resemble IV-type isotherms. Integral and differential pore distribution curves obtained by N_2-sorptiometry exhibit out-of-layers pores of 4-5 nm and 10-20 nm. Na-birnessites, Sr- and Ba-buserites possess external B.E.T surfaces of 75.6, 49.2 and 93.6 m^2/g respectively. Considerable adsorption volumes of 14, 17 cm^3/g for P/P0 = 0.05 for Na-birnessites and Ba-buserites are assessed by Ar-sorptiometry. Differential pore distribution curves confirm inner-layer micropores of 5 to 7 Å with a B.E.T specific area of 76.2 m^2/g for Na-birnessites and 51.8 m^2/g for Ba-buserites. Na-birnessites and Sr-, Ba-buserites possess enhanced ionic exchanging capacity, acting as a "sink" for heavy metal cations such as Fe^{2+}, Fe^{3+}, Co^{2+}, Ni^{2+}, As^{3+}. The retention of U, Cs and Sr radioisotopes by them unfolds their salient anti-pollution potential for soil and subwater ecosystems.

Keywords: Na-birnessites, Sr-, Ba-buserites, one- and two-dimensional layers, porous media, adsorption/desorption properties, ion exchange capacity, heavy metal cation trap

1. Introduction

The history of the name birnessite derives from the region called Birness, from where Jones and Milne reported at first on this material [1]. It importance is related to the its manganese content which classify it as the main Mn-containing phase in soil, marine and nodules [1, 2]. Beyond this fact, what makes this mineral important is its characteristic two dimensional layered structure built of edge- and corner-sharing MnO_6 octahedral sheets separated by a single water molecule layer and random cations [4,5]. The latter cause a spacing varying from 7-7.1 Å [5]. Upon further hydrating at certain conditions they convert reversibly to buserites which have a similar structure but consist of two single molecule water layers enlarging the interlayer space around 10 Å [4,6,7]. Since water is loosely bound to the buserite structure, it can be lost easily upon drying yielding back birnessites [4,6,7]. This inter-conversion is of great importance for various topics and especially for manganese distribution in the nature. The special structure of birnessite and buserite bears several unusual properties such as pronounced adsorptive properties and ion exchanging [8-13]. In spite of the industrial applications of the latter [14-16, 17-20] deriving from this property, increasing interest is paid for their application as anticontamintats

[10,12,21,22] in the environmental remediation. Numerous studies have unveiled their adsorbing/exchanging capacities of various alkaline metal cations [7,10,8,24], transition metals cations [9,11,13,22,23] or even hazardous nuclear wastes containing uranium cations [5]. Due to the importance of these materials and their continuously reevaluation, this study aims to shed light on the structural and adsorptive properties of Na-birnessite and emphasise their cation sorptive/exchanging properties.

2. Results and Discussion

2.1 Structure of birnessites and buserites

Golden et al. were the first to report on the layered structure of birnessites. They found the chemical formula $Na_4Mn_{14}O_{27}*9H_2O$ for the synthetic Na-birnessites classifying it to the orthorhombic crystal system. The structure of Na-birnessite consisted of two-dimensional sheets of edge-shared MnO_6 octahedra, spaced at 7 Å and occupied by Mn^{3+}/Mn^{4+} species. This distance between layers could accommodate a single layer water molecules and exchangeable Na ions [6]. Latter studies of Le Goff et al. on Na-birnessites and buserites based on infrared and absorption spectroscopy investigations reported the chemical formula $Na0._{32}MnO_2*0.67H_2O$ for the dried Na-birnessite. Although the oxidation state of manganese is represented as 4, according to them it was merely 3.68 [4]. They could classify the Na-birnessite lamellar structure in the monoclinic space group of C2/m with Na ions and water molecules occupying the prismatic holes formed between the octahedral layers with a typical interlayer distance of 7.1. This interlayer distance reported by them was in full accordance to the previous investigations of Post and Veblen which determined the crystal structure of synthetic sodium, magnesium and potassium, birnessite using TEM and the Rietveld method [25]. Upon drying, Na-birnesites lose their single water molecule layer which leads to a decrease of the interlayer spacing of 5.6 Å [7]. Buserites in comparison to birnessites have a greater interlayer spacing of 9.3-10 Å [7], and contain double-water molecule layers between the two-dimensional edge-shared MnO_6 octahedral layers. They easily lose one water layer transforming to the respective stable Na-birnessites [4,7]. This transformation is interlaced with an interlayer shifting of approx. 0.3 Å. Due to the ability to maintain or lose the second water layer they are classified to unstable and stable buserites [7]. Buserites which lose reversibly one layer of water molecules upon drying and regain it upon stirring in water represent the unstable ones. Luo et al. showed that this process is strongly dependent on the preparation method and proposed a double aging method for the synthesis of stable Na-buserites at ambient conditions for longer times [7]. A schematic which summarizes all is described above on the reversible transformation dry-birnessite--birnessite-buserite is exhibited in fig. 1.

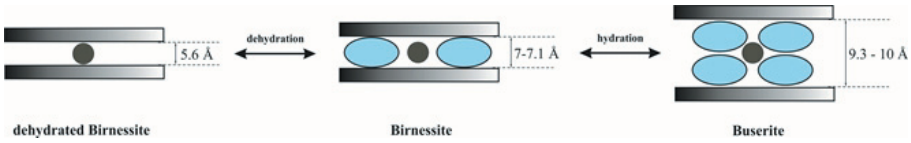

Figure 1: The reversible conversion of birnessite to dehydrated birnessite (left) and buserite (right). The top and bottom layers represent edge-sharing MnO_6 octahedra. The given distances between octahedral layers are based on the literatures [4,5,7].

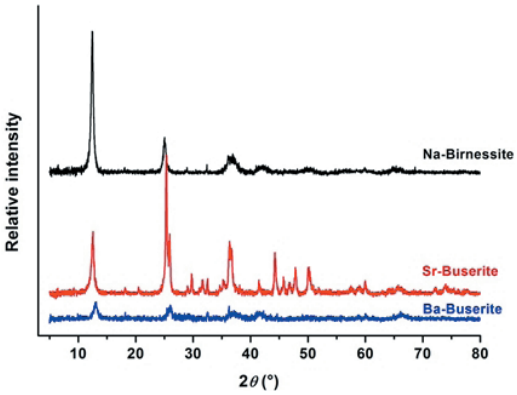

Figure 2: Measured XRD powder patterns of Na-birnessites, Sr- and Ba- busserites.

The measured diffraction pattern of Na-birnessites (Fig. 2) shows a good match with the pattern published by Prieto & Rives [26], which indexed and refined it in the monoclinic system with the lattice constants $a_0 = 5.039$ Å, $b_0 = 2.822$ Å, $c_0 = 7.366$ Å, $\beta = 103$ º. Indeed, literature data unveils that in most cases Na-birnessites crystallize in the monoclinic crystal system [4,27,28]. As reported by them, this is due to the high polarizing effect of the alkali cations (Li^+, Na^+, K^+) toward the water molecules which constrain the layered structure to maintain the monoclinic symmetry. The measured sample of Sr-buserite revealed a good crystallinity as shown by the powder pattern of fig. 2. In opposite to it, the powder pattern of Ba-buserite resembled more to XRD pattern of a nano-crystalline sample. Both diffraction patterns of measured buserites (Fig. 2) matched well to the measured pattern of Na-birnessites, especially for the position of the main reflections. This similarity to the diffraction pattern of Na-birnessites is due to the instability of Sr- and Ba-buserites at ambient conditions for long times as reported by Luo [7]. He found that Ba-buserite change direcly to Ba--birnessite upon drying, meanwhile Sr-buserite can retain the buserite structure up to 1 h after drying. For the latter, this conversion occurs gradually and partially. This fact explains the presence of some buserite structure reflections with low relative intensities, in the measured powder pattern of Sr-buserites.

2.2 Porosity and BET surface area

N_2 sorptiometric measurements were taken to determine the porosity and BET surface area of Na-birnessite, Sr- and Ba-buserite. The adsorption isotherms and the respective differential pore distributions are plotted in fig. 3. At the first glance, the adsorption isotherms of Na-birnessite (Fig 3a) and Ba-buserite (Fig. 3e) are characterized by a similar initial and maximal N_2 adsorption volume. Anyway, a close observation of the adsorption data unveils a light advantage of the initial and final adsorption volumes of Ba-buserite (13.32 cm^3/g vs. 15.91 cm^3/g) and (135.27 cm^3/g vs. 157.71 cm^3/g) making a difference in the adsorption volumes of approx. 20 cm^3/g.

Sr-buserites showed a poorer adsorption behavior in comparison to Na-birnessites and Ba-buserites. Its initial and final adsorption volumes consisted merely of 8.73 cm^3/g and 94.67 cm^3/g. The differential pore distributions of the measured samples (Fig. 3b,d,f) displayed the presence of the microporosity in all of them and an overall external porosity increasing in the order Sr-buserite < Na-birnessite < Ba-buserite. Since the N_2 kinetic molecule diameter is 3.64 Å [29] the N_2 molecule stericity impedes its entrance and accommodation in the free space between the interlayers, which in the case of Na-buserite in dried form is reported 1.94 Å. The BET specific surface area for these three samples was measured by this adsorbate and is shown in fig. 4. As expected and in full accordance to the adsorption isotherms and differential pore distributions, Ba-buserite shows the highest specific area 93.64 m^2/g followed by Na-birnessite with 75.57 m^2/g and Sr-buserite 49.16 m^2/g. Indeed, the determined BET specific surface area of Na-birnessites was slightly above the maximal border value of 72 m^2/g reported by Wong and Cheng [21] and much higher than the literature values [26,30]. To overcome the difficulty of the proper determination of the sample porosity due to the inaccessibility of N_2 entering the inlayer space of these materials, complementary

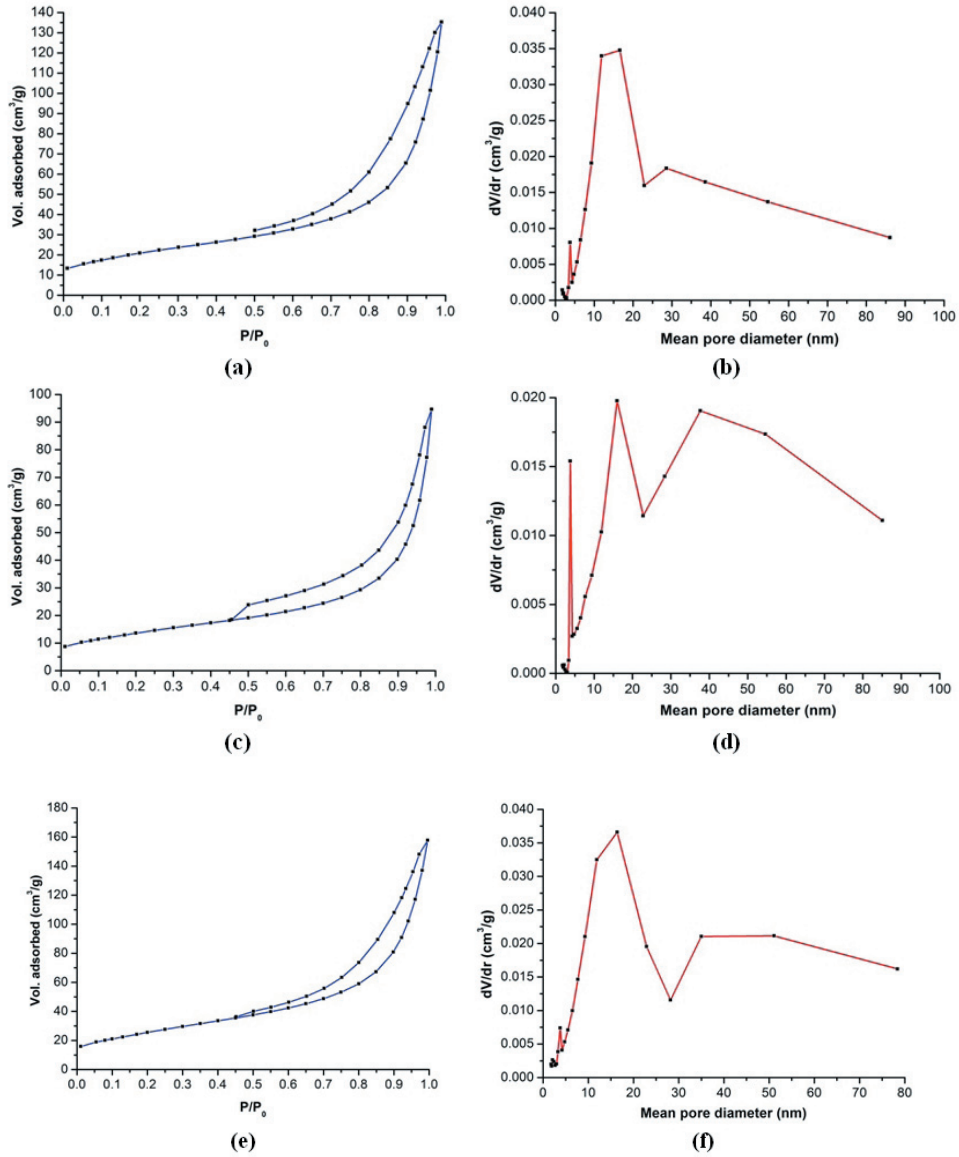

Figure 3: Adsorption desorption hysteresis of: (a) Na-birnessite, (c) Sr-buserite and (e) Ba-buserite; differential pore distribution of: (b) Na-birnessite, (d) Sr-buserite and (f) Ba-buserite.

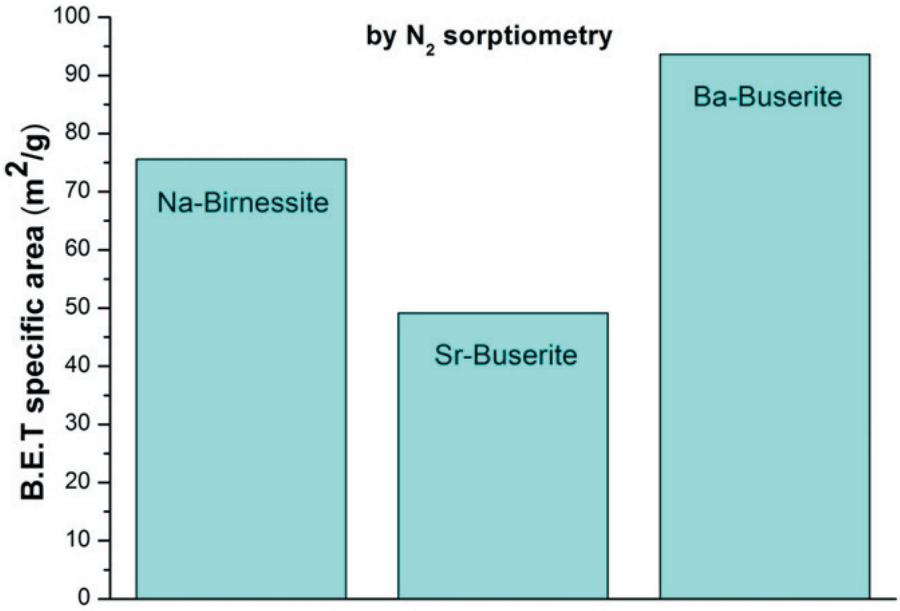

Figure 4: BET surface area of Na-birnessites, Sr- and Ba-buserites determined by N_2 sorptiometry.

Ar-sorptiometric measurements were taken for the samples of Na-birnessite and Ba-buserite. Ar atoms have a smaller kinetic diameter 3.4 [21] and hence can better access the pores. The Ar-adsorption isotherms of both samples were recorded for a relative pressure of 0.05 (Fig. 5a). The recorded Ar-adsorption isotherms exhibit slightly lower initial adsorption volumes compared to the N_2 adsorption data. Again Ba-buserite shows the highest adsorption volume of 17 cm^3/g, compared to 14 cm^3/g for Na-birnessite.

The differential pore distribution calculated according to the Horvath-Kawazoe equation (Fig. 5b) for both samples reveals the main pore distribution with mean diameters varying from 0.3 to 1.2 nm, and the maximum value at 7 Å. This is the most reported value of the interlayer distance in birnessites. This fact reinforces the conclusion regarding the instability of the Sr- and Ba-buserites at ambient conditions and emphasizes their partial or total conversion into the respective birnessites. These measurements also endorse the fact that the exchange of Na^+ with Ba^{2+} increases the porosity in the birnessite structure.

Complementary BET specific area determination based on Ar-sorptiometric measurements of Na-birnessite and Ba-buserite samples (Fig. 6) exhibited a larger BET specific area of the latter (60 vs. 64 m^2/g). Anyway these values are lower in comparison to the BET values reported above for the N_2-sorptric data and slightly above the value 55 m^2/g reported for Na-birnessite by Wong and Cheng [21]. The discrepancy between the BET surface area determined by N_2-sorptiometry and Ar-sorptiometry occurs due to the difference between the shapes of N_2 molecule and Ar atom, their polarisabilities and their surface packing behavior. Na-birnessite showed reveals a larger BET specific surface area compared to its external surface (60 m^2/g vs 57 m^2/g). The opposite was observed for Ba-buserites which showed a larger external surface area instead (64 m^2/g vs. 69 m^2/g).

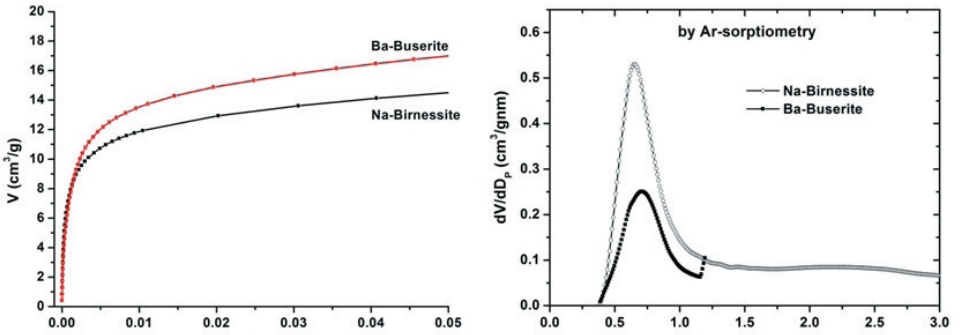

Figure 5: (a) Ar-adsorption isotherms of Na-birnessite and Ba-Buserite, (b) differential pore distribution of the samples of Na-birnessite and Ba-Buserite determined by Ar-sorptiometry.

The BET surface area determined for Ba-buserites is inferior in comparison to the approximate value 200 m^2/g reported by Jeffries and Stumm [8]. This indicates that the product obtained and reported in this study, claimed as Ba-buserite was probably an intermediate of Na-birnessite and Ba-buserite. This conclusion is fully endorsed by the finding of Luo et al. who reported the same while exchanging of Na with Ba in instable Na-buserite [7].

2.3 Cation exchanging and environmental protection

2.3.1 The role of birnessites

The physical properties of the nonstoichiometric manganese oxides, i.e. birnessites and buserites have a considerable effect on their adsorption properties. Although we didn't performed yet cationic adsorption studies with the synthesized materials, there is plenty of information in the literature reporting on the cationic adsorption/exchanging properties of birnessites and buserites. At one hand the cation adsorption in such layered materials occurs in the space between the octahedral layers. At the other hand, the cation exchanging process in them with the environmental cations occurs in two levels, namely a) exchanging with the cations situated between the octahedral layers, which is the quite frequent for most of them, b) exchanging with the manganese cations, occupying octahedral holes. The cation exchanging in birnessites and buserites has a considerable contribution in the environmental remedy. Rives, Arco and Prieto [10] reported on a partial cation exchange of Na- and K- containing birnessites when they were introduced to solutions containing Li^+, Mg^{2+} and Cu^{2+}. The reported exchanging order was $L^+ > Mg^{2+} > Cu^{2+}$. Since the cation exchange occurred between the interlayers ones and those introduced by the environment, it wasn't associated with the change of the interlayers spacing in them. Feng et al [11] found L-type adsorption isotherms of heavy metals from the aqueous environment. The adsorption was concentration dependent and increased sharply when the equilibrium concentration of the heavy metals was increased. From all the tested manganese oxides type structures, they reported on the enhanced adsorbing properties of birnessites toward Pb^{2+}, Cu^{2+} Zn^{2+}, Co^{2+} and Cd^{2+}. Lead was adsorbed the most followed by the others according to the given sequence. They also proposed that the cation adsorption process occurred in their hydroxylation form where the adsorbed amount was proportional to the respective hydrolysis constants. Table 1 exhibits the reported maximal adsorbed values for the mentioned cations.

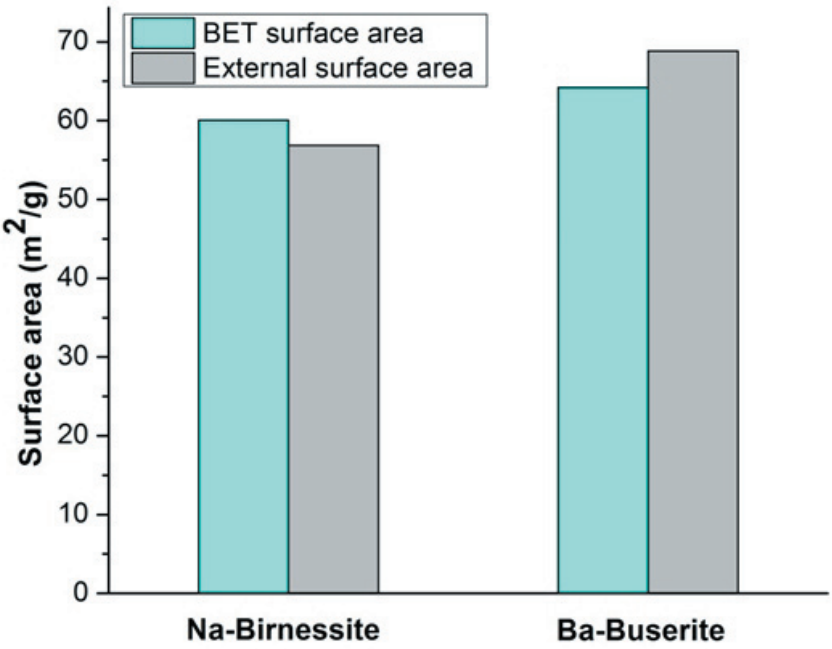

Figure 6: BET and external surface area of Na-birnessites, Sr- and Ba-buserites determined by Ar sorptiometry.

Adsorbing material	Maximal adsorption values of some heavy metals (mmol/kg)				
	Pb (0.396 nm)*	Co (0.35 nm)*	Cu (0.349 nm)*	Cd (0.371 nm)*	Zn (0.35 nm)*
Birnessite	148	189	190	168	189

Table 1: Maximal adsorption values of five heavy metals by birnessite [11].

The radius of the hydrated ion was calculated $r_{ion} + 2r_{H2O}$, rion was reported by Shannon [31]

Similar studies performed by McKenzie and Tebo et al. [9,23] in this field, revealed increased adsorption/exchanging capacities of birnesites toward the cationic species as follows $Pb^{2+} > Cu^{2+} > Co^{2+} > Ni^{2+} > Zn^{2+} > Mn^{2+} > Ca^{2+} > Mg^{2+}$. Manganese oxidation state plays the most important role in this sequence followed by the distributions of the cations in the layers and interlayers respectively [13,22]. Meanwhile, Villalobos et al. [32] found that the adsorption/exchanging capacity for Pb^{2+} among others was dependent on the birnessite specific area. According to Wong et al. [21] the great sorption capacity of Pb^{2+} in comparison to the other heavy metals is interlaced with its ability to occupy interlayer space in birnessite and their surface edge sites. All the adsorption/exchanging processes involving greater ions than the present ones are associated by the enlargement of the interlayer distance and birnessite cell distortion. Al-Attar and Dyer [5] reported increases of b-dimension in birnessite cell due to high uranium sorption

on Li-, Cs- and Ba-birnessites. Since the process is pH dependent, the best distribution coefficients values reported for Li- and Ca-birnessites in deionised water 2.71 x 106 and 1.67 x 106 ml/g respectively were achieve at pH = 6. In contrast to them, transition metal birnessites showed low adsorption/exchange values ranging between 34–184 ml/g.

Despite of the above distinctive exchanging properties between interlayer situated cations and the environmental ones, as mentioned previously, birnessites take part also to the cation exchanging between $Mn^{3+}/^{4+}$ occupying the octahedral holes and the environmental ones. In such process Mn plays the role of the oxidation agent. Feng et al. reported on the considerable amounts of Cr^{3+} adsorbed on birnessite reaching up to (1330.0 mmol/kg). The adsorption of Cr^{3+} occurring of at the interface induced new equilibria between it and Mn, leading to its further oxidation to Cr^{6+}. Due to the surface characteristics, once Cr^{6+} was formed it desorbed back from the birnessite surface into the solution. This process attributes to birnesites environmental remediation properties since Cr^{6+} is less toxic than Cr^{3+} [11]. Dias et al. [12] proved a similar behavior of synthetic birnessites toward As^{3+}. The contact of As^{3+} with the birnessite surface caused its direct oxidation to As^{5+} and the consequent reduction of Mn^{4+} to Mn^{3+} and Mn^{2+}. The maximal As^{3+} adsorption level reported by them was approx. 20 mg As/g.

2.3.2 The role of buserites

Similar to birnessites, busserites as their derivatives or precursors possess ion adsorption/exchange properties. Murray et al. [24] were the first to report on the adsorption/exchange of Ni^{2+}, Cu^{2+}, Co^{2+} Ca^{2+} at high concentrations from buserites. Jeffries and Stumm [8] reported later on the adsorption of two valent ions of Ca^{2+}, Zn^{2+} and Cu^{2+} from their aqueous solutions. At a pH values varying from 2-7 they found the following buserite adsorption sequence: $Ca^{2+} < Zn^{2+} < Cu^{2+}$. At normal pH values ranging from 6-8 buserites show enhanced adsorption capacities, decreasing considerably their concentrations in see waters. They also stressed the fact of the complicity of the heavy metal adsorption process regarding the released hydrogen ions from the surface. Later studies of Luo et al. [7] unveil the feasibility of obtaining stable buserites of Mg^{2+}, Ca^{2+}, and Sr^{2+} from Na-buserite. They demonstrated also the formation of stable buserites from the treatment of unstable Na-buserite with some transition metal cations, such as Mg^{2+}, Cu^{2+}, Zn^{2+}, Ni^{2+}, Co^{2+}, and Mn^{2+}.All these latter buserites formed, although considered stable at ambient conditions, upon heating they displayed higher instability in comparison to Mg-busserites. The latter were obtained very quick due to ion exchange from the unstable buserite. Different from all of these, the exchange of Na with Ba led to the formation of an intermediate product between birnessite and busserite. All of this cationic adsorption exchanges similar to birnessites were related with significantly increased interlayer spacing.

3. Experimental Section

We reported in this study the synthesis of Na--birnessite and the attempt of the synthesis of Sr- and Ba-buserites. The synthesized samples revealed significant differences in their XRD powder patterns. The XRD pattern of the Na--birnessites matched well with the literature reported pattern, assigning it hence to the monoclinic system. The claimed Sr- and Ba-buserite patterns displayed also close similarities with reported ones. The N_2 adsorption measurements unveiled the presence of micropores in all samples. The overall external porosity of them increased in the order Sr-buserite < Na-birnessite < Ba-buserite. Ba-buserite shows the highest specific area 93.64 m^2/g followed by Na-birnessite with 75.57 m^2/g and Sr-buserite 49.16 m^2/g. The complementary Ar-sorptiometric measurements for Na-birnessite and Ba-buserite recorded for a relative pressure of 0.05 exhibited slightly lower initial adsorption volumes compared to the N_2 adsorption data. Ba-buserite showed the highest adsorption volume of 17 cm^3/g, compared to 14 cm^3/g for Na-birnessite. A mean diameter of 7 Å obtained by the differential pore distribution calculated according to the Horvath-Kawazoe equation reinforced the conclusion regarding the instability of the Sr- and Ba-buserites at ambient

conditions and emphasized their partial or total conversion into the respective birnessites. Complementary BET specific area determination based on Ar-sorptiometric measurements showed a higher specific area in the case of Ba-birnessite compared to Na-birnessite. The latter, show a higher specific aree compared to the external surface, meanwhile the opposite was observed for Ba-buserite. The BET surface area determined for Ba-buserites was inferior in comparison to the one indicated in the literature concluding that the claimed as Ba-buserite was probably an intermediate of Na-birnessite and Ba-buserite. The adsorptive/exchanging properties of birnessites and buserites toward alkali- and transition heavy metal cations, for the remedy of the environment from their contamination are emphasized.

4. Conclusions

We reported in this study the synthesis of Na--birnessite and the attempt of the synthesis of Sr- and Ba-buserites. The synthesized samples revealed significant differences in their XRD powder patterns. The XRD pattern of the Na--birnessites matched well with the literature reported pattern, assigning it hence to the monoclinic system. The claimed Sr- and Ba-buserite patterns displayed also close similarities with reported ones. The N_2 adsorption measurements unveiled the presence of micropores in all samples. The overall external porosity of them increased in the order Sr-buserite < Na-birnessite < Ba-buserite. Ba-buserite shows the highest specific area 93.64 m^2/g followed by Na-birnessite with 75.57 m^2/g and Sr-buserite 49.16 m^2/g. The complementary Ar-sorptiometric measurements for Na-birnessite and Ba-buserite recorded for a relative pressure of 0.05 exhibited slightly lower initial adsorption volumes compared to the N_2 adsorption data. Ba-buserite showed the highest adsorption volume of 17 cm^3/g, compared to 14 cm^3/g for Na-birnessite. A mean diameter of 7 Å obtained by the differential pore distribution calculated according to the Horvath-Kawazoe equation reinforced the conclusion regarding the instability of the Sr- and Ba-buserites at ambient conditions and emphasized their partial or total conversion into the respective birnessites. Complementary BET specific area determination based on Ar-sorptiometric measurements showed a higher specific area in the case of Ba-birnessite compared to Na-birnessite. The latter show a higher specific surface compared to the external one, meanwhile the opposite was observed for Ba-buserite. The BET surface area determined for Ba-buserites was inferior in comparison to the one indicated in the literature concluding that the claimed as Ba-buserite was probably an intermediate of Na-birnessite and Ba-buserite. The adsorptive/exchanging properties of birnessites and buserites toward alkali- and transition heavy metal cations, for the remedy of the environment from their contamination are emphasized.

Acknowledgments

The financial support from Metallomic Scientific Network V4MSNet (project 11440027) is greatly acknowledged.

Conflicts of Interest

The authors declare they have no potential conflicts of interests concerning drugs, products,services or another research outputs in this study. The Editorial Board declares that the manuscript met the ICMJE „uniform reguirements“ for biomedical papers.

References

1. Jones, L. H. P., Milne, A. A. Mineral. Birnessite, a new manganese oxide mineral from Aberdeenshire, Scotland. Mineral. Mag., 1956, 31, 283-288.
2. Bricker, O. Some stability relations in system Mn-O2-H2O at 25 ºC and 1 atmosphere total pressure. Am. Mineral., 1965, 50, 1296-1354.
3. Giovanoli, R.; Burki, P. Comparison of X-ray evidence of marine manganese nodules and non-marine manganese ore deposits. Chimia, 1975, 29, 266-269.
4. Le Goff, P., Baffler, N., Bach, S., Pereira-Ramos, J. P. Synthesis, ion exchange and electrochemical properties of lamellar phyllomanganates of the birnessite group. Mat. Res. Bul., 1996, 31(1), 63-75.
5. Al-Attar, L., Dyer, A. Sorption behaviour of uranium on birnessite, a layered manganese oxide. J. Mater. Chem., 2002, 12, 1381-1386.
6. Golden, D. C., Chen C. C., Dixon, J. B. Transformation of birnessite to buserite, todorokite, and manganite under mild

hydrothermal treatment. Clays Clay Miner., 1987, 35(4), 271-280.
7. Luo, J., Zhang, Q., Huang, A., Giraldo, O., Suib, S. L. Double-Aging Method for Preparation of Stabilized Na-Buserite and Transformations to Todorokites Incorporated with Various Metals. Inorg. Chem., 1999, 38, 6106-6113.
8. Jeffries, D. S., Stumm, W. The metal-adsorption chemistry of buserite. Can.Mineral., 1976, 14, 16-22.
9. Mc Kenzie, R.M. The adsorption of lead and other heavy metals on oxides of manganese and iron. Aust. J. Soil Res., 1980, 18, 61-73.
10. Rives, V., Del Arco, M., Prieto, O. Birnesitas obtenidas mediante cambio iónico. Evolución estructural con la calcinación. (Birnessites obtained through ionic exchange. Structural evolution with the calcination). Bol. Soc. Esp. Ceram. V., 2004, 43(2), 142-147.
11. Feng, X. H., Zhai, L. M., Tan, W. F., Liu, F., He, J. Z. Adsorption and redox reactions of heavy metals on synthesized Mn oxide minerals. Environ Pollut., 2007, 147(2), 366-73.
12. Dias, A., Sá, R. G., Spitale, M. C., Athayde, M., Ciminelli, V. S.T. Microwave-hydrothermal synthesis of nanostructured Na-birnessites and phase transformation by arsenic(III) oxidation. Mat. Res. Bul., 2008, 43, 1528-1538.
13. Zhao, W., Wang, Q.Q., Liu, F. Pb2+ adsorption on birnessite affected by Zn2+ and Mn2+ pretreatments. J. Soils Sediment., 2010, 10, 870-878.
14. Pereira-Ramos, J. P., Badour, R., Bach, S., Baffier, N. Electrochemical and structural characteristics of some lithium intercalation materials synthesized via a sol-gel process: V2O5 and manganese dioxides-based compounds. Solid State Ionics, 1992, 701, 3-56.
15. Bach, S., Pereira-Ramos, J. P., Baffier, N. Electrochemical sodium insertion into the sol-gel birnessite manganese dioxide. Electrochim. Acta, 1993, 38, 1695-1700.
16. Bach, S., Pereira-Ramos, J. P., Baffier, N. Synthesis and Characterization of Lamellar MnO2 Obtained from Thermal Decomposition of NaMnO4 for Rechargeable Lithium Cells. J. Solid State Chem., 1995, 120, 70-73.
17. Shen, Y. F., Zerger, R. P., DeGuzman, R. N., Suib, S. L., McCurdy, L., Potter, D. I.; O'Young, C. L. Manganese oxide octahedral molecular sieves: preparation, characterization, and applications. J. Chem. Soc., Chem. Commun., 1992, 1213-1214.
18. Jiang, S. P., Ashton, W. R., Tseung, A. C. C. An observation of homogeneous and heterogeneous catalysis processes in the decomposition of H2O2 over MnO2 and Mn(OH)2. J. Catal., 1991, 131, 88-94.
19. Nitta, M. Characteristics of manganese nodules as adsorbents and catalysts, a review. Appl. Catal., 1984, 19, 151-176.
20. Yin, Y. G., Xu, W. Q., Shen, Y. F., Suib, L. S. Studies of Oxygen Species in Synthetic Todorokite-like Manganese Oxide Octahedral Molecular Sieves. Chem. Mater., 1994, 6(10), 1803-1808.
21. Wong, S.-T., Cheng, S. Synthesis and Characterization of Pillared Buserite. Inorg. Chem., 1992, 31, 1165-1172.
22. Gaillot, A.C., Drits, V.A., Manceau, A., Lanson, B. Structure of the synthetic K-rich phyllomanganate birnessite obtained by high-temperature decomposition of KMnO4: substructures of K-rich birnessite from 1000 ºC experiment. Micropor. Mesopor. Mat., 2007, 98, 267-282.
23. Tebo, B.M., Bargar, J.R., Clement, B.G., Dick, G.J., Murray, K.J., Parker, D., Verity, R., Webb, S.M. Biogenic manganese oxides: properties and mechanisms of formation. Annu. Rev. Earth Planet. Sci., 2004, 32, 287-328.
24. Murray, D. J., Healey T. W., Fuerstenau, D. W. The adsorption of aqueous metal on colloidal hydrous manganese oxide. In Advances in Chemistry, Series 79, Adsorption from Aqueous Solution. Amer. Chem. Soc., 1968, 74-81.
25. Post, J. E., Veblen, D. R. Crystal-structure determinations of synthetic sodium, magnesium, and potassium birnessite using TEM and the Rietveld method. Am. Miner., 1990, 75, 477.
26. Prieto, O., Rives, V. Preparation and characterization of nonstoichiometric manganese oxides. Bol. Soc. Esp. Cerám. Vidrio, 2000, 39(3), 233-238.
27. Brock, S. L., Duan, N., Tian, Z. R., Giraldo, O., Zhou H., Suib. S. L. A review of porous manganese oxide materials. Chem. Mater., 1998, 10, 2619-2628.
28. K. Kuma, A. Usui, W. Palawsky, B. Gedulin y G. Arrhenius. "Crystal structure of synthetic 7 Å and 10 Å manganates substituted by mono- and divalent cations". Miner. Mag., 1994, 58, 425-447.
29. Breck, D. W. Zeolite Molecular Sieves; Wiley: New York, 1973, pp 636.
30. Cornell, R. M., Giovanoli, R. Transformation of hausmannite into birnessite in alkaline media. Clays Clay Miner., 1988, 36(3), 249-257.
31. Shannon, R. D. Revised Effective Ionic Radii and Systematic Studies of Interatomic Distances in Halides and Chalcogenides. Acta Cryst., 1976, A32, 751-767.
32. Villalobos, M., Bargar, J., Sposito, G., Mechanisms of Pb(II) sorption on a biogenic manganese oxide. Environ. Sci. & Technol., 2005, 39, 569-576.

The article is freely distributed under license Creative Commons (BY-NC-ND). But you must include the author and the document can not be modified and used for commercial purposes.

Immunohistochemical detection of metallothionein

Gabriella Emri[1*], Eszter Emri[1], Livia Beke[2], Gábor Boros[1], Csaba Hegedűs[1], Eszter Janka[1], Emese Gellén[1], Gábor Méhes[2] and Éva Remenyik[1]

[1] Department of Dermatology, Faculty of Medicine, University of Debrecen, Nagyerdei krt. 98, H-4032 Debrecen, Hungary – European Union; E-Mails: emeszti@gmail.com; borosgabor27@gmail.com; hegeduscsaba88@gmail.com; janka.eszter.a@gmail.com; emesegellen@med.unideb.hu; remenyik@med.unideb.hu

[2] Institute of Pathology, Faculty of Medicine, University of Debrecen, Nagyerdei krt. 98, H-4032 Debrecen, Hungary – European Union; E-Mails: beke.livia@gmail.com; mehes.gabor@med.unideb.hu;

* Author to whom correspondence should be addressed; E-Mail: gemri@med.unideb.hu;
Tel.: +36-52-255-602; Fax: +36-52-255-736.

Received:10.8.2015 / Accepted:27.8.2015 / Published: 1.10.2015

All human tissues consist of a wide variety of cells that have an impact on each other. Human diseases that are caused by genetic alterations and/or environmental factors can be characterized by morphological and functional changes in tissues. Both aspects are important to better understand the pathomechanism of a disease and to find new therapeutic targets. Immunohistochemistry identifies the expression, intracellular localization as well as tissue distribution of various proteins, while morphology of tissue can also be assessed precisely. It is used for routine diagnostics as well as for research. However, antigen specific assay standardization and the use of appropriate positive and negative tissue controls are very important to interpret the findings in a way that ensures the biological relevance. Abnormal metallothionein function and expression have been implicated in various human diseases, including cancer. Immunohistochemistry provides an excellent opportunity to gain an insight into the role of MT in the pathogenesis of diseases.

Keywords: metallothionein antibodies; metallothionein tissue expression; immunohistochemistry

1. Introduction

Zinc (Zn (II)) is an essential microelement, it has critical role in normal health and development [1]. Binding of Zn (II) to zinc coordination motifs in proteins stabilizes the structure or influences the function. The prevalence of genes encoding zinc proteins is estimated to be over 3% of the 32,000 identified genes. Over 300 Zn (II)-dependent enzymes have been defined and characterized [2]. It has been shown that Zn (II) can regulate the DNA-binding activity of zinc finger transcription factors [3]. The Zn (II)-metallothionein (MT)/thionein pair, which is an important component of cellular Zn (II) homeostasis, is critical to sequester or release Zn(II) depending on the local redox state, thereby influencing the function of numerous enzymes and transcription factors that control cell proliferation, apoptosis and signalling pathways [4,5]. Abnormal MT function and expression have been implicated in various human diseases, including cancer [6]. There are at least 10 isoforms of MT in human body, which are expressed in a tissue specific pattern and may play distinct roles in the various cell types. MT-I and MT-II isoforms are present in all cells throughout the body, MT-III was first isolated as a growth inhibiting factor (GIF) from brain neurons, MT-IV is located in stratified epithelium [6]. Transcription of MT-I and MT-II can be induced by inflammatory cytokines (IL-6, TNF-α, interferons), lipopolysaccharids, glucocorticoids, free radicals, antioxidants or

heavy metals. MT is a cytosolic protein in resting cells, but it can be translocated transiently to the cell nucleus during cell proliferation and differentiation [7].

Immunohistochemistry (IHC) identifies the expression, intracellular localization as well as tissue distribution of various proteins, while morphology of tissue can also be assessed precisely [8]. IHC detection of MT in tissue samples is a very important option to study its role in the pathogenesis of diseases. Special IHC methods such as multiple immunolabeling using serial sections of tissue blocks or double staining technique provide an opportunity to study correlations between MT expression and important cell and tissue functions [9]. Tissue microarray allows simultaneous examination of large number of tissues on a single microscope slide; therefore it is very suitable to evaluate the diagnostic, prognostic or predictive role of the MT expression [9].

2.Immunohistochemical detection of metallothionein

The IHC technique is a combination of immunologic and chemical reactions visualized with a photonic microscope [8]. It can be divided in pre-analytical, analytical and post-analytical phases. It starts with tissue fixation, embedding, and tissue sectioning, followed by deparaffinization, antigen retrieval, blocking of non-specific activities, incubation with the primary antibody, and labeling of the antigen-antibody reaction, and ends with slide counterstaining, coverslipping and evaluation (Figure 1.). Most commonly, formalin-fixation and paraffin-embedding (FFPE) is used for its ability to preserve tissue indefinitely for morphologic examination [8,10]. Heat-induced epitope retrieval was proved to restore the immunoreactivity of tissues fixed in formalin [8]

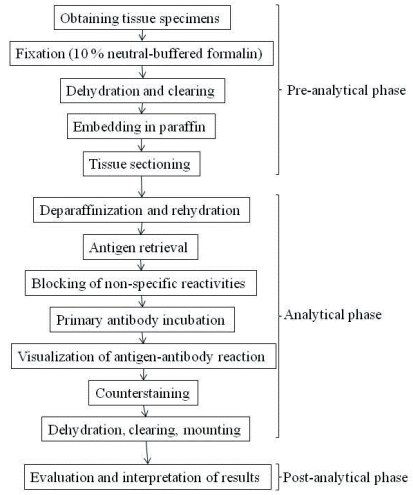

Figure 1: Outline of standard immunohistochemical protocol [8,11,12].

2.1 Pre-analytical phase of immunohistochemistry

The aim of fixation is to maintain morphological features and to preserve tissue suitable for a range of staining and IHC [11]. Adequate tissue fixation is very important to stabilize proteins and prevent tissue decay. Tissue fixation may be accomplished by physical (freeze) and/or chemical (coagulative and cross-linking) methods. For IHC purposes, the fixative of choice is a 10% neutral-buffered formalin solution. The specimen should be placed in fixative immediately after it is removed from the patient. The volume of formalin should be 10 to 20 times the volume of specimen. Delayed, too short or too long fixation can lead to false IHC results [8]. Formaldehyde penetrates the tissue very quickly, but fixes it very slowly; 16-24 h fixation time is required for a tissue specimen of 1-4 mm in diameter. Large specimens should be cut into slices 4 to 5 mm thick for further fixation [11].

Tissue processing refers to a series of steps that include removal of the extractable water and lipids from the tissue, usually in an automated manner, then infiltration and embedding in a support matrix (paraffin) so that the tissue can be stabilized and cut easily [11]. The specimens are cut on a rotary microtome into sections 3 to 5 μm thick. Sections that will be used for IHC

should be mounted on glass slides specially coated or charged to ensure better adherence [11]. Long-term storage of tissue sections is not recommended, because photo-oxidation of sections results in loss of antigenicity [8]. Detection of certain antigens has the limitation of requiring fresh tissue. In this case the specimen is obtained fresh and kept moist until it is oriented and embedded in optimal cutting temperature (OCT) compound, then the specimen is snap frozen [11]. The tissue is then sectioned at 6 µm. Occasionally, special tissue processing (e.g., decalcification, demelanization) is required prior to the immunostaining, but epitopes can be destroyed by an aggressive procedure [8]. The standard of protocol for tissue fixation and processing must be developed for each antigens and tissue type. It is worth to highlight that pre-analytical factors influence the success of a subsequent nucleic acid analysis as well [10].

2.2 Analytical phase of immunohistochemistry

Tissue sections mounted on coated or charged glass slides are deparaffinized and rehydrated before antigen retrieval (AR). Incomplete deparaffinization causes suboptimal or incomplete staining because of incomplete tissue penetration by the antibody [12]. Heat- and/or protease--induced AR is a procedure which reverses the structural changes induced by the fixation and tissue processing [8]. AR techniques are critical for antigen unmasking, optimal results require control of the pH and temperature of retrieval solutions and controlled enzymatic digestion [12]. The mechanism of heat to restore the immunoreactivity of formalin-fixed tissues is not completely clear, the dissociation of irrelevant proteins from target peptides, hydrolysis of methylene cross-links, restoring the native electrostatic charges, mobilization of trace paraffin etc. can be involved [8]. Enzymatic treatment is optimal only for few antigens and can alter tissue morphology or destroy epitopes [8].

Antigen epitopes consist of 5-6 amino acid residues, and are classified as linear or conformational [8]. Antigens may consist of multiple identical or distinct epitopes. Antigen-antibody binding involves hydrophobic, van der Waals, and electrostatic interactions. The best diluents buffer for primary antibody is 0.05 to 0.1 M Tris buffer (pH 6.0) [8]. Background reactivity due to ionic interactions can be reduced by increasing the NaCl concentration in the buffer, but it can reduce the antigen-antibody binding [8]. Detergents (e.g., Tween 20) are also used to facilitate antigen-antibody binding by solubilizing membrane proteins; they are usually incorporated into dilution/rinse buffers [8]. Antibody concentrates and pre-diluted preparations must be optimized for usage at the correct dilution [12]. The affinity of an antibody for an antigen affects the sensitivity and specificity of an immunological reaction [8]. The overall binding intensity between antibodies and a multivalent antigen is described by avidity. Polyclonal antibodies usually have higher avidity, but lower specificity compared with monoclonal antibodies [8]. The high specificity, however, does not eliminate the possibility of cross-reactivity with other antigens, because the target epitopes can be part of multiple proteins and peptides.

The most frequent reason for the failure of IHC is the poor quality of the primary antibody used. However, nonspecific background staining, less than optimal specific staining, or no staining require a careful evaluation of all components involved in each step of the IHC technique [13].

2.2.1 Detection system

Primary (direct detection), secondary or tertiary (indirect detection) antibodies labelled with enzymes, metals or fluorescent compounds are used to visualize the antigen-antibody reaction [8,12]. The detection system must be compatible with the species tested. The most common label is the horseradish peroxidase, which produces a coloured precipitate at the site of the antigen--antibody reaction in the presence of its specific substrate and chromogens. Endogenous peroxidase activity has to be blocked before incubation with primary antibody. Chromogen entrapment, precipitation and contaminants may lead to false-positive interpretation of an IHC test [12]. Three-step techniques are more sensitive, e.g., the labelled streptavidin-biotin (LSAB) method, which is widely used. In this case, a biotinylated secondary antibody binds

to the primary antibody attached to the tissue antigen, and the biotinylated complex is detected by streptavidin that has been conjugated to the enzyme. Nevertheless, the endogenous biotin-associated background staining has led to increasing use of labelled polymer-based detection systems that are characterized by greater sensitivity, specificity, and suitable for manual and automated IHC platforms. Simultaneous or sequential multiple labelling using various detection systems can be used to localize different antigens in the same sections. Quantum dot labelling is a promising new tool for multispectral analysis [8].

Frozen sections can be more appropriate to examine the expression of certain proteins. In this case, immunofluorescence is used for detection of antigen-antibody reaction. Primary (or secondary) antibodies are linked to a fluorescent label such as fluorescein isothiocyanate to allow visualization using a fluorescence microscope [12]. Compared to frozen sections, paraffin-embedded tissues offer the advantage of better preservation of cellular details and permanency of the reaction [11].

2.3 Post-analytical phase of immunohistochemistry

Post-analytical phase of IHC includes assay standardization/validation, control performance, and interpretation of IHC results [8,14]. IHC assay standardization is important to obtain consistent and reproducible results within each laboratory and comparable results among laboratories [8]. Standardization is the process of optimizing the test method (reagents and protocols). Guidelines for antigen-, tissue- and species-specific standardization of IHC examinations should be based on currently available published evidence and modern understanding of quality assurance principles as applied to IHC in general [15]. Furthermore, diagnostic IHC laboratories must meet the ISO 15189 standards or standards of operation as defined by the Clinical Laboratory Improvement Amendments, respectively [16]. In non-accredited laboratories, IHC tests should be validated by documentation of internal and external quality assessments [17]. Use of quality controls is required for technical calibration and analytical validation [14]. Positive tissue control is defined as tissue that is known to contain the antigen of interest. Positive and negative tissue controls must be fixed and stained in the same way as the tested specimen [8]. Positive tissue control in the tested specimen is designated as internal positive tissue control, e.g., MT immunoreactivity in basal layer of normal epidermis (Figure 2.). Negative reagent controls are used to confirm the specificity of the test and to assess the degree of nonspecific background staining present by omitting the primary antibody [14]. Validation detects any cross-reactivity of the selected antibodies with unrelated antigens, and cross-reactivity among different tissues and among different species, examines the variables that affect the IHC reaction, such as fixation time and storage of unstained tissue sections, and may include comparison of results among different laboratories using similar techniques [8]. Whenever possible, validation compares the sensitivity of IHC detection to the gold standard method of detection for the Ag in question.

According to the Clinical and Laboratory Standards Institute suggestions, the IHC report should include the cellular location and tissue distribution of the tested antigen, semi-quantitative evaluation of the immunoreactivity, along with an interpretation of the test results [8,13-15]. The report should contain demographic information, the tissue that was tested, disease characteristics, and the antibody used. IHC scoring schemes are based on a subjective assessment of the labelling intensity and percent positive cells by a pathologist. Recently, it has been demonstrated that software algorithms are able to properly indicate the disease-relevant regions in digitized tissue images and quantify the area and optical density of positive staining [18,19]. Advantages of an automated digital IHC image analysis are that it is unbiased, precise in ranges of staining that appear weak to the eye, and produces continuous data [18].

2.4 Antibodies for metallothionein immunodetection

In mammals, four tandemly clustered MT genes are known [20]. In humans, MT-I has

undergone duplication events that have resulted in 13 duplicate isoforms, five of which have been predicted to be no active forms [20]. All genes encode for conserved peptide chains that retain 20 invariant metal-binding cysteines. A total of 9 and 11 cysteines are required to form protein domains that bind three and four divalent metal ions [21]. MT-I and MT-II are 61-residue proteins, MT-III holds an extra residue in the β-domain and a six-residue long insertion in the α-domain, whereas MT-IV shares an additional residue in the β-domain [20]. In humans, the transcription of MT-I and MT-II isoforms is induced by various stimuli [21]. The expression of MT-II, MT-IE and MT-IX can be detected in most types of tissue, whereas the expression of other MT-I isoforms seems to be restricted to some tissues [20]. MT-III is constitutive tissue--specific isoform, it is expressed in human brain and in some other tissues [20]. MT-IV mRNA expression has been reported in stratified squamous epithelium in mouse, no data exist on the expression of MT-IV in humans [20].

In order to investigate protein expression, the most widely used primary antibody to detect MT-I/II proteins in FFPE tissues of a number of different species is a monoclonal mouse antibody (Clone E9, Dako) reacting with a single and highly conserved epitope formed by the last 5-7 residues of the N-terminus of the β-domain of MT-I and MT-II [22-25]. The immunogen was horse self-polymerized MT-I and MT-II. In previous studies a specific polyclonal antibody that was generated against rat liver MT in rabbits was used efficiently to detect MT expression also in humans [7,26,27]. Furthermore, due to the difference in the amino acid sequence, specific monoclonal and polyclonal antibodies against MT-III could be generated and used successfully in IHC tests [22,28-30]. Further progress in the development of primary antibodies against MT isoforms would be important for future investigations. Nevertheless, IHC studies to date have greatly contributed to the current knowledge on the functions of MT in the human body.

2.5 Tissue specific expression of metallothionein proteins

MT-I and MT-II can be expressed in all cells throughout the body, however, IHC examinations were able to reveal that not all cells express MT to the same extent in healthy tissues [27]. In addition, several factors, e.g., proliferation status, age, can influence the expression of MT. For example, in normal human skin, strong MT-I/II immunostaining can be detected in basal keratinocytes of epidermis and hair follicle outer root sheath, hair matrix cells and the secretory coil, but not in the exocrine portion of eccrine glands [31]. In hyperplastic epidermis the increased MT expression represents an increase in the germinative pool size [32]. Accordingly, the protein levels of MT-I and MT-II have been shown to decrease significantly with increasing age simultaneously with the decrease of keratinocyte proliferation [33]. Nartey et al. investigated the distribution of MT during human development [34]. They found that MT levels are higher in the fetal liver than in the adult liver; in addition, MT is localized in the nucleus and the cytoplasm of human fetal and neonatal hepatocytes, whereas MT is mainly expressed in the cytoplasm of adult liver cells. In the fetal and neonatal human kidney, MT is localized primarily in the nucleus and the cytoplasm of the proximal tubular epithelial cells, whereas in the adult kidney, intraluminal MT localization was also observed [34].

MT-III expression has been investigated by IHC in rats [28]. Some astrocytes in the deep layers of cortex, ependymal cells, some glomerular and tubular cells in the kidney, some glandular epithelial cells in the dorsolateral lobe of prostate, some Sertoli cells and Leydig cells in the testis, and taste bud cells in the tongue showed MT-III immunostaining [28].

2.5.1 Metallothionein expression in response to exogenous agents

It is thought that MTs exert cytoprotective effects against heavy metal toxicity and oxidative stress [27]. IHC is suitable method to investigate the expression of MT in various tissues in response to an exogenous agent. An example is the elevated nuclear and cytoplasmic

MT expression of periportal hepatocytes, proximal tubular epithelial cells, intestinal columnar epithelial cells and Paneth cells in rats during dietary copper or zinc overloads, and upon exposure to cadmium [25,35,36]. Furthermore, the hepatic MT levels were increased in both the nucleus and cytoplasm of hepatocytes in mice upon thioacetamide exposure [37], and in rats upon exposure to 2,3,7,8-tetrachlorodibenzo-p-dioxin [38]. Increased MT-I and MT-II expression in the renal proximal tubular cells of rats upon administration of doxorubicin might indicate a protective mechanism against the pro-apoptotic effect of this cytostatic agent [39]. The MT levels have been found to be elevated in the epidermis after acute ultraviolet radiation exposure [40].

2.5.2 Metallothionein expression in inflammatory conditions

MT knockout mice appear relatively healthy, but they show an impaired response to stress [5]. MT expression is induced by a variety of pro- and anti-inflammatory mediators including glucocorticoids, reactive oxygen species, antioxidants, endotoxin, acute phase cytokines, furthermore, MT have a wide range of functions in cellular homeostasis and immunity [41]. Altered expression of MT has been shown in many inflammatory conditions. For example, an IHC study on renal biopsies from patients with lupus nephritis showed the depletion of MT-I and MT-II protein expression in the proximal tubular epithelial cells compared with healthy kidney specimens [42]. Moreover, a tubular MT score below the median value of the cohort predicted a poor renal outcome. Tissue infiltrating MT-positive cells could be shown in colonic biopsies from patients with inflammatory bowel disease and acute infectious colitis [43]. In another study, the mucosal MT concentration in colonic tissue samples from patients with inflammatory bowel disease has been found to be lower compared with normal mucosa tissue samples suggesting an antioxidant imbalance in the intestinal mucosa of these patients [44,45]. In a dextran sulfate sodium-induced intestinal inflammation mouse model MT-positive cells were detected in the lamina propria and submucosal layer and were mainly co-localized in macrophages [46]. Nevertheless, the increase of colonic myeloperoxidase activity levels and pro-inflammatory cytokine production induced by dextran sulfate sodium was significantly higher in the MT-I/II knockout animals compared with the wild-type mice suggesting that MT plays a protective role against colitis [46].

MT expression was analyzed in the central nervous system of mice with experimental autoimmune encephalomyelitis [47]. MT-I/II seemed to be produced mainly by reactive astrocytes and activated macrophages. It was assumed that the elevation of MT expression level in tissue may act on the inflammatory microenvironment suppressing pro-inflammatory cytokine production of macrophages, decreasing apoptotic cell death in neurons and oligodendrocytes, and enhancing tissue repair [47].

2.5.3 Metallothionein expression in cancer

MT expression in tissues has been studied most intensively in human cancers [48]. The results suggest that change in MT levels might play a role in the conversion of a potentially malignant lesion to a malignant carcinoma. For example, significantly higher MT-I/II and MT-III expression was noted in actinic keratosis and cutaneous squamous cell cancer, as compared with normal skin epidermis, whereas very low levels of MT-III expression were found in basal cell cancer [22,29]. A significantly higher MT-I/II expression was also observed in oral squamous cell carcinoma tissues comparing with normal and oral leukoplakia epithelial tissues [49]. High MT expression was detected in pancreas adenocarcinoma tissues compared with pancreatic serous cystadenoma or healthy pancreatic tissue samples [50]. Analysis of MT-I/II expression in prostate epithelial cells showed higher MT expression in tissues derived from benign prostatic hyperplasia than in those derived from prostate cancer [51]. Furthermore, IHC analysis of specimens from normal colorectal mucosa, adenomas, carcinomas and lymph node metastases revealed the down-regulation of MT-I/II expression in association with colorectal cancer progression [52]. Janssen et al. confirmed that the MT concentrations

of colorectal adenomas, carcinomas and liver metastases are lower than that of corresponding normal mucosa, however, they have found that a relatively high MT content might be associated with the aggressiveness of colorectal cancers [53]. Meta-analysis of IHC studies led to the conclusion that significantly increased MT-I/II expression can be detected in head and neck, and ovarian cancers, respectively, compared with healthy tissues, but significantly decreased MT expression can be observed in liver tumours compared with normal liver tissue [54]. It seems that the expression of MT is not universal to all human tumours, but may depend on the differentiation status and proliferative index of tumours, along with other tissue factors and gene mutations [48]. The various tumours may also differ in the intracellular localization of MT. For example, we observed nuclear MT-I/II staining in benign melanocytic nevi and intensive cytoplasmic and nuclear staining in malignant melanomas (Figure 2.) [9]. Cytoplasmic and nuclear MT-I/II expression was significantly higher in endometrial cancer cells compared with cells in benign hyperplasia of endometrium, however, the nuclear MT expression correlated better with histologic grade [55].

Changes in MT expression (up- or down-regulation) may be associated with a more aggressive phenotype and therapeutic resistance, ultimately resulting in a worse prognosis [6,21]. Weinlich et al. have found that high MT levels in tumour cells are associated with reduced survival in patients with malignant melanoma [56]. We confirmed that high expression of MT-I/II in melanoma cells is significantly more frequent in primary cutaneous malignant melanoma with haematogenous metastases [9]. In bladder cancer patients a high MT expression in tumour tissues was linked to shorter tumour-specific survival and increased recurrence rates [57]. IHC analysis of specimens from renal cell carcinoma revealed that MT immunostaining is associated with significantly worse prognosis [58]. The absence of MT expression in ovarian cancer samples correlated with improved progression-free survival in patients treated with adjuvant platinum-based chemotherapy [59]. Nevertheless, the role of MT in metastasis formation remains to be confirmed, and experimental evidence for its oncogenic role is still lacking.

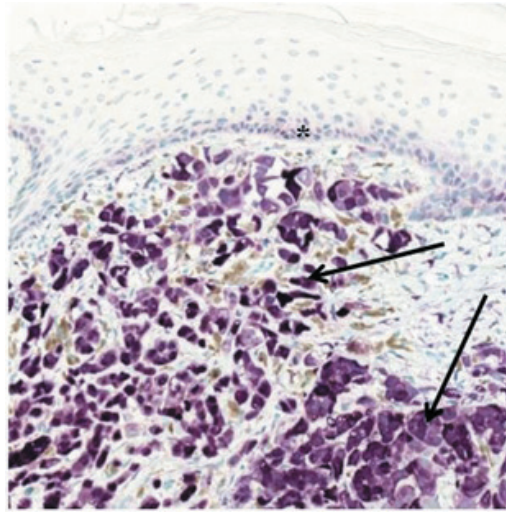

Figure 2: Expression of MT-I/II in primary cutaneous malignant melanoma cells (arrows). The keratinocytes (asterisks) of epidermal basal layer served as internal positive tissue controls. The IHC detection was based on an immunoperoxidase reaction using VIP chromogenic substrate. The slides were counterstained with methyl-green. Original magnification is x20.

3. Conclusions

Zn (II) is essential in fine-tuned orchestration of basic cell functions such as proliferation, gene expression and stress response. Besides metal detoxification, MT can release/bind Zn (II) with high affinity and regulates the availability of Zn (II) in various cell compartments thereby influencing the function of many transcription factors and enzymes [5]. It might explain why we can detect changes in the expression of MT in cancer, and calls for further investigations in this field. Moreover, the availability of zinc from MT is controlled by the local redox status [4]. Alterations in reactive oxygen species homeostasis are thought to be involved in the pathogenesis of various diseases, including cancers [6]. IHC is suitable to demonstrate MT expression in its morphological and functional

context; therefore, it is an important element of the investigations. Assay standardization and the use of appropriate positive and negative tissue controls are very important to interpret the findings correctly.

Acknowledgments

This work was supported by the European Social Fund TÁMOP-4.2.2.A-11/1/KONV-2012-0031, the Hungarian Scientific Research Fund OTKA K68401 and NK101680, and the Metallomic Scientific Network V4MSNet (project 11440027).

Conflicts of Interest

The authors declare no conflict of interest.

The authors declare they have no potential conflicts of interests concerning drugs, products, services or another research outputs in this study. The Editorial Board declares that the manuscript met the ICMJE „uniform reguirements“ for biomedical papers.

References

1. Schwartz, J.R.; Marsh, R.G.; Draelos, Z.D. Zinc and skin health: Overview of physiology and pharmacology. Dermatologic surgery : official publication for American Society for Dermatologic Surgery [et al.] 2005, 31, 837-847; discussion 847.
2. Berg, J.M.; Shi, Y. The galvanization of biology: A growing appreciation for the roles of zinc. Science 1996, 271, 1081-1085.
3. Roesijadi, G.; Bogumil, R.; Vasak, M.; Kagi, J.H. Modulation of DNA binding of a tramtrack zinc finger peptide by the metallothionein-thionein conjugate pair. The Journal of biological chemistry 1998, 273, 17425-17432.
4. Maret, W. The function of zinc metallothionein: A link between cellular zinc and redox state. The Journal of nutrition 2000, 130, 1455S-1458S.
5. Davis, S.R.; Cousins, R.J. Metallothionein expression in animals: A physiological perspective on function. The Journal of nutrition 2000, 130, 1085-1088.
6. Thirumoorthy, N.; Shyam Sunder, A.; Manisenthil Kumar, K.; Senthil Kumar, M.; Ganesh, G.; Chatterjee, M. A review of metallothionein isoforms and their role in pathophysiology. World journal of surgical oncology 2011, 9, 54.
7. Cherian, M.G. The significance of the nuclear and cytoplasmic localization of metallothionein in human liver and tumor cells. Environmental health perspectives 1994, 102 Suppl 3, 131-135.
8. Ramos-Vara, J.A.; Miller, M.A. When tissue antigens and antibodies get along: Revisiting the technical aspects of immunohistochemistry--the red, brown, and blue technique. Veterinary pathology 2014, 51, 42-87.
9. Emri, E.; Egervari, K.; Varvolgyi, T.; Rozsa, D.; Miko, E.; Dezso, B.; Veres, I.; Mehes, G.; Emri, G.; Remenyik, E. Correlation among metallothionein expression, intratumoural macrophage infiltration and the risk of metastasis in human cutaneous malignant melanoma. Journal of the European Academy of Dermatology and Venereology : JEADV 2013, 27, e320-327.
10. Bass, B.P.; Engel, K.B.; Greytak, S.R.; Moore, H.M. A review of preanalytical factors affecting molecular, protein, and morphological analysis of formalin-fixed, paraffin-embedded (ffpe) tissue: How well do you know your ffpe specimen? Archives of pathology & laboratory medicine 2014, 138, 1520-1530.
11. Elenitsas, R.; Nousari, C.H.; Seykora, J.T. Laboratory methods. In Lever's histopathology of the skin, 9th ed.; Elder, D.E.; Elenitsas, R.; Johnson, J., B. L.; Murphy, G.F., Eds. Lippincott Williams & Wilkins: Philadelphia, USA, 2005; pp 59-67.
12. Ramdial, P.K.; Bastian, B.C.; Goodlad, J.; McGrath, J.A.; Lazar, A. Specialized techniques in dermatopathology. In Mckee's pathology of the skin, 4th ed.; Calonje, E.; Brenn, T.; Lazar, A.; McKee, P.H., Eds. Elsevier Saunders: 2012; Vol. 1, pp 32-37.
13. Ward, J.M.; Rehg, J.E. Rodent immunohistochemistry: Pitfalls and troubleshooting. Veterinary pathology 2014, 51, 88-101.
14. Ramos-Vara, J.A.; Kiupel, M.; Baszler, T.; Bliven, L.; Brodersen, B.; Chelack, B.; Czub, S.; Del Piero, F.; Dial, S.; Ehrhart, E.J., et al. Suggested guidelines for immunohistochemical techniques in veterinary diagnostic laboratories. Journal of veterinary diagnostic investigation : official publication of the American Association of Veterinary Laboratory Diagnosticians, Inc 2008, 20, 393-413.
15. Taylor, C.R. New revised clinical and laboratory standards institute guidelines for immunohistochemistry and immunocytochemistry. Applied immunohistochemistry & molecular morphology : AIMM / official publication of the Society for Applied Immunohistochemistry 2011, 19, 289-290.
16. Elliott, K.; McQuaid, S.; Salto-Tellez, M.; Maxwell, P. Immunohistochemistry should undergo robust validation equivalent to that of molecular diagnostics. Journal of clinical pathology 2015.
17. Nielsen, S. External quality assessment for immunohistochemistry: Experiences from nordiqc. Biotechnic & histochemistry : official publication of the Biological Stain Commission 2015, 90, 331-340.
18. Rizzardi, A.E.; Johnson, A.T.; Vogel, R.I.; Pambuccian, S.E.; Henriksen, J.; Skubitz, A.P.; Metzger, G.J.; Schmechel, S.C. Quantitative comparison of immunohistochemical staining measured by digital image analysis versus pathologist visual scoring. Diagnostic pathology 2012, 7, 42.
19. Varghese, F.; Bukhari, A.B.; Malhotra, R.; De, A. Ihc profiler: An open source plugin for the quantitative evaluation and automated scoring

of immunohistochemistry images of human tissue samples. PloS one 2014, 9, e96801.
20. Moleirinho, A.; Carneiro, J.; Matthiesen, R.; Silva, R.M.; Amorim, A.; Azevedo, L. Gains, losses and changes of function after gene duplication: Study of the metallothionein family. PloS one 2011, 6, e18487.
21. Pedersen, M.O.; Larsen, A.; Stoltenberg, M.; Penkowa, M. The role of metallothionein in oncogenesis and cancer prognosis. Progress in histochemistry and cytochemistry 2009, 44, 29-64.
22. Zamirska, A.; Matusiak, L.; Dziegiel, P.; Szybejko-Machaj, G.; Szepietowski, J.C. Expression of metallothioneins in cutaneous squamous cell carcinoma and actinic keratosis. Pathology oncology research : POR 2012, 18, 849-855.
23. Hifumi, T.; Miyoshi, N.; Kawaguchi, H.; Nomura, K.; Yasuda, N. Immunohistochemical detection of proteins associated with multidrug resistance to anti-cancer drugs in canine and feline primary pulmonary carcinoma. The Journal of veterinary medical science / the Japanese Society of Veterinary Science 2010, 72, 665-668.
24. Dincer, Z.; Jasani, B.; Haywood, S.; Mullins, J.E.; Fuentealba, I.C. Metallothionein expression in canine and feline mammary and melanotic tumours. Journal of comparative pathology 2001, 125, 130-136.
25. Mullins, J.E.; Fuentealba, I.C. Immunohistochemical detection of metallothionein in liver, duodenum and kidney after dietary copper-overload in rats. Histology and histopathology 1998, 13, 627-633.
26. Nartey, N.; Cherian, M.G.; Banerjee, D. Immunohistochemical localization of metallothionein in human thyroid tumors. The American journal of pathology 1987, 129, 177-182.
27. Thirumoorthy, N.; Manisenthil Kumar, K.T.; Shyam Sundar, A.; Panayappan, L.; Chatterjee, M. Metallothionein: An overview. World journal of gastroenterology : WJG 2007, 13, 993-996.
28. Hozumi, I.; Suzuki, J.S.; Kanazawa, H.; Hara, A.; Saio, M.; Inuzuka, T.; Miyairi, S.; Naganuma, A.; Tohyama, C. Metallothionein-3 is expressed in the brain and various peripheral organs of the rat. Neuroscience letters 2008, 438, 54-58.
29. Pula, B.; Tazbierski, T.; Zamirska, A.; Werynska, B.; Bieniek, A.; Szepietowski, J.; Rys, J.; Dziegiel, P.; Podhorska-Okolow, M. Metallothionein 3 expression in normal skin and malignant skin lesions. Pathology oncology research : POR 2015, 21, 187-193.
30. Sens, M.A.; Somji, S.; Lamm, D.L.; Garrett, S.H.; Slovinsky, F.; Todd, J.H.; Sens, D.A. Metallothionein isoform 3 as a potential biomarker for human bladder cancer. Environmental health perspectives 2000, 108, 413-418.
31. van den Oord, J.J.; De Ley, M. Distribution of metallothionein in normal and pathological human skin. Archives of dermatological research 1994, 286, 62-68.
32. Karasawa, M.; Nishimura, N.; Nishimura, H.; Tohyama, C.; Hashiba, H.; Kuroki, T. Localization of metallothionein in hair follicles of normal skin and the basal cell layer of hyperplastic epidermis: Possible association with cell proliferation. The Journal of investigative dermatology 1991, 97, 97-100.
33. Ma, C.; Li, L.F.; Chen, X. Expression of metallothionein-i and ii in skin ageing and its association with skin proliferation. The British journal of dermatology 2011, 164, 479-482.
34. Nartey, N.O.; Banerjee, D.; Cherian, M.G. Immunohistochemical localization of metallothionein in cell nucleus and cytoplasm of fetal human liver and kidney and its changes during development. Pathology 1987, 19, 233-238.
35. Santon, A.; Giannetto, S.; Sturniolo, G.C.; Medici, V.; D'Inca, R.; Irato, P.; Albergoni, V. Interactions between zn and cu in lec rats, an animal model of wilson's disease. Histochemistry and cell biology 2002, 117, 275-281.
36. Tanimoto, A.; Hamada, T.; Higashi, K.; Sasaguri, Y. Distribution of cadmium and metallothionein in cdcl2-exposed rat kidney: Relationship with apoptosis and regeneration. Pathology international 1999, 49, 125-132.
37. Oliver, J.R.; Jiang, S.; Cherian, M.G. Augmented hepatic injury followed by impaired regeneration in metallothionein-i/ii knockout mice after treatment with thioacetamide. Toxicology and applied pharmacology 2006, 210, 190-199.
38. Nishimura, N.; Miyabara, Y.; Suzuki, J.S.; Sato, M.; Aoki, Y.; Satoh, M.; Yonemoto, J.; Tohyama, C. Induction of metallothionein in the livers of female sprague-dawley rats treated with 2,3,7 ,8-tetrachlorodibenzo-p-dioxin. Life sciences 2001, 69, 1291-1303.
39. Chmielewska, M.; Symonowicz, K.; Pula, B.; Owczarek, T.; Podhorska-Okolow, M.; Ugorski, M.; Dziegiel, P. Expression of metallothioneins i and ii in kidney of doxorubicin-treated rats. Experimental and toxicologic pathology : official journal of the Gesellschaft fur Toxikologische Pathologie 2015, 67, 297-303.
40. Ablett, E.; Whiteman, D.C.; Boyle, G.M.; Green, A.C.; Parsons, P.G. Induction of metallothionein in human skin by routine exposure to sunlight: Evidence for a systemic response and enhanced induction at certain body sites. The Journal of investigative dermatology 2003, 120, 318-324.
41. Lynes, M.A.; Hidalgo, J.; Manso, Y.; Devisscher, L.; Laukens, D.; Lawrence, D.A. Metallothionein and stress combine to affect multiple organ systems. Cell stress & chaperones 2014, 19, 605-611.
42. Faurschou, M.; Penkowa, M.; Andersen, C.B.; Starklint, H.; Jacobsen, S. The renal metallothionein expression profile is altered in human lupus nephritis. Arthritis research & therapy 2008, 10, R76.
43. Devisscher, L.; Hindryckx, P.; Lynes, M.A.; Waeytens, A.; Cuvelier, C.; De Vos, F.; Vanhove, C.; Vos, M.D.; Laukens, D. Role of metallothioneins as danger signals in the pathogenesis of colitis. The Journal of pathology 2014, 233, 89-100.
44. Kruidenier, L.; Kuiper, I.; Van Duijn, W.; Mieremet-Ooms, M.A.; van Hogezand, R.A.; Lamers, C.B.; Verspaget, H.W. Imbalanced secondary mucosal antioxidant response in inflammatory bowel disease. The Journal of pathology 2003, 201, 17-27.
45. Ioachim, E.; Michael, M.; Katsanos, C.; Demou, A.; Tsianos, E.V. The immunohistochemical expression of metallothionein in inflammatory

bowel disease. Correlation with hla-dr antigen expression, lymphocyte subpopulations and proliferation-associated indices. Histology and histopathology 2003, 18, 75-82.
46. Tsuji, T.; Naito, Y.; Takagi, T.; Kugai, M.; Yoriki, H.; Horie, R.; Fukui, A.; Mizushima, K.; Hirai, Y.; Katada, K., et al. Role of metallothionein in murine experimental colitis. International journal of molecular medicine 2013, 31, 1037-1046.
47. Espejo, C.; Carrasco, J.; Hidalgo, J.; Penkowa, M.; Garcia, A.; Saez-Torres, I.; Martinez-Caceres, E.M. Differential expression of metallothioneins in the cns of mice with experimental autoimmune encephalomyelitis. Neuroscience 2001, 105, 1055-1065.
48. Cherian, M.G.; Jayasurya, A.; Bay, B.H. Metallothioneins in human tumors and potential roles in carcinogenesis. Mutation research 2003, 533, 201-209.
49. Pontes, H.A.; de Aquino Xavier, F.C.; da Silva, T.S.; Fonseca, F.P.; Paiva, H.B.; Pontes, F.S.; dos Santos Pinto, D., Jr. Metallothionein and p-akt proteins in oral dysplasia and in oral squamous cell carcinoma: An immunohistochemical study. Journal of oral pathology & medicine : official publication of the International Association of Oral Pathologists and the American Academy of Oral Pathology 2009, 38, 644-650.
50. Sliwinska-Mosson, M.; Milnerowicz, H.; Rabczynski, J.; Milnerowicz, S. Immunohistochemical localization of metallothionein and p53 protein in pancreatic serous cystadenomas. Archivum immunologiae et therapiae experimentalis 2009, 57, 295-301.
51. Lee, J.D.; Wu, S.M.; Lu, L.Y.; Yang, Y.T.; Jeng, S.Y. Cadmium concentration and metallothionein expression in prostate cancer and benign prostatic hyperplasia of humans. Journal of the Formosan Medical Association = Taiwan yi zhi 2009, 108, 554-559.
52. Arriaga, J.M.; Levy, E.M.; Bravo, A.I.; Bayo, S.M.; Amat, M.; Aris, M.; Hannois, A.; Bruno, L.; Roberti, M.P.; Loria, F.S., et al. Metallothionein expression in colorectal cancer: Relevance of different isoforms for tumor progression and patient survival. Human pathology 2012, 43, 197-208.
53. Janssen, A.M.; van Duijn, W.; Oostendorp-Van De Ruit, M.M.; Kruidenier, L.; Bosman, C.B.; Griffioen, G.; Lamers, C.B.; van Krieken, J.H.; van De Velde, C.J.; Verspaget, H.W. Metallothionein in human gastrointestinal cancer. The Journal of pathology 2000, 192, 293-300.
54. Gumulec, J.; Raudenska, M.; Adam, V.; Kizek, R.; Masarik, M. Metallothionein - immunohistochemical cancer biomarker: A meta-analysis. PloS one 2014, 9, e85346.
55. Jagielski, L.; Jelen, M.; Kobierzycki, C.; Jagielska, G.; Blok, R. Increase of nuclear expression of metallothionein i/ii in neoplastic transformation of the endomnetrium. Ginekologia polska 2015, 86, 182-187.
56. Weinlich, G.; Eisendle, K.; Hassler, E.; Baltaci, M.; Fritsch, P.O.; Zelger, B. Metallothionein - overexpression as a highly significant prognostic factor in melanoma: A prospective study on 1270 patients. British journal of cancer 2006, 94, 835-841.
57. Hinkel, A.; Schmidtchen, S.; Palisaar, R.J.; Noldus, J.; Pannek, J. Identification of bladder cancer patients at risk for recurrence or progression: An immunohistochemical study based on the expression of metallothionein. Journal of toxicology and environmental health. Part A 2008, 71, 954-959.
58. Tuzel, E.; Kirkali, Z.; Yorukoglu, K.; Mungan, M.U.; Sade, M. Metallothionein expression in renal cell carcinoma: Subcellular localization and prognostic significance. The Journal of urology 2001, 165, 1710-1713.
59. Woolston, C.M.; Deen, S.; Al-Attar, A.; Shehata, M.; Chan, S.Y.; Martin, S.G. Redox protein expression predicts progression-free and overall survival in ovarian cancer patients treated with platinum-based chemotherapy. Free radical biology & medicine 2010, 49, 1263-1272.

The article is freely distributed under license Creative Commons (BY-NC-ND). But you must include the author and the document can not be modified and used for commercial purposes.

MALDI-TOF MSI and electrochemical detection of metallothionein in chicken liver after cadmium exposure

Roman Guran[1,2]*, Iva Blazkova[1,2], Renata Kensova[1,2], Lukas Richtera[1,2], Lucie Blazkova[1,2], Ondrej Zitka[1,2], Rene Kizek[1,2] and Vojtech Adam[1,2]

[1] Department of Chemistry and Biochemistry, Mendel University in Brno, Zemedelska 1, 613 00 Brno, Czech Republic; E-Mails: iva.blazkova@seznam.cz (I.B.), R.Kensova@seznam.cz (R.K.), oliver@centrum.cz (L.R.), BlazkovaLu@seznam.cz (L.B.), zitkao@seznam.cz (O.Z.), kizek@sci.muni.cz (R.K.), vojtech.adam@mendelu.cz (V.A.)

[2] Central European Institute of Technology, Brno University of Technology, Technicka 10, 616 00 Brno, Czech Republic

* Author to whom correspondence should be addressed; E-Mail: r.guran@email.cz; Tel.: +420 545 133 350; Fax: +420 545 212 044.

Received:10.9.2015 / Accepted:20.9.2015 / Published:1.10.2015

Metallomics is an area that studies the interactions of metal ions with proteins and other biomolecules and their function in living organisms. Metallothioneins (MTs) belong to a large family of metalloproteins in this field. As it is known, the presence of Cd^{2+} ions causes higher expression of MTs. Therefore we focused on determination of MT and Cd content in liver from chicken embryos (model organism) by electrochemistry and atomic absorption spectroscopy (AAS) after the exposure of chicken embryos to different concentrations of $Cd(NO_3)_2$. We also determined the spatial distribution of MT in chicken liver tissue slices by matrix assisted laser desorption/ionization time-of-flight mass spectrometry imaging (MALDI-TOF MSI) and evaluated the toxicity of $Cd(NO_3)_2$ to chicken embryos. Finally, we attempted to find the correlation between 2D MSI maps of MT and concentration of MT in chicken liver.

Keywords: metallothionein; Cd toxicity; chicken liver; MALDI MSI

1. Introduction

Metallothioneins (MTs) are intracellular, low-molecular weight, proteins where cysteines form at least one third of all protein amino acids and thiol groups serve as pockets for coordination with divalent metal ions, especially Zn and Cu [1]. Metallothioneins are connected with cancer development, protection of organism against environmental pollution effects and also with chemoresistance of cells. Their main functions include detoxification of heavy metals, maintenance of ion homeostasis and protection against oxidative stress. MTs exist in all kind of mammalian cells. Four isoforms of human MT (MT-1, MT-2, MT-3, MT 4) were found so far [2] and according to UniProt database two chicken MTs (MT1 and MT3) have been reported. The expression of MTs in the liver can be induced by several metals and drugs. MTs serve as cellular regulators by coordination of essential metals (Zn, Cu) and reducing the toxicity of heavy metals (Cd, Pb) [3].

MTs can be detected electrochemically in Brdicka solution. Here, three characteristic signals are measured for construction of electrochemical fingerprint of MT: RS_2Co (about -1.3 V), Cat1 (-1.4 V) and Cat2 (-1.5 V). The obtained voltammograms are then analyzed by mathematical model [4,5].

Cadmium (Cd), a non-essential heavy metal and a selective toxicant, is accumulated mainly in the kidneys where it causes cellular injury [6]. Cd ions stimulate expression of MTs and toxicity occurs when the concentration of Cd ions exceeds the buffering capacity of intracellular MTs [7]. Cd naturally occurs in the environment as a pollutant from agriculture and industry [8-10]. Cadmium is a known teratogen

and can cause damage to chicken embryos [11]. Cadmium levels can be determined by different methods. In this study, atomic absorption spectroscopy (AAS) method was used as described in our previous work [12].

Matrix assisted laser desorption/ionization time-of-flight mass spectrometry imaging (MALDI TOF MSI) is an imaging technique used for determining spatial distribution of various molecules (biomarkers) in a variety of tissue samples. MALDI is "soft" ionization technique, which does not completely fragment the molecules of analytes and therefore a molecular weight of whole analyte can be measured [13]. MALDI-TOF has been used for detection of cancer biomarkers of different tumors, namely; gastrointestinal tumors, tumors of respiratory system, renal and bladder tumors, prostate, breast and ovarian tumors [14]. In this study we have used MALDI-TOF MSI for imaging MT in chicken liver for the first time.

The purpose of this study was the detection of MT in liver from chicken embryos exposed to different concentrations of cadmium by electrochemistry and MALDI-TOF MSI. Also, we attempted to find some correlation between measured MT concentrations and administered concentrations of cadmium.

2. Results and Discussion

Chicken embryos were divided into control group and five groups exposed to the 100 µl solutions of $Cd(NO_3)_2$ with total cadmium amount: 3.75, 7.5, 15, 30 and 60 µg/egg. A control group was administered with the same volume of pure water. Each group contained ten chicken embryos/fertilized eggs.

Cadmium toxicity was evaluated using Kaplan-Meier survival analysis [15]. It showed (Fig. 1C) that 5 hours after application of $Cd(NO_3)_2$ solutions or pure water into chicken embryos the overall survival of chicken embryos will

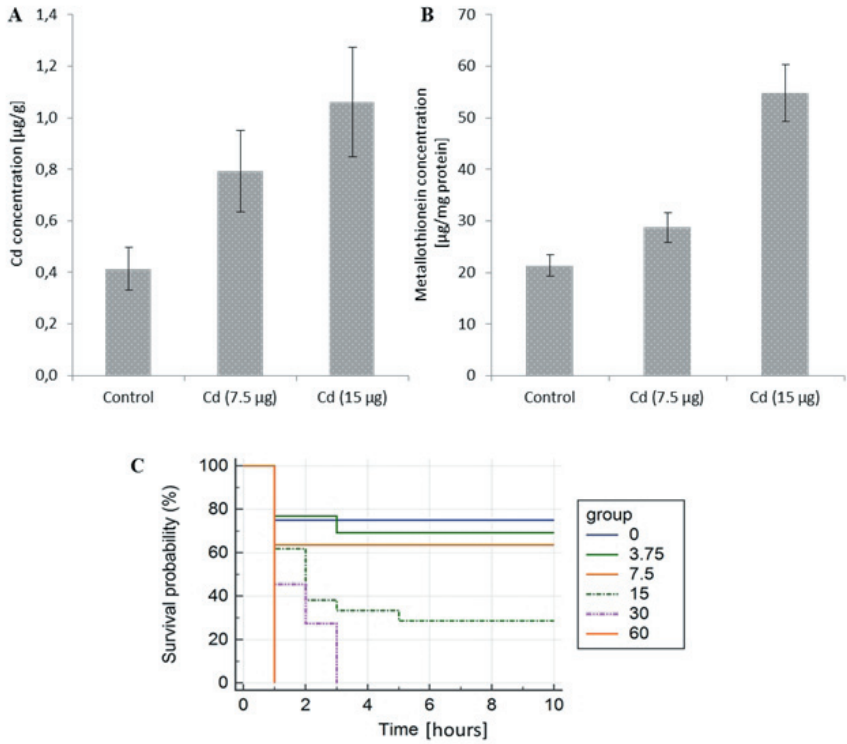

Figure 1: (A) Determination of concentration of Cd relative to the weight of liver from chicken embryos. Cd was measured by AAS (paragraph 3.6.). (B) Determination of concentration of metallothionein (MT) relative to the total protein amount measured in liver from chicken embryos. MT was measured by differential pulse voltammetry (DPV) using Brdicka solution (paragraph 3.4.). (C) Kaplan-Meier survival analysis of chicken embryos after the application of 0, 3.75, 7.5, 15, 30 and 60 µg/egg of cadmium in the form of Cd^{2+} ions – these concentrations are shown as groups with different color according to the legend.

be 0 % for group 60 and 30, cca 30 % for group 15, cca 62 % for group 7.5, cca 70 % for group 3.75 and cca 75 % for control group (group 0). The number of group means total amount of administered Cd in µg/egg. For other analyses were used samples only from groups 15, 7.5 and 0 because chicken embryos from groups 60 and 30 were dead and the difference of group 3.75 from group 0 is not so significant as in the case of group 7.5 and 15.

Liver samples were extracted from chicken embryos in the 17th day of their growth and were further processed for determining cadmium and metallothionein concentrations and total protein content. The AAS analysis of Cd content and differential pulse voltammetric (DPV) analysis of MT content gave similar results (Fig. 1A, 1B). The determined concentrations of Cd in liver samples had the same trend as determined concentrations of MT.

This highlights a fact that MTs are expressed more in the presence of heavy metals and that

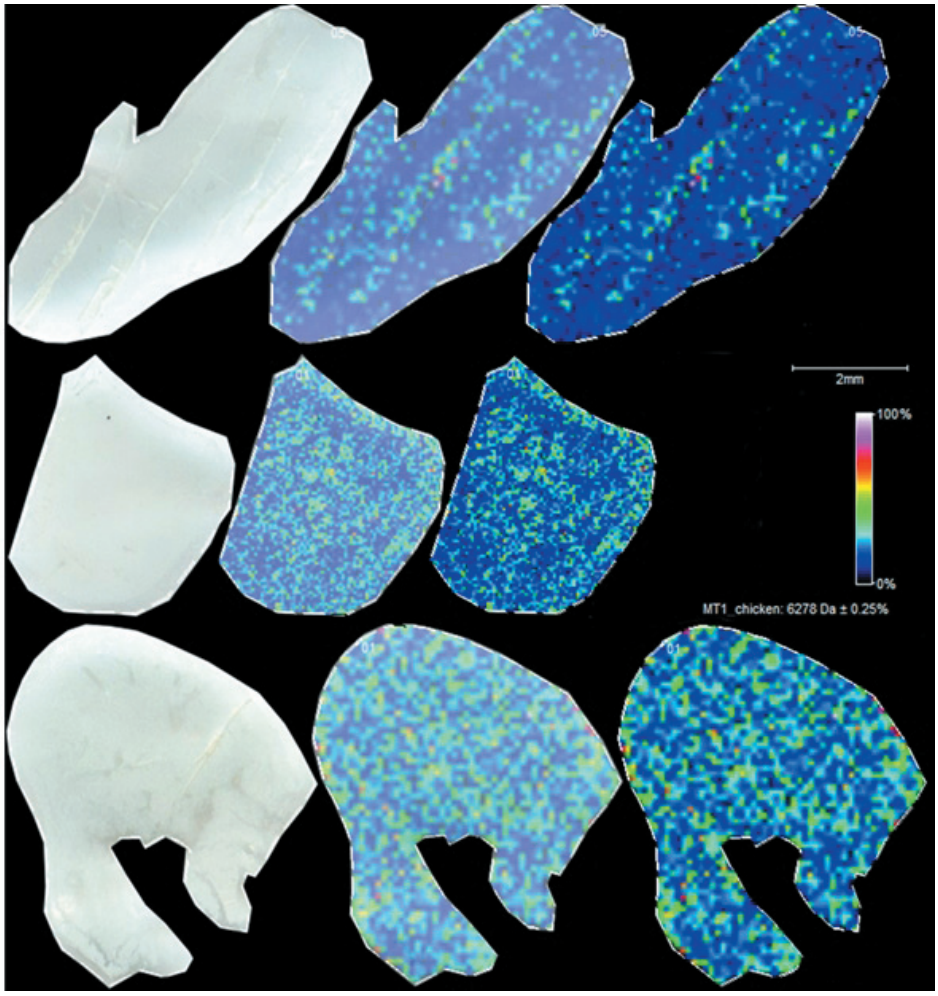

Figure 2. MALDI mass spectrometry images of spatial distribution of chicken metallothionein MT1 (6277 Da) in liver from chicken embryo after exposure to Cd: (A) control sample (0 µg of Cd), (B) 7.5 µg of Cd and (C) 15 µg of Cd. Pictures on the left represent scanned images of liver slices, pictures on the right represent results from MSI, and pictures in the middle represent scanned images of liver slices merged with results from MSI and.

they bind these metals [16,17].

To support these results further a MALDI-TOF mass spectrometry imaging was used to obtain spatial distribution of MT in liver from chicken embryos. Typically, cryo sectioned frozen tissue samples are used for MALDI MSI, but formalin-fixed and paraffin-embedded (FFPE) tissue samples can be used too [18]. In this work, FFPE liver from chicken embryos was chosen because of optimized method of deparaffinization and antigen retrieval [19].

Results from MALDI TOF MSI are shown in Fig. 2. Chicken metallothionein MT1 with molecular weight 6277 Da was detected by MALDI--TOF MSI, and was verified in UniProt database. Liver from chicken embryos exposed to 0 (Fig. 2A), 7.5 (Fig. 2B) and 15 (Fig. 2C) μg/egg of Cd were analyzed. Obtained results indicate that with higher concentration of Cd in liver, higher amounts of chicken MT1 were detected. This was in correlation with results from DPV and AAS analyses. A spatial distribution of MT1 showed that MT1 is uniformly expressed in whole liver tissue and the expression sites cannot be determined precisely. However, these data have shown that MALDI-TOF MSI can be used for determination of MT in FFPE chicken liver tissue which can be used in future experiments.

3. Experimental Section

3.1 Chemicals and material

All chemicals used in this study were purchased from Sigma Aldrich (St. Louis, MO, USA) in ACS purity unless noted otherwise. Acetate buffer of pH 5 was prepared by titrating 0.2 M acetic acid with 0.2 M sodium acetate then diluted with water and used as a supporting electrolyte. The pH was measured using pH meter WTW inoLab (Weilheim, Germany). High purity deionized water (Milli-Q Millipore 18.2 MΩ.cm^{-1}, MA, USA) was used throughout the study.

3.2 Model organism

The fertilized eggs of Lenghorn hen (Integra, a.s., Zabcice, Czech Republic) were incubated at 37 °C and relative humidity of 55% in the incubator (RCom 50 MAX, Gyeongnam, Korea). The experiments were performed with embryos in 7th developmental day. The toxicity of Cd^{2+} was analyzed after the application of 100 μl of $Cd(NO_3)_2 \bullet 4H_2O$ (37.5, 75, 150, 300 or 600 μg.ml^{-1} Cd^{2+}). This solution was applied through a small hole in a shell on the chorioallantoic membrane. Chicken embryo controls were exposed to 100 μl of deionized water (n = 5). 17th developmental day, the embryos were removed from the shell and after the extraction of liver, a few samples were used for MALDI-TOF MSI (paragraph 3.7.) and other samples were frozen and kept for other analysis. The samples were stored in -80 °C until assayed.

3.3 Sample preparation for MT electrochemical detection

100 mg of thawed embryo's liver samples were used for MT analysis according to protocol [20]: samples were mixed with 1 ml of 0.1 M phosphate buffer (pH 7.0) and homogenized by ultrasonic needle for 2 minutes. After homogenization, samples were shaken at 8 °C for 20 minutes and centrifuged for 10 minutes at 4 °C. 10 μl of supernatant was mixed with 990 μl of the phosphate buffer and samples were further denatured at 99 °C for 20 minutes in a thermomixer (Eppendorf 5430, Hamburg, Germany) and centrifuged for 10 minutes (Eppendorf 5402, Hamburg, Germany) to remove bulk proteins and peptides that interfere in the electrochemical response.

3.4 Metallothionein determination

Levels of MT in all tissues were determined by the differential pulse voltammetry with Brdicka electrolyte (1 mM $Co(NH_3)_6Cl_3$, and 1 M ammonia buffer (NH_3(aq) and NH_4Cl, pH = 9.6)) using previous protocol [21]. Differential pulse voltammetric measurements were performed using the 747 VA Stand instrument connected to a 693 VA Processor and 695 Autosampler (Metrohm, Herisau, Switzerland), and a standard reaction cuvette with three electrodes (working electrode was a hanging mercury drop electrode with a drop area of 0.4 mm^2, Ag/AgCl/3M KCl electrode was used as reference electrode and platinum electrode was used as auxiliary electrode) and also a

cooled sample holder and measurement cell to 4 °C (Julabo F25, Julabo, Seelbach, Germany). The analyzed samples were deoxygenated prior to measurements by purging with argon (99.999%) saturated with water for 120 s. The parameters of the measurement were as follows: initial potential of -0.7 V, end potential of -1.75 V, modulation time 0.057 s, time interval 0.2 s, step potential 2 mV, modulation amplitude -250 mV, Eads = 0 V, volume of injected sample 5 µl. Measurements were done in electrochemical cell with total volume of 2 ml (5 µl of sample and 1995 µl Brdicka solution).

3.5 Determination of total protein content

Total protein was determined by using the SKALAB CBT 600T kit (Skalab, Svitavy, Czech Republic) according to manufacturer´s instructions.

3.6 Atomic absorption spectroscopy (AAS)

Cadmium was determined using 280Z Agilent Technologies atomic absorption spectrometer (Agilent, USA) with electrothermal atomization. Cadmium ultrasensitive hollow cathode lamp (Agilent, USA) was used as the radiation source (lamp current 4 mA). The spectrometer was operated at 228.8 nm resonance line with spectral bandwidth of 0.5 nm. The sample volume 20 µl was injected into the graphite tube. The flow of argon inert gas was 300 ml.min-1. Zeeman background correction was used with field strength 0.8 Tesla. Cadmium was determined in the presence of palladium chemical modifier.

3.7 MALDI-TOF mass spectrometry imaging

Preparation of tissue samples

The extracted embryo's liver samples were paraffinized according to [22]. Then they were cut into 10 µm thin slices using microtome Leica SM2010 R (Baria s.r.o., Prague, Czech Republic) and they were mounted onto ITO (indium-tin oxide) glass slides (Bruker Daltonik GmbH, Bremen, Germany). The conductivity of surface was checked by ohmmeter. Deparaffinization and antigen retrieval were performed according to protocol by Casadonte et al. [19]. Position of tissue slices was marked by at least three marks by white pencil corrector. Then the glass slides with samples were scanned by Epson Perfection V500 Office (Epson Europe B.V., Amsterdam, Netherlands) with resolution 2400 DPI. MALDI matrix was sprayed onto glass slides with samples by Bruker ImagePrep (Bruker Daltonik GmbH, Bremen, Germany). As MALDI matrix, 2,5-dihydroxybenzoic acid (DHB) (Sigma-Aldrich, St. Louis, MO, USA) was used. DHB was prepared in concentration of 30 $mg.ml^{-1}$ in 50% methanol and 0.2% TFA. MALDI matrix mixtures were thoroughly vortexed and ultrasonicated using Bandelin 152 Sonorex Digital 10P ultrasonic bath (Bandelin electronic GmbH, Berlin, Germany) for 2 minutes at 50 % of intensity at room temperature. The samples were ready for analysis after drying.

Mass spectrometry imaging

The mass spectrometry experiments were performed on a MALDI-TOF mass spectrometer Bruker ultrafleXtreme (Bruker Daltonik GmbH, Bremen, Germany). Data acquisition and processing of mass spectra was performed on flexControl 3.4 and flexAnalysis 2.2 softwares, while analysis of MSI data was done on flexImaging 3.0 software. Firstly, scanned images of tissue slices were loaded into flexImaging 3.0 while MALDI adapter with glass slides was loaded into mass spectrometer. Then, the position of MALDI adapter was changed according to white marks on glass slides in the way, that MALDI adapter was moved in flexControl to a position of white marks and on each mark the position was pointed manually in flexImaging by mouse pointer – thus the position of tissue slices was programmed into the mass spectrometer. Next, regions of acquisition were highlighted by mouse pointer in flexImaging and raster width of approximately 100 µm was chosen. Before MALDI MSI, the measuring method was standardized and mass spectrometer was calibrated on a mixture of peptide and protein calibration standards (Bruker Daltonik GmbH, Bremen, Germany). The laser power was set to 65 %. MALDI MSI was performed in linear positive mode in the m/z range 2–20 kDa. The MS spectra were acquired by averaging 1600 sub spectra from a total of 1600 laser shots

per raster spot. Automatic method of MALDI MSI was then initiated. The mass spectra were automatically loaded into flexAnalysis, where they were processed (baseline substraction was performed), and finally the processed spectra were automatically loaded into flexImaging.

Preparation of MALDI MSI images

Final preparation of MSI images was made in flexImaging by selecting peak of chicken metallothionein 1 (MT1) – the molecular weight of chicken MT1 was chosen according to UniProt database (www.uniprot.org). From a peak molecular weight a mass filter was made in the format "(molecular weight + atomic weight of hydrogen) ± 0.25 %". Finally, images of tissue slices with used mass filters of selected peaks were used for preparation of final MALDI MSI images, which were made in GIMP 2.8 (www.gimp.org).

3.8 Statistical analysis

Data were processed using MICROSOFT EXCEL (Microsoft, WA, USA). The results are expressed as an average ± standard deviation (SD) unless otherwise noted.

4. Conclusions

In our work, cadmium toxicity was connected with expression of metallothionein. With higher amounts of cadmium injected to chicken embryos, higher amounts of metallothionein were detected. This was further supported by MALDI-TOF mass spectrometry imaging of metallothionein in liver from chicken embryos. In liver tissue with higher amount of cadmium, higher metallothionein peak intensities were detected corresponding to higher concentration of metallothionein. To our current knowledge this was the first use of MALDI-TOF MSI for detection of metallothionein from formalin--fixed and paraffin-embedded tissue sample.

Acknowledgments

The work was supported by V4 Metallomic Scientific Network TD 11440027.

Conflicts of Interest

The authors declare no conflict of interest.

The authors declare they have no potential conflicts of interests concerning drugs, products, services or another research outputs in this study. The Editorial Board declares that the manuscript met the ICMJE „uniform reguirements" for biomedical papers.

References

1. Lynes, M.A.; Hidalgo, J.; Manso, Y.; Devisscher, L.; Laukens, D.; Lawrence, D.A. Metallothionein and stress combine to affect multiple organ systems. Cell Stress & Chaperones 2014, 19, 605-611.
2. Pinter, T.B.J.; Irvine, G.W.; Stillman, M.J. Domain selection in metallothionein 1a: Affinity-controlled mechanisms of zinc binding and cadmium exchange. Biochemistry 2015, 54, 5006-5016.
3. Klaassen, C.D.; Liu, J.; Choudhuri, S. Metallothionein: An intracellular protein to protect against cadmium toxicity. Annual Review of Pharmacology and Toxicology 1999, 39, 267-294.
4. Vyslouzilova, L.; Krizkova, S.; Anyz, J.; Hynek, D.; Hrabeta, J.; Kruseova, J.; Eckschlager, T.; Adam, V.; Stepankova, O.; Kizek, R. Use of brightness wavelet transformation for automated analysis of serum metallothioneins- and zinc-containing proteins by western blots to subclassify childhood solid tumours. Electrophoresis 2013, 34, 1637-1648.
5. Sobrova, P.; Vyslouzilova, L.; Stepankova, O.; Ryvolova, M.; Anyz, J.; Trnkova, L.; Adam, V.; Hubalek, J.; Kizek, R. Tissue specific electrochemical fingerprinting. Plos One 2012, 7.
6. Yang, H.; Shu, Y. Cadmium transporters in the kidney and cadmium-induced nephrotoxicity. International Journal of Molecular Sciences 2015, 16, 1484-1494.
7. Sabolic, I.; Breljak, D.; Skarica, M.; Herak-Kramberger, C.M. Role of metallothionein in cadmium traffic and toxicity in kidneys and other mammalian organs. Biometals 2010, 23, 897-926.
8. Krystofova, O.; Trnkova, L.; Adam, V.; Zehnalek, J.; Hubalek, J.; Babula, P.; Kizek, R. Electrochemical microsensors for the detection of cadmium(ii) and lead(ii) ions in plants. Sensors 2010, 10, 5308-5328.
9. Supalkova, V.; Petrek, J.; Baloun, J.; Adam, V.; Bartusek, K.; Trnkova, L.; Beklova, M.; Diopan, V.; Havel, L.; Kizek, R. Multi-instrumental investigation of affecting of early somatic embryos of spruce by cadmium(ii) and lead(ii) ions. Sensors 2007, 7, 743-759.
10. Kovarova, J.; Kizek, R.; Adam, V.; Harustiakova, D.; Celechovska, O.; Svobodova, Z. Effect of cadmium chloride on level of metallothionein in carp. Sensors 2009, 9, 4789-4803.
11. Thompson, J.; Hipwell, E.; Loo, H.V.; Bannigan, J. Effects of cadmium on cell death and cell proliferation in chick embryos. Reprod. Toxicol.

2005, 20, 539-548.
12. Kensova, R.; Blazkova, I.; Vaculovicova, M.; Milosavljevic, V.; Blazkova, L.; Hynek, D.; Kopel, P.; Novotna, M.; Zehnalek, J.; Pohanka, M., et al. The effect of cadmium ions and cadmium nanoparticles on chicken embryos and evaluation of organ accumulation. Int. J. Electrochem. Sc. 2015, 10, 3623-3634.
13. Yates, J.R. Mass spectrometry and the age of the proteome. Journal of Mass Spectrometry 1998, 33, 1-19.
14. Merlos Rodrigo, M.A.; Zitka, O.; Krizkova, S.; Moulick, A.; Adam, V.; Kizek, R. Maldi-tof ms as evolving cancer diagnostic tool: A review. Journal of Pharmaceutical and Biomedical Analysis 2014, 95, 245-255.
15. Goel, M.K.; Khanna, P.; Kishore, J. Understanding survival analysis: Kaplan-meier estimate. International Journal of Ayurveda Research 2010, 1, 274-278.
16. Hockner, M.; Dallinger, R.; Stuerzenbaum, S.R. Metallothionein gene activation in the earthworm (lumbricus rubellus). Biochemical and Biophysical Research Communications 2015, 460, 537-542.
17. Sheng, Z.; Yang, W.X.; Zhu, J.Q. Metallothionein from pseudosciaena crocea: Expression and response to cadmium-induced injury in the testes. Ecotoxicology 2015, 24, 779-794.
18. De Sio, G.; Smith, A.J.; Galli, M.; Garancini, M.; Chinello, C.; Bono, F.; Pagni, F.; Magni, F. A maldi-mass spectrometry imaging method applicable to different formalin-fixed paraffin-embedded human tissues. Molecular Biosystems 2015, 11, 1507-1514.
19. Casadonte, R.; Caprioli, R.M. Proteomic analysis of formalin-fixed paraffin-embedded tissue by maldi imaging mass spectrometry. Nat. Protocols 2011, 6, 1695-1709.
20. Tmejova, K.; Hynek, D.; Kensova, R.; Blazkova, I.; Vyslouzilova, L.; Stepankova, O.; Pohanka, M.; Zehnalek, J.; Vaculovicova, M.; Adam, V., et al. Electrochemical analysis of metallothionein in chicken exposed to cadmium ions. Int. J. Electrochem. Sc. 2015, 10, 3923-3934.
21. Krejcova, L.; Fabrik, I.; Hynek, D.; Krizkova, S.; Gumulec, J.; Ryvolova, M.; Adam, V.; Babula, P.; Trnkova, L.; Stiborova, M., et al. Metallothionein electrochemically determined using brdicka reaction as a promising blood marker of head and neck malignant tumours. Int. J. Electrochem. Sc. 2012, 7, 1767-1784.
22. Berril, M. Histology protocols. https://www.trentu.ca/biology/berrill/histology/histology_protocols.htm (7.9.2015),

The article is freely distributed under license Creative Commons (BY-NC-ND). But you must include the author and the document can not be modified and used for commercial purposes.

REVIEW

The use of MALDI MSI for the study of different tissues

Roman Guran[1,2*], Lucie Vanickova[3,4], Ondrej Zitka[1,2], Vojtech Adam[1,2] and Rene Kizek[1,2]

[1] Department of Chemistry and Biochemistry, Mendel University in Brno, Zemedelska 1, 613 00 Brno, Czech Republic; E-Mails: zitkao@seznam.cz , vojtech.adam@mendelu.cz, kizek@sci.muni.cz

[2] Central European Institute of Technology, Brno University of Technology, Technicka 10, 616 00 Brno, Czech Republic

[3] Laboratory of Chemical Ecology, Institute of Chemistry and Biotechnology, Federal University of Alagoas, Av. Lourival de Melo Mota, s/n, Tabuleiro, 57072-970 Maceió, Brazil; E-Mail: luci.vanickova@gmail.com

[4] Institute of Organic Chemistry and Biochemistry, AS CR, Flemingovo nam. 2, 166 10 Prague, Czech Republic

* Author to whom correspondence should be addressed; E-Mail: r.guran@email.cz;
Tel.: +420 545 133 350; Fax: +420 545 212 044.

Received:2.7.2015 / Accepted:7.7.2015 / Published:1.10.2015

Matrix-assisted laser desorption/ionization mass spectrometry imaging technique (MALDI MSI) has mainly focused on imaging the spatial distribution of biomarkers, drugs and metabolites in different tissues. Due to ion suppression, MALDI MSI is usually used in the *m/z* range from 0 to 30 kDa. To detect a wide range of analyte concentrations, it is necessary to prepare tissue samples appropriately; cryosectioning has been found to be a successful method. There is also a need to process an enormous amount of formaldehyde-fixed tissue samples from histopatology/histochemistry. This article presents a short history and recent progress in MALDI MSI techniques for the imaging of diverse tissues.

Keywords: MALDI imaging; biomarker; tumor; skin; insect; plant

1. Introduction

The matrix assisted laser desorption/ionization (MALDI) technique was introduced by Karas et al. in 1985 [1]. Three years later, the same research group published a first study on the utilization of this ionization method for mass spectrometry of proteins [2]. Since its introduction, MALDI mass spectrometry was developed rapidly. Nowadays, it is routinely used for characterization of peptides, proteins and identification of bacteria. Because of its soft biomolecules ionization, MALDI was found to be useful for mass spectrometry imaging of a variety of samples where information regarding the spatial distribution of molecules is needed. At the turn of the third millennium, MALDI mass spectrometry imaging (MALDI MSI, MALDI imaging) was firstly applied for the determination of protein expression in mammalian tissues [3]. Usually, MALDI is combined with time-of-flight mass spectrometry (TOF MS), because it measures complete mass spectra over wide mass ranges at the same time [4]. There also exist other types of mass spectrometers connected with MALDI, such as Fourier transform ion cyclotron resonance mass spectrometers (FT-ICR MS) or linear ion trap with orbitrap mass spectrometers (LTQ Orbitrap MS) [5-7]. Currently, the MALDI MSI technique is the subject of comprehensive research to improve it in different ways – time of analysis [8,9], spatial resolution [10], and sensitivity and detection of different analytes [11,12]. Information gained from MALDI MSI can be correlated with immunohistochemical images [13] or with images from other techniques such

as magnetic resonance imaging (MRI) [14] or laser ablation-inductively coupled plasma mass spectrometry/atomic emission spectrometry (LA-ICP MS/AES) [15]. There exist several extensive reviews on recent progress in MALDI MSI and on the development of MALDI imaging techniques that are recommended to readers with interest in this field [16-18].

In the following paragraphs, a brief description of the current state of the use of MALDI MSI in research on different analytes in tissues will be given.

2. MALDI MSI in study of various tissues

In order for MALDI MSI analyses to generate reproducible data, proper sample preparation is crucial. Usually, various organs [19,20], plant tissues [21], bacterial colonies [22] or cells [23] are analyzed. There are different ways of preparing tissue sections depending on the state of tissue sample – whether it is fresh, frozen (-80 °C), conserved in ethanol or fixed in formaldehyde and embedded in paraffin [24,25]. The most frequently analyzed tissues are liver, kidneys, lungs, brain, heart and all types of tumors. The preferred preparation of tissue is quick and deep freezing of fresh samples – this minimalizes the degradation of analytes and fixes their spatial distribution. Rapid freezing of the entire tissue is crucial to prevent the sample from cracking and the formation of ice crystals. The tissue sample is firstly wrapped in thin aluminum foil and then is immersed repeated in the freezing liquid (nitrogen, ethanol, isopropanol). Afterwards, the tissue sample is stored at -40 or -80 °C, depending on the used freezing liquid. The optimal thickness of frozen tissue sections, made in cryotome is 5-20 µm. Fixation of frozen tissue sections on the conductive ITO (indium-tin oxide) glass slide is generally conducted by dehydration – usually a glass slide with tissue is briefly soaked in 70% ethanol and then soaked for a few minutes in 90% and 100% ethanol. For protein analysis, prior to the application of matrix, lipids and salts are washed away with ethanol and water or other organic solvents (xylene, chloroform). To desalt tissue samples prior to lipid analysis a solution of ammonium acetate or ammonium formate is recommended [23].

A general MALDI MSI workflow consists of cutting the tissue into slices, scanning the glass slide, applying a matrix solution, measuring the mass spectra, and analyzing the data using 2D mass maps (Fig. 1). For MALDI MSI of tissue sections that have been formalin-fixed and paraffin-embedded, sample preparation is more complicated. Paraffin can suppress ionization, and formaldehyde fixation causes dehydration, denaturation, crosslinking (methylene bridges), and the precipitation and agglutination of proteins, which prevents detection. Therefore, the deparaffination of tissue samples by incubation in xylene for a few minutes is needed. Then, rehydration is carried out by soaking the slides with the tissue samples in a series of ethanol solutions gradually decreasing in concentration. Antigens are recovered by breaking methylene bridges of cross-linked proteins at high temperatures and incubating in buffers differing in pH and ionic strength [13].

2.1 MALDI MSI of tumors

Tumors are the most frequently studied tissues by MALDI MSI. Oncology research plays an important role in the rapid development of MALDI MSI techniques.

The majority of researchers are searching for new cancer biomarkers or for distributions of drugs and their metabolites inside tumor tissue. In order to obtain the necessary data, sample preparation and matrix application must be optimized for each type of investigated analyte. Some analytes suffer from ion suppression, for example, and require different methods for their study.

Nearly all types of tumors have been investigated by MALDI MSI techniques. The most often applied MALDI MSI technique is MALDI-TOF MSI. For example, a time-of-flight detector was used to image metabolites in colorectal liver cancer metastases in a mouse model [26]. The applied matrix was N (1 naphthyl)ethylenediamine dihydrochloride (NEDC). This matrix was proven to be useful in the analysis of oligosaccharides and glycerophospholipids. In another study, MALDI-TOF MSI was com-

bined with MALDI-FT-ICR MSI to visualize and quantify the distribution of the anticancer drug, irinotecan, and its active metabolite, SN-38, in colon cancer (in a murine model) [27]. Rodrigo et al. reviewed that MALDI-TOF MSI was also used in studies of gastrointestinal cancer, cancer of the respiratory system, renal and bladder cancer, and prostate, breast and ovarian cancer, in order to find new cancer biomarkers or to study the spatial distribution of anticancer drugs in tumors [28].

MALDI-LTQ Orbitrap MSI is another technique that has been used for drug imaging in human lung tumor sections and rat xenograft tissue sections, where thin sections were exposed to pharmaceutical drugs (erlotinib, gefitinib, and tiotropium), and were characterized by microenvironment localization [31]. This method was also applied in a study, where a comparison between two different ways of carrying out pulmonary drug administration (inhalation of a nebulized aerosol of aqueous

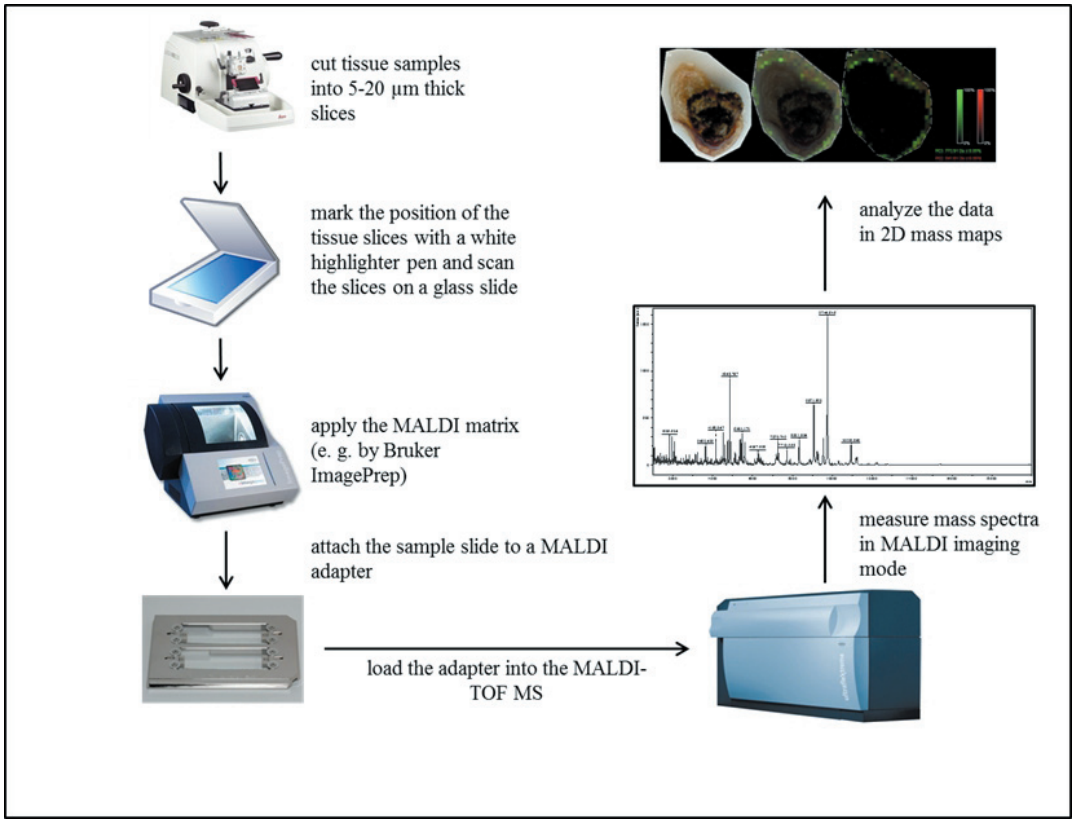

Figure 1: The scheme of typical MALDI MSI workflow.

MALDI-FT-ICR MSI was employed in in situ studies of lipids in head and neck tumors [29], where it served for gaining high resolution data sets for higher mass accuracy and better interpretation of lipidome, and in a study, where it helped to find and optimize an ex vivo model for better and faster optimization of sample preparation procedures in MALDI drug imaging studies [30].

drug solutions and intratracheal administration) was carried out in guinea pigs (model organism). Results indicated different distributions of the drug in connection with different method of administration [32].

2.2 MALDI MSI of other tissues

The (analytical) power of MALDI MSI has been demonstrated in many studies and with diverse types of tissues. For example, dermato-

logy/cosmetics use MALDI MSI to investigate the effect of age and peptide applications on the skin [33]. In other study from the fields of cosmetics and forensics, MALDI MSI was used to investigate reactions of hydrogen peroxide with cocaine in hair to provide information whether cocaine and his reaction products can be detected in hair after bleaching. It was found that all compounds of interest are in the hydrogen peroxide and wash solutions, and thus all evidence of cocaine use might be lost after a hair bleaching treatment [34]. An interesting study on MALDI MS/MS imaging of the drug tilidine in hair after external contamination revealed that for correct segmental hair analysis it is necessary to collect hair samples not only several weeks after intake but also within the first days after intake [35]. Another study on detection of blood in fingerprints revealed that MALDI MSI can support existing presumptive tests by detecting the molecules of haem and haemoglobin through their *m/z* ratios. Moreover, MALDI MSI is compatible with other methods employed for enhancing fingerprints contaminated by blood [36].

Mammalian retinas have also been investigated, and high resolution MALDI MSI was used to obtain information about the distribution of lipids on the retina [37]. Resolution at the level of a single cell was achieved.

Mesenchymal stem cells were investigated by MALDI MSI for the characterization of lipid markers of chondrogenic differentiation [38], and 20 different lipid species were identified.

Several studies focused on MALDI MSI of plant tissues. Soares et al. investigated hesperidin and rutin in Citrus sinensis grafted on Citrus limonia after infection by Xylella fastidiosa [39]. They suggested that hesperidin plays a role in the plant-pathogen interaction. In previous study, hypericin (a red anthraquinone-derivative with medicinal properties) and related phytochemicals were investigated in the leaves of Hypericum species by high resolution MALDI MSI [40]. Yet another study focused on using MALDI MSI to detect fungicide residue on wheat leaf surfaces, demonstrating the potential of MALDI MSI for monitoring the distribution of agrochemicals on leaves [41].

Insects have also been the subject of MALDI MSI. Klein et al. investigated plant-pest chemical interfaces inside leaves, specifically the interactions between soybean and aphids and rice and bacteria were studied [42]. Whole-body sections and various organs of the rove beetle, Paederus riparius, were investigated by atmospheric pressure high resolution scanning microprobe MALDI MSI to locate metabolites of the defensive compounds pederin, pseudopederin and pederon [43]. An interesting study from Brazil focused on queen bee signals in the stingless bee Friesella schrottkyi and illustrated the spatial distribution of active compounds on queen bees [44]. The spatial distribution of lipids in Drosophila melanogaster was also analyzed by MALDI MSI to provide more information about this model organism [45].

3. Conclusion

It is clear that MALDI MSI has potential in different research fields. Some significant improvements of MALDI imaging techniques have been made and surely these techniques will undergo important improvements and modernization to serve analyze tumors and other tissues. Further developments and the combination of MALDI MSI with other imaging techniques or quantitative methods will result in wider use of MALDI MSI, and clinical methods using MALDI MSI could be validated and applied in routine analytical processes in laboratories.

MALDI MSI can be used as supportive technique in clinical research, mainly in oncology. Finding new cancer biomarkers is so important that all suitable methods should be tested. The task for researchers is to find relevant analytical standards and make MALDI MSI a standard analytical method as soon as possible.

List of abbreviations

AES … atomic emission spectrometry
FT … Fourier transform
ICP … inductively coupled plasma
ICR … ion cyclotron resonance
ITO … indium-tin oxide
LA … laser ablation
LTQ … linear ion trap/linear trap quadrupole

MALDI … matrix assisted laser desorption/ ionization
MRI … magnetic resonance imaging
MS … mass spectrometry/spectrometer
MSI … mass spectrometry imaging
NEDC … N (1 naphthyl)ethylenediamine dihydrochloride
TOF … time-of-flight

Acknowledgments

The authors acknowledge Dr. Tara Massad for the language corrections and valuable comments on the early version of the manuscript. The financial support from "CEITEC–start_up" project (CZ.1.05/1.1.00/02.0068) and doctoral project "MALDI-IMAGE" (PGS27_2014) is greatly acknowledged.

Conflicts of Interest

The authors declare no conflict of interest.

References

1. Karas, M.; Bachmann, D.; Hillenkamp, F. Influence of the wavelength in high-irradiance ultraviolet-laser desorption mass-spectrometry of organic-molecules. Analytical Chemistry 1985, 57, 2935-2939.
2. Karas, M.; Hillenkamp, F. Laser desorption ionization of proteins with molecular masses exceeding 10000 Daltons. Analytical Chemistry 1988, 60, 2299-2301.
3. Stoeckli, M.; Chaurand, P.; Hallahan, D.E.; Caprioli, R.M. Imaging mass spectrometry: A new technology for the analysis of protein expression in mammalian tissues. Nature Medicine 2001, 7, 493-496.
4. Caprioli, R.M.; Farmer, T.B.; Gile, J. Molecular imaging of biological samples: Localization of peptides and proteins using MALDI-TOF MS. Analytical Chemistry 1997, 69, 4751-4760.
5. Solouki, T.; Marto, J.A.; White, F.M.; Guan, S.H.; Marshall, A.G. Attomole biomolecule mass analysis by matrix-assisted laser-desorption ionization fourier-transform ion-cyclotron resonance. Analytical Chemistry 1995, 67, 4139-4144.
6. Strupat, K.; Kovtoun, V.; Bui, H.; Viner, R.; Stafford, G.; Horning, S. MALDI produced ions inspected with a linear ion trap-orbitrap hybrid mass analyzer. Journal of the American Society for Mass Spectrometry 2009, 20, 1451-1463.
7. Chen, B.M.; Lietz, C.B.; Li, L.J. In situ characterization of proteins using laserspray ionization on a high-performance MALDI-LTQ-Orbitrap mass spectrometer. Journal of the American Society for Mass Spectrometry 2014, 25, 2177-2180.
8. Bednarik, A.; Kuba, P.; Moskovets, E.; Tomalova, I.; Krasensky, P.; Houska, P.; Preisler, J. Rapid matrix-assisted laser desorption/ionization time-of-flight mass spectrometry imaging with scanning desorption laser beam. Analytical Chemistry 2014, 86, 982-986.
9. Prentice, B.M.; Chumbley, C.W.; Caprioli, R.M. High-speed MALDI MS/MS imaging mass spectrometry using continuous raster sampling. Journal of Mass Spectrometry 2015, 50, 703-710.
10. Korte, A.R.; Yandeau-Nelson, M.D.; Nikolau, B.J.; Lee, Y.J. Subcellular-level resolution MALDI-MS imaging of maize leaf metabolites by MALDI-linear ion trap-Orbitrap mass spectrometer. Analytical and Bioanalytical Chemistry 2015, 407, 2301-2309.
11. Flinders, B.; Morrell, J.; Marshall, P.S.; Ranshaw, L.E.; Clench, M.R. The use of hydrazine-based derivatization reagents for improved sensitivity and detection of carbonyl containing compounds using MALDI-MSI. Analytical and Bioanalytical Chemistry 2015, 407, 2085-2094.
12. Wang, X.D.; Han, J.; Yang, J.C.; Pan, J.X.; Borchers, C.H. Matrix coating assisted by an electric field (MCAEF) for enhanced tissue imaging by MALDI-MS. Chemical Science 2015, 6, 729-738.
13. Caldwell, R.L.; Gonzalez, A.; Oppenheimer, S.R.; Schwartz, H.S.; Caprioli, R.M. Molecular assessment of the tumor protein microenvironment using imaging mass spectrometry. Cancer Genomics & Proteomics 2006, 3, 279-287.
14. Acquadro, E.; Cabella, C.; Ghiani, S.; Miragoli, L.; Bucci, E.M.; Corpillo, D. Matrix-assisted laser desorption ionization imaging mass spectrometry detection of a magnetic resonance imaging contrast agent in mouse liver. Analytical Chemistry 2009, 81, 2779-2784.
15. Bianga, J.; Bouslimani, A.; Bec, N.; Quenet, F.; Mounicou, S.; Szpunar, J.; Bouyssiere, B.; Lobinski, R.; Larroque, C. Complementarity of MALDI and LA ICP mass spectrometry for platinum anticancer imaging in human tumor. Metallomics 2014, 6, 1382-1386.
16. Dreisewerd, K. Recent methodological advances in MALDI mass spectrometry. Analytical and Bioanalytical Chemistry 2014, 406, 2261-2278.
17. Rompp, A.; Spengler, B. Mass spectrometry imaging with high resolution in mass and space. Histochemistry and Cell Biology 2013, 139, 759-783.
18. Svatos, A. Mass spectrometric imaging of small molecules. Trends in Biotechnology 2010, 28, 425-434.
19. Sun, N.; Ly, A.; Meding, S.; Witting, M.; Hauck, S.M.; Ueffing, M.; Schmitt-Kopplin, P.; Aichler, M.; Walch, A. High-resolution metabolite imaging of light and dark treated retina using MALDI- FTICR mass spectrometry. Proteomics 2014, 14, 913-923.
20. Wang, H.Y.J.; Wu, H.W.; Tsai, P.J.; Liu, C.B.; Zheng, Z.F. Matrix-assisted laser desorption/ionization mass spectrometry imaging of cardiolipins in rat organ sections. Analytical and Bioanalytical Chemistry 2014, 406, 565-575.
21. Shroff, R.; Schramm, K.; Jeschke, V.; Nemes, P.; Vertes, A.; Gershenzon, J.; Svatos, A. Quantification of plant surface metabolites by matrix-assisted laser desorption-ionization mass spectrometry imaging: Glucosinolates on Arabidopsis thaliana

leaves. Plant Journal 2015, 81, 961-972.
22. Louie, K.B.; Bowen, B.P.; Cheng, X.L.; Berleman, J.E.; Chakraborty, R.; Deutschbauer, A.; Arkin, A.; Northen, T.R. „Replica-extraction-transfer" nanostructure-initiator mass spectrometry imaging of acoustically printed bacteria. Analytical Chemistry 2013, 85, 10856-10862.
23. Nimesh, S.; Mohottalage, S.; Vincent, R.; Kumarathasan, P. Current status and future perspectives of mass spectrometry imaging. International Journal of Molecular Sciences 2013, 14, 11277-11301.
24. Kriegsmann, J.; Kriegsmann, M.; Casadonte, R. MALDI TOF imaging mass spectrometry in clinical pathology: A valuable tool for cancer diagnostics. International Journal of Oncology 2015, 46, 893-906.
25. Thomas, A.; Chaurand, P. Advances in tissue section preparation for MALDI imaging MS. Bioanalysis 2014, 6, 967-982.
26. Wang, J.N.; Qiu, S.L.; Chen, S.M.; Xiong, C.Q.; Liu, H.H.; Wang, J.Y.; Zhang, N.; Hou, J.; He, Q.; Nie, Z.X. MALDI-TOF MS imaging of metabolites with a N (1 naphthyl)ethylenediamine dihydrochloride matrix and its application to colorectal cancer liver metastasis. Analytical Chemistry 2015, 87, 422-430.
27. Buck, A.; Halbritter, S.; Spath, C.; Feuchtinger, A.; Aichler, M.; Zitzelsberger, H.; Janssen, K.P.; Walch, A. Distribution and quantification of irinotecan and its active metabolite SN-38 in colon cancer murine model systems using MALDI MSI. Analytical and Bioanalytical Chemistry 2015, 407, 2107-2116.
28. Rodrigo, M.A.M.; Zitka, O.; Krizkova, S.; Moulick, A.; Adam, V.; Kizek, R. MALDI-TOF MS as evolving cancer diagnostic tool: A review. Journal of Pharmaceutical and Biomedical Analysis 2014, 95, 245-255.
29. Krasny, L.; Hoffmann, F.; Ernst, G.; Trede, D.; Alexandrov, T.; Havlicek, V.; Guntinas-Lichius, O.; von Eggeling, F.; Crecelius, A.C. Spatial segmentation of MALDI FT-ICR MSI data: A powerful tool to explore the head and neck tumor in situ lipidome. Journal of the American Society for Mass Spectrometry 2015, 26, 36-43.
30. Huber, K.; Aichler, M.; Sun, N.; Buck, A.; Li, Z.; Fernandez, I.E.; Hauck, S.M.; Zitzelsberger, H.; Eickelberg, O.; Janssen, K.P., et al. A rapid ex vivo tissue model for optimising drug detection and ionisation in MALDI imaging studies. Histochemistry and Cell Biology 2014, 142, 361-371.
31. Vegvari, A.; Fehniger, T.E.; Rezeli, M.; Laurell, T.; Dome, B.; Jansson, B.; Welinder, C.; Marko-Varga, G. Experimental models to study drug distributions in tissue using MALDI mass spectrometry imaging. Journal of Proteome Research 2013, 12, 5626-5633.
32. Zecchi, R.; Trevisani, M.; Pittelli, M.; Pedretti, P.; Manni, M.E.; Pieraccini, G.; Pioselli, B.; Amadei, F.; Moneti, G.; Catinella, S. Impact of drug administration route on drug delivery and distribution into the lung: An imaging mass spectrometry approach. European Journal of Mass Spectrometry 2013, 19, 475-482.
33. Mondon, P.; Hillion, M.; Peschard, O.; Andre, N.; Marchand, T.; Doridot, E.; Feuilloley, M.G.J.; Pionneau, C.; Chardonnet, S. Evaluation of dermal extracellular matrix and epidermal-dermal junction modifications using matrix-assisted laser desorption/ionization mass spectrometric imaging, in vivo reflectance confocal microscopy, echography, and histology: Effect of age and peptide applications. Journal of Cosmetic Dermatology 2015, 14, 152-160.
34. Cuypers, E.; Flinders, B.; Bosman, I.J.; Lusthof, K.J.; Van Asten, A.C.; Tytgat, J.; Heeren, R.M.A. Hydrogen peroxide reactions on cocaine in hair using imaging mass spectrometry. Forensic Science International 2014, 242, 103-110.
35. Poetzsch, M.; Baumgartner, M.R.; Steuer, A.E.; Kraemer, T. Segmental hair analysis for differentiation of tilidine intake from external contamination using LC-ESI-MS/MS and MALDI-MS/MS imaging. Drug Testing and Analysis 2015, 7, 143-149.
36. Bradshaw, R.; Bleay, S.; Clench, M.R.; Francese, S. Direct detection of blood in fingermarks by MALDI MS profiling and imaging. Science & Justice 2014, 54, 110-117.
37. Ly, A.; Schone, C.; Becker, M.; Rattke, J.; Meding, S.; Aichler, M.; Suckau, D.; Walch, A.; Hauck, S.M.; Ueffing, M. High-resolution MALDI mass spectrometric imaging of lipids in the mammalian retina. Histochemistry and Cell Biology 2015, 143, 453-462.
38. Rocha, B.; Cillero-Pastor, B.; Eijkel, G.; Bruinen, A.L.; Ruiz-Romero, C.; Heeren, R.M.A.; Blanco, F.J. Characterization of lipidic markers of chondrogenic differentiation using mass spectrometry imaging. Proteomics 2015, 15, 702-713.
39. Soares, M.S.; da Silva, D.F.; Forim, M.R.; da Silva, M.F.d.G.F.; Fernandes, J.B.; Vieira, P.C.; Silva, D.B.; Lopes, N.P.; de Carvalho, S.A.; de Souza, A.A., et al. Quantification and localization of hesperidin and rutin in Citrus sinensis grafted on C. limonia after Xylella fastidiosa infection by HPLC-UV and MALDI imaging mass spectrometry. Phytochemistry 2015, 115, 161-170.
40. Kusari, S.; Sezgin, S.; Nigutova, K.; Cellarova, E.; Spiteller, M. Spatial chemo-profiling of hypericin and related phytochemicals in Hypericum species using MALDI-HRMS imaging. Analytical and Bioanalytical Chemistry 2015, 407, 4779-4791.
41. Annangudi, S.P.; Myung, K.; Adame, C.A.; Gilbert, J.R. MALDI-MS imaging analysis of fungicide residue distributions on wheat leaf surfaces. Environmental Science & Technology 2015, 49, 5579-5583.
42. Klein, A.T.; Yagnik, G.B.; Hohenstein, J.D.; Ji, Z.Y.; Zi, J.C.; Reichert, M.D.; MacIntosh, G.C.; Yang, B.; Peters, R.J.; Vela, J., et al. Investigation of the chemical interface in the soybean-aphid and rice-bacteria interactions using MALDI-mass spectrometry imaging. Analytical Chemistry 2015, 87, 5294-5301.
43. Bhandari, D.R.; Schott, M.; Rompp, A.; Vilcinskas, A.; Spengler, B. Metabolite localization by atmospheric pressure high-resolution scanning

microprobe matrix-assisted laser desorption/ ionization mass spectrometry imaging in whole-body sections and individual organs of the rove beetle Paederus riparius. Analytical and Bioanalytical Chemistry 2015, 407, 2189-2201.
44. Nunes, T.M.; Mateus, S.; Favaris, A.P.; Amaral, M.; von Zuben, L.G.; Clososki, G.C.; Bento, J.M.S.; Oldroyd, B.P.; Silva, R.; Zucchi, R., et al. Queen signals in a stingless bee: Suppression of worker ovary activation and spatial distribution of active compounds. Scientific Reports 2014, 4.
45. Niehoff, A.C.; Kettling, H.; Pirkl, A.; Chiang, Y.N.; Dreisewerd, K.; Yew, J.Y. Analysis of Drosophila lipids by matrix-assisted laser desorption/ ionization mass spectrometric imaging. Analytical Chemistry 2014, 86, 11086-11092.

The article is freely distributed under license Creative Commons (BY-NC-ND). But you must include the author and the document can not be modified and used for commercial purposes.

Utilization of graphene oxide electrophoretic deposition for construction of electrochemical sensors and biosensors

Jana Vlachova[1,2*], Jan Labuda[3], David Hynek[1,2], Ondrej Zitka[1,2] and Rene Kizek[1,2]

[1] Laboratory of Metallomics and Nanotechnologies, Department of Chemistry and Biochemistry, Mendel University in Brno, Zemedelska 1, CZ-613 00 Brno, Czech Republic; E-Mails: vlachova.jana@centrum.cz (V.J.), d.hynek@email.cz (D.H.), zitkao@seznam.cz (O.Z.), kizek@sci.muni.cz (R.K.)

[2] Central European Institute of Technology, Brno University of Technology, Technicka 3058/10, CZ-616 00 Brno, Czech Republic;

[3] Institute of Analytical Chemistry, Faculty of Chemical and Food Technology, Slovak University of Technology in Bratislava, Radlinského 9 81237, Bratislava, Slovakia; E-Mails: jan.labuda@stuba.sk (J.L.)

* Author to whom correspondence should be addressed; E-Mail: vlachova.jana@centrum.cz

Received:18.6.2015 / Accepted:20.6.2015 / Published: 1.10.2015

This review summarizes and discusses electrophoretic methods for the fabrication deposited graphene and graphene-based structures. Graphenes are commonly dispersed in organic solvents or in water. Deposition procedures are performed mostly under constant voltage and deposition time seems to be an important parameter for influence prepared graphene structures. It was shown that electrophoretically deposited graphene layers have excellent properties suitable for electrochemical sensors and biosensors construction, e.g. high electrical conductivity and large surface area. Electrophoretic deposition enables also preparation of material which combines graphene with metal nanoparticles or polymers.

Keywords: graphene oxide, electrophoretic deposition, sensor, biosensor

1. Introduction

Graphene and graphene oxide (GO) has attracted increasing interest of many scientists because of its unique properties which find application across many fields. Enormous number of papers regarding to graphene and graphene oxide are focused on improvement of preparation of these materials, their deposition on substrates and formation of novel graphene structures which enhance detection abilities of electrodes as sensitivity and electron transfer.

This mini-review focuses on the fabrication of GO-based electrodes prepared by electrophoretic deposition (EPD) and their utilization in electrochemical sensors and biosensors.

2. Graphene oxide

Graphene oxide along with carbon nanotubes, nanofibers, fullerens, nanodiamonds and nanocomposites are important carbon-based materials [1] which have been widely used for various applications as a catalyst of chemical reactions [2], luminescent nanomaterial [3,4], nanocomposite [5-8] and drug deliver [4,9]. Especially in electrochemistry, application of graphene oxide is employed in the photovoltaic device [10], chemical sensor and biosensors [11,12] due to wide electrochemical potential window, low charge-transfer resistance and great electrochemical activity [13].

Although the structure of GO was studied by several authors, amorphous character of GO and lack of analytical technique for its characterizing make an obstacles in GO characterization. Thus, despite numerous attempts to propose precise structure of GO, an unambiguous model has not been clarified yet, only the Lerf-Klinowski model is thought to be the most acceptable [14,15]. GO is formed of monolayer of carbon atoms which creates of two-dimensional hexagonal lattice with oxygenated functionalities as a carboxylic acid group, hydroxyl and epoxy groups [15]. The consequences of oxygenated groups on surface are hydrophilicity and solubility of GO in water and other organic solvents [16]. Through these oxygenated groups

and non-covalent binding via π-π stacking, cation-π or van der Waals interactions on the sp2 networks, GO can be easily modified by diverse small molecules and polymers which lead to improvement of electrical, thermal and mechanical properties of graphene oxide [15].

The GO is commonly prepared by oxidation of graphite using various methods. Three most popular methods were proposed by Brodie [17], Staudenmaier [18] and Hummers [19]. The shortest and recently most used method is the Hummers method [20]. Preparation and functionalization of GO-based electrodes can be performed by several methods. Basic approach involves simple evaporation of GO suspension on the electrode surface. Unfortunately, layer formed using this method causes aggregation of GO and nonuniform deposition [21]. Using of spin-coater is more sophisticated method which create thin continuous layer [22]. Langmuir-Blodgett [23] and layer-by-layer [24] method are another alternative approaches mainly useful for sensors fabrication. Interesting method of GO deposition, which creates uniform layer, is vacuum filtration [25]. This method involves filtration of GO sheets suspension through porous membrane where GO sheets lodge and form a film. This film can be transferred onto electrode by gently pressing the film against electrode surface [21]. Direct pattering using for example inject printing of GO also offers opportunity how create layer of GO directly onto substrates [26]. The last approach for modification of electrodes is electrophoretic deposition which is described below.

3. Electrophoretic deposition

Electrophoretic deposition is a two-step process in which charged particles, dispersed or suspended in a liquid medium, move toward conductive substrate of opposite charge through the application of external electric field and then deposit on it [27,28]. According to the charge of deposited particles, there exist two types of EPD. When the particles are negatively charged, application of the electric field causes deposition of particles on positively charge electrode (anode). This process is called anodic EPD. Opposite to this process is EDP of positively charged particles on negatively charged electrode (cathode) which is called cathodic EPD [28].

EPD is simple short-time process which requires cost-efficient equipment and provides the possibility of scaling up to large dimensions [27]. The main factors influencing EPD, among others, are applied voltage, deposition time, distance between electrodes and properties of used solvent. Via alteration of these parameters the thickness and morphology of deposited layer can be easily controlled [28]. Due to EPD, it is possible to modify any shape of conductive surface by GO with diverse kind of molecules as metal ions [29], particles [30], carbon nanotubes [31], biopolymers [32] and so to create a compact thin film as well as complex 3D structures [13,27,28]. A disadvantage is EPD performed in an aqueous medium where the application of voltage higher then 3-4 V leads to the formation of gas bubbles because of water electrolysis. Decomposition of water can be avoided by using alternating current where the main influencing factor is frequency [33,34]. Comparison of different reports shows wide variation of EPD condition. For example, applied voltage ranges from 5 up to 300 V, deposition time ranges from few seconds to half hour and GO is dispersed in water or organic solvents. Worth noticing is that only few papers describe creation of gas bubbles during EPD from water where high voltages were applied while other authors did not mention it [27].

4. Sensors and biosensors

Various structures of pure GO or modified with metal ions, particles or biopolymers prepared by electrophoretic deposition have a wide potential for application in sensors and biosensors. High sensitivity of electrodes modified with GO allows miniaturization of detection systems into portable device. Such sensors could find usage in fields as an food quality control or clinical diagnosis [13].

4.1 Sensors for clinical diagnosis

GO-based electrodes offer a new approach for sensors used in clinical diagnosis. For example reduced GO-$Ni(OH)_2$ composite for nonenzy-

matic glucose sensing was prepared by EPD on gold electrode from mixture of reduced GO (rGO) with $NiCl_2 \cdot 6\ H_2O$ in ethanol at 50 V for 20 seconds. Ni^{2+} ions decorated negatively charged GO sheet and such positively charged rGO-Ni^{2+} sheets in electric field move to cathode and deposit on it (Figure 1). rGO-$Ni(OH)_2$ composite was accomplished by cycling in 0.1 M NaOH. Electrochemical measurement of glucose on rGO-$Ni(OH)_2$ modified electrode was based on electrooxidation of $Ni(OH)_2$ on NiOOH in alkaline solution following oxidation of glucose to gluconic acid while NiOOH reduce back to $Ni(OH)_2$ [35].

Another possibility of utilization of graphene material as graphene nanowalls is for DNA

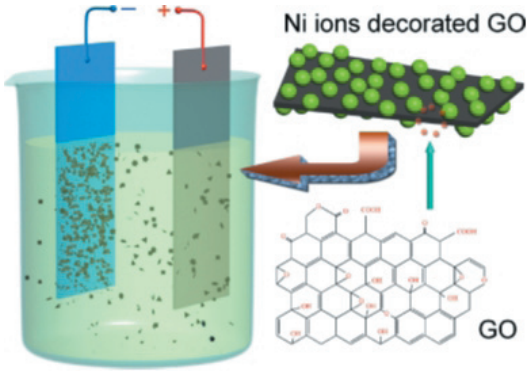

Figure 1: Schema of EPD of GO-Ni^{2+} sheets. Ni^{2+} ions decorated negatively charged GO sheet and such positively charged rGO-Ni^{2+} sheets in electric field move to cathode and deposit on it. (Reprinted with permission from ref 8. Copyright 2013 American Chemical Society.)

xture of GO and $Mg(NO_3)_2 \cdot 6\ H_2O$ on the similar principle as was written above. EPD was carried out in aqueous suspension of GO-Mg^{2+} sheets at 30 V for 10 minutes and such modified electrode was subsequently reduced by hydrazine vapor for 1 hour. An Electrode modified by the graphene nanowalls was able to detect all four free bases simultaneously even bases bounded in ssDNA and dsDNA in femtomolar concentrations. Due to high sensitivity, authors were able to detect single-based mismatch in sequence of DNA [36].

Later this modification was used for the determination of leukemia and normal blood cells based on an electrochemical detection of the guanine oxidation. It was found that the current signal of guanine was significantly higher in the case of leukemia cells than in normal cell and, moreover, the peak position of leukemia cells was observed at lower potential 0.61 V than in normal cell 0.76 V [37]. Previous study of free and bounded guanine showed the position of peaks at 0.57 V and 0.71 V, respectively [36]. The authors concluded that the higher signal and shift of potential to lower values for leukemia cells could be consequence of increased concentration of free guanine in electrolyte. This increased concentration could be caused by penetration of extremely sharped edges of graphene nanowalls into the cells and release of overexpressed free guanine from

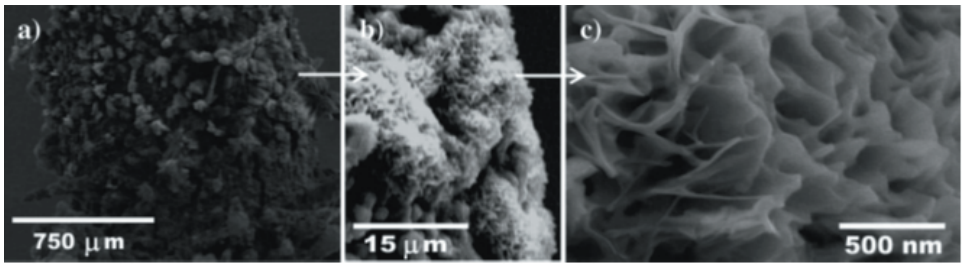

Figure 2: Images of electrode modified by graphene nanowalls obtained using field-emission scanning electron microscopy working at 15 kV. (Reprinted with permission from ref 36. Copyright 2012 American Chemical Society.)

sensors (Figure 2). Graphene nanowalls were created by EPD on graphite electrode from mi-

cancer cells [37]. Possible indicator of renal as well as liver diseases is increased level of

urea in serum, blood or urine. For urea sensing, the mesoporous silica particle embedded GO platform was created. EPD on indium tin oxide (ITO) glass substrate was performed at 120 V for 2 minutes in mixture of SiO_2 particles and GO in acetonitrile and with addition of $Mg(NO_3)_2 \cdot 6 H_2O$ as an electrolyte and to ensure creation of surface charge on the GO. After EPD, the immobilization of urease and glutamate dehydrogenase (GLDH) enzymes was carried out to create biosensor for urea sensing. The electrochemical detection of urea was performed in the presence of nicotinamide adenine dinucleotide (NADH) and α-ketoglutarate using cyclic voltammetry in phosphate buffer saline containing $[Fe(CN)_6]^{3-/4-}$. Increased concentration of urea triggers system lead to the decomposition of urea by urease, then electrons are transfered to α-ketoglutarate which is transformed to 2-L-glutamete by GLDH. Finally, 2-L-glutamete reduces $[Fe(CN)_6]^{3-}$ to $[Fe(CN)_6]^{4-}$ which is oxidized back on the electrode surface (Figure 3) [30].

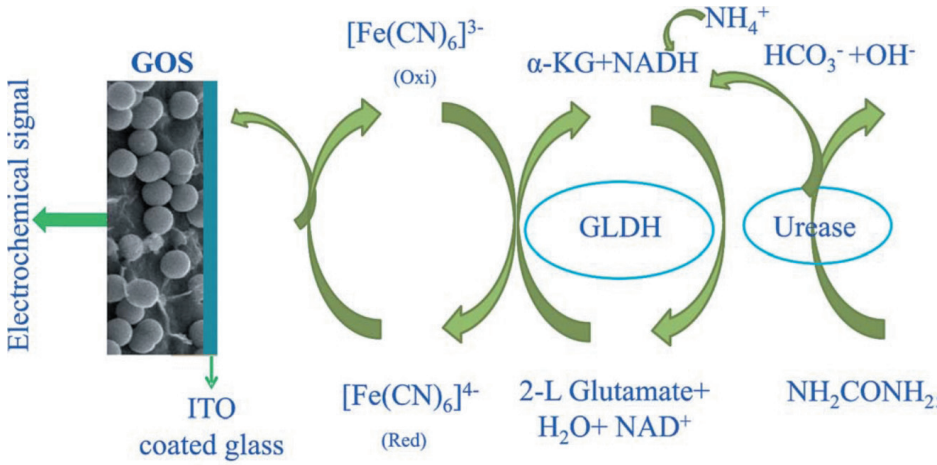

Figure 3: Schema of urea sensing using GO-based bioelectrode. Electrons from urea decomposition are transferred via GLDH, α-ketoglutarate and $[Fe(CN)_6]^{3-}$ to electrode surface. (Reprinted from ref 30.)

4.2 Sensors for food analysis

The graphene-based sensors can be used in food analysis as well as in clinical diagnosis. These sensors can be utilized for detection of nutrients or food toxins. Quercetin is natural flavonoid which plays important role in medical and nutritional science because of its antioxidant activity, cardiovascular protection and anti-inflammatory activity. Due these properties, detection of quercetin has become conscious of increased interest. Such sensor for quercetin was prepared by EPD at 1.7 V from aqueous solution of graphene with addition of KCl on glassy carbon electrode and after modified with β-cyclodextrin by electro-polymerization. Detection of quercetin using such modified electrode was studied in real samples of tea and honeysuckle [32].

For food quality control, the detection of food toxin is very important. Alfatoxin B1 is secondary fungal metabolite produced by Aspergillus flavus and Aspergillus parasiticus which is responsible for human hepatocellular carcinoma. The utilization of graphene oxide could be useful platform for creation of immunosensor for alfatoxin B1 detection. For example, electrode modified with rGO-Mg^{2+} sheets using EPD at 60-70 V for 2 minutes was functionalized with monoclonal antibody for alfatoxin B1 and then utilized for the electrochemical sensing studies of alfatoxin [38,39].

Overview of EPD conditions for modifications of electrode by GO described above is shown in Table 1.

GO modification	solvent	voltage	time	application	reference
rGO-$Ni(OH)_2$	ethanol	50 V	20 s	glucose detection	[35]
rGO-Mg^{2+} sheets	water	30 V	10 min	DNA detection	[36]
rGO-Mg^{2+} sheets	water	30 V	10 min	leukemia cell detection	[37]
rGO	water	150 V	20 s	lysozyme detection	[40]
GO-SiO_2 particles	acetonitrile	120 V	2 min	urea detection	[30]
GR/β-cyclodextrin	water	1.7	–	quercetin detection	[32]
rGO-Mg^{2+} sheets	acetonitrile	60-70 V	2 min	aflatoxin B1 detection	[38,39]

5. Conclusions

This review summarizes the utilization of GO-based electrodes prepared by the electrophoretic deposition for application in sensors and biosensors. The electrodes for such application can be modified by pure graphene oxide, graphene oxide with SiO_2 particles or biopolymers. However, the most often modification of the GO-based electrodes used in sensors and biosensors is the modification by metal ions. Electrophoretic deposition of such GO-M+ sheets leads to the formation of 3D structures of graphene oxide which cause an increase of the active surface of electrode and improve an electron transfer from analyte to the electrode surface which result in significant increase of the sensitivity.

Acknowledgments

Financial support from NanoBioTECell P102/11/1068 and the Scientific Grant Agency VEGA of the Slovak Republic (Project No 1/0361/14) is highly acknowledged.

Conflicts of Interest

State any potential conflicts of interest here or "The authors declare no conflict of interest".

The authors declare they have no potential conflicts of interests concerning drugs, products, services or another research outputs in this study. The Editorial Board declares that the manuscript met the ICMJE „uniform requirements" for biomedical papers.

References

1. Cha, C.; Shin, S.R.; Annabi, N.; Dokmeci, M.R.; Khademhosseini, A. Carbon-based nanomaterials: Multifunctional materials for biomedical engineering. ACS Nano 2013, 7, 2891-2897.
2. Pyun, J. Graphene oxide as catalyst: Application of carbon materials beyond nanotechnology. Angewandte Chemie International Edition 2011, 50, 46-48.
3. Jeon, S.-J.; Kwak, S.-Y.; Yim, D.; Ju, J.-M.; Kim, J.-H. Chemically-modulated photoluminescence of graphene oxide for selective detection of neurotransmitter by "turn-on" response. Journal of the American Chemical Society 2014, 136, 10842-10845.
4. Sun, X.; Liu, Z.; Welsher, K.; Robinson, J.T.; Goodwin, A.; Zaric, S.; Dai, H. Nano-graphene oxide for cellular imaging and drug delivery. Nano research 2008, 1, 203-212.
5. Jasinski, J.B.; Ziolkowska, D.; Michalska, M.; Lipinska, L.; Korona, K.P.; Kaminska, M. Novel graphene oxide/manganese oxide nanocomposites. RSC Advances 2013, 3, 22857-22862.
6. Yang, X.; Tu, Y.; Li, L.; Shang, S.; Tao, X.-m. Well-dispersed chitosan/graphene oxide nanocomposites. ACS Applied Materials & Interfaces 2010, 2, 1707-1713.
7. Maheshkumar, K.V.; Krishnamurthy, K.;

Sathishkumar, P.; Sahoo, S.; Uddin, E.; Pal, S.K.; Rajasekar, R. Research updates on graphene oxide-based polymeric nanocomposites. Polymer Composites 2014, 35, 2297-2310.
8. Zhang, H.; Zhang, X.; Zhang, D.; Sun, X.; Lin, H.; Wang, C.; Ma, Y. One-step electrophoretic deposition of reduced graphene oxide and ni(oh)2 composite films for controlled syntheses supercapacitor electrodes. The Journal of Physical Chemistry B 2013, 117, 1616-1627.
9. Liu, J.; Cui, L.; Losic, D. Graphene and graphene oxide as new nanocarriers for drug delivery applications. Acta Biomaterialia 2013, 9, 9243-9257.
10. Yin, Z.; Sun, S.; Salim, T.; Wu, S.; Huang, X.; He, Q.; Lam, Y.M.; Zhang, H. Organic photovoltaic devices using highly flexible reduced graphene oxide films as transparent electrodes. ACS Nano 2010, 4, 5263-5268.
11. Shao, Y.; Wang, J.; Wu, H.; Liu, J.; Aksay, I.A.; Lin, Y. Graphene based electrochemical sensors and biosensors: A review. Electroanalysis 2010, 22, 1027-1036.
12. Sharma, P.; Tuteja, S.K.; Bhalla, V.; Shekhawat, G.; Dravid, V.P.; Suri, C.R. Bio-functionalized graphene–graphene oxide nanocomposite based electrochemical immunosensing. Biosensors and Bioelectronics 2013, 39, 99-105.
13. Gao, H.; Duan, H. 2d and 3d graphene materials: Preparation and bioelectrochemical applications. Biosensors and Bioelectronics 2015, 65, 404-419.
14. He, H.; Klinowski, J.; Forster, M.; Lerf, A. A new structural model for graphite oxide. Chemical Physics Letters 1998, 287, 53-56.
15. Dreyer, D.R.; Park, S.; Bielawski, C.W.; Ruoff, R.S. The chemistry of graphene oxide. Chemical Society Reviews 2010, 39, 228-240.
16. Zhu, Y.; Murali, S.; Cai, W.; Li, X.; Suk, J.W.; Potts, J.R.; Ruoff, R.S. Graphene and graphene oxide: Synthesis, properties, and applications. Advanced Materials 2010, 22, 3906-3924.
17. Brodie, B.C. On the atomic weight of graphite. Philosophical Transactions of the Royal Society of London 1859, 149, 249-259.
18. Staudenmaier, L. Verfahren zur darstellung der graphitsäure. Berichte der deutschen chemischen Gesellschaft 1898, 31, 1481-1487.
19. Hummers, W.S.; Offeman, R.E. Preparation of graphitic oxide. Journal of the American Chemical Society 1958, 80, 1339-1339.
20. Ciszewski, M.; Mianowski, A. Survey of graphite oxidation methods using oxidizing mixtures in inorganic acids. CHEMIK 2013, 67, 267-274.
21. Chen, D.; Feng, H.; Li, J. Graphene oxide: Preparation, functionalization, and electrochemical applications. Chemical Reviews 2012, 112, 6027-6053.
22. Becerril, H.A.; Mao, J.; Liu, Z.; Stoltenberg, R.M.; Bao, Z.; Chen, Y. Evaluation of solution-processed reduced graphene oxide films as transparent conductors. ACS Nano 2008, 2, 463-470.
23. Li, X.; Zhang, G.; Bai, X.; Sun, X.; Wang, X.; Wang, E.; Dai, H. Highly conducting graphene sheets and langmuir-blodgett films. Nat Nano 2008, 3, 538-542.
24. Ramesha, G.K.; Sampath, S. Electrochemical reduction of oriented graphene oxide films: An in situ raman spectroelectrochemical study. The Journal of Physical Chemistry C 2009, 113, 7985-7989.
25. Eda, G.; Lin, Y.-Y.; Miller, S.; Chen, C.-W.; Su, W.-F.; Chhowalla, M. Transparent and conducting electrodes for organic electronics from reduced graphene oxide. Applied Physics Letters 2008, 92, 233305.
26. Dua, V.; Surwade, S.P.; Ammu, S.; Agnihotra, S.R.; Jain, S.; Roberts, K.E.; Park, S.; Ruoff, R.S.; Manohar, S.K. All-organic vapor sensor using inkjet-printed reduced graphene oxide. Angewandte Chemie International Edition 2010, 49, 2154-2157.
27. Chavez-Valdez, A.; Shaffer, M.S.P.; Boccaccini, A.R. Applications of graphene electrophoretic deposition. A review. The Journal of Physical Chemistry B 2013, 117, 1502-1515.
28. Besra, L.; Liu, M. A review on fundamentals and applications of electrophoretic deposition (epd). Progress in Materials Science 2007, 52, 1-61.
29. Wu, Z.-S.; Pei, S.; Ren, W.; Tang, D.; Gao, L.; Liu, B.; Li, F.; Liu, C.; Cheng, H.-M. Field emission of single-layer graphene films prepared by electrophoretic deposition. Advanced Materials 2009, 21, 1756-1760.
30. Abraham, S.; Ciobota, V.; Srivastava, S.; Srivastava, S.K.; Singh, R.K.; Dellith, J.; Malhotra, B.D.; Schmitt, M.; Popp, J.; Srivastava, A. Mesoporous silica particle embedded functional graphene oxide as an efficient platform for urea biosensing. Analytical Methods 2014, 6, 6711-6720.
31. Lu, T.; Pan, L.; Li, H.; Nie, C.; Zhu, M.; Sun, Z. Reduced graphene oxide–carbon nanotubes composite films by electrophoretic deposition method for supercapacitors. Journal of Electroanalytical Chemistry 2011, 661, 270-273.
32. Zhang, Z.; Gu, S.; Ding, Y.; Shen, M.; Jiang, L. Mild and novel electrochemical preparation of β–cyclodextrin/graphene nanocomposite film for super-sensitive sensing of quercetin. Biosensors and Bioelectronics 2014, 57, 239-244.
33. Neirinck, B.; Fransaer, J.; Vleugels, J.; Van der Biest, O. Aqueous electrophoretic deposition at high electric fields. Key Engineering Materials 2009, 412, 33-38.
34. Chávez-Valdez, A.; Boccaccini, A.R. Innovations in electrophoretic deposition: Alternating current and pulsed direct current methods. Electrochimica Acta 2012, 65, 70-89.
35. Subramanian, P.; Niedziolka-Jonsson, J.; Lesniewski, A.; Wang, Q.; Li, M.; Boukherroub, R.; Szunerits, S. Preparation of reduced graphene oxide-ni(oh)2 composites by electrophoretic deposition: Application for non-enzymatic glucose sensing. Journal of Materials Chemistry A 2014, 2, 5525-5533.
36. Akhavan, O.; Ghaderi, E.; Rahighi, R. Toward single-DNA electrochemical biosensing by graphene nanowalls. ACS Nano 2012, 6, 2904-2916.
37. Akhavan, O.; Ghaderi, E.; Rahighi, R.; Abdolahad, M. Spongy graphene electrode in electrochemical

detection of leukemia at single-cell levels. Carbon 2014, 79, 654-663.
38. Srivastava, S.; Kumar, V.; Ali, M.A.; Solanki, P.R.; Srivastava, A.; Sumana, G.; Saxena, P.S.; Joshi, A.G.; Malhotra, B.D. Electrophoretically deposited reduced graphene oxide platform for food toxin detection. Nanoscale 2013, 5, 3043-3051.
39. Basu, J.; Datta, S.; RoyChaudhuri, C. A graphene field effect capacitive immunosensor for sub-femtomolar food toxin detection. Biosensors and Bioelectronics 2015, 68, 544-549.
40. Subramanian, P.; Lesniewski, A.; Kaminska, I.; Vlandas, A.; Vasilescu, A.; Niedziolka-Jonsson, J.; Pichonat, E.; Happy, H.; Boukherroub, R.; Szunerits, S. Lysozyme detection on aptamer functionalized graphene-coated spr interfaces. Biosensors and Bioelectronics 2013, 50, 239-243.

The article is freely distributed under license Creative Commons (BY-NC-ND). But you must include the author and the document can not be modified and used for commercial purposes.

REVIEW

Influence of Different Inducers on Ligninolytic Enzyme Activities

Martina Vrsanska[1]*, Alena Buresova[1], Pavel Damborsky[2], Vojtech Adam[1]

[1] Department of Chemistry and Biochemistry, Faculty of Agronomy, Mendel University in Brno, Zemedelska 1, CZ-613 00 Brno, Czech Republic, European Union; E-Mail: alena.buresova@mendelu.cz (AB), vojtech.adam@mendelu.cz (VA)

[2] Institute of Chemistry, Faculty of Chemical and Food Technology, Slovak University of Technology in Bratislava, Radlinskeho 9, 812 37 Bratislava, Slovak republic, European Union; E-Mail: chempada@savba.sk (PD)

* Author to whom correspondence should be addressed; E-Mail: xvrsansk@mendelu.cz;
Tel.: +420 734 252 656.

Received:26.6.2015 / Accepted: 26.6.2015 / Published:1.10.2015

White rot fungi are important for their efficient, various and complex ligninolytic enzyme system, which is able to degrade wide variety of compounds including lignin. These enzymes are desirable for using in various industrial and bioremediation applications. However, ligninolytic enzymes are produced by fungi only in small quantities, so their use in biotechnological processes is limited due to low productivity and high economic costs. Thus, there is a great demand in induction, enhancement and stabilization of ligninolytic enzymes. The main scope of this review is to briefly summarize general and specific concepts about induction of ligninolytic enzymes produced by white rot basidiomycetes.

Keywords: white-rot fungi; enzyme activity; inducer;

1. Introduction

Enzymes have a wide range of technological applications in various fields of human activities such as food, textile, paper and pharmaceutical industries. Enzymes also play very important role in biological remediation [1], the process leading to the removal, detoxification or transformation of various organic pollutants in environment. They are also applied in nanobiotechnology, where they are used as biosensors, the analytical tools for the analysis of bio-material samples [2]. The use of enzymes for this purpose, however, entails certain limitations. These are mainly the high cost of commercial preparations and therefore are constantly looking for new, cheaper and natural sources.

One of the potencial enzyme producers are fungi that have broad enzymatic equipment. They are currently the focus of considerable attention due to their diverse application [3].

Fungi are able to decompose, or cause to deteriorate a huge variety of materials and compounds such a different type of wood, textile, stored paper, plastics, leather and diverse materials using for wrapping [4].

Species of basidiomycetes are considered to be a very interesting group of fungi including different ecological groups such as white rot, brown rot, and leaf litter fungi [5, 6]. Among them, only the white rot fungi are able to efficiently decompose lignin due to the production of ligninolytic enzymes. Lignin, a complex aromatic biopolymer, makes structural rigidity to wood and protects it from microbial attack [7] and it is extremely recalcitrant to degradation [8]. Ligninolytic enzymes are also capable of degrading various environmental pollutants, including polycyclic aromatic hydrocarbons, synthetic dyes, pesticides, polychlorinated biphenyls, herbicides and many other xenobiotics. However, ligninolytic enzymes from white rot fungi are only secreted in small amounts, so their using in industrial applications has been limited due to low productivity and high economic cost [9, 10]. A higher enzyme activity guarantees a higher and faster transformation of the target substrate and improves the applicability and effectiveness of enzyme-catalyzed processes [11].

The main scope of the review is to briefly encompass general and specific concepts about possibilities, how to increase enzyme activity of white rot fungi using natural or synthetic inducers.

2. Ligninolytic Enzymes of White Rot Fungi

Each of white rot basidiomycetes produced different enzymes, depending on cultivation conditions. Secretion of enzymes is influenced by different aspects, such as fungal species, culture type, aeration and cultivation time [12, 13, 14, 15]. These enzymes are usually produced extracellulary as secondary metabolites and they can degrade different plant materials and can colonize lot of environmental parts [16].

Fungi can secrete various isoforms of the same enzyme [14]. These isoenzymes are different in their stability, optimal pH and temperature and affinity for different substrates [16, 17].

The most important ligninolytic enzymes of white rot fungi are phenol oxidase laccase (Lac, E.C. 1.10.3.2) [18] and three heme peroxidases: lignin peroxidase (LiP, E.C.1.11.1.14), Mn dependant peroxidase (MnP, E.C. 1.11.1.13) [19] and versatile peroxidase (VP, E.C. 1.11.1.16) [20]. Other enzymes, secreted by white rot fungi, are associated with ligninolytic enzymes in lignin degradation but are unable to degrade lignin alone. For example, glyoxal oxidase (E.C. 1.2.3.5) and superoxide dismutase (E.C. 1.15.1.1) produce the H_2O_2 required by LiP and MnP [21].

Laccase is blue copper oxidase which contains four copper atoms per molecule in the catalytic center and catalyzes the four electron reduction of oxygen to water [22, 23]. Laccase is able to oxidize a huge variety of organic or inorganic compounds, including phenols (e.g. catechol, hydroquinone, 2,6-dimethoxyphenol and syringaldazine) [24, 25], aromatic amines and ascorbate [26]. Laccase is often produced in the form of numerous isoenzymes [27].

Lignin peroxidase is glycosylated protein containing heme. In the presence of endogenously produced peroxide, LiP catalyzes the oxidation of aromatic non-phenolic lignin structures to give aryl-cation radicals [28]. The oxidative lignin degradation requires the presence of veratryl alcohol, which is the substrate for LiP and also secreted fungal metabolite [29].

Mangan dependent peroxidase is also enzyme containg heme. It catalyzes H_2O_2 dependent oxidation of Mn^{2+} to highly reactive Mn^{3+}. After the cation Mn^{3+} subsequently oxidizes phenolic parts of lignin to produce free radicals. The high reactivity of Mn^{3+} is stabilized by chelators (oxalate, malonate, maleate), which are secreted by fungus [30].

Versatile peroxidase has catalytic properties of LiP and MnP. VP secreted by P. eryngii showed high sequence and structural homology with LiP, but also comprises a binding site for Mn^{2+}. It is not yet clear how much VP are expanded, but their presence suggests a close relationship with LiP and MnP [30].

Some white rot basidiomycetes contain all of these lignin-modifying enzymes, while others contain only one or two of these enzymes [31].

3. Induction of Fungal Enzyme Activity

Enzyme activity can be affected by many factors. The most critical factors are concentration of carbon, nitrogen and inducer agent [32]. The inducer is a specific molecule that induces synthesis of the relevant inducible enzyme and is usually a substrate for a given enzyme. The inducers are natural (wood, wheat, straw, fruit, etc.) [33, 34, 35, 36] or synthetic compounds (2,5-xylidine, guaiacol, ferulic acid, 2,6- dimethoxyphenol etc.) [37, 28, 38, 39, 40], which depending on the enzyme.

3.1 Nitrogen, and Carbon Sources, and Natural Inducers

Amount of carbon, nitrogen and inducer is considered to be limiting for large scale production of fungal enzymes [10]. It is well known that the white rot fungus, Phanerochaete chrysosporium, cultivated in synthetic medium, produces LiP and MnP only under nitrogen-limited conditions [41]. However, it was found that in the presence of lignocellulosic substrate, a high nitrogen concentration stimulates these enzymes production [34, 42, 43]. Previous studies have proved that both the nature and

concentration of nitrogen sources are powerful nutrition factors regulating ligninolytic enzyme secretion [44, 45, 46].

Songulashvili et al. [34] tested several inorganic and organic nitrogen sources in submerged fermentation of wheat bran to improve enzyme production by Ganoderma lucidum. The maximal value of laccase activity was revealed in supplementation of culture medium with KNO_3. The same compound slightly stimulated MnP accumulation. Among organic compounds, peptone appeared to be the appropriate nitrogen source for laccase accumulation. Levin et al. [47] used different nitrogen sources (amino acids, yeast extract, peptone) and found that the highest laccase activity was with L-glutamic acid by Trametes trogii.

The concentrate of carbon in nutrient medium and lignocellulosic substrate play important role in enzyme expression [48, 49]. Galhaup et al. [48] studied that the expressive production of laccase by Trametes pubescens started when the glucose concentration in the growth medium was a certain low, critical concentration. Cellobiose and glucose that were efficiently and quickly utilized by T. pubescens resulted in high levels of laccase activity [12]. According to Bettin et al. [50] the laccase activity in Pleurotus sajor-caju cultivation in glucose media was higher than those obtained with lactose. The contrary, lactose appeared to be the best carbon source for the laccase production by Pseudotrametes gibbosa and good for the enzyme secretion by Cerrena unicolor and Fomes fomentarius. In addition, glycerol also had significant accumulation of laccase by these three fungi [12].

Many authors used wheat straw, sawdust or bran as a substrate for increase enzyme activity [34, 51, 52, 53, 54]. Stajic et al. [35] studied that the medium carbon sources mandarine peels and grapevine sawdust for Pleurotus eryngii and Pleurotus ostreatus were the best for highest laccase activity. Makela et al. [55] found the maximal LiP activities and noticeable levels of MnP, when they used wood as a carbon source with milled alder as inducer. Bazanella et al. [56] tested agricultural and food wastes as substrate for Pleurotus pulmonarius. The highest activities of laccase were found in wheat bran, pineapple peel and orange peel. The highest activities of Mn peroxidase were obtained in pineapple peel cultures.

3.2 Synthetic Inducers

Enzyme activity can be increased not only by addition of the natural inducers, but also using synthetic inducers. It has been reported [37, 49, 57] that the addition of aromatic compound 2,5-xylidine induces several times more the laccase activities of white rot basidiomycetes. Another aromatic compounds such as ferulic acid, guaiacol, veratryl alcohol and 1-hydroxybenzotriazole have been used to increase laccase secretion [58, 59, 60]. Kuhar et al. [39] and Wang et al. [61] used ferulic acid as inducer for the highest laccase activity.

Novotný et al. [40] used Tween 80 and MnP activity was increased. Gassara et al. [62] observed that addition of Tween 80 caused the highest values of MnP activity produced by P. chrysosporium. Also in the work of Usha et al. [63] Tween 80 stimulated the production of ligninolytic enzymes secreted by Stereum ostrea. Munoz et al. [64] studied laccase of P. eryngii in the glucose medium, which contained ammonium-tartrate, and they obtained two isoenzymes with laccase activity.

Some solvents can be used to dissolve water-insoluble molecules for studies of their activity as enzyme inducers. For example dimethyl sulfoxide or ethanol are very often used as solvents to dissolve water-insoluble compounds for determination of enzyme activities. However, ethanol is also used as an active solvent to induce enzyme activity [65]. Lee et al. [66] added ethanol as a solvent to a medium containing glucose as the carbon source, laccase activity by T. versicolor increased. They also observed a mediators effect of ethanol on laccase production by Grifola frondosa and Coriolus hirsutus.

3.3 Metal Inducers

Some heavy metals are necessary for fungi, some aren't, but they can be toxic, when present in excess [33]. Usually the metals start to be toxic in concentration only a few times greater than those required [67]. The essential

fungal metals include copper, iron, zinc, nickel, manganese and molybdenum. Nonessential metals are chromium, cadmium, mercury lead and silver [68].

For white rot fungi the most important metal is manganese and copper. It has been reported that manganese plays a regulatory role in the expression of LiP, MnP, Lac and in the degradation of lignin [68, 69]. Copper is a cofactor in the catalytic center of laccase. Tinoco et al. [70] induce laccase secretion in Pleurotus ostreatus through culture medium optimization containing lignin and Cu^{2+} as inducers.

The positive synergistic effect was showed between Cu^{2+} and lignin, where the activity increased 60-fold. Metal responsive elements have also been identified in several laccase genes [33], what can explain the positive effect of copper ion on laccase level. Palmieri et al. [71] also observed supplementation of P. ostreatus cultures with Cu^{2+} and higher secretion of all laccase isoenzymes by the fungus. This result is similar to work of Khammuang et al. [72], where high levels of laccase activity after addition of Cu^{2+} were observed. The presence of copper in the catalytic center of the enzyme has been known for a lot time, but the importance of regulation role of copper in laccase production has just recently been studied [33]. The positive effect of the addition of metal ions on the production of enzyme was studied by lot of authors [42, 55, 62, 71-77, 83-85] (Table 1)

The induction of laccase by other metals, that are able to cause oxidative stress, was studied with T. pubescens by Galhaup et al. [78]. They also observed that laccase activity secreted by P. ostreatus was increased by the addition of 1-5 mM cadmium.

Extracellular enzymes must face high concentrations of metals, because they are not protected by the cell-associated metal-detoxication mechanism. When metals enter into the cell, they are able to influence the production of extracellular enzymes on the levels of transcriptional and translational regulation [33]. It seems, that low concentrations of essential heavy metals are necessary for the development of the ligninolytic enzyme system [79]. Addition of low concentrations of zinc and cooper into the metal-free synthetic cultivation medium increased the activity of LiP and MnP of P. chrysosporium [79].

4. Conclusion

White rot basidiomycetes have efficient, various and complex ligninolytic enzyme system. They have been successfully applied for treatment and decomposition of different phenolic compounds, dyes and other xenobiotics. The use of enzymes for the treatment or the removal of environmental and industrial pollutants has attracted increasing attention because of their high efficiency and high selectivity. The main issue of their implementation at industrial scale is the low yield of ligninolytic enzymes in most white rot fungi. For a more efficient secretion of these enzymes are necessary inducers of enzyme activity. Inducers have varies forms, they can be as natural substrates (straw, wood, lignin) or they can be added into medium as synthetic compounds (2,5-xylidine, ferulic acid, guaiacol, etc.). Induction of enzyme activity also can be cause by addition of some nitrogen source such as KNO_3, peptone, ammonium tartrate, etc. Many recombinant microorganisms overproduce many industrial enzymes, high expression of laccase and peroxidases in heterologous systems has not been achieved yet, they still have to be obtained from natural sources, also these enzymes are generally secreted in low quantities. It is evident that the potential applications of these enzymes in industrial and environmental technologies demand lot of amounts of these enzymes at low cost, that in future will increase the demand for potential inducers of enzyme activities.

Conflicts of Interest

The authors declare they have no potential conflicts of interests concerning drugs, products, services or another research outputs in this study. The Editorial Board declares that the manuscript met the ICMJE „uniform reguirements“ for biomedical papers.

References

1. Whiteley, C.D.; Lee, D.J. Enzyme technology and biological remediation. Enzyme Microb. Technol. 2006, 38, 291–316.

2. Gupta, R.; Chaudhury, N.K. Entrapment of in biomolecules in sol-gel matrix for application in biosensors: Problem and future prospects. Biosensors and Bioelectronics 2007, 22, 2387–2399.
3. Guimarães, L.H.S et al. Screening of filamentous fungi for production of enzymes of biotechnological interest. Braz. J. Microbiol. 2006, 37.
4. Tišma, M. et al. White rot fungi in phenols, dyes and other xenobiotics treatment-a brief review Croat. J. Food Sci. Technol. 2010, 34–47.
5. Blanchette, R.A. Degradation of the lignocellulosic complex in wood. Canadian Journal of Botany 1995, 73, 999–1010.
6. Worrall, J.J. et al. Comparision of wood decay among diverse lignicolous fungi. Mycologia 1997, 89, 199–219.
7. Higuchi, T. Lignin biochemistry biosynthesis and biodegradation. Wood Sci. Technol. 1990, 24, 23–63.
8. Kirk, T.K.; Farrell R.L. Enzymatic combustion: the microbial degradation of lignin. Annu. Rev. Microbiol. 1987, 41, 465–505.
9. Flores, et al. Selection of Trichoderma strains capable of increasing laccase production by Pleurotus ostreatus and Agaricus bisporus in dual cultures. J Appl Microbiol 2009, 106, 249–57.
10. Rivera-Hoyos, C.M. et al. Fungal laccases. Fungal Bio Rev 2013, 27, 67–82.
11. Rao, M.A. et al. Enzymes as useful tools for environmental purposes. Chemosphere 2014, 107, 145–162.
12. Elisashvili, V.; Kachlishvili, E. Physiological regulation of laccase and manganese peroxidase production by white rot basidiomycetes. Journal of Biotechnology 2009, 144, 37–42.
13. Bonugli-Santos, R.C. et al. Production of laccase, manganese peroxidase and lignin peroxidase by Brazilian marine-derived fungi. Enzyme and Microbial Technology 2010, 46, 32–37.
14. Leontievsky, A. et al. Yellow laccase of Panus tigrinus oxidises non-phenolic substrates without electron-transfer mediators. FEBS Letters 1997, 413, 446–448.
15. Brijwani K. et al. Fungal Laccases: Production, Function, and Applications in Food Processing. Enzyme Research 2010, 10.
16. Heinzkill, M. et al. Characterization of laccases and peroxidases from wood rotting fungi. Appl. and Environ. Microbiology 1998, 64, 1601–1606.
17. Assavanig, A. et al. Isolation, characterization and function of laccase from Trichoderma. Appl. Microbiol. Biotechnol. 1992, 38, 198–202.
18. Thurston, C.F. The structure and function of fungal laccases. Microbiology 1994, 140, 19–26.
19. Orth, A.B.; Tien, M. Biotechnology of lignin degradation. The Mycota. II. Genetics and Biotechnology 1995, 287–302.
20. Ruiz-Dueñas, F.J. et al. A new versatile peroxidase from Pleurotus. Biochem. Soc. Trans. 2001, 29, 116–122.
21. Leonowicz, A. et al. Biodegradation of lignin by white rot fungi. Fungal Genet Biol 1999, 27, 175–185.
22. Giardina, P et al. Laccases: a never-ending story. Cell. Mol. Life Sci. 2010, 67, 369–385.
23. Jořenek, M.; Zajoncová, L. Biotechnologický význam lakasy a její charakteristika. Chem. Listy 2003, 107, 921–928.
24. Thurston, C.F. et al. The structure and function of fungal laccases. Microbiology 1994, 140, 19–26.
25. Eggert, C. et al. A fungal metabolite mediates degradation of non-phenolic lignin structures and synthetic lignin by laccase. FEBS Lett. 1996, 391, 44–148.
26. Madhavi, V.; Lele, S.S. Laccase: Properties and Application. BioResources 2009, 4, 1694–1717.
27. Šušla, M.; Svobodová K. Ligninolytické enzymy jako účinné nástroje pro biodegradaci obtížně rozložitelných organopolutantů. Chem. Listy 2006, 100, 889–895.
28. Hatakka, A.I. Biodegradation of lignin. Lignin, humic substances and coal. Biopolymers 2001, 1, 129–180.
29. Hammel, K.E.; Cullen, D. Role of fungal peroxidases in biological ligninolysis. Current Opinion in Plant Biology 2008, 11, 349–355.
30. Hofrichter, M. et al. New and classic families of secreted fungal heme peroxidases. Appl. Microbiol Biotechnol 2010, 87, 871–897.
31. Hatakka, A. Lignin-modifying enzymes from selected white rot fungi: production and role in lignin degradation. FEMS Microbiol. Rev. 1994, 13, 125–135.
32. Majeau, J.A. et al. Laccases for removal of recalcitrant and emerging pollutants. Bioresour. Technol. 2010, 101, 2331–2350.
33. Baldrian P. Interactions of heavy metals with white rot fungi. Enzyme and Microbial Technology 2003, 32, 78–91.
34. Songulashvili, G. et al. Basidiomycetes laccase and manganese peroxidase activity in submerged fermentation of food industry wastes. Enzyme and Microbial Technology 2007, 41, 57–61.
35. Stajic, M. et al. Effect of different carbon and nitrogen sources on laccase and peroxidases production by selected Pleurotus species. Enzyme and Microbial Technology 2006, 38, 65–73.
36. Jiang, X. et al. Effects of nitrogen addition and litter properties on litter decomposition and enzyme activities of individual fungi. Applied Soil Ecology 2014, 80, 108–115.
37. Min, K.L. et al. Characterization of a Novel Laccase Produced by the Wood-Rotting Fungus Phellinus ribis. Archives of Biochemistry and Biophysics 2001, 392, 279–286.
38. Arora, D.S.; Gill P.K. Effects of various media and supplements on laccase production by some white rot fungi. Bioresource Technology 2001, 77, 89–91.
39. Kuhar, F.; Papinutti L. Optimization of l accase production by two strains of Ganoderma lucidum using phenolic and metallic inducers. Rev Argent Microbiol. 2014, 46, 144–149.
40. Novotný, Č. et al. Ligninolytic fungi in bioremediation: extracellular enzyme production and degradation rate. Soil Biology & Biochemistry. 2004, 36, 1545–1551.
41. Reddy, C.A.; D'Souza T.M. Physiology and molecular biology of the lignin peroxidases of Phanerochaete chrysosporium. FEMS Microbiol Rev. 1994, 13, 137–52.

42. Saparrat, M.C.N. et al. Induction, Isolation, and Characterization of Two Laccases from the White Rot Basidiomycete Coriolopsis rigida. Appl. and Envir. Microbiol. 2002, 1534–1540.
43. Kapich, A.N. et al.. Effect of lignocellulose-containing substrate on production of ligninolytic peroxidases in submerged cultures of Phanerochaete chrysosporium ME-446. Enzyme Microb. Technol. 2004, 34, 187–95.
44. Galhaup, C. et al. Increased production of laccase by the wood-degrading basidiomycete Trametes pubescens. Enzyme Microb. Technol. 2002, 30, 529–36.
45. Zakariashvili, N.G.; Elisashvili, V.I. Regulation of Cerrena unicolor lignocellulolytic activity by a nitrogen source in culture medium. Microbiology (Moscow) 1992, 62, 525–8.
46. Sun, X. et al. Production of lignocellulolytic enzymes by Trametes gallica and detection of polysaccharide hydrolase and laccase activities in polyacrylamide gels. J. Basic Microbiol. 2004, 44, 220–231.
47. Levin, L. et al. Effect of nitrogen sources and vitamins on ligninolytic enzyme production by some whiterot fungi. Dye decolorization by selected culture filtrates. Bioresource Technology 2010, 101, 4554–4563.
48. Galhaup, C. et al. Characterization of the major laccase isoenzyme from Trametes pubescens and regulation of its synthesis by metal ions. Microbiology 2002, 148, 2159–2169.
49. Elisashvili, V. et al. Physiological regulation of edible and medicinal higher basidiomycetes lignocellulotic enzymes activity. Int. J. Med. Mushr. 2002, 4, 159–166.
50. Bettin, F. et al. Production of laccases in submerged process by Pleurotus sajor-caju PS-2001 in relation to carbon and organic nitrogen sources, antifoams and Tween 80. J. Ind. Microbiol. Biotechnol. 2008, 36, 1–9.
51. Hossain, S.M. Effect of wheat straw powder on enhancement of ligninolytic enzyme activity using Phanerochate chrysosporium. Indian Journal of Biochemistry 2008, 502–507.
52. Fang, Z. et al. Identification of a laccase Glac15 from Ganoderma lucidum 77002 and its application in bioethanol production. Biotechnology for Biofuels 2015, 8, 54.
53. Rodrigues, M.A.M. et al. Effect of enzyme extracts isolated from white rot fungi on chemical composition and in vitro digestibility of wheat straw. Animal Feed Science and Technology 2008, 141, 326–338.
54. Parenti, A. et al. Induction of laccase activity in the white rot fungus Pleurotus ostreatus using water polluted with wheat straw extracts. Bioresource Technology 2013, 133, 142–149.
55. Makela, M.R. et al. Effect of copper, nutrient nitrogen, and wood-supplement on the production of lignin-modifying enzymes by the white rot fungus Phlebia radiata. Fungal biology 2013, 117, 62–70.
56. Bazanella, G.C. et al. Production of laccase and manganese peroxidase by Pleurotus pulmonarius in solid-state cultures and application in dye decolorization. Folia Microbiol (Praha) 2013, 58, 641–7.
57. Revankar, M.S. et al. Solid-state fermentation for enhanced production of laccase using indigenously isolated Ganoderma sp. Appl. Biochem. Biotechnol. 2007, 143, 16–26.
58. Kocyigit, A. et al. Production of laccase from Trametes trogii TEM H2: a newly isolated white rot fungus by air sampling. Journal of Basic Microbiology 2012, 52, 1–9.
59. Revankar, M.S.; Lele, S.S. Enhanced production of laccase using a new isolate of white rot fungus WR-1. Process Biochem. 2006, 41, 581–588.
60. Collins, P.J.; Dobson, A.D.W. Regulation of laccase gene transcription in Trametes versicolor. Appl. Environ. Microbiol. 1997, 63, 3444–3450.
61. Wang, F. et al. Enhanced laccase production by Trametes versicolor using corn steep liquor as both nitrogen source and inducer. Bioresource Technology 2014, 166, 602–605.
62. Gassara, F. et al. Screening of agro-industrial wastes to produce ligninolytic enzymes by Phanerochaete chrysosporium. Biochemical Engineering Journal 2010, 49, 388–394.
63. Usha, K.Y. et al. Enhanced Production of Ligninolytic Enzymes by a Mushroom Stereum ostrea. Biotechnol Res Int 2014, 8154–95.
64. Munoz, C. Laccase isoenzymes of Pleurotus eryngii: characterization, catalytic properties and participation in activation of molecular oxygen and Mn2+ oxidation. Appl Environ Microbiol 1997, 63, 2166–74.
65. Shah, V. et al. Influence of dimethyl sulfoxide on extracellular enzyme production by Pleurotus ostreatus. Biotechnology Letter 2006, 651–655.
66. Lee, I.Y. et al. Enhanced production of laccase in Trametes versicolor by the addiction of ethanol. Biotechnol. Lett. 1999, 21, 965–968.
67. Hughes, M.N.; Poole, R.K. Metal speciation and microbial growth the hard (and soft) facts. J. Gen. Microbiol. 1991, 137, 725–34.
68. Gadd, G.M. Interactions of fungi with toxic metals. New Phytol 1993, 124, 25–60.
69. Shimada, M. et al. Possible biochemical roles of oxalic acid as a low molecular weight compound involved in brown-rot and white-rot decays. J. Biotechnol. 1997, 53, 101–113.
70. Tinoco, R. et al. Increasing Pleurotus ostreatus laccase production by culture medium optimization and copper/lignin synergistic induction. J. Ind. Microbiol. Biotechnol. 2011, 38, 531–540.
71. Palmieri, G. et al. Copper Induction of Laccase Isoenzymes in the Ligninolytic Fungus Pleurotus ostreatus. Applied and Envir. Microbiology 2000, 920–924.
72. Khammuang, S. et al. Copper induction of laccases by Lentinus polychrous under liquid-state-fermentation. Biocatalysis and Agricultural Biotechnology 2013, 2, 357–362.
73. Levin, L. et al. Copper induction of lignin-modifying enzymes in the white rot fungusTrametes trogii. Mycologia 2002, 94, 377–383.
74. Bonnarme, P.; Jeffries, T.W. Mn(II) Regulation of Lignin Peroxidases and Manganese-Dependent Peroxidases from Lignin-Degrading White Rot Fungi. Applied and Environ. Microbiol. 1990,

210–217.
75. Minussi, R. C. et al. Laccase induction in fungi and laccase/N–OH mediator systems applied in paper mill effluent. Bioresource Technology 2007, 98 158–164.
76. Fonseca, M.I. et al. Copper inducing effect on laccase production of white rot fungi native from Misiones (Argentina). Enzyme and Microbial Technology 2010, 46, 534–539.
77. Levin, L. et al. Optimization of lignocellulolytic enzyme production by the white rot fungus Trametes trogii in solid-state fermentation using response surface methodology. Biochemical Engineering Journal 2008, 39, 207–214.
78. Galhaup, C.; Haltrich, D. Enhanced formation of laccase activity by the white rot fungus Trametes pubescens in the presence of copper. Appl Microbiol Biotechnol 2001, 56, 225–32.
79. Asgher, M. Characterization of a novel manganese peroxidase purified from solid state culture of Trametes versicolor IBL-04. Bioresources 2011, 6, 4317–4330.
80. Kneževič, A. et al. The effect of trace elements on wheat straw degradation by Trametes gibbosa. International Biodeterioration & Biodegradation 2014,96, 152–156.
81. Murugesan, K. et al. Effect of metal ions on reactive dye decolorization by laccase from Ganoderma lucidum. Journal of Hazardous Materials 2009, 168, 523–529.
82. Cordi, L. et al. Fungal laccase: copper induction, semi-purification, immobilization, phenolic effluent treatment and electrochemical measurement. African Journal of Biotechnology 2007, 10, 1255–1259.

The article is freely distributed under license Creative Commons (BY-NC-ND). But you must include the author and the document can not be modified and used for commercial purposes.

Interaction of nanocarrier apoferritin with cytotoxic drug molecules

Simona Dostalova[1,2*], Monica Vazzana[1,3], Marketa Vaculovicova[1,2], Vojtech Adam[1,2] and Rene Kizek[4]

[1] Department of Chemistry and Biochemistry, Faculty of Agronomy, Mendel University in Brno, Zemedelska 1, CZ-613 00 Brno, Czech Republic, Emails: simona1dostalova@gmail.com (S.D.);; marketa.ryvolova@seznam.cz (M.V.); vojtech.adam@mendelu.cz (V.A.); kizek@sci.muni.cz (R.K.)

[2] Central European Institute of Technology, Brno University of Technology, Technicka 3058/10, CZ-616 00 Brno, Czech Republic

[3] Department of Biological and Environmental Sciences, University of Messina, Piazza Salvatore Pugliatti, 98122 Messina, Italy, Email: monicavazzana@libero.it (M.V.)

* Author to whom correspondence should be addressed; E-Mail: simona1dostalova@gmail.com; Tel.: +420-5-4513-3350; Fax: +420-5-4521-2044.

Received: 19.6.2015 / Accepted:19.6.2015 / Published: 1.10.2015

In this work, the encapsulation of cytotoxic drug doxorubicin (DOX) in protein nanocarrier apoferritin was studied. Two encapsulation protocols, using the disassembly and reassembly of apoferritin molecules in different surrounding pH and infusion method of encapsulation, were compared. The changes in size distribution and zeta potential of apoferritin in dependence to the pH changes, doxorubicin encapsulation and apoferritin:doxorubicin number of molecules ratio (1:14; 1:28; 1:56) were observed. The encapsulation efficiency at 1:56 apoferritin:doxorubicin ratio was 70% via pH changing method and 88% via infusion method. The release of doxorubicin molecules from nanocarrier after 14 days of storage at -20; 4; 20 and 37 °C was studied using capillary electrophoresis with laser induced fluorescence detection. The most stable was the storage at -20 °C with the infusion encapsulation method (after 14 days 0.32% DOX release). Due to very low release of cytotoxic drug molecules from apoferritin, apoferritin seems to be a suitable nanocarrier. Based on the size distribution changes, encapsulation efficiency and doxorubicin release, the infusion encapsulation method seems more promising.

Keywords: apoferritin; doxorubicin; fluorescence; nanocarrier; nanomedicine

1. Introduction

Naturally occurring or artificially prepared proteins can be employed in various fields including basic research [1-4], industry [5-8], immuno-based assays [9-12], detection of many different analytes [13-16], conventional medicine [17-20] or nanomedicine [21-24]. The first nanomedicine formulation ever approved by the FDA was a PEGylated bovine serum albumin in 1990, named Adagen® [25]. Out of the 44 FDA-approved nanomedicine formulations, 10 are polymer-protein conjugates or albumin nanoparticles [26-28] and novel protein-based nanocarriers are still being developed [29-32].

The use of proteins as nanocarriers has many advantages in comparison with artificial nanocarriers [33]. The immune response of patient's body to protein nanocarriers is much lower, especially for the proteins naturally occurring in humans or after surface modification with polyethyleneglycol [34]. Moreover, they can usually self-assemble to form uniform cages with an extraordinary binding capacity for various drugs. They are also biodegradable, and have abundant renewable sources [35]. The high binding capacity of protein nanocarriers owns to multiple functional groups in their primary sequence allowing for different interactions

with therapeutic molecules [36]. Drug molecules can also be reversibly encapsulated in some proteins' three-dimensional hollow cage [37].

The most frequently studied protein as a nanocarrier is a human serum albumin, the most abundant protein in blood plasma (about 60% of the total plasma protein count) [38]. Albumin is a globular protein containing 585 amino acids (with one tryptophan residue) and three homologous domains stabilized by disulfide bridges [39]. The ligands, either organic or inorganic, usually bind to the many hydrophobic cavities in albumin subdomains, making this protein an important regulator of intercellular fluxes and, moreover, drug behavior in vivo [40]. Ligands can interact with both C=O and C-N albumin groups, resulting in changes in its secondary structure [41]. Albumin nanoparticles were used for delivery of cytostatic drugs, siRNAs, vaccines or radiodiagnostics [42-45].

Protein apoferritin is also studied as a possible nanocarrier [29,46-48]. Apoferritin is also naturally found in human body as a major iron-binding protein. Apoferritin forms a hollow rhombic dodecahedral shell with outer diameter of 12-13 nm and an inner diameter of 7-8 nm [49]. The ligands can thus not only interact with amino acid residues of apoferritin but also be encapsulated in its hollow cavity. Many amino acid side chains of apoferritin 24 subunits interact to form hydrophobic cores, but there is also a large number of polar and hydrophilic residues, allowing for interaction with various molecules [50]. Some substances can bind to the apoferritin surface through hydrogen bonding (non-ionic molecules) or electrostatic interactions (ionic molecules) [51]. The apoferritin shell contains both hydrophobic and hydrophilic channels, allowing small molecules to enter the cavity via diffusion [52]. Its subunits can also be reversibly disassociated via the change of surrounding environment to encapsulate bigger molecules after reassembling [53]. In this work, we studied the interactions of cytotoxic drug doxorubicin with the apoferritin protein. Two encapsulation methods were compared, the pH changing and infusion method.

2. Results and Discussion

2.1 The encapsulation protocol

In this work, we studied the interactions of cytotoxic drug doxorubicin with protein nanocarrier apoferritin. To this end, two methods of doxorubicin encapsulation in apoferritin were evaluated. Fig. 1 shows the protocols of the two presented encapsulation methods. One of the methods employs the ability of apoferritin to reversibly disassociate its subunits in highly acidic pH and reassemble in the neutral pH, thus encapsulating any molecules mixed with disassembled apoferritin (Fig. 1A). The infusion method (Fig. 1B) allows the doxorubicin to enter the apoferritin cavity by diffusion through the channels in the apoferritin shell. The excess molecules of doxorubicin were removed in both methods by filtration through Amicon 3K centrifugal units.

2.2 The characterization of nanocarrier size and zeta potential

The influence of pH changes and doxorubicin encapsulation on the size distribution of created nanocarrier was evaluated (Fig. 2). In this experiment, the apoferritin:doxorubicin molecule ratio was 1:14. The native size of protein complex apoferritin in water (pH 6.9) was 16 nm with a small portion of 250 nm particles (Fig. 2A) and a zeta potential of -13.7 mV. Due to the pH changes, the structure of apoferritin was disassembled and reassembled, however, the reassembly process is not completely correct and part of the subunits can aggregated, creating nanoparticles of 160 nm or 5 000 nm in addition to the correctly reassembled 16 nm particles (Fig. 2B). The apoferritin was diluted in water after the disassembly/reassembly process and its zeta potential was -9.93 mV at pH 7.0.

After the encapsulation of doxorubicin via the pH changing method, particles of 16 nm and 300 nm were observed, with zeta potential of -19.5 mV at pH 7.2 (Fig. 2C). The size distribution of apoferritin with doxorubicin encapsulated via the infusion method was highly similar to the native apoferritin, with 16 nm particles and portion of 200 nm particles (Fig. 2D). However, the zeta potential of apoferritin with encapsu-

lated doxorubicin via the infusion method was decreased compared to native apoferritin, -19.5 mV at pH 7.3

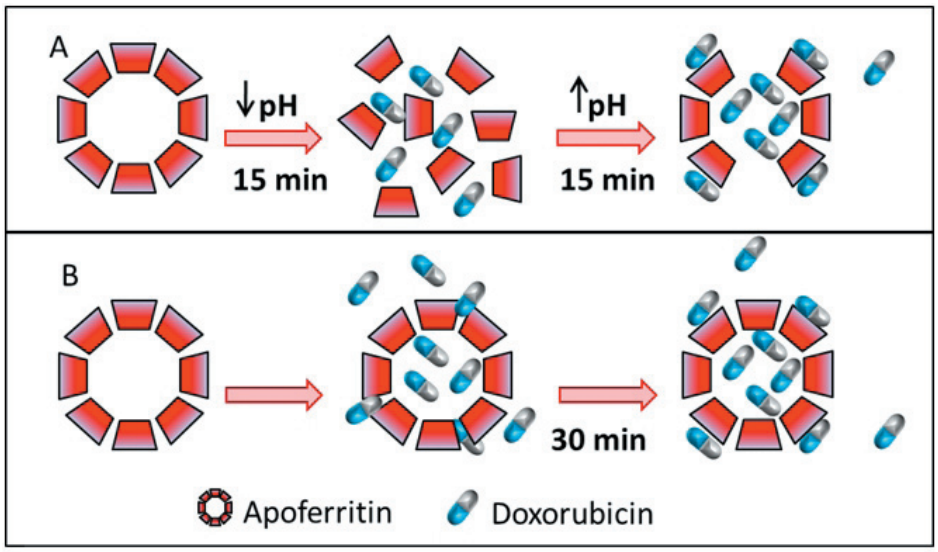

Figure 1: The encapsulation protocols compared in this work with subsequent removal of excess doxorubicin molecules by filtration through Amicon 3K centrifugal units at for 15 min at 25 °C and 6000×g and rinsing 3 times with water. (a) The encapsulation of doxorubicin molecules in apoferritin using the pH changing method. The apoferritin subunits were disassociated by acidification to pH 2.8 and mixed with doxorubicin for 15 min at 25 °C and 60 rpm. After that the pH was increased to 7.2 and the sample was mixed for 15 min at 25°C and 60 rpm to reassemble the apoferritin structure and allow the doxorubicin molecules to be encapsulated in apoferritin cavity. (b) The encapsulation of doxorubicin molecules in apoferritin using the infusion method. The apoferritin was mixed with doxorubicin for 30 min at 25 °C and 60 rpm.

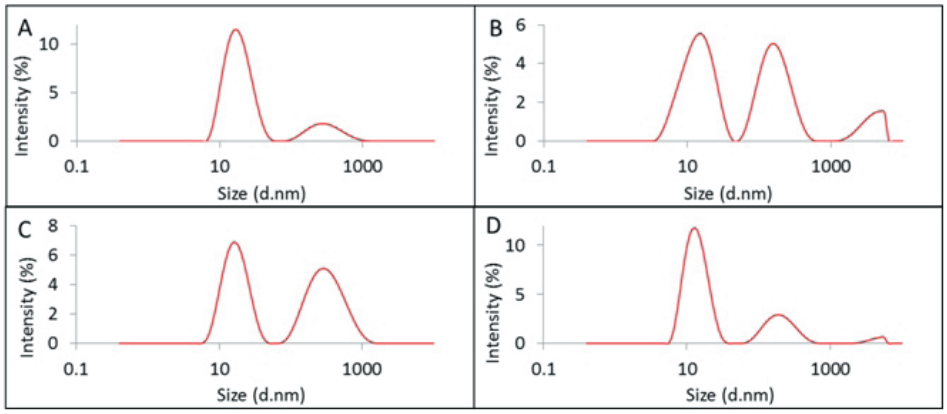

Figure 2: The changes of apoferritin size distribution by intensity due to the pH changes and doxorubicin encapsulation. (a) The size distribution by intensity of apoferritin in water, pH 6.9. (b) The size distribution by intensity of apoferritin in water after the pH changes, pH 7.0. (c) The size distribution by intensity of apoferritin with encapsulated doxorubicin via the pH changing method, pH 7.2. (d) The size distribution by intensity of apoferritin with encapsulated doxorubicin via the infusion method, pH 7.3.

The influence of apoferritin:doxorubicin ratio on the size distribution of created nanocarrier was further evaluated (Fig. 3). The size distribution of apoferritin with encapsulated doxorubicin via the pH changing encapsulation method changed with the increasing concentration of doxorubicin by increasing the portion of particles with 300 nm or more (Fig. 3A, C, E). However, no such changes in the size distribution were observed in the infusion encapsulation method with the increasing doxorubicin concentration (Fig. 3 B, D and F).

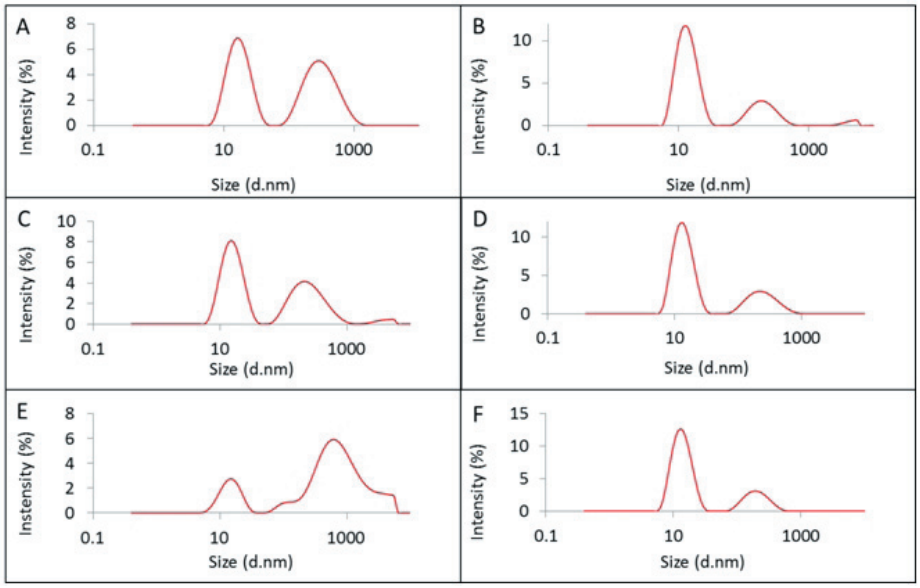

Figure 3: The changes of apoferritin size distribution by intensity due to the different apoferritin:doxorubicin ratio during encapsulation. (**a, c, e**) The size distribution by intensity of apoferritin with encapsulated doxorubicin via the pH changing method (**b, d, f**) The size distribution by intensity of apoferritin with encapsulated doxorubicin via the infusion method. (**a, b**) The apoferritin:doxorubicin ratio 1:14. (**c, d**) The apoferritin:doxorubicin ratio 1:28. (**e, f**) The apoferritin:doxorubicin ratio 1:56.

2.3 The efficiency of doxorubicin encapsulation in apoferritin nanocarrier using different methods

To evaluate the encapsulation efficiency the optical properties of doxorubicin were used – its absorption maximum at 480 nm and emission maximum at 600 nm. Absorbance and fluorescence spectra of created nanocarriers were measured after the encapsulation of doxorubicin molecules in apoferritin via the pH changing and infusion method and subsequent removal of excess doxorubicin molecules (Fig. 4). The apoferritin:doxorubicin molecule ratio was 1:56.

Following encapsulation, both the absorbance and fluorescence of doxorubicin is significantly decreased. Fig. 4A shows the decrease of doxorubicin absorbance after the encapsulation very similarly in both encapsulation methods, 1.95× using the infusion encapsulation method and 2× using the pH changing method. The decrease of doxorubicin fluorescence was also observed (Fig. 4B) and it differed significantly between the individual encapsulation methods – 6.61× decrease of fluorescence using the infusion method and 7.4× using the pH changing method.

After the subsequent removal of excess doxorubicin molecules by filtration and adjusting the sample volume to original, the absorbance (Fig. 4C) and fluorescence (Fig. 4D) spectra were measured again. After comparison with absorbance and fluorescence spectra before filtration, it was observed that 88% of doxorubi-

cin molecules were encapsulated in apoferritin using the infusion method, while only 70% were encapsulated using the pH changing method.

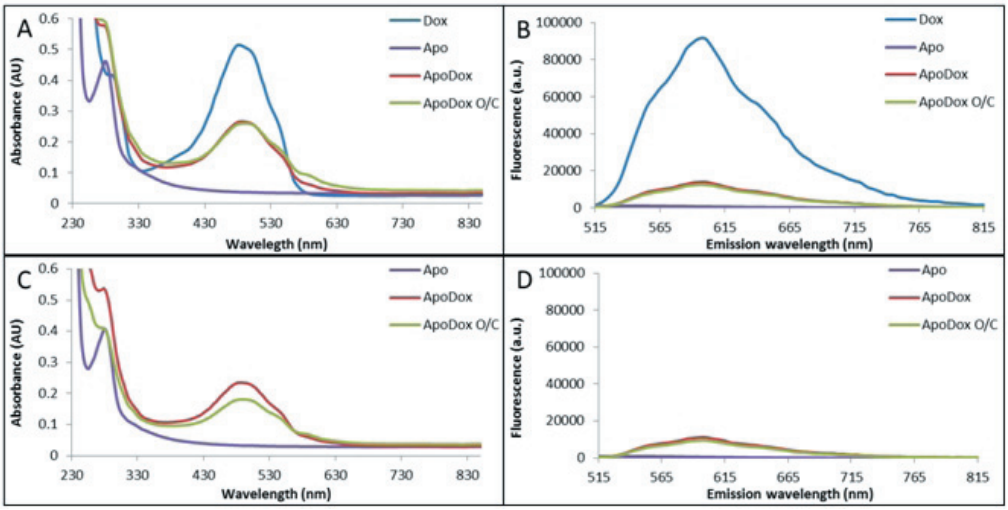

Figure 4: The absorbance (**a, c**) and emission (**b, d**) spectra of apoferritin with encapsulated doxorubicin via the pH changing (ApoDox O/C) and infusion (ApoDox) method after encapsulation (**a, b**) and after subsequent removal of excess doxorubicin molecules (**c, d**). The apoferritin:doxorubicin ratio was 1:56. Emission was measured at excitation wavelength 480 nm.

2.4 The release of doxorubicin molecules from apoferritin during a long-term storage

To evaluate the apoferritin stability the release of doxorubicin molecules from apoferritin during a storage for 14 days at different temperatures (-20; 4; 20 and 37 °C) was observed using capillary electrophoresis with laser induced fluorescence detection. In contrast to known literature [29,48] it was observed that, following encapsulation, part of doxorubicin molecules is located inside the apoferritin cavity and part on its surface. This is concluded based on the change in zeta potential of apoferritin after encapsulation of doxorubicin and by the behavior of apoferritin with encapsulated doxorubicin in electric field (Fig. 5). Doxorubicin showed two distinct peaks after separation in capillary electrophoresis (Fig. 5A). Apoferritin with encapsulated doxorubicin via both encapsulation methods showed a third peak with electrophoretic mobility corresponding to apoferritin in addition to the two peaks corresponding to doxorubicin (Fig. 5B). During the separation by capillary electrophoresis the doxorubicin molecules from the apoferritin surface are probably released by the surrounding electric field [54]. This behavior was observed in apoferritin with encapsulated doxorubicin via both pH changing and infusion method.

The height of peak corresponding to apoferritin with encapsulated doxorubicin after 1; 2; 3; 6; 10 and 14 days of storage was used to compare the release from nanocarriers prepared via different encapsulation methods and storage at different temperatures (Fig. 6). After 6 days of storage in all temperatures, the peak height of apoferritin with encapsulated doxorubicin was increased which can be caused by the transfer of more doxorubicin molecules from the apoferritin surface to its cavity. After longer storage the release of doxorubicin molecules from apoferritin cavity is very limited. The encapsulation of doxorubicin via the pH changing method caused higher (2.7×) release of doxorubicin molecules from apoferritin (Fig. 6A-D). This can probably be caused by the fact, that reassembly of apoferritin after pH changes is not complete but there appear two hole defects on opposite apoferritin poles [53] and

doxorubicin can leave the apoferritin cavity through these defects.

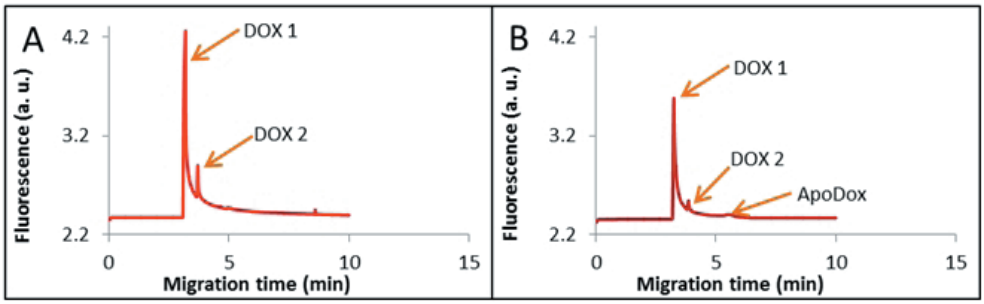

Figure 5: The behavior of doxorubicin (**a**) and apoferritin with encapsulated doxorubicin via both the pH changing and infusion method (**b**) during capillary electrophoresis with laser induced fluorescence detection using fused silica capillary with internal diameter of 75 μm and total length of 64.5 cm (54 cm to detector window); the separation voltage of 20 kV and hydrodynamic injection by 3 psi for 10 s.

The lowest release was observed after storage at -20 °C with 0.75% of released doxorubicin encapsulated via the pH changing method (Fig. 6A) and 0.32% via the infusion method (Fig. 6E) after 14 days of storage. Thus it can be concluded, that apoferritin with encapsulated doxorubicin is the most stable after storage at -20 °C. After 14 days of storage at 4 °C, the release was 1.67% with encapsulation via pH changing method (Fig. 6B) and 0.29% via the infusion method (Fig. 6F). The highest release and thus the lowest stability was observed after storage at 20 °C, with 2.44% of released molecules with encapsulation via pH changing method (Fig. 6C) and 2.02% via infusion method (Fig. 6G). After 14 days of storage at 37 °C, 1.47% of doxorubicin was released with encapsulation via pH changing method (Fig. 6D) and 1% via the infusion method (Fig. 6H).

3. Experimental Section

3.1 Chemicals

All chemicals of ACS purity were obtained from Sigma-Aldrich (St. Louis, MO, USA) unless stated otherwise. The deionized water was prepared using reverse osmosis equipment Aqual 25 (Aqual s.r.o., Brno, Czech Republic). The deionized water was further purified by using apparatus Milli-Q Direct QUV equipped with an UV lamp from Millipore (Billerica, MA, USA), exhibiting a resistance of 18 MΩ. The pH was measured using pH meter WTW inoLab (Weilheim, Germany).

3.2 The encapsulation of doxorubicin in apoferritin via pH changing method

1 mg of apoferritin (20 μL of 50 mg/mL) was mixed with 67.2 μg of doxorubicin (200 μL of 336 μg/mL) with a molar ratio of apoferritin:-doxororubicin 1:56 and 100 μL of water. Using 2.5 μL of 1 M HCl the pH was lowered to 2.8 to disassociate the apoferritin subunits. The sample was mixed for 15 min at 25 °C and 60 rpm. The pH was changed to 7.2 with 2.7 μL of 1M NaOH and the sample was shaken for 15 min at 25 °C and 60 rpm to reassemble the subunits and encapsulate the doxorubicin in apoferritin hollow. The excess doxorubicin molecules were removed by filtration using the centrifugation in Amicon 3K centrifugal units for 15 min at 25 °C and 6000×g. The samples were rinsed with water 3 times. Water was added after the filtration to fill the sample to its original volume.

3.3 The encapsulation of doxorubicin in apoferritin via infusion method

1 mg of apoferritin (20 μL of 50 mg/mL) was mixed with 67.2 μg of doxorubicin (200 μL of 336 μg/mL) with a molar ratio of apoferritin:-doxororubicin 1:56 and 100 μL of water.

The sample was shaken for 30 min at 25 °C and 60 rpm. The excess doxorubicin molecules were removed by filtration using the centrifugation in Amicon 3K centrifugal units for 15 min at 25 °C and 6000×g. The samples were rinsed

with water 3 times. Water was added after the filtration to fill the sample to its original volume.

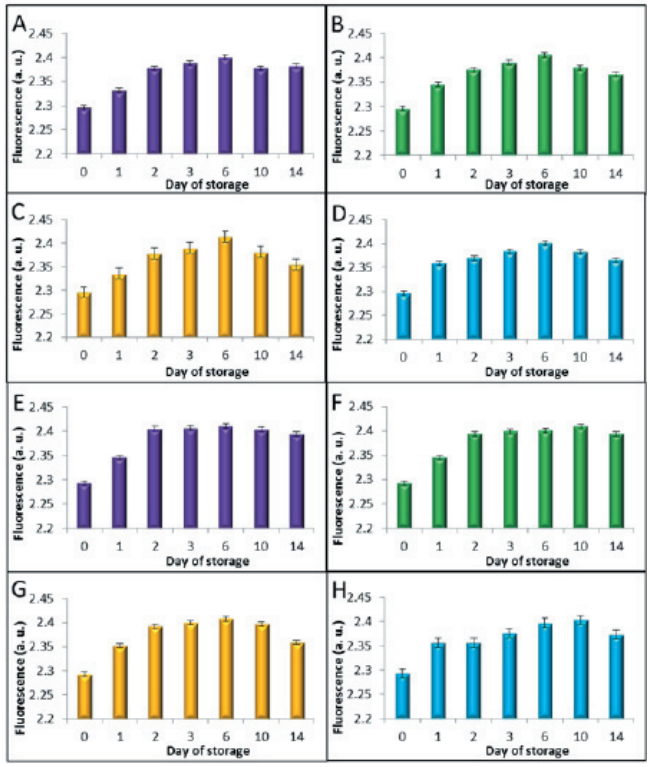

Figure 6: The release of doxorubicin from apoferritin nanocarrier during 14 days of storage at -20 °C (**a, e**), 4 °C (**b, f**); 20 °C (**c, g**) and 37 °C (**d, h**). The encapsulation was performed via both the pH changing (a-d) and infusion method (**e-h**). The release was measured using fused silica capillary with internal diameter of 75 μm and total length of 64.5 cm (54 cm to detector window); the separation voltage of 20 kV and hydrodynamic injection by 3 psi for 10 s.

3.4 Characterization of nanocarrier size

The average particle size and size distribution were determined by quasi elastic laser light scattering with a Malvern Zetasizer (NANO-ZS, Malvern Instruments Ltd., Worcestershire, United Kingdom). The zeta potential was determined by laser Doppler micro-electrophoresis with a Malvern Zetasizer. Nanoparticles in distilled water solution of 1.5 mL were put into a polystyrene latex cell and measured at a detector angle of 173°, a wavelength of 633 nm, temperature 25 °C and a refractive index of 1.33.

3.5 The encapsulation efficiency

The efficiency of doxorubicin encapsulation in apoferritin was evaluated using the optical properties of doxorubicin. The absorbance (wavelength 230-850 nm) and fluorescence (excitation wavelength 480 nm, emission 515-815 nm) spectra of the resulting nanocarriers were measured using the TECAN Infinite 200 PRO microtitration plate reader (Männedorf, Switzerland).

3.6 The release of doxorubicin molecules from apoferritin nanocarrier during 14 days

The created apoferritin nanocarrier with encapsulated doxorubicin using both pH changing and infusion encapsulation method was stored for 14 days at -20; 4; 20 and 37 °C. After 1; 2; 3; 6; 10 and 14 days of storage the nanocarrier fluorescence was measured using the capillary electrophoresis with laser induced fluorescence

detection CE 7100, Agilent Technologies (Santa Clara, CA, USA). Fused silica capillary with internal diameter of 75 µm and with the total length of 64.5 cm (54 cm to detector window) was used. The separation voltage of 20 kV and hydrodynamic injection by 3 psi for 10 s was employed.

4. Conclusions

Two methods for doxorubicin encapsulation in apoferritin nanocarrier were compared in this study. Standard, pH changing method showed 70% encapsulation efficiency, while the infusion method showed 88% encapsulation efficiency. A very low release of doxorubicin molecules from apoferritin nanocarrier after storage for 14 days at different temperatures was observed with the most stable using the infusion encapsulation method and storage at -20 °C.

Acknowledgments

The authors gratefully acknowledge financial support from the Grant Agency of the Czech Republic (NANOCHEMO GA CR 14-18344S) and PGS28_2014.

Conflicts of Interest

The authors declare they have no potential conflicts of interests concerning drugs, products,services or another research outputs in this study. The Editorial Board declares that the manuscript met the ICMJE „uniform reguirements“ for biomedical papers.

References

1. Chayaratanasin, P.; Barbieri, M.A.; Suanpairintr, N.; Adisakwattana, S. Inhibitory effect of clitoria ternatea flower petal extract on fructose-induced protein glycation and oxidation-dependent damages to albumin in vitro. BMC complementary and alternative medicine 2015, 15, 546.
2. Kim, K.-W.; Kim, B.-M.; Moon, H.-W.; Lee, S.-H.; Kim, H.-R. Role of c-reactive protein in osteoclastogenesis in rheumatoid arthritis. Arthritis research & therapy 2015, 17, 563.
3. Moran, G.; Carcamo, C.; Concha, M.; Folch, H. Expression of the protein serum amyloid a in response to aspergillus fumigatus in murine models of allergic airway inflammation. Rev. Iberoam. Micol. 2015, 32, 25-29.
4. Tsushima, H.; Okazaki, K.; Ishihara, K.; Ushijima, T.; Iwamoto, Y. Ccaat/enhancer-binding protein beta promotes receptor activator of nuclear factor-kappa-b ligand (rankl) expression and osteoclast formation in the synovium in rheumatoid arthritis. Arthritis research & therapy 2015, 17, 532.
5. Fujiwara, M.; Imura, T. Transparent silica thin films prepared from sodium silicate and bovine serum albumin with petal effect. Ceram. Int. 2015, 41, 7565-7572.
6. Rasala, B.A.; Mayfield, S.P. Photosynthetic biomanufacturing in green algae; production of recombinant proteins for industrial, nutritional, and medical uses. Photosynth. Res. 2015, 123, 227-239.
7. Zhao, Y.; Zhao, Y.Z.; Xu, H.L.; Yang, Y.Q. A sustainable slashing industry using biodegradable sizes from modified soy protein to replace petro-based poly(vinyl alcohol). Environ. Sci. Technol. 2015, 49, 2391-2397.
8. Zhao, Y.Z.; Zhao, Y.; Yang, Y.Q. Modified soy protein to substitute non-degradable petrochemicals for slashing industry. Ind. Crop. Prod. 2015, 67, 466-474.
9. Heger, Z.; Cernei, N.; Krizkova, S.; Masarik, M.; Kopel, P.; Hodek, P.; Zitka, O.; Adam, V.; Kizek, R. Paramagnetic nanoparticles as a platform for fret-based sarcosine picomolar detection. Sci Rep 2015, 5.
10. Krizkova, S.; Ryvolova, M.; Hynek, D.; Eckschlager, T.; Hodek, P.; Masarik, M.; Adam, V.; Kizek, R. Immunoextraction of zinc proteins from human plasma using chicken yolk antibodies immobilized onto paramagnetic particles and their electrophoretic analysis. Electrophoresis 2012, 33, 1824-1832.
11. Van Zoelen, S.A.; Ozkan, O.; Inceoglu, B. Antigenic cross-reactivity anti-birtoxin antibody against androctonus crassicauda venom. J. Arthropod.-Borne Dis. 2015, 9, 176-183.
12. Zitka, O.; Krizkova, S.; Skalickova, S.; Dospivova, D.; Adam, V.; Kizek, R. Microfluidic tool coupled with electrochemical assay for detection of lactoferrin isolated by antibody-modified paramagnetic beads. Electrophoresis 2013, 34, 2120-2128.
13. Abdelwahab, M.; Loa, C.C.; Wu, C.C.; Lin, T.L. Recombinant nucleocapsid protein-based enzyme-linked immunosorbent assay for detection of antibody to turkey coronavirus. J. Virol. Methods 2015, 217, 36-41.
14. Heger, Z.; Zitka, O.; Fohlerova, Z.; Rodrigo, M.A.M.; Hubalek, J.; Kizek, R.; Adam, V. Use of green fluorescent proteins for in vitro biosensing. Chem. Pap. 2015, 69, 54-61.
15. Minnaard, M.C.; Van De Pol, A.C.; De Groot, J.A.H.; De Wit, N.J.; Hopstaken, R.M.; Van Delft, S.; Goossens, H.; Ieven, M.; Lammens, C.; Little, P., et al. The added diagnostic value of five different c-reactive protein point-of-care test devices in detecting pneumonia in primary care: A nested case-control study. Scand. J. Clin. Lab. Invest. 2015, 75, 291-295.
16. Sonaimuthu, P.; Cheong, F.W.; Chin, L.C.; Mahmud, R.; Fong, M.Y.; Lau, Y.L. Detection of human malaria using recombinant plasmodium knowlesi merozoire surface protein-1 (msp-119) expressed in escherichia coli. Experimental parasitology 2015, 153, 118-122.
17. Kassir, R.; Blanc, P.; Tibalbo, L.M.B.; Breton, C.;

Lointier, P. C-reactive protein and procalcitonin for the early detection of postoperative complications after sleeve gastrectomy: Preliminary study in 97 patients. Surg. Endosc. 2015, 29, 1439-1444.
18. Liyasova, M.S.; Ma, K.; Lipkowitz, S. Molecular pathways: Cbl proteins in tumorigenesis and antitumor immunity-opportunities for cancer treatment. Clin. Cancer Res. 2015, 21, 1789-1794.
19. Numbenjapon, N.; Chamnanwanakij, S.; Sangaroon, P.; Simasathien, S.; Watanaveeradej, V. C-reactive protein as a single useful parameter for discontinuation of antibiotic treatment in thai neonates with clinical sepsis. Journal of the Medical Association of Thailand = Chotmaihet thangphaet 2015, 98, 352-357.
20. Zali, H.; Zamanian-Azodi, M.; Tavirani, M.R.; Baghban, A.A.Z. Protein drug targets of lavandula angustifolia on treatment of rat alzheimer's disease. Iran. J. Pharm. Res. 2015, 14, 291-302.
21. Heger, Z.; Cernei, N.; Blazkova, I.; Kopel, P.; Masarik, M.; Zitka, O.; Adam, V.; Kizek, R. Gammafe2o3 nanoparticles covered with glutathione-modified quantum dots as a fluorescent nanotransporter. Chromatographia 2014, 77, 1415-1423.
22. Janu, L.; Stanisavljevic, M.; Krizkova, S.; Sobrova, P.; Vaculovicova, M.; Kizek, R.; Adam, V. Electrophoretic study of peptide-mediated quantum dot-human immunoglobulin bioconjugation. Electrophoresis 2013, 34, 2725-2732.
23. Rodrigues, S.; Cordeiro, C.; Seijo, B.; Remunan-Lopez, C.; Grenha, A. Hybrid nanosystems based on natural polymers as protein carriers for respiratory delivery: Stability and toxicological evaluation. Carbohydr. Polym. 2015, 123, 369-380.
24. Sahebalzamani, M.; Biazar, E.; Shahrezaei, M.; Hosseinkazemi, H.; Rahiminavaie, H. Surface modification of phbv nanofibrous mat by laminin protein and its cellular study. Int. J. Polym. Mater. Polym. Biomat. 2015, 64, 149-154.
25. Syiam, M.M.; El-Aziem, M.A.; Soliman, M.E.M. Adagen: Adaptive interface agent for x-ray fracture detection. Ieee: New York, 2004; p 354-357.
26. Alconcel, S.N.S.; Baas, A.S.; Maynard, H.D. Fda-approved poly(ethylene glycol)-protein conjugate drugs. Polym. Chem. 2011, 2, 1442-1448.
27. Gommans, G.M.M.; Boer, R.O.; van Dongen, B.A.; van der Schors, T.G.; de Waard, J.W.D. Optimisation of 99mtc-nanocoll sentinel node localisation in carcinoma of the breast. Eur. J. Nucl. Med. 2000, 27, 744-744.
28. O'Shaughnessy, J.A.; Blum, J.L.; Sandbach, J.F.; Savin, M.; Fenske, E.; Hawkins, M.J.; Baylor-Charles, A. Weekly nanoparticle albumin paclitaxel (abraxane) results in long-term disease control in patients with taxane-refractory metastatic breast cancer. Breast Cancer Res. Treat. 2004, 88, S65-S65.
29. Blazkova, I.; Nguyen, V.H.; Dostalova, S.; Kopel, P.; Stanisavljevic, M.; Vaculovicova, M.; Stiborova, M.; Eckschlager, T.; Kizek, R.; Adam, V. Apoferritin modified magnetic particles as doxorubicin carriers for anticancer drug delivery. Int. J. Mol. Sci. 2013, 14, 13391-13402.
30. Chen, C.H.; Hu, H.Y.; Qiao, M.X.; Zhao, X.L.; Wang, Y.J.; Chen, K.; Chen, D.W. Anti-tumor activity of paclitaxel through dual-targeting lipoprotein-mimicking nanocarrier. J. Drug Target. 2015, 23, 311-322.
31. Mottaghitalab, F.; Farokhi, M.; Shokrgozar, M.A.; Atyabi, F.; Hosseinkhani, H. Silk fibroin nanoparticle as a novel drug delivery system. J. Control. Release 2015, 206, 161-176.
32. Zhou, Z.L.; Badkas, A.; Stevenson, M.; Lee, J.Y.; Leung, Y.K. Herceptin conjugated plga-phis-peg ph sensitive nanoparticles for targeted and controlled drug delivery. Int. J. Pharm. 2015, 487, 81-90.
33. Dostalova, S.; Munzova, D.; Vaculovicova, M.; Kizek, R. Delivery of doxorubicin using protein nanocarriers. J. Metallomics Nanotech. 2014, 1, 34-38.
34. Ma, Y.J.; Nolte, R.J.M.; Cornelissen, J. Virus-based nanocarriers for drug delivery. Adv. Drug Deliv. Rev. 2012, 64, 811-825.
35. Elzoghby, A.O.; Samy, W.M.; Elgindy, N.A. Protein-based nanocarriers as promising drug and gene delivery systems. J. Control. Release 2012, 161, 38-49.
36. Elzoghby, A.O.; Samy, W.M.; Elgindy, N.A. Albumin-based nanoparticles as potential controlled release drug delivery systems. J. Control. Release 2012, 157, 168-182.
37. Elzoghby, A.O.; El-Fotoh, W.S.A.; Elgindy, N.A. Casein-based formulations as promising controlled release drug delivery systems. J. Control. Release 2011, 153, 206-216.
38. Chen, T.; Zhu, X.; Chen, Q.; Ge, M.; Jia, X.; Wang, X.; Ge, C. Interaction between z-ligustilide from radix angelica sinensis and human serum albumin. Food Chem. 2015, 186, 292-297.
39. Sugio, S.; Kashima, A.; Mochizuki, S.; Noda, M.; Kobayashi, K. Crystal structure of human serum albumin at 2.5 angstrom resolution. Protein Eng. 1999, 12, 439-446.
40. Varshney, A.; Rehan, M.; Subbarao, N.; Rabbani, G.; Khan, R.H. Elimination of endogenous toxin, creatinine from blood plasma depends on albumin conformation: Site specific uremic toxicity & impaired drug binding. PLoS One 2011, 6.
41. Liu, Y.; Chen, M.M.; Jiang, L.G.; Song, L. Stereoselective interaction of cinchona alkaloid isomers with bovine serum albumin. Food Chem. 2015, 181, 170-178.
42. Kunda, N.K.; Alfagih, I.M.; Dennison, S.R.; Tawfeek, H.M.; Somavarapu, S.; Hutcheon, G.A.; Saleem, I.Y. Bovine serum albumin adsorbed pga-co-pdl nanocarriers for vaccine delivery via dry powder inhalation. Pharm. Res. 2015, 32, 1341-1353.
43. Sharma, R.I.; Pereira, M.; Schwarzbauer, J.E.; Moghe, P.V. Albumin-derived nanocarriers: Substrates for enhanced cell adhesive ligand display and cell motility. Biomaterials 2006, 27, 3589-3598.
44. Son, S.; Song, S.; Lee, S.J.; Min, S.; Kim, S.A.; Yhee, J.Y.; Huh, M.S.; Kwon, I.C.; Jeong, S.Y.; Byun, Y., et al. Self-crosslinked human serum albumin nanocarriers for systemic delivery of polymerized sirna to tumors. Biomaterials 2013, 34, 9475-9485.
45. Yuan, A.; Wu, J.H.; Song, C.C.; Tang, X.L.; Qiao,

Q.; Zhao, L.L.; Gong, G.M.; Hu, Y.Q. A novel self-assembly albumin nanocarrier for reducing doxorubicin-mediated cardiotoxicity. J. Pharm. Sci. 2013, 102, 1626-1635.
46. Heger, Z.; Skalickova, S.; Zitka, O.; Adam, V.; Kizek, R. Apoferritin applications in nanomedicine. Nanomedicine 2014, 9, 2233-2245.
47. Munzova, D.; Dostalova, S.; Vaculovicova, M.; Kizek, R. Apoferritin: Nanocarrier for targeted drug delivery. J. Metallomics Nanotech. 2014, 1, 50-54.
48. Tmejova, K.; Hynek, D.; Kopel, P.; Dostalova, S.; Smerkova, K.; Stanisavljevic, M.; Nguyen, V.H.; Nejdl, L.; Vaculovicova, M.; Krizkova, S., et al. Electrochemical behaviour of doxorubicin encapsulated in apoferritin. Int. J. Electrochem. Sci. 2013, 8, 12658-12671.
49. Haussler, W. Structure and dynamics in apoferritin solutions with paracrystalline order. Chem. Phys. 2003, 292, 425-434.
50. Crichton, R.R.; Declercq, J.P. X-ray structures of ferritins and related proteins. Biochim. Biophys. Acta-Gen. Subj. 2010, 1800, 706-718.
51. Liu, F.; Du, B.J.; Chai, Z.; Zhao, G.H.; Ren, F.Z.; Leng, X.J. Binding properties of apoferritin to nicotinamide and calcium. Eur. Food Res. Technol. 2012, 235, 893-899.
52. Granier, T.; Gallois, B.; Dautant, A.; Destaintot, B.L.; Precigoux, G. Comparison of the structures of the cubic and tetragonal forms of horse-spleen apoferritin. Acta Crystallogr. Sect. D-Biol. Crystallogr. 1997, 53, 580-587.
53. Kim, M.; Rho, Y.; Jin, K.S.; Ahn, B.; Jung, S.; Kim, H.; Ree, M. Ph-dependent structures of ferritin and apoferritin in solution: Disassembly and reassembly. Biomacromolecules 2011, 12, 1629-1640.
54. Konecna, R.; Nguyen, H.V.; Stanisavljevic, M.; Blazkova, I.; Krizkova, S.; Vaculovicova, M.; Stiborova, M.; Eckschlager, T.; Zitka, O.; Adam, V., et al. Doxorubicin encapsulation investigated by capillary electrophoresis with laser-induced fluorescence detection. Chromatographia 2014, 77, 1469-1476.

The article is freely distributed under license Creative Commons (BY-NC-ND). But you must include the author and the document can not be modified and used for commercial purposes.

Study of cell penetrating peptide and Europium(III) and Terbium(III) Schiff base complexes interaction

Vedran Milosavljevic[1,2], Pavel Kopel [1,2+], Miguel Angel Merlos Rodrigo[1,2+] , Kristyna Cihalova[1,2+], Amitava Moulick [1,2+], Dorota Wawrzak[3,+] and Rene Kizek[1,2*]

[1] Department of Chemistry and Biochemistry, Laboratory of Metallomics and Nanotechnologies, Mendel University in Brno, Zemedelska 1, CZ-613 00 Brno, Czech Republic - European Union; E-mails: grizlidripac@gmail.com (VM), paulko@centrum.cz (PK), merlos19792003@hotmail.com (MAMR), kriki.cihalova@seznam.cz (KC), amitavamoulick@gmail.com (AM), kizek@sci.muni.cz (RK)

[2] Central European Institute of Technology, Brno University of Technology, Technicka 3058/10, CZ-616 00 Brno, Czech Republic - European Union;

[3] Institute of Chemistry, Environmental Protection and Biotechnology, Jan Dlugosz University of Czestochowa, Armii Krajowej 13/15, PL-42-201 Czestochowa, Poland - European Union; E-mail: d.wawrzak@ajd.czest.pl (DW)

* Author to whom correspondence should be addressed; E-Mail: kizek@sci.muni.cz; Tel.: +420-5-4513-3350; Fax: +420-5-4521-2044.

Received:18.6.2015 / Accepted:1.9.2015 / Published: 1.10.2015

Eu(III) and Tb(III) Schiff base complexes are applicable in various fields such as sensing, assays, screening protocols in vitro, imaging studies in cellulo or in vivo. Fluorescent europium and terbium complexes and their interaction with cell penetrating peptide (KKKRKC) can represent an excellent key for understanding pathway of peptide transportation though cell membrane and the application of Schiff base complexes as potential antibacterial drugs. Mass spectrometry (MALDI TOF) and spectrophotometry measurements have been used for study of complex formation between Eu(III) and Tb(III) Schiff base complex with cell penetrating peptide.

Keywords: Schiff base; mass spectrometry; spectrophotometry; europium; terbium; cell penetrating peptide.

1. Introduction

During the last decade newly developed potential therapeutic drugs such as proteins, nucleic acids, and new types of hydrophilic drugs are being reported. However, these drugs mostly have limitations due to their inability to reach the appropriate intracellular targets as a consequence of poor possibility to penetrate through cell membranes or deactivation by resistance mechanisms that transport these compounds out of the cell, both limiting their interaction with intracellular targets [1,2]. It has been also reported that poor cell specificity and normal cell cytotoxicity are common in application of standard technique for drug delivery systems, such as microinjection, electroporation, liposomal formulation and use of viral vectors [3-5]. In the search for new anticancer agents and drug delivery systems, cell penetrating peptides (CPP) attracted attention due to their possibilities for intracellular delivery of a wide range of macromolecules. CPP are short peptides consisting of less than 30 amino acids. CPP structures are mostly composed of positively charged amino acids (e.g. Arg, Lys and His) providing them possibility to translocate through the cell membrane by various mechanism, including endocytosis, and easily deliver various cell-impermeable covalently or noncovalently conjugated bioactive cargo such as proteins [6],

nucleic acid [7], siRNA [8], peptide nucleic acid [9] and quantum dots [10]. CPPs as delivery agents were in focus of many investigations with the aim to increase stability and efficiency of cargo delivery avoiding the problem of cytotoxicity effect, lack of cell specificity and unexpected side effects. However, it has been shown that side effects on normal cells during cancer therapy or antibacterial application are minimized [11-13]. Peptides as drug carriers offer some advantages over other carriers as they are relatively easy to modify with various organic or inorganic materials, especially with compounds that have fluorescent properties, enabling easy tracking of drugs after application and for better understanding of the structure and functions of biological systems [14]. Many of luminescent materials such as organic fluorophores [15], recombinant proteins [16], semiconductor nanoparticles [17], and emissive metal complexes [18] are being used for peptide labeling. Application of organic dyes has many limitations associated with poor extinction coefficient or quantum yield and low stability against bleaching. However, on the other hand, metal complexes, especially rare earth metal-based materials show excellent optical properties since the f–f emission lines of Pr(III), Sm(III), Eu(III), Tb(III), Dy(III) and Tm(III) ions are in the visible range [19,20]. Especially great attention attracts luminescent rare-earth metal complexes with Eu(III) and Tb(III) as the excited states of these ions are less sensitive to vibrational quenching by intra or intermolecular energy transfer to adjacent high--energy vibrators such as hydroxyl groups [21]. Comparing metal-rare complex with quantum dots (QDs), they have long life time fluorescence and the fluorescence wavelength of Ln(III) ions is not sensitive to particle size, where the study of the function and properties of these compounds is simplified in comparison to QDs [22]. However, Ln(III) complexes are mostly used for study of their magnetic properties and imagine purpose, only few scientific reports are dealing with application of the complexes in biological applications [23-25].

Based on this consideration, we were interested in preparation of Schiff bases 2-[(E)--2-pyridylmethyleneamino]-N-[2-[(E)-2-pyridylmethyleneamino]ethyl]ethanamine (S-5) and 2-[(E)-2-pyridylmethyleneamino]-N,N--bis[2-[(E)-2-pyridylmethyleneamino]ethyl] ethanamine (S-6) and their europium(III) and terbium(III) complexes Eu(III)-S-5 and Tb(III)--S-6 with luminescent properties in order to study their interaction with cell penetrating peptide and possible biological applications. The compounds were evaluated against several bacterial species with respect to their toxicity.

2. Results and Discussion

2.1 UV/VIS measurement

Luminescence studies were conducted at room temperature, observing absorbance and fluorescence properties of KKKRKC cell penetrating peptide, Eu(III) and Tb(III) Schiff base complexes and interaction between cell penetrating peptide and Eu(III) and Tb(III) Schiff base complexes. Concentrations of cell penetrating peptide and Eu(III) and Tb(III) Schiff base complex samples were set on 1 mM, and the changes in the absorption spectra were monitored by spectrophotometry. The absorbance maxima of all samples were observed and it is found that all samples have maximum absorbance at 266 nm (Fig. 1a and 1b). However, from the results obtained after mixing of peptide with Eu(III) and Tb(III) Schiff base complexes a gradual decrease of the peptide-complex absorbance can be clearly observed if we compare it with absorbance of the complexes, concluding that interaction between peptide and complexes is confirmed. This can be explained using Lewis theory of acid and base, where europium and terbium ions represent acid part of complex, while nitrogen or oxygen bases can be bond via donor-acceptor bonding, in which peptide ligand transfers electron charge towards the metal center, forming interaction with the electron donor atoms leading to formation of peptide-complex structure [19,26,27].

An excitation wavelengths of 266 nm was taken in order to determine the maximum wavelength of emission of the mixed Eu(III) and Tb(III). Schiff base complexes and their interaction with cell penetrating peptide were measured. From the obtained results it can be

seen that maximum emission peaks of Tb(III)--S-5 and Tb(III)-S-6 were found at 355 nm, 450 nm, 480 nm, 500 nm and 545 nm (Fig. 1c). This can be explained by f-f transition coming from electron or energy transfer processes which is assigned to the 5D4-7FJ with J = 6–0, reported by Shintoyo et al. [28]. However, in the case of Tb(III)-S-5 and Tb(III)-S-6 complex with peptide the same position peaks as in case of only complex emission were found, while also high emission peak was found at 305 nm for which we can assume that they belong to peptide-complex interaction via donor-acceptor bond mentioned before. In the case of Eu(III)--S-5 and Eu(III)-S-6 maximum emission peaks have been found at 365 nm, 455 nm, 475 nm, 490 nm, 615 nm and 700 nm (Fig. 1d), due to f-f emission of electron or energy transfer processes which is assigned to the 5D0-7FJ with J = 4–0 transitions [28]. The same results have been obtained for Eu(III)-S-5 and Eu(III)-S-6 complex with peptide, with high emission peak at 305 nm, which probably belongs to peptide--complex interaction.

2.2 Mass spectrometry measurement

To confirm that interactions between cell penetrating peptide with Eu(III) and Tb(III) Schiff base complex and complex itself were formed, mass spectrometry (MALDI-TOF) was applied. The main observed signals shown in (Fig. 2a and 2b) were assigned as follows: [Peptide^{+}H]$^{+}$ (*m/z* 790.63). It is evident that a proposed intramolecular complex, metal-peptide, was found, as shown in Figure 2c, 2d, 2e and 2f: [peptide--Eu(III)-H]+ (*m/z* 952.86), [2peptide-Eu(III)$^{\cdot}$H]$^{+}$ (m/z 1740.54); [peptide-2ClEu(III)$^{\cdot}$H]$^{+}$ (*m/z* 892.54), [peptide-Eu(III)-H]$^{+}$ (m/z 952.86), [2peptide-Eu(III)-H]$^{+}$ (*m/z* 1739.53); [peptide--2Cl-HTb(III)]+ (m/z 878.77), [peptide-Tb(III)--2Cl-H]+ (*m/z* 1041.89), [2peptide-2Tb(III)--$H_2O^{\cdot}$H]+ (m/z 1918.69) and [peptide-2Cl-H]$^{+}$ Tb(III)(*m/z* 878.73), [peptide-Tb(III)-2Cl-H]$^{+}$ (*m/z* 1041.83), [2peptide-2Tb(III)-H_2O-H]$^{+}$ (*m/z* 1918.54). The intensity of peptide signal without incubation with metal was lower than with metal complexes in both cases (Eu(III) and Tb(III)). The spectra Tb(III)-S-5-peptide and Tb(III)-S-6-peptide showed no significant

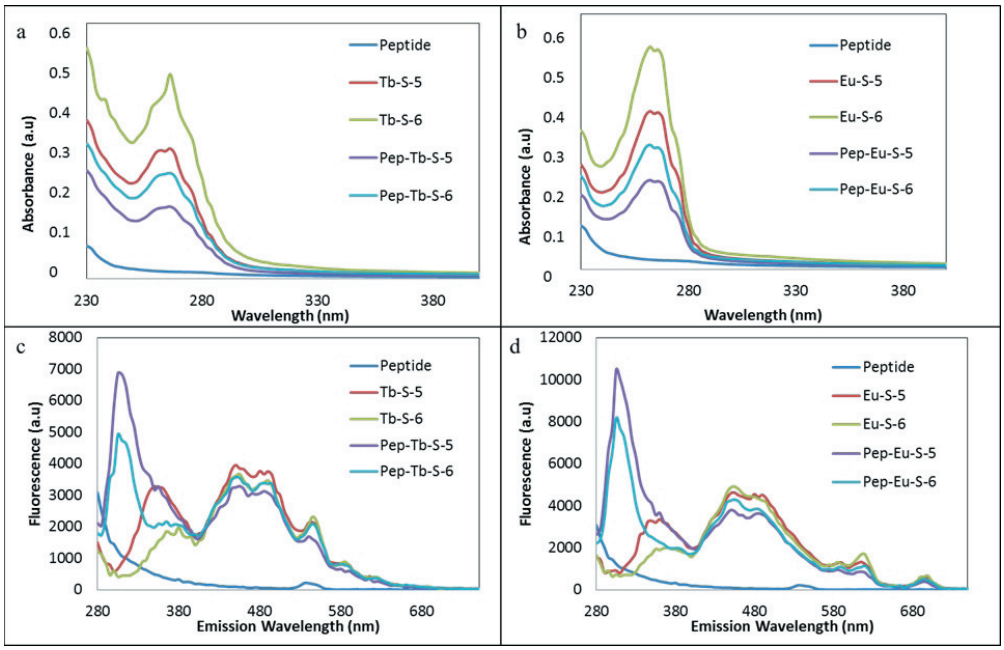

Figure 1: (a) Absorption and fluorescence spectra of cell penetrating peptide, Tb(III)-S-5 and Tb(III)-S-6 Schiff base complex. (b) Absorption and fluorescence spectra of cell penetrating peptide, Eu(III)-S-5 and Eu(III)-S-6 Schiff base complex.

difference in the formation of complexes. We cannot confirm the type of bonding that occurs between the metal and the peptide by MALDI-TOF, however from the results it is obvious that complexes between peptide and Eu(III) and Tb(III) are formed [29,30]. From the results we can conclude, that Schiff bases are replaced by peptides during reaction and 1:1 lanthanides complexes or dimers are formed. This conclusion can be explained by affinity of lanthanides to oxygen atoms which are present in peptides. Much stronger bonds are therefore formed in comparison with nitrogen coordination in the case of Schiff bases.

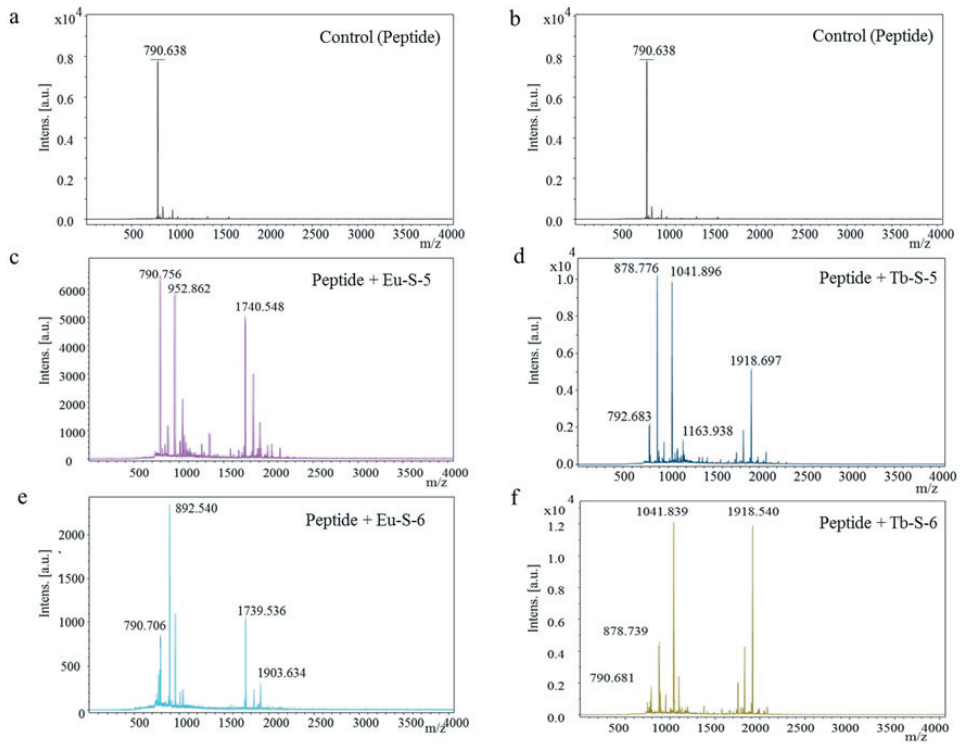

Figure 2: (a,b) Mass spectra of peptide. (c) Mass spectrum of peptide interaction with Eu(III)-S-5 complex, (d) Tb(III)-S-5 complex, (e) Eu(III)-S-6 complex, (f) Tb(III)-S-6 complex.

*2.3 Influence of Eu(III) and Tb(III) Schiff base complex on **E. coli***

Today it is well known that growth of microorganisms can be limited by heavy metal ions which can be incorporated into a variety of materials and as such they perform strong antibacterial activity [31,32]. Effect of Eu(III) and Tb(III) Schiff base complex on *E. coli* was conducted by method of determination of growth dependences, where the 50% inhibitory concentration (IC_{50}) was determined. In this experiment antimicrobial activity of Eu(III) (S-5 and S-6) and Tb(III) (S-5 and S-6) Schiff base complex conjugates with cell penetrating peptide were determined. Obtained results show that Eu(III)-S-5 and Eu(III)-S-6 conjugate with cell penetrating peptide (Fig. 3a, 3b) have stronger antimicrobial effect. In the case of *E. coli* treated with Eu(III)-S-5 and Eu(III)-S-6, there was minimal inhibitory concentration (MIC) determined after addition of 0.125 mM and totally inhibitory concentration (TIC) after application of 5 mM. IC_{50} for Eu(III)-S-5 was statistically calculated as 1.6 mM (Fig. 3a). Also, the same results were obtained for Eu(III)-S-6, only in the case of this sample IC_{50} was determined as 1.3 mM (Fig. 3b). In appli-

cation of Tb(III)-S-5 and Tb(III)-S-6 conjugate with cell penetrating peptide the minimal inhibitory concentration (MIC) was 0.125 mM and the total inhibitory concentration (TIC) was 5 mM (Fig. 3c, 3d). However, treatment of *E. coli* with Tb(III)-S-5 showed that IC_{50} was statistically calculated as 2.5 mM (Fig. 3c). After application of Tb(III)-S-6 on *E. coli* results showed that total inhibitory concentration (TIC) is not sufficient for inhibition, because in the case of this sample IC_{50} was calculated as 10 mM (Fig. 3d), what indicates lower toxicity of Tb(III)-S-6 on bacterial strains in comparison to the other three samples, which correlates with lower concentration values required for the bacterial inhibition.

However, to confirm that metal-peptide complex have main role in antibacterial activity, peptide conjugate with S-5 and S-6 Schiff base without Terbium and Europium were applied on E. coli. Results show that treatment of E. coli with S-5 Schiff base conjugate with cell penetrating peptide showed that IC_{50} was statistically calculated at 19.2 mM and for S-6 Schiff base conjugate with cell penetrating peptide at 20 mM. Due to that we can conclude that main role in antibacterial activity have samples that contain Schiff base complex with Terbium and Europium. Antibacterial effect of applied samples come from Schiff base complex with Terbium and Europium and peptide, with ability to easily penetrate the bacterial cell membrane by coordination of metal ion through oxygen or nitrogen donor atom with lipopolysaccharide (LPS) causing the damage of cell membrane. Atabay et. al, report application of monometallic complexes with $PdCl_2$ and ZnX_2, were ligand acts as a chelating tridentate or bidentate, through two of the nitrogen atoms in the imidazole ring and the sulfur atom of the bridging group together with two chloride ions forming a rare five coordinate complex

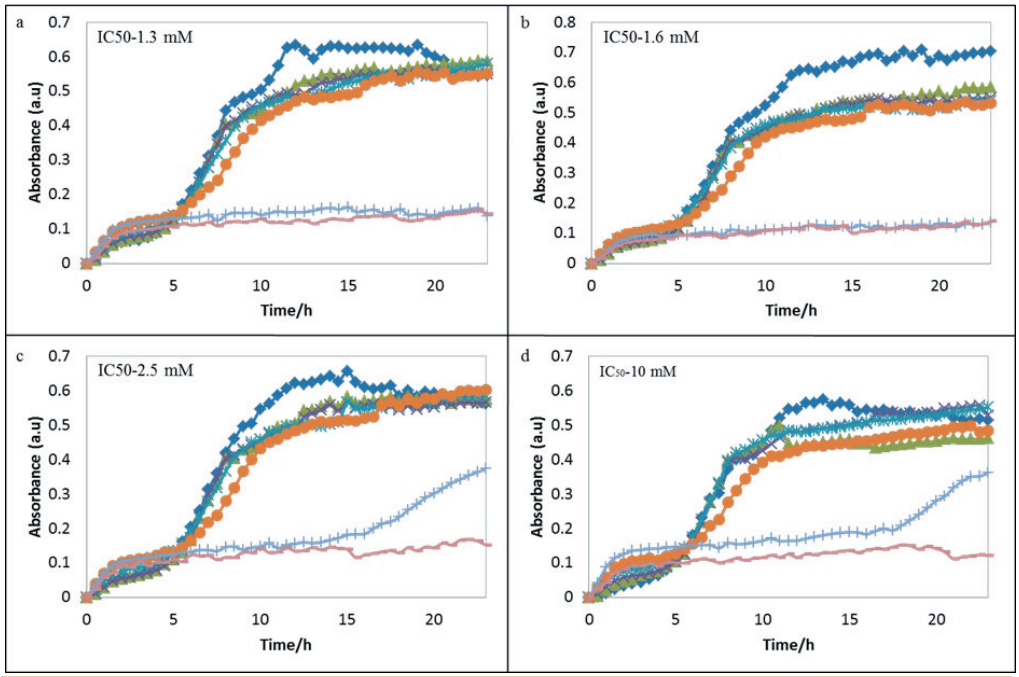

Figure 3: Spectrophotometric determination of growth curves obtained by treatment with 0, 0.125, 0.312, 0.625, 1, 2.5 and 5 mM concentration of Eu(III) and Tb(III) Schiff base complex conjugate with cell penetrating peptide of: (a) E. coli after application of Eu(III)-S-5 conjugate with CPP. (b) E. coli after application of Eu(III)-S-6 conjugate with CPP. (c) E. coli after application of Tb(III)-S-5 conjugate with CPP. (d) E. coli after application of Tb(III)-S-6 conjugate with CPP.

and tetrahedral complexes, which have strong antibacterial activity [33,34].

3. Experimental Section

3.1 Chemicals

2-pyridinecarboxaldehyde, diethylenetriamine, tris(2-aminoethyl)amine, europium(III) chloride, terbium(III) chloride, methanol, glycerol, glucose, tryptophan, yeast extract were purchased from Sigma–Aldrich Co. (St. Louis, MO, USA). Deionized water underwent demineralization by reverse osmosis using an Aqua Osmotic 02 (Aqua Osmotic, Czech Republic) and was subsequently purified using a Millipore RG (MiliQ water, 18 M, Millipore Corp., Billerica, MA, USA).

3.2 Synthesis of KKKRKC peptide

For synthesis, Liberty Blue peptide synthesizer was used (CEM, Matthews, NC, USA). The sequences and monoisotopic molecular weights of synthesized peptides were as follows: KKKRKC - 790 Da. Deblock of Fmoc protecting group was performed with 20 % piperidine v/v in DMF. Coupling was achieved using N,N,N',N'-tetramethyl-O-(1H-benzotriazol-1-yl)uronium hexafluorophosphate (HBTU), N,N-diisopropylethylamine (DIEA) and DMF. Cleavage of side chain protecting groups was performed by treating the peptide resin with 95 % trifluoroacetic acid v/v, 2.5 % H_2O v/v and 2.5 % TIPS v/v for 30 minutes at 38 °C under microwave irradiation. Isolation of peptide was performed by centrifugation (6000 rpm, 3 min) under cold diethylether.

3.3 Synthesis of Eu(III)-S-5 and Tb(III)-S-5 Schiff base complexes

2-pyridinecarboxaldehyde (2850 µl) and diethylenetriamine (1080 µl) were added in 35 mL of methanol and refluxed for 6 h. After cooling, methanol was added to 50 ml. Tb(III)$Cl_3 \cdot 6H_2O$ (0.435 g) or Eu(III)$Cl_3 \cdot 6H_2O$ (0.366 g) was dissolved in 50 ml of water. After that Schiff base (5 ml) was added to the solution with stirring. Solutions were heated at 80 °C for 2 h. After that the solutions were filtered and water was added to reach 100 ml with final concentration 10 mM.

3.4 Synthesis of Eu(III)-S-6 and Tb(III)-S-6 Schiff base complexes

2-pyridinecarboxaldehyde (2850 µl) and tris(2-aminoethyl)amine (1498 µl) were added in 35 mL of methanol and refluxed for 6 h. After cooling, methanol was added to 50 ml. Tb(III)$Cl_3 \cdot 6H_2O$ (0.435 g) or Eu(III)$Cl_3 \cdot 6H_2O$ (0.366 g) were dissolved separately in 50 ml of water. After that Schiff base (5 ml) was added to the both solutions with stirring. The solutions were heated at 80 °C for 2 h. After that solutions were filtered and water was added to reach 100 ml with final concentration 10 mM.

3.5 Cultivation of bacterial strains

Staphylococcus aureus (NCTC 8511), Escherichia coli (NCTC 13216) and methicillin-resistant Staphylococcus aureus (7111 2/A8) were obtained from the Czech Collection of Microorganisms, Faculty of Science, Masaryk University, Brno, Czech Republic. The strains were stored as a spore suspension in 20% (v/v) glycerol at -20°C. Prior to use in this study, the strains were thawed and the glycerol was removed by washing with distilled water.

The composition of cultivation medium was as follows: glucose 10 g/l, tryptone 10 g/l and yeast extract 5 g/l, sterilized MilliQ water with 18 MΩ. pH of the cultivation medium was adjusted at 7.4 before sterilization. The sterilization of the media was carried out at 121 °C for 30 min in sterilizer (Tuttnauer 2450EL, Israel). The prepared cultivation media were inoculated with bacterial cultures or yeasts into 25 ml Erlenmeyer flasks. After inoculation, bacteria and yeasts were cultivated for 24 h on a shaker at 600 rpm and 37 °C. Strains, cultivated under these conditions, were diluted by cultivation medium to $OD_{600} = 0.1$ and used in the following experiments.

3.6 Determination of growth curves

The procedure for the evaluation of the antimicrobial effect of tested compounds consisted in measuring of the absorbance using the apparatus Multiskan EX (Thermo Fisher Scientific, Germany) and subsequent analysis in the form of growth curves. Bacteria and yeasts were

cultivated in GTY medium for 24 h with shaking and were diluted with GTY medium using Specord spectrophotometer 210 (Analytik, Jena, Germany) at a wavelength of 600 nm to absorbance 0.1. On the microplate, these cultures were mixed with various concentrations of peptide and peptide-Eu(III) and Tb(III) Schiff base complex or S. aureus alone as a control for measurements. The concentrations of all samples were 0; 7.8; 15.6; 31.3; 62.5; 125; 250 and 500 μg/ml. Total volume in the microplate wells was always 300 μl. The measurements were carried out at time 0, then each half-hourly for 24 h at 37 °C and a wavelength of 600 nm. The obtained values were analyzed in graphical form as growth curves for each variant individually. Software STATISTICA (data analysis software system), version 10.0 (Tulsa, OK, USA) was used for data processing. The half-maximal concentrations (IC50) were calculated from logarithmic regression of sigmoidal dose-response curve. The general regression model was used to analyse differences between the combinations of compounds.

3.7 UV/Vis spectrophotometry

Measurements of peptide and europium(III) and terbium(III) Schiff base complexes fluorescence were conducted by a multifunctional microplate reader Tecan Infinite 200 PRO (Tecan group Ltd., Männedorf, Switzerland). The absorbance scans were recorded in the range of 200–800 nm each 5 nm. Emission wavelengths from 260 nm to 850 nm were measured at different excitation wavelengths (280 nm, 350 nm, and 400 nm) with 200 μl of the sample placed on a Costar UV-transparent, acrylic copolymer, flat bottom, 96 well plate (Sigma–Aldrich Co. St. Louis, MO, USA). All measurements were performed at 30 °C controlled by the Tecan Infinite 200 PRO (TECAN, Switzerland).

3.8 Matrix-assisted laser desorption/ ionization (MALDI-TOF)

The mass spectrometry experiments were performed on a MALDI-TOF/TOF mass spectrometer Bruker Ultraflextreme (Bruker Daltonik GmbH, Germany) equipped with a laser operating at wavelength of 355 nm with an accelerating voltage of 25 kV, cooled with nitrogen and a maximum energy of 43.2 μJ with repetition rate 2000 Hz in linear and positive mode, and with software for data acquisition and processing of mass spectra flexControl version 3.4 and flexAnalysis version 2.2. The matrix used in the MALDI method was α-cyano--4-hydroxycinnamic acid (CCA) (Bruker). The matrix was prepared in TA30 (30% acetonitrile, 0.1% trifluoroacetic acid solution). Mixture was thoroughly vortexed and ultrasonicated using Bandelin 152 Sonorex Digital 10P ultrasonic bath (Bandelin electronic GmbH, Germany) to 2 minutes 50% of intensity at ambient temperature. Working standard solutions were prepared daily by dilution of the stock solutions. The sample solutions were TA30. The solutions for analysis were mixed in ratio of 1:1 (matrix/substance). After obtaining a homogeneous solution, 1μl was applied on the target and dried under atmospheric pressure and ambient temperature. A mixture of peptide calibrations standard (Bruker) was used to externally calibrate the instrument. The MS spectra were typically acquired by averaging 20 sub spectra from a total of 500 shots of the laser (Smartbeam 2. Version: 1_0_38.5).

4. Conclusions

We have successfully synthesized and conjugated the Eu(III) and Tb(III) Schiff base complexes with KKKRKC cell penetrating peptide. All interactions between peptide and Eu(III) and Tb(III) Schiff complex were confirmed by spectrophotometric and mass spectrometry studies. UV/VIS spectra of Tb(III)-S-5-peptide and Tb(III)-S-6-peptide in the presence and absence of Schiff base affirmed an increase in peak intensity of complex and decrease in free Schiff base spectra indicating the formation of metal-peptide complex. The spectra of Tb(III)-S-5-peptide and Tb(III)-S-6-peptide show no significant difference in the formation of complexes by MALDI-TOF. Even though we cannot confirm the type of bonding that occurs between the metal and the peptide by MALDI-TOF, it is obvious that complexes between peptide and Eu(III) and Tb(III) Schiff base are formed. Europium and Terbium ions represent

the acid part of complex according to the Lewis acid theory where the nitrogen or oxygen bases can be bound via donor-acceptor bond, while peptide ligand transfers electron charge toward the metal center, forming interaction with the electron donor atoms. This property resulting in reduced metal ion polarity, through partial sharing of the positive charge with donor atoms of the ligand, enables higher antimicrobial activity. In other words, the chelation of peptide-Schiff base complex leads to increase in lipophilic properties allowing the complex penetration through lipid layers of the bacterial membrane [35]. Due to that reason Schiff base can easily penetrate the cell membrane by coordination of metal ions via donor-acceptor theory with lipopolysaccharide leading directly to membrane damage. Metal-peptide complex due to that in the future can shows great potential in biological application as antibacterial drug, however it is necessary conduct more experiment on metal rare complex and their application as antibacterial drug.

Acknowledgments

The financial support from the project CEITEC CZ.1.05/1.1.00/02.0068 is highly acknowledged. The authors thank Radek Chmela for his skilful technical assistance.

Conflicts of Interest

The authors declare they have no potential conflicts of interests concerning drugs, products, services or another research outputs in this study. The Editorial Board declares that the manuscript met the ICMJE „uniform requirements“ for biomedical papers.

References

1. Torchilin, V. Intracellular delivery of protein and peptide therapeutics. Drug discovery today. Technologies 2008, 5, e95-e103.
2. Perez-Tomas, R. Multidrug resistance: Retrospect and prospects in anti-cancer drug treatment. Current Medicinal Chemistry 2006, 13, 1859-1876.
3. Pujals, S.; Giralt, E. Proline-rich, amphipathic cell-penetrating peptides. Advanced Drug Delivery Reviews 2008, 60, 473-484.
4. Elmquist, A.; Langel, U. In vitro uptake and stability study of pvec and its all-d analog. Biological Chemistry 2003, 384, 387-393.
5. Vives, E.; Brodin, P.; Lebleu, B. A truncated hiv-1 tat protein basic domain rapidly translocates through the plasma membrane and accumulates in the cell nucleus. Journal of Biological Chemistry 1997, 272, 16010-16017.
6. Floren, A.; Maeger, I.; Langel, U. Uptake kinetics of cell-penetrating peptides. In Cell-penetrating peptides: Methods and protocols, Langel, U., Ed. 2011; Vol. 683, pp 117-128.
7. Johnson, L.N.; Cashman, S.M.; Kumar-Singh, R. Cell-penetrating peptide for enhanced delivery of nucleic acids and drugs to ocular tissues including retina and cornea. Molecular Therapy 2008, 16, 107-114.
8. Chiu, Y.L.; Ali, A.; Chu, C.Y.; Cao, H.; Rana, T.M. Visualizing a correlation between sirna localization, cellular uptake, and rnai in living cells. Chemistry & Biology 2004, 11, 1165-1175.
9. Turner, J.J.; Ivanova, G.D.; Verbeure, B.; Williams, D.; Arzumanov, A.A.; Abes, S.; Lebleu, B.; Gait, M.J. Cell-penetrating peptide conjugates of peptide nucleic acids (pna) as inhibitors of hiv-1 tat-dependent trans-activation in cells. Nucleic Acids Research 2005, 33, 6837-6849.
10. Yukawa, H.; Kagami, Y.; Watanabe, M.; Oishi, K.; Miyamoto, Y.; Okamoto, Y.; Tokeshi, M.; Kaji, N.; Noguchi, H.; Ono, K., et al. Quantum dots labeling using octa-arginine peptides for imaging of adipose tissue-derived stem cells. Biomaterials 2010, 31, 4094-4103.
11. Heitz, F.; Morris, M.C.; Divita, G. Twenty years of cell-penetrating peptides: From molecular mechanisms to therapeutics. British Journal of Pharmacology 2009, 157, 195-206.
12. Geisler, I.; Chmielewski, J. Cationic amphiphilic polyproline helices: Side-chain variations and cell-specific internalization. Chemical Biology & Drug Design 2009, 73, 39-45.
13. Mussbach, F.; Franke, M.; Zoch, A.; Schaefer, B.; Reissmann, S. Transduction of peptides and proteins into live cells by cell penetrating peptides. Journal of Cellular Biochemistry 2011, 112, 3824-3833.
14. Miller, L.W.; Cornish, V.W. Selective chemical labeling of proteins in living cells. Current Opinion in Chemical Biology 2005, 9, 56-61.
15. Domaille, D.W.; Que, E.L.; Chang, C.J. Synthetic fluorescent sensors for studying the cell biology of metals. Nature Chemical Biology 2008, 4, 168-175.
16. Shaner, N.C.; Steinbach, P.A.; Tsien, R.Y. A guide to choosing fluorescent proteins. Nature Methods 2005, 2, 905-909.
17. Weng, J.F.; Ren, J.C. Luminescent quantum dots: A very attractive and promising tool in biomedicine. Current Medicinal Chemistry 2006, 13, 897-909.
18. Gonzalez, D.; Lokhande, N.; Vadde, S.; Zhao, Q.; Cassill, A.; Renthal, R. Luminescence resonance energy transfer in the cytoplasm of live escherichia coli cells. Biochemistry 2011, 50, 6789-6796.
19. Eliseeva, S.V.; Buenzli, J.-C.G. Lanthanide luminescence for functional materials and biosciences. Chemical Society Reviews 2010, 39, 189-227.
20. Bunzli, J.C.G.; Piguet, C. Taking advantage of luminescent lanthanide ions. Chemical Society

Reviews 2005, 34, 1048-1077.
21. Dickins, R.S.; Parker, D. Signalling reversible anion binding in aqueous media. Macrocyclic Chemistry: Current Trends and Future Perspectives 2005, 121-+.
22. Shen, J.; Sun, L.-D.; Yan, C.-H. Luminescent rare earth nanomaterials for bioprobe applications. Dalton Transactions 2008, 5687-5697.
23. Zangana, K.H.; Pineda, E.M.; Winpenny, R.E.P. Tetrametallic lanthanide(iii) phosphonate cages: Synthetic, structural and magnetic studies. Dalton Transactions 2014, 43, 17101-17107.
24. Wu, Y.; Morton, S.; Kong, X.; Nichol, G.S.; Zheng, Z. Hydrolytic synthesis and structural characterization of lanthanide-acetylacetonato/hydroxo cluster complexes - a systematic study. Dalton Transactions 2011, 40, 1041-1046.
25. Hauser, C.P.; Thielemann, D.T.; Adlung, M.; Wickleder, C.; Roesky, P.W.; Weiss, C.K.; Landfester, K. Luminescent polymeric dispersions and films based on oligonuclear lanthanide clusters. Macromolecular Chemistry and Physics 2011, 212, 286-296.
26. Thielemann, D.T.; Wagner, A.T.; Roesch, E.; Koelmel, D.K.; Heck, J.G.; Rudat, B.; Neumaier, M.; Feldmann, C.; Schepers, U.; Braese, S., et al. Luminescent cell-penetrating pentadecanuclear lanthanide clusters. Journal of the American Chemical Society 2013, 135, 7454-7457.
27. Galindo-Murillo, R.; Cheatham, T.E., III. DNA binding dynamics and energetics of cobalt, nickel, and copper metallopeptides. Chemmedchem 2014, 9, 1252-1259.
28. Shintoyo, S.; Fujinami, T.; Matsumoto, N.; Tsuchimoto, M.; Weselski, M.; Bienko, A.; Mrozinski, J. Synthesis, crystal structure, luminescent and magnetic properties of europium and terbium complexes with a bidentate benzoate and a tripod n-7 ligand containing three imidazole, ln(iii)(h3l)benzoate (clo4)(2)center dot h2o center dot 2meoh (ln(iii) = eu-iii and tb-iii). Polyhedron 2015, 91, 28-34.
29. Bassett, A.P.; Magennis, S.W.; Glover, P.B.; Lewis, D.J.; Spencer, N.; Parsons, S.; Williams, R.M.; De Cola, L.; Pikramenou, Z. Highly luminescent, triple- and quadruple-stranded, dinuclear eu, nd, and sm(iii) lanthanide complexes based on bis-diketonate ligands. Journal of the American Chemical Society 2004, 126, 9413-9424.
30. Hampe, O.; Klyatskaya, S.; Karpuschkin, T.; Vonderach, M.; Weis, P.; Ruben, M.; Kappes, M.M. Mass spectrometric characterization of a dinuclear terbium phthalocyaninato complex. International Journal of Mass Spectrometry 2012, 325, 183-188.
31. Martinez-Abad, A.; Sanchez, G.; Lagaron, J.M.; Ocio, M.J. On the different growth conditions affecting silver antimicrobial efficacy on listeria monocytogenes and salmonella enterica. International Journal of Food Microbiology 2012, 158, 147-154.
32. Percival, S.L.; Thomas, J.; Linton, S.; Okel, T.; Corum, L.; Slone, W. The antimicrobial efficacy of silver on antibiotic-resistant bacteria isolated from burn wounds. International Wound Journal 2012, 9, 488-493.
33. Chohan, Z.H.; Farooq, M.A.; Scozzafava, A.; Supuran, C.T. Antibacterial schiff bases of oxalylhydrazine/diamide incorporating pyrrolyl and salicylyl moieties and of their zinc(ii) complexes. Journal of Enzyme Inhibition and Medicinal Chemistry 2002, 17, 1-7.
34. Agh-Atabay, N.M.; Dulger, B.; Gucin, F. Structural characterization and antimicrobial activity of 1,3-bis(2-benzimidazyl)-2-thiapropane ligand and its pd(ii) and zn(ii) halide complexes. European Journal of Medicinal Chemistry 2005, 40, 1096-1102.
35. Osowole, A.A.; Kolawole, G.A.; Fagade, O.E. Synthesis, characterization and biological studies on unsymmetrical schiff-base complexes of nickel(ii), copper(ii) and zinc(ii) and adducts with 2,2 ,-dipyridine and 1,10-phenanthroline. Journal of Coordination Chemistry 2008, 61, 1046-1055.

The article is freely distributed under license Creative Commons (BY-NC-ND). But you must include the author and the document can not be modified and used for commercial purposes.

ARTICLE

HPV Detection in Leukocyte Samples of Spinocellular Carcinomas Using PCR

Ana Maria Jimenez Jimenez [1,2] , Lourdes Maria Herrera-Quintana[3], Simona Dostalova[1,2], Zbynek Heger [1,2], Branislav Ruttkay-Nedecky[1,2], and Rene Kizek [1,2*]

[1] Department of Chemistry and Biochemistry, Faculty of Agronomy, Mendel University in Brno, Zemedelska 1, CZ-613 00 Brno, Czech Republic, European Union; E-Mail: anuskajj@hotmail.com (A. J. J.); lourdesherrera@correo.ugr.es (L.H.Q.); Esedinka@seznam.cz (S. D.); heger@mendelu.cz (Z. H.); brano.ruttkay@seznam.cz (B. R. N.); kizek@sci.muni.cz (R. K.)

[2] Central European Institute of Technology, Brno University of Technology, Technicka 3058/10, CZ-616 00 Brno, Czech Republic, European Union.

[3] Department of Physiology, Faculty of Pharmacy, Institute of Nutrition and Food Technology, Biomedical Research Centre, University of Granada, Spain.

* Author to whom correspondence should be addressed; E-Mail: kizek@sci.muni.cz;
Tel.: +420-5-4513-3350; Fax: +420-5-4521-2044.
Received:18.6.2015 / Accepted:8.7.2015 / Published:1.10.2015

Head and neck cancer are a malignant tumours originating in the upper aerodigestive tract, including the oral cavity, larynx, pharynx and nasopharynx. The vast majority of head and neck cancers are squamous cell carcinomas (HNSCC) arising from the epithelial membranes of these regions. The environmental pollution, high alcohol consumption and smoking are associated with this type of cancer, and also human papilloma virus (HPV) is involved in HNSCC carcinogenesis. Many different methodologies have been developed for detection of HPV virus. This manuscript is dealing with the HPV detection in leukocyte samples of 103 patients with spinocellular carcinomas using PCR method for detection and subtypes identification. 56 positives samples were detected for HPV papillomavirus. Further, the positives samples were tested with HPV type-specific primers and 21.4% were HPV 16 type and 12.5% were HPV 18 type. 7% of these samples were positive for both HPV16 and HPV18 type.

Keywords: Human papillomavirus; head and neck cancer; PCR.

1. Introduction

Head and neck squamous cell carcinomas (HNSCCs) are malignant tumors of epidermal keratinocytes, that affect mainly the lip, oral cavity, nasal cavity, paranasal sinuses, pharynx, and larynx [1]. HNSCCs grow locally and infrequently metastasize [2]. This carcinomas are one of the major forms of skin cancer, which arises from the uncontrolled multiplication of epithelial cells or other cell types such as keratinocytes, tonofilament bundles, desmosomes, or structures involved in cell-to-cell adhesion [3]. At the time of diagnosis, HNSCCs spread to the lymph nodes of the neck, and this is often the first sign of the disease. The surgery and radiation are the common therapy against this cancer [4].

The HNSCCs is the sixth leading cancer by incidence worldwide and eighth by death. There are 0.5 million new cases a year worldwide [5]. The environmental pollution and wrong life style, which are associated with the squamous cell carcinomas, involve following risk factors: tobacco smoking, alcohol consumption, UV light, particular chemicals used in certain workplaces, and certain strains of viruses, such as human papillomavirus (HPV) [6].

Human papillomaviruses (HPVs) are small DNA viruses with a strict tropism for human epithelial cells. In general, HPV infections are asymptomatic and persist for 18–24 months before they are cleared by the immune system of the host [7]. Tumorigenicity of HPVs differs markedly among HPV genotypes [8]. This virus

has been associated with HNSCCs in the areas of the oropharynx, lung, fingers, and anogenital region [1]. Functional loss of p53 tumor suppressor gene, mutations in Ras protooncogenes, and certain chromosomal aberrations are characteristics of cancer caused by HPVs [9].

Many different methods are able to give information about the presence of HPVs in biological samples. The combination of a sensitive test, and a specific test, could allow for the best potential to accurately establish the presence or absence of HPVs [10,11].The mainly utilized tests for HPV identification among others, are polymerase chain reaction (PCR) testing, real time PCR, in situ hybridization analysis (IS), immunohistochemical (IHC) staining for tumor suppressor protein p16, and southern blotting assays [11].

The methodology for polymerase chain reaction (PCR) is an indispensable technique used in molecular biology in research labs to amplify a single copy of DNA generating thousands to millions of copies of chosen DNA sequence [12]. This technique has a big variety of applications like DNA cloning for DNA sequencing, DNA-based phylogeny, or functional analysis of genes; the diagnosis of hereditary diseases; the identification of genetic fingerprints and the detection and diagnosis of infectious diseases. PCR can be extensively modified to perform a wide array of genetic manipulations [10,13].

Patients	Age	Histological group	Localization	Grade	Stage	Metastasis
92% Men	69	97% Spinocellular	73% Dissem	95%High	49% I-II 51% III-IV	5%
8% Women	64	99% Spinocelullar	81% Dissem	93%High	69% I-II 51% III-IV	6%

Table 1: Clinical characterization of patients. Analysis the medical information obtained from patients with head and neck cancer from St. Anne´s University Hospital in Brno, differentiating between men and women and their clinical histological data.

In HPV detection the PCR represents a highly-sensitive and cost-effective method. It can be used to detect as little as one copy of a DNA sequence from paraffin-embedded tissues or fresh tissues from biopsies [14]. The disadvantages of PCR techniques are that they have lower specificity, they do not allow distinction between all HPV types that are present in the neoplastic cells and non-neoplastic and they cannot distinguish between episomal and integrated HPV DNA[15]. Furthermore, the presence of latent viruses leads to false positive results due to the ability of PCR to detect just a few copies of HPV DNA per cell. Different attempts have been made to resolve this issue through the use of real-time PCR, which provides a quantitative analysis of viral load [16].

The combined results of immunocytochemical detection of p16 protein and the detection of HPV DNA by specific PCR enable better discrimination between latent and carcinogenic HPV infections and thus can provide information on the prognosis of HNSCC patients and facilitate therapeutic decisions[17].

The detection of the viral oncoproteins E6 and E7 requires technique that is restricted to the research laboratory, like RNA extraction and polymerase chain reaction amplification. The development of RNA in situ hybridization (ISH) probes complementary to E6/E7 mRNA permits direct visualization of viral transcripts in routinely processed tissues and has opened the door for accurate HNSCC detection in the clinical care setting [18].

2. Results and Discussion

2.1 Clinical Characterization of Patients

In this study 103 DNA samples were isolated from leukocytes of patients with head and neck cancer from St. Anne´s University Hospital in Brno and purified using QIAamp DNA Mini Kit. The average age of the patients was 69 years for

men and 64 years for women.

92% of the patients were men and 8% women, with major diagnosis for both which was oropharynx cancer with spinocellular histological type, followed with adenocarcinomas and basaliomas. Only a low percentage of the high grade tumors in men and women were found. These men presented a 51% of this cancer in the stage III-IV, with a 5% of metastasis, while the women presented a 69% of this cancer in the stage I-II, with a 6% of metastasis (Table.1).

2.2 PCR detection and subtypes identification

The samples were analyzed using PCR with specific primers for HPV detection and subtypes identification. DNA from leukocytes samples was tested using GP5/GP6 set of primers located within the L1 region of HPV genome. Furthermore, the samples were also tested with type-specific primers for HPV types 16 and 18

Figure 1: Scheme of HPV detection using PCR. First, GP5/GP6 primers for HPV detection were used. Next, the 56 HPV positive samples were analyzed with the type-specific primers for HPV-16 and HPV-18, obtaining 12 samples of HPV16, 7 samples of HPV-18 and 4 samples were HPV-16 and HPV-18 at the same time.

(Fig. 1).The quality of the isolated DNA, was determined with β-actin gene. 85 of the 103 DNA samples were β-actin positive and thus, adequate for further analysis. In this group of samples, 56 positives samples were detected for HPV which were obtained in 65.9% cases. We identified the subtypes with type-specific primers for HPV-16 and HPV-18 obtaining 21.4% of HPV-16 type and 12.5% of HPV-18 type. 7% of these samples were HPV-16 and HPV-18 positives at the same time and were determined as high grade tumors (Fig.2).

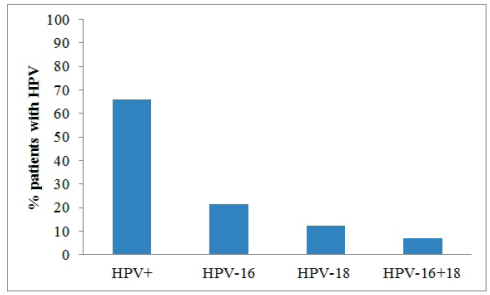

Figure 2: HPV detection and subtypes identification of the patients by PCR method. GP5/GP6 primers were used for HPV detection (65.9%) and HPV16-18 primer for subtyping (21.4% HPV-16, 12.5% HPV-18 and a 7% for HPV16-18).

2.3 Sequencing analysis

The HPV positive samples were also checked by PCR sequencing. After purification and sequencing of these samples, they were studied by in silico analysis using BLAST searches and Clustalw Multiple Sequence Alignment, obtaining 73% of identities with full length sequence of L1 HPV major capsid protein (Fig.3).

2.4 Discussion

We have used in our study the polymerase chain reaction (PCR) method for HNSCCs detection in leukocyte samples, because is a highly-sensitive, fast and cost-effective method. The PCR methods enable the detection of large number of HPV genotypes and also can increase significantly the positivity rate of HPV DNA detection in samples with a low DNA copy number. In conclusion, we preselected the samples using sets of primers located within the L1 region of HPV genome (GP5/GP6 primers) and with an additional amplification to typing of PCR--positive samples with the HPV type-specific primers (HPV16-18 primers). The samples were also tested by PCR sequencing and by in silico analysis, where was obtained a 73% of identities with the sequence of L1 HPV major capsid protein, which confirms the presence of HPV.

The first studies that used the set of GP5/GP6 primers for HPV detection were done in samples of patients with cervical cancer. Jacobs et al, introduced a GP5/GP6 PCR-based procedure in which they included Southern blot

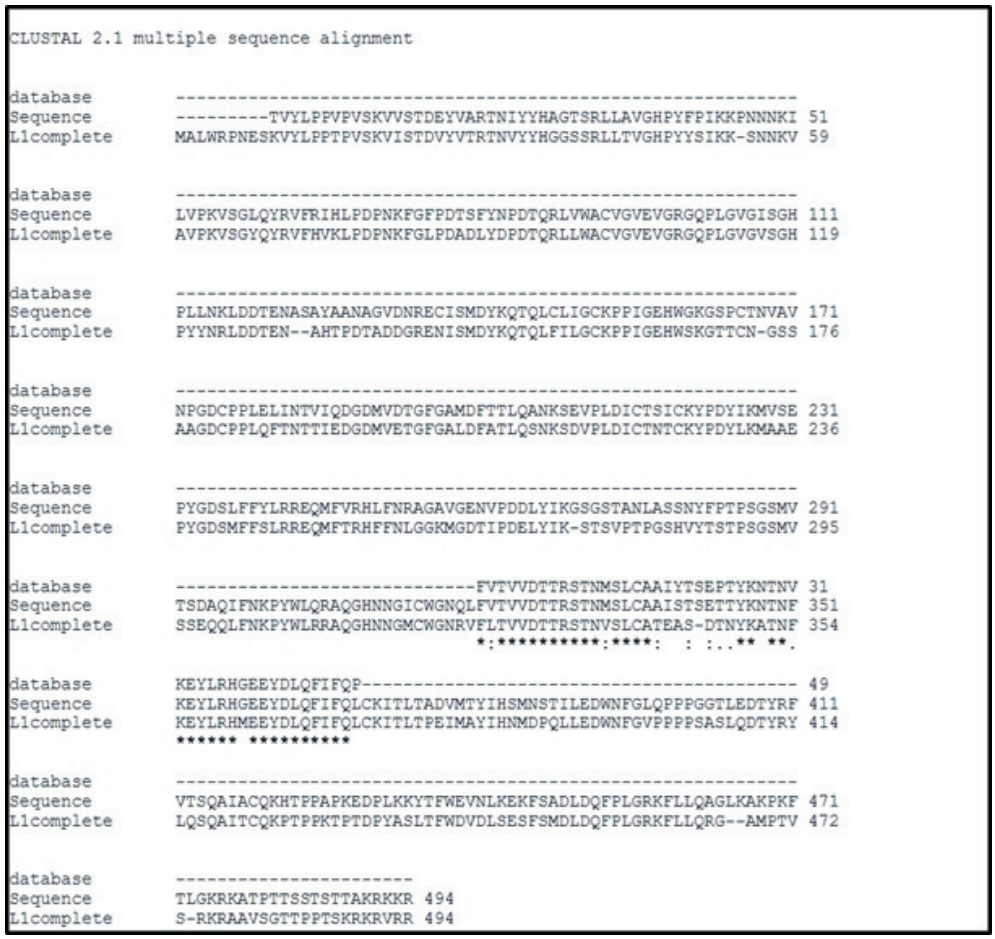

Figure 3: Multiple sequence alignment using ClustalW2. The sequences used in this alignment were, sequence of the amplicon obtained with the GP5/GP6 set of primers (called database), the sequence obtained from analysis of our samples (called Sequence), and a complete sequence of L1 gene (called L1 complete).

hybridization of PCR products with cocktails of radioactively labeled HPV type-specific internal oligonucleotides to detect a broad spectrum of genital HPV genotypes in one PCR[19]. De Roda Husman et al observed that the GP5/GP6 PCR method provided an increased detection of HPV level in poorly cervical scrapes[20]. Baay et al, compared the efficacies of three general primer pairs (GP5/6, CPI/IIG, MY09/11) for the detection of HPV DNA in formaldehyde-fixed paraffin-embedded carcinomas. The efficacy of each primer pair increased in HPV DNA detection in a 87.6%[21].

3. Experimental Section

3.1 Clinical specimens

A total of 103 histopathologically confirmed head and neck cancer subjects were involved in the study. The samples were collected from St. Anne´s University Hospital, Department of Otorhinolaryngology and Head and Neck Surgery. Enrolment of patients into realized clinical study was approved by the Ethic Committee of the Faculty of Medicine, Masaryk University, Brno, Czech Republic.

Primer	Sequence (5'-3')	Reference
GP5 GP6	TTTGTTACTGTGGTAGATAC GAAAAATAAACTGTAAATCA	(Snijders et al., 1990[22])
HPV16fw HPV16rv	CCCAGCTGTAATCATGCATGGAGA GTGTGCCCATTAACAGGTCTTCCA	(Soler et al., 1991[23])
HPV18fw HPV18rv	CGACAGGAACGACTCCAACGA GCTGGTAAATGTTGATGATTAACT	(Soler et al., 1991[23])
β-actin fw β-actin rv	CCTGAACCCTAAGGCCAACC GCAATGCCTGGGTACATGGT	(Ueyama et al.,1987[24])

Table 2: List of primers used in this study [25].

3.2 Extraction and quantification of DNA

DNA was isolated and purified from leukocytes using QIAamp DNA Mini Kit (Qiagen, Venlo, Netherlands), following the manufacturer's instructions. The concentration of purified DNA was determined using multimode reader Infinite 200 (Tecan, Männedorf, Switzerland).

3.3 Polymerase chain reaction (PCR)

The 142 base-pair long sequence of L1 gene was amplified using GP5 and GP6 primers. The PCR mixture from New England Biolabs (UK), containing the PCR buffer (10 mM Tris–HCl, pH 8.3, 50 mM KCl with 2.5 mM $MgCl_2$ included) 0.05 mM of each dNTP and 0.05 mM of GP5 and GP6 primers (Table 2). The DNA amplification was carried out during 40 cycles that included the denaturation at 94°C for 30 s, the annealing at 45°C for 30 s and the primer extension at 72°C for 30 s.

The positive samples for HPV were analyzed using PCR with the HPV-16 and HPV-18 primers. The PCR amplicons reached length of 202 bp for HPV-16 and 272 bp for HPV-18. The PCR mixture from New England Biolabs (UK), containing the PCR buffer (10 mM Tris–HCl, pH 8.3, 50 mM KCl with 2.5 mM $MgCl_2$ included) 0.05 mM of each dNTP and 0.05 mM of each couples of primers (Table 1). The DNA amplification was carried out during 40 cycles that included the denaturation at 94°C for 30 s, the annealing at 58°C for 30 s and the primer extension at 72°C for 30 s.

As the internal quality control of the isolated DNA, β-actin gene (600bp) was used. The PCR mixture from New England Biolabs (UK), contained the PCR buffer (10 mM Tris–HCl, pH 8.3, 50 mM KCl with 2.5 mM $MgCl_2$ included) 0.05 mM of each dNTP and 0.05 mM of each couples of primers (Table 2). The DNA amplification was carried out during 40 cycles that included the denaturation at 94°C for 30 s, the annealing at 58°C for 30 s and the primer extension at 72°C for 45 s. Each PCR product was analysed using electrophoresis on 1% agarose gels stained with ethidium bromide.

3.4 Sequencing

GenomeLab DTCS Quick Start kit (Beckman Coulter, USA) with 20 ng of purifed amplified DNA from the PCRs was used for the sequencing reaction. The cycling conditions were as follows: 30 cycles of denaturation at 96 °C for 20 s; annealing at 50 °C for 20 s and 60 °C for DNA synthesis for 4 min. DNA fragments from this reaction were purified using magnetic particles CleanSEQ (Beckman Coulter, USA). DNA sequencing was performed on Genetic Analysis System CEQ 8000 (Beckman Coulter, USA). After denaturation at 90 °C for 2 min, the fluorescence-marked DNA fragments were separated in 33 cm capillary with 75 μm i.d.

(Beckman Coulter, USA), which was filled with a linear polyacrylamide denaturing gel (Beckman Coulter, USA). The separation was performed at capillary temperature of 50 ºC and voltage of 4.2 kV for 85 min.

3.5 Sequence analyses

Sequence analyses were performed using, BLASTX algorithm available from the NCBI (http://blast.ncbi.nlm.nih.gov/;[26]) and ClustalW2 algorithm available at EBI (http://www.ebi.ac.uk/Tools/clustalw2/;[27]).

4. Conclusions

The polymerase chain reaction is a suitable method enabling the detection of HPVs and differentiation between different subtypes. Many different HPV tests are available. All of the methods are able to give information about the presence of HPV in biological samples. The majority of carcinomas are caused by the most common and high risk HPV types, HPV-16 and HPV-18, which contain the E6-E7 oncogenes. The patients infected with one type of HPV were significantly more likely to harbor additional HPV types. Thus, evaluation of risk rate of heterogeneous coinfections has to be further done to determine the effects on head and neck cancer development.

Acknowledgments

Financial support from SPINCANCER NT/14337 is highly acknowledged.

Conflicts of Interest

The authors declare they have no potential conflicts of interests concerning drugs, products,services or another research outputs in this study. The Editorial Board declares that the manuscript met the ICMJE „uniform reguirements“ for biomedical papers.

References

1. Syrjanen, S. Human papillomavirus (hpv) in head and neck cancer. J. Clin. Virol. 2005, 32, S59-S66.
2. Syrjanen, S.; Rautava, J. Hpv and oral health response. J. Am. Dent. Assoc. 2012, 143, 442-444.
3. Syrjanen, K.J.; Chang, F.; Syrjanen, S.M. Hpv infections in etiology of benign and malignant sinonasal, bronchial and oesophageal squamous cell lesions. Medimond S R L: 40128 Bologna, 2000; p 169-179.
4. Janicek, M.F.; Averette, H.E. Cervical cancer: Prevention, diagnosis, and therapeutics. CA-Cancer J. Clin. 2001, 51, 92-114.
5. Badulescu, F.; Crisan, A.; Badulescu, A.; Schenker, M. Recent data about the role of human papillomavirus (hpv) in oncogenesis of head and neck cancer. Rom. J. Morphol. Embryol. 2010, 51, 437-440.
6. Chen, A.Y.; DeSantis, C.; Jemal, A. Us mortality rates for oral cavity and pharyngeal cancer by educational attainment. Arch. Otolaryngol. Head Neck Surg. 2011, 137, 1094-1099.
7. Schwartz, S. Papillomavirus transcripts and posttranscriptional regulation. Virology 2013, 445, 187-196.
8. Tsao, K.-C.; Huang, C.-G.; Kuo, Y.-B.; Chang, T.-C.; Sun, C.-F.; Chang, C.A.; Yang, S.-L.; Chan, E.-C. Prevalence of human papillomavirus genotypes in northern taiwanese women. Journal of Medical Virology 2010, 82, 1739-1745.
9. Garnett, T.O.; Duerksen-Hughes, P.J. Modulation of apoptosis by human papillomavirus (hpv) oncoproteins. Arch. Virol. 2006, 151, 2321-2335.
10. Gagnon, D.; Fradet-Turcotte, A.; Archambault, J. A quantitative and high-throughput assay of human papillomavirus DNA replication. Methods in molecular biology (Clifton, N.J.) 2015, 1249, 305-316.
11. Venuti, A.; Paolini, F. Hpv detection methods in head and neck cancer. Head and neck pathology 2012, 6 Suppl 1, S63-74.
12. Haugg, A.M.; Rennspiess, D.; zur Hausen, A.; Speel, E.J.M.; Cathomas, G.; Becker, J.C.; Schrama, D. Fluorescence in situ hybridization and qpcr to detect merkel cell polyomavirus physical status and load in merkel cell carcinomas. Int. J. Cancer 2014, 135, 2804-2815.
13. Rodel, F.; Wieland, U.; Fraunholz, I.; Kitz, J.; Rave-Frank, M.; Wolff, H.A.; Weiss, C.; Wirtz, R.; Balermpas, P.; Fokas, E., et al. Human papillomavirus DNA load and p16(ink4a) expression predict for local control in patients with anal squamous cell carcinoma treated with chemoradiotherapy. International journal of cancer. Journal international du cancer 2015, 136, 278-288.
14. Heidegger, I.; Pichler, R.; Muller, B.; Klocker, H.; Oswald, D.; Haid, B.; Zelger, B.; Horninger, W.; Oswald, J. Is real-time pcr the correct method to evaluate the incidence of human papillomavirus in prepuces of asymptomatic boys and men? World J. Urol. 2014, 32, 1199-1204.
15. Micalessi, M.I.; Boulet, G.A.; Bogers, J. A real-time pcr approach based on spf10 primers and the innolipa hpv genotyping extra assay for the detection and typing of human papillomavirus. Methods in molecular biology (Clifton, N.J.) 2015, 1249, 27-35.
16. Sahiner, F.; Kubar, A.; Gumral, R.; Ardic, M.; Yigit, N.; Sener, K.; Dede, M.; Yapar, M. Efficiency of my09/11 consensus pcr in the detection of multiple hpv infections. Diagn. Microbiol. Infect. Dis. 2014, 80, 43-49.
17. Linxweiler, M.; Bochen, F.; Wemmert, S.; Lerner, C.; Hasenfus, A.; Bohle, R.M.; Al-Kadah, B.;

Takacs, Z.F.; Smola, S.; Schick, B. Combination of p16(ink4a)/ki67 immunocytology and hpv polymerase chain reaction for the noninvasive analysis of hpv involvement in head and neck cancer. Cancer Cytopathol. 2015, 123, 219-229.
18. Westra, W.H. Detection of human papillomavirus (hpv) in clinical samples: Evolving methods and strategies for the accurate determination of hpv status of head and neck carcinomas. Oral Oncol. 2014, 50, 771-779.
19. Jacobs, M.V.; Snijders, P.J.F.; vandenBrule, A.J.C.; Helmerhorst, T.J.M.; Meijer, C.; Walboomers, J.M.M. A general primer gp5+/gp6+-mediated pcr-enzyme immunoassay method for rapid detection of 14 high-risk and 6 low-risk human papillomavirus genotypes in cervical scrapings. Journal of Clinical Microbiology 1997, 35, 791-795.
20. De Roda Husman, A.-M.; Walboomers, J.M.M.; Van Den Brule, A.J.C.; Meijer, C.J.L.M.; Snijders, P.J.F. The use of general primers gp5 and gp6 elongated at their 3‘ ends with adjacent highly conserved sequences improves human papillomavirus detection by pcr. J. Gen. Virol. 1995, 76, 1057-1062.
21. Baay, M.F.D.; Quint, W.G.V.; Koudstaal, J.; Hollema, H.; Duk, J.M.; Burger, M.P.M.; Stolz, E.; Herbrink, P. Comprehensive study of several general and type-specific primer pairs for detection of human papillomavirus DNA by pcr in paraffin-embedded cervical carcinomas. Journal of Clinical Microbiology 1996, 34, 745-747.
22. Snijders, P.J.F.; Vandenbrule, A.J.C.; Schrijnemakers, H.F.J.; Snow, G.; Meijer, C.; Walboomers, J.M.M. The use of general primers in the polymerase chain-reaction permits the detection of a broad-spectrum of human papillomavirus genotypes. J. Gen. Virol. 1990, 71, 173-181.
23. Soler, C.; Allibert, P.; Chardonnet, Y.; Cros, P.; Mandrand, B.; Thivolet, J. Detection of human papillomavirus type-6, type-11, type-16 and type-18 in mucosal and cutaneous lesions by the multiplex polymerase chain-reaction. J. Virol. Methods 1991, 35, 143-157.
24. Ueyama, H.; Kurokawa, K.; Sasaki, I.; Ueda, K. Characterization of acidic actin in mouse sarcoma-180 cells. Cell Structure and Function 1987, 12, 463-470.
25. Husnjak, K.; Grce, M.; Magdic, L.; Pavelic, K. Comparison of five different polymerase chain reaction methods for detection of human papillomavirus in cervical cell specimens. J. Virol. Methods 2000, 88, 125-134.
26. Altschul, S.F.; Madden, T.L.; Schaffer, A.A.; Zhang, J.H.; Zhang, Z.; Miller, W.; Lipman, D.J. Gapped blast and psi-blast: A new generation of protein database search programs. Nucleic Acids Res. 1997, 25, 3389-3402.
27. Larkin, M.A.; Blackshields, G.; Brown, N.P.; Chenna, R.; McGettigan, P.A.; McWilliam, H.; Valentin, F.; Wallace, I.M.; Wilm, A.; Lopez, R., et al. Clustal w and clustal x version 2.0. Bioinformatics 2007, 23, 2947-2948.

The article is freely distributed under license Creative Commons (BY-NC-ND). But you must include the author and the document can not be modified and used for commercial purposes.

Characterization of carbon quantum dots by capillary electrophoresis with laser-induced fluorescence detections

Marketa Vaculovicova [1,2], Simona Dostalova [1,2], Vedran Milosavljevic [1,2], Pavel Kopel [1,2], Vojtech Adam [1,2] and Rene Kizek [1,2**]

[1] Department of Chemistry and Biochemistry, Faculty of Agronomy, Mendel University in Brno, Zemedelska 1, CZ-613 00 Brno, Czech Republic, European Union; marketa.ryvolova@seznam.cz (M. V.), simona1dostalova@gmail.com (S. D.), grizlidripac@gmail.com (V. M.), paulko@centrum.cz (P. K.), vojtech.adam@mendelu.cz (V. A.), kizek@sci.muni.cz (R. K.)

[2] Central European Institute of Technology, Brno University of Technology, Technicka 3058/10, CZ-616 00 Brno, Czech Republic, European Union;

* Author to whom correspondence should be addressed; E-Mail: simona1dostalova@gmail.com; Tel.: +420-5-4513-3350; Fax: +420-5-4521-2044.

Received: 3.9.2015 / Accepted:9.9.2015 / Published: 1.10.2015

Interestingly, even though the absorption maximum of prepared capped carbon quantum dots (CQDs) is 210 nm and the emission maximum is 392 nm, using capillary electrophoresis with laser-induced fluorescence detection (CE-LIF) with excitation wavelength of 470 nm and long pass emission filter (510 nm) a signal was observed. Application of separation technique reviled presence of two different species, which corresponded to two well-resolved peaks present in the electropherogram. This fact is probably caused by presence of particles of different sizes.

Keywords: carbon quantum dots; fluorescence; capillary electrophoresis

1. Introduction

Recently, semiconductor quantum dots (QDs) have been established as a valuable tool for labeling and sensing [1-3]. However, semiconductor quantum dots possess certain limitations such as high toxicity due to the use of heavy metals in their production. It is known that heavy metals are highly toxic even at relatively low levels, which may prove prohibitive to any clinical studies. This prompted the creation of carbon-based fluorescent nanoparticles (CQDs) to replace semiconductor QDs due to their low toxicity, biocompatibility, low cost and chemical inertness in addition to having similar fluorescence properties [4]. Similarly to semiconductor QD, fluorescent carbon nanoparticles can employed for chemical sensing applications - monitoring of metal ion content [5,6], pH sensing [7], biosensing [8] and/or in vivo imaging [9,10].

Even though the capillary electrophoresis (CE) is an extremely valuable separation analytical method and in combination with laser-induced fluorescence detection provides exceptionally low limits of detection, its application to analysis of fluorescent carbon nanomaterials is relatively limited [11]. In contrast to stationary fluorescence spectrometry, CE is capable to reveal the presence of various species in the sample due to their different electrophoretic mobility.

In this work, preparation of CQDs from various precursors such as citric acid, sucrose and multiwall carbon nanotubes were synthetized, optically characterized by fluorescence spectrometry and investigated by capillary electrophoresis with laser-induced fluorescence detection.

2. Results and Discussion

2.1 Spectrometric characterization

The solutions of CQDs were prepared from different carbon precursors (citric acid, sucrose

and multiwall carbon nanotubes) according to the procedures described above. Photographs of obtained solutions under illumination by UV light (254 and 312 nm) and ambient light are shown in Fig. 1.

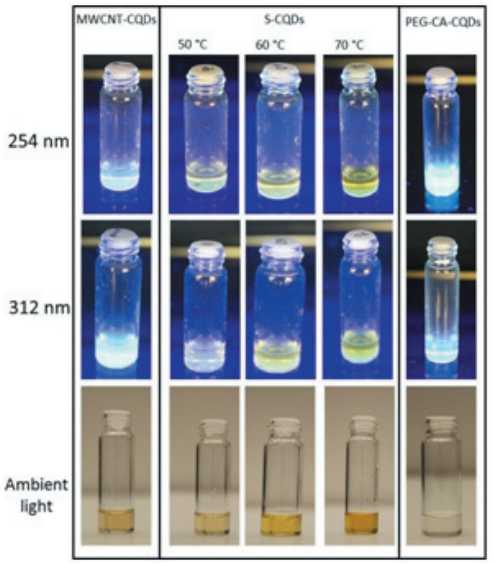

Figure 1: Photographs of various types of CQDs solutions (MWCNT-CQDs, S-CQDs, PEG-CA-CQDs) under UV (254 and 312 nm) and ambient light illumination.

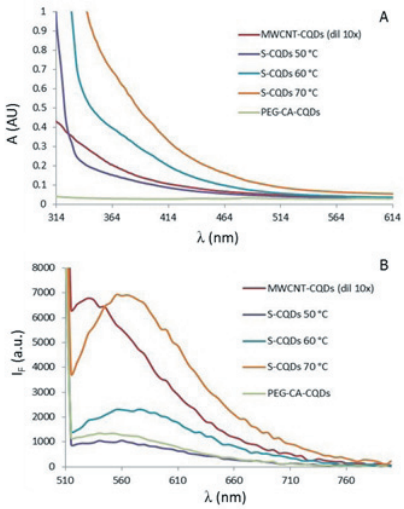

Figure 2: (A) Absorbance spectra of synthetized CQDs. (B) Emission spectra of synthetizes CQDs after excitation by 480 nm.

The obtained solutions were optically characterized using spectrophotometry and fluorescence spectrometry. The best fluorescence properties were detected in case of MWCNT-CQDs followed by S-CQDs and PEG-CA-CQDs (Fig. 2). All synthetized CQDs absorbed the light in the UV range of the spectra the as shown in Fig. 2A. Above the wavelength of 500 nm, the absorbance decreased below 0.2 AU in case of all types of CQDs. Therefore, the excitation by the light with the wavelength of 488 nm (excitation light source of CE-LIF instrument) is not optimal; however, as shown in Fig. 2B, some signal was obtained even under such suboptimal conditions. The most intensive signal was obtained in case of S-CQDs (70 °C) and MWCNT-CQDs. MWCNT-CQDs had to be even 10-times diluted to obtain measurable signal.

2.2 Capillary electrophoresis with laser-induced fluorescence detection

2.2.1 PEG-CA-CQDs

Besides the stationary fluorescence spectrometry, also CE-LIF analysis of CQDs was carried out to investigate the number of species present in the solution. As shown in Fig. 3, in the case of PEG-CA-CQDs, there are two species present. The CE-LIF signal is very low due to the non-ideal setting of the CE-LIF instrument for analysis PEG-CA-CQDs (absorption maximum of PEG-CA-CQDs is 210 nm and the excitation wavelength of the CE-LIF instrument is 488 nm). However, still two species can be recognized in the solution.

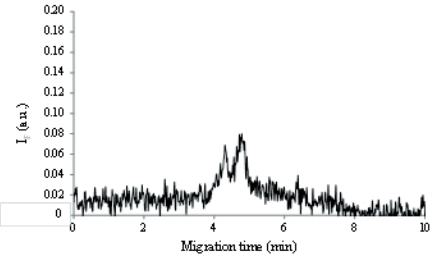

Figure 3: CE-LIF of PEG-CA-CQDs. Separation conditions: internal diameter - 75 μm, length - 54/64.5 cm, separation voltage - 20 kV, hydrodynamic injection - 0.5 psi, 5 s, electrolyte - 20 mM sodium borate, pH 9.

2.2.2 S-CQDs

Second precursor tested for CQDs preparation is the sucrose. It was found out that the preparation temperature has a significant influence on the fluorescence properties. In this case, temperatures of 50 60 and 70 °C were tested. Two peaks were recognized in the electropherogram – 6.1 min and 6.6 min. the major peak with migration time of 6.6 min was used for quantification and evaluation. As shown in Fig. 4, the preparation temperature of 70 °C provided nanoparticles of significantly higher fluorescence compared to 50 °C (5.8-times) and 60 °C (1.8-times). In comparison with PEG-CA--CQDs, the CE-LIF signal of S-CQDs (50 °C) was 4-times higher.

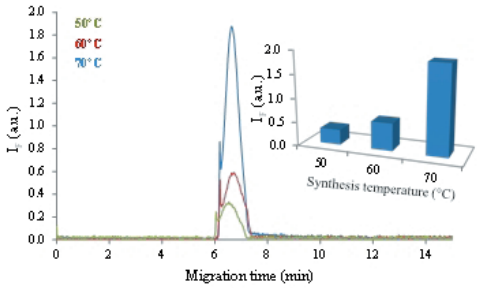

Figure 4: CE-LIF of S-CQDs prepared by using 50, 60 and 70 °C. Separation conditions: internal diameter - 75 µm, length - 54/64.5 cm, separation voltage - 20 kV, hydrodynamic injection - 0.5 psi, 5 s, electrolyte - 20 mM sodium borate, pH 9. Inset: Dependence of the peak height on the preparation temperature.

2. 2. 3. MWCNT-CQDs

MWCNT-CQDs provided the best fluorescence properties from all carbon precursors used. As shown in the Fig. 5, the signal obtained by CE-LIF analysis of MWCNT-CQDs was 8.6-times higher compared to the S-CQDs (70 °C). Similarly to S-CQDs, two peaks are present in the electropherogram of MWCNT-CQDs (4.2 and 4.35 min). As shown in the inset of Fig.4, the fluorescence signal is linearly dependent on concentration with regression equation of y = 14.568x + 1.5459 and determination coefficient R^2=0.9954.

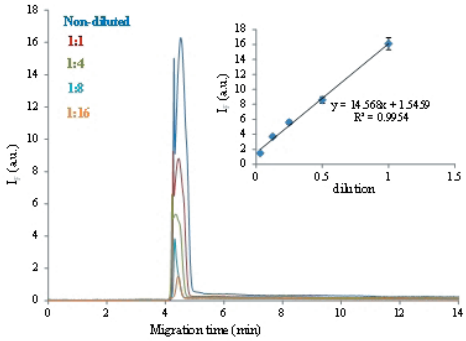

Figure 5: CE-LIF of MWCNT-CQDs. Separation conditions: internal diameter - 75 µm, length - 54/64.5 cm, separation voltage - 20 kV, hydrodynamic injection - 0.5 psi, 5 s, electrolyte - 20 mM sodium borate, pH 9. Inset: Dependence of the peak height on the dilution by separation electrolyte.

Based on the CE-LIF data, the electrophoretic mobilities of all CQDs were calculated (migration times of major peaks were used) according to the equation 1. Migration time of coumarin 334 used as a electroosmotic flow marker was 4.06 min. The obtained values of electrophoretic mobilities are summarized in Tab. 1. It follows from the results that S-CQDs possess the most negative charge, which is caused probably due to the preparation procedure.

$$\mu_{El} = (l_{eff} \times l_{tot} / t_{migCQDs} \times V) - (l_{eff} \times l_{tot} / t_{migEOF} \times V) \quad (1)$$

μ_{El} – electrophoretic mobility,
l_{eff} – effective capillary length,
ltot – total capillary length,
t_{migEOF} – migration time of the electroosmotic flow,
$t_{migCQDs}$ – migration time of CQDs.

CQDs type	Electrophoretic mobility ($\times 10^{-9} m^2 V^{-1} s^{-1}$)
PEG-CA-CQDs	-4.125
S-CQDs	-26.439
MWCNT-CQDs	-5.866

3. Experimental Section

3.1 Synthesis of fluorescence carbon nanoparticles (CQDs)

3.1.1 Polyethyleneglycol-capped citric acid-based CQDs (PEG-CA-CQDs)

The solution of ethylene glycol (10 mL), PEG-8000 (1 g) and citric acid (1 g) in a 100 mL three-neck flask was heated at 180 °C for 3 h under nitrogen flow, and then cooled down to ambient temperature. Mili-Q water was then added and the mixture was stirred for a couple of minutes. The obtained solutions were purified for 24 h by dialysis against Mili-Q water with a D-Tube maxi dialyzer to remove ethylene glycol.

3.1.2 Sucrose-based CQDs (S-CQDs)

H_3PO_4 (70%, 10 mL) was added with stirring to a solution of sucrose (1 g) in water (5 mL). After 30 min stirring, 2 ml of mixture was pipetted to a glass vial and heated in Multiwave 3000 Microwave Reaction System (Anton Paar, Graz, Austria) using rotor 64MG5. Reaction conditions were as follows – power 300 W, time 10 min and temperatures 50, 60 and 70 °C. After cooling, the samples were neutralized with water solution of Na_2CO_3 (4 g in 15 ml). Neutralized solutions were left overnight and formed dark brown precipitates were removed by centrifugation (10000 rpm, 20 min, 20 °C). Thus, obtained supernatants were used for measurements.

3.1.3 Multiwall carbon nanotubes-based CQDs (MWCNT-CQDs)

MWCNT (0.1 g) were heated in 3:1 mixture of H_2SO_4 : HNO_3 (10 ml) under reflux at 140 °C for 8 h. After cooling acetone (10 ml) was added. The mixture was left overnight and Na_2CO_3 (10.6 g) in water (80 ml) was added with stirring. Brown oily viscous liquid was collected on bottom of tube after centrifugation (25000 rpm, 20 min, 20 °C). Water layer was used for fluorescence measurement.

3.2 Fluorescence spectrometry and spectrophotometry

Absorbance and fluorescence spectra were measured using the TECAN microtitration plate reader Infinite 200 PRO (Switzerland) using 50 µL of the sample in the UV transparent 96-well plate. Each absorbance value is an average of 5 measurements.

3.3 Capillary electrophoresis with laser-induced fluorescence detection (CE-LIF)

The electrophoretic behavior was analyzed by CE-LIF (PACE MDQ, Beckman Coulter, USA) using fused silica capillary with internal diameter of 75 µm was used 54/64.5 cm.

The separation voltage of 20 kV and hydrodynamic injection by 0.5 psi for 5 s was employed. 20 mM sodium borate buffer pH 9 was used as a separation electrolyte. The signal was detected with laser-induced fluorescence after excitation with argon ion laser (488 nm) and emission wavelength in the range 510-530 nm. Coumarin 334 was used as a electroosmotic flow marker.

4. Conclusions

It was found out that MWCNT-CQDs provided the best optical properties and were the most suitable for CE-LIF analysis with 488 nm excitation light source. For further labeling purposes the MWCNT-CQDs will be used. On the other hand, the S-CQDs exhibited the most negative electrophoretic mobility suggesting their negative charge compared to the other CQD types, which were very slightly negative or neutral.

Acknowledgments

Financial support from SIX CZ.1.05/2.1.00/03.0072 is highly acknowledged.

Conflicts of Interest

The authors declare they have no potential conflicts of interests concerning drugs, products, services or another research outputs in this study. The Editorial Board declares that the manuscript met the ICMJE „uniform requirements“ for biomedical papers.

References

1. Chan, W.C.W.; Maxwell, D.J.; Gao, X.H.; Bailey, R.E.; Han, M.Y.; Nie, S.M. Luminescent quantum dots for multiplexed biological detection and imaging. Curr. Opin. Biotechnol. 2002, 13, 40-46.
2. Medintz, I.L.; Uyeda, H.T.; Goldman, E.R.; Mattoussi, H. Quantum dot bioconjugates for imaging, labelling and sensing. Nat. Mater. 2005, 4, 435-446.

3. Michalet, X.; Pinaud, F.F.; Bentolila, L.A.; Tsay, J.M.; Doose, S.; Li, J.J.; Sundaresan, G.; Wu, A.M.; Gambhir, S.S.; Weiss, S. Quantum dots for live cells, in vivo imaging, and diagnostics. Science 2005, 307, 538-544.
4. Lim, S.Y.; Shen, W.; Gao, Z.Q. Carbon quantum dots and their applications. Chem. Soc. Rev. 2015, 44, 362-381.
5. Guo, Y.M.; Zhang, L.F.; Zhang, S.S.; Yang, Y.; Chen, X.H.; Zhang, M.C. Fluorescent carbon nanoparticles for the fluorescent detection of metal ions. Biosens. Bioelectron. 2015, 63, 61-71.
6. Yin, P.P.; Ai, K.L.; Li, M.L.; Sun, G.Y. Highly fluorescent carbon nanoparticles for sensitive detection of iron (iii). Chin. J. Anal. Chem. 2014, 42, 1427-1433.
7. Li, H.T.; Ming, H.; Liu, Y.; Yu, H.; He, X.D.; Huang, H.; Pan, K.M.; Kang, Z.H.; Lee, S.T. Fluorescent carbon nanoparticles: Electrochemical synthesis and their ph sensitive photoluminescence properties. New J. Chem. 2011, 35, 2666-2670.
8. Ouyang, X.Y.; Liu, J.H.; Li, J.S.; Yang, R.H. A carbon nanoparticle-based low-background biosensing platform for sensitive and label-free fluorescent assay of DNA methylation. Chem. Commun. 2012, 48, 88-90.
9. Fang, Y.X.; Guo, S.J.; Li, D.; Zhu, C.Z.; Ren, W.; Dong, S.J.; Wang, E.K. Easy synthesis and imaging applications of cross-linked green fluorescent hollow carbon nanoparticles. ACS Nano 2012, 6, 400-409.
10. Ruan, S.B.; Wan, J.Y.; Fu, Y.; Han, K.; Li, X.; Chen, J.T.; Zhang, Q.Y.; Shen, S.; He, Q.; Gao, H.L. Pegylated fluorescent carbon nanoparticles for noninvasive heart imaging. Bioconjugate Chem. 2014, 25, 1061-1068.
11. Hu, Q.; Paau, M.C.; Zhang, Y.; Chan, W.; Gong, X.J.; Zhang, L.; Choi, M.M.F. Capillary electrophoretic study of amine/carboxylic acid-functionalized carbon nanodots. J. Chromatogr. A 2013, 1304, 234-240.

The article is freely distributed under license Creative Commons (BY-NC-ND). But you must include the author and the document can not be modified and used for commercial purposes.

ARTICLE

Modification of anti-DNA antibodies with carbon quantum dots

Simona Dostalova [1,2*], Marketa Vaculovicova [1,2], Sona Krizkova [1,2], Lukas Richtera [1,2], Pavel Kopel [1,2] and Rene Kizek [1,2]

[1] Department of Chemistry and Biochemistry, Faculty of Agronomy, Mendel University in Brno, Zemedelska 1, CZ-613 00 Brno, Czech Republic, European Union; simona1dostalova@gmail.com (S. D.), marketa.ryvolova@seznam.cz (M. V.), sonakrizk@centrum.cz (S. K.), oliver@centrum.cz (L. R.), paulko@centrum.cz (P. K.), kizek@sci.muni.cz (R. K.)

[2] Central European Institute of Technology, Brno University of Technology, Technicka 3058/10, CZ-616 00 Brno, Czech Republic, European Union;

* Author to whom correspondence should be addressed; E-Mail: simona1dostalova@gmail.com; Tel.: +420-5-4513-3350; Fax: +420-5-4521-2044.

Received: 3.9.2015 / Accepted:20.9.2015 / Published:1.10.2015

The anti-DNA antibodies are produced in patients with autoimmune disease called systemic lupus erythematodes. They can be reactive against double or single stranded DNA or DNA modified with some other molecules. Using the variety of antibodies it is possible to determine the structure of studied DNA. In this work, we used 4 anti-DNA antibodies produced in egg yolk after immunization of hens with DNA-mBSA antigen – anti-dsDNA, anti-ssDNA, afi-dsDNA and afi-ssDNA. The reactivity of these antibodies was evaluated using the dot blot method with different lengths and concentrations of DNA antigen. The most reactive antibodies (anti-ssDNA) were modified with carbon quantum dots synthesized from multiwall carbon nanotubes and this modification was verified by ELISA-like method with fluorescent detection and fluorescence resonance energy transfer between DNA and quantum dots was observed, increasing the sensitivity of the DNA detection.

Keywords: anti-DNA antibodies; carbon quantum dots; DNA structure; fluorescence imaging

1. Introduction

Antibodies represent a specialized glycoprotein group and form the main base of vertebrate immune system. There are 5 immunoglobulin classes in mammalian serum: IgG, IgM, IgA, IgD and IgE [1]. In avian species the immunoglobulins G are replaced by highly functionally similar immunoglobulins Y and there are also IgA and IgM present [2]. Antibodies are often used in variety of applications, including ELISA for the detection of various analytes [3], virions [4] or tumor markers [5], cell capture for subsequent analysis [6] and magnetic immunoseparation [7,8]. For bulk production, antibodies extracted from chicken egg yolks immunized with the specific antigen are often used [9].

Anti-DNA antibodies were first discovered in 1957 [10] and they can bind to single stranded or double stranded DNA [11,12]. Anti-dsDNA antibodies can be found in the blood of systemic lupus erythematodes (SLE) patients. This autoimmune disease is manifesting by formation of immunocomplexes [13]. The antibodies usually belong to class IgM in normal patients or IgG in SLE patients [14] and they can be transiently found in the blood of patients with some viral infections (HIV, BK or B19 virus) [15]. Anti-dsDNA antibodies usually bind to sugar-phosphate backbone, base pairs or some double strand conformations. Anti-ssDNA antibodies should be able to bind to bases, nucleotides, oligonucleotides and sugar-phospate backbone [16]. Commercially available are also antibodies against DNA adducts such as those with cisplatin [17]. The combination of suitable antibodies can help identify the secondary structures of

DNA [18].

To enhance the antigen detection limit it is possible to label the antibodies with highly fluorescent nanoparticles such as quantum dots (QDs) [3]. QDs have unique fluorescent characteristics, including wide absorbance spectrum with narrow emission spectrum, high quantum yield or excellent photostability [19]. They are usually formed by a semiconductor crystals, such as CdTe, CdS or ZnS, but they can also be prepared from carbon materials with polymer coating [6]. These materials include nanodiamonds [20], graphene [21], graphite [22], single- and multi-wall carbon nanotubes [23], citric acid [24] or sucrose [25]. The prepared carbon quantum dots usually show high fluorescence under UV light [26].

In this work, we studied anti-DNA antibodies produced in chicken egg yolks as a tool for DNA structure detection. We used four different anti-DNA antibodies: anti-dsDNA, afi-dsDNA, anti-ssDNA and afi-ssDNA. Their reactivity towards various sized DNA molecules was evaluated using dot blot method. The successful modification of anti-DNA antibodies with carbon quantum dots was determined by ELISA-like method with fluorescent detection.

2. Results and Discussion

2.1 The reactivity of anti-DNA antibodies and DNA of different lengths

The reactivity of 4 different types of anti-DNA antibodies (anti-dsDNA, afi-dsDNA, anti-ssDNA and afi-ssDNA) to different lengths of double and single stranded DNA was evaluated using the dot blot assay on Zeta Probe membrane with high affinity to DNA. 6 different DNA samples were immobilized on the membrane in the order described in Fig. 1A – double and single stranded oligonucleotide (12 bp), double and single stranded DNA fragment (498 bp) and double and single stranded genomic DNA from bacteriophage λ (48502 bp). To determine which part of DNA serves as an antigen for anti-DNA antibodies, we used two concentrations of different DNA lengths – the same molar concentration (15 nM, Fig. 1B) and same mass concentration (100 µg/mL, Fig. 1C). The antibodies used were produced in chicken egg yolk after hen immunization. Anti-chicken antibody labeled with horseradish peroxidase was used for colorimetric detection of antibody-DNA binding. Table 1 shows the quantification of the observed bands intensity

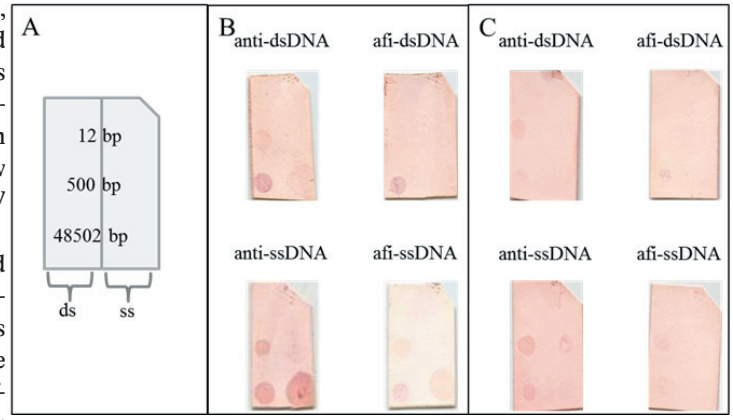

Figure 1: The dot blot assay for evaluation of antibody reactivity with single and double stranded DNA of different length. (A) The sample order on Zeta Probe membrane. (B) Dot blot assay with 15 nM DNA and 22 µg/mL of antibodies. (C) Dot blot assay with 100 µg/mL of DNA and 22 µg/mL of antibodies.

None of the tested antibodies were able to bind to oligonucleotides, either single stranded or double stranded. The anti-dsDNA antibody was able to bind to double stranded DNA fragment and both double and single stranded genomic DNA. With the same molar concentrations of DNA, the anti-dsDNA antibody bound most to the double stranded genomic DNA and the binding to double stranded DNA fragment and single stranded genomic DNA was similar. However, with the same mass concentrations of used DNA, the anti-dsDNA antibody bound equally to all three of these samples. From these results, it can be concluded that this antibody probably binds to the DNA mass (i.e. certain number of bases), not to a special part of DNA

molecule. The afi-dsDNA was prepared by affinity purification of anti-dsDNA antibodies. This antibody was able to bind only to the double stranded genomic DNA, it was non-reactive to any shorter or single stranded DNA.

Antibody	DNA	15 nM DNA	100 µg/mL DNA
Anti-dsDNA	ds-12 bp	0	0
	ss-12 bp	0	0
	ds-500 bp	40	40
	ss-500 bp	0	0
	ds-48502 bp	56	35
	ss-48502 bp	35	30
Afi-dsDNA	ds-12 bp	0	0
	ss-12 bp	0	0
	ds-500 bp	0	0
	ss-500 bp	0	0
	ds-48502 bp	45	31
	ss-48502 bp	0	0
Anti-ssDNA	ds-12 bp	0	0
	ss-12 bp	0	0
	ds-500 bp	51	46
	ss-500 bp	18	0
	ds-48502 bp	39	50
	ss-48502 bp	56	41
Afi-ssDNA	ds-12 bp	0	0
	ss-12 bp	0	0
	ds-500 bp	18	33
	ss-500 bp	0	0
	ds-48502 bp	24	34
	ss-48502 bp	19	0

Table 1: The colorimetric intensity quantification of dot blot assay.

The anti-ssDNA antibody was the most reactive, it was able to bind to both single and double stranded DNA fragment and genomic DNA. With the same molar concentrations of DNA, the antibody bound most equally the double stranded DNA fragment and single stranded genomic DNA. The reactivity to single stranded DNA fragment was poor. With the same mass concentrations of DNA, the antibody equally bound to double stranded DNA fragment and single and double stranded genomic DNA. There was no reactivity to single stranded DNA fragment. Overall, the anti-ssDNA antibody is more reactive to double stranded DNA than single stranded which can be caused by the immunization process during which the single stranded DNA can form double strands with its complementary molecules. The afi-ssDNA was prepared in a similar way to the afi-dsDNA. With the same molar concentrations of DNA, this antibody bound to double stranded DNA fragments and single and double stranded genomic DNA, but in the case of same concentrations of DNA, the afi-ssDNA antibody bound only to double stranded DNA fragment and genomic DNA. These antibodies probably bind to some part of DNA molecule, but the reactivity is also dependent on the DNA mass.

2.2 Characterization of carbon quantum dots

The most reactive antibodies (anti-ssDNA) were subsequently modified with carbon quantum dots synthesized from multiwall carbon nanotubes (MWCNT-CQDs). Fig. 2A shows these quantum dots under ambient

and UV (254 and 312 nm). Fig. 2B shows the absorbance spectrum of MWCNT-QDs. The absorption of these quantum dots is the highest for light of smaller wavelengths (UV light). However, their fluorescence intensity increased in dependence to the increasing excitation wavelength with the excitation maximum at 330 nm. with no MWCNT-QDs modification (Fig. 3A) showed no fluorescence using this excitation. In case of antibodies modified with MWCNT--QDS there was very low fluorescence observed and only with the highest DNA concentration (100 µg/mL) (Fig. 3B). However, high fluorescence was observed with the excitation at

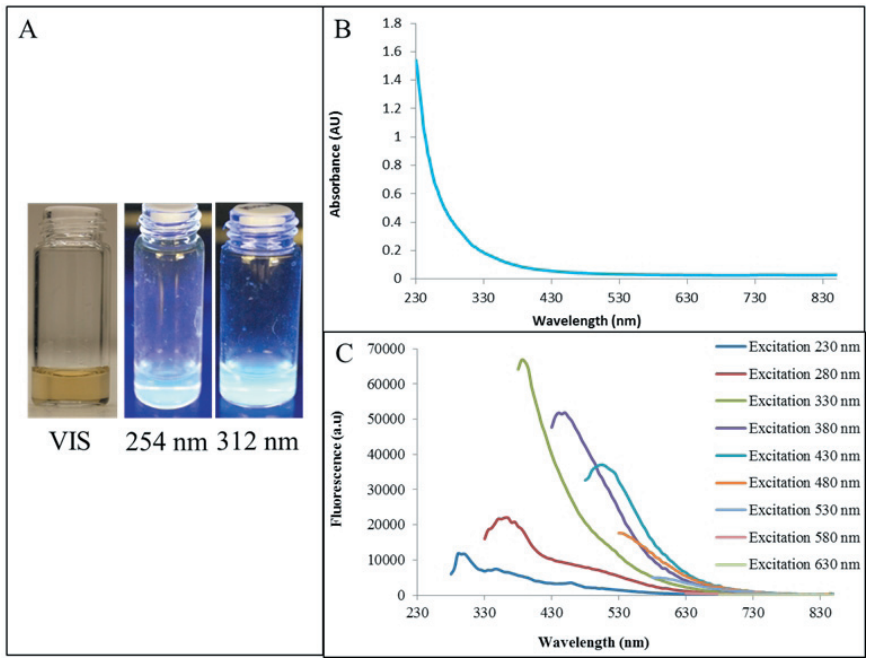

Figure 2: The characterization of MWCNT-CQDs. (A) Visualization under ambient and UV (254 and 312 nm) light. (B) Absorbance spectrum of MWCNT-CQDs. (C) The fluorescence spectra of MWCNT-CQDs after various excitation wavelength.

2.3 Modification of anti-DNA antibodies with carbon quantum dots

These quantum dots were used for the modification of anti-ssDNA antibodies. The successful modification was verified by ELISA-like method with fluorescent detection (Fig. 3). The double stranded DNA fragments were immobilized on the surface of microtiter plate well and the rest of the surface was blocked by milk powder in PBS. The samples were then incubated with antibodies with and without MWCNT-QDs modification and excess molecules of antibodies were removed by washing. The fluorescence of MWCNT-QDs was measured using their excitation maximum at 330 nm. Antibodies 230 nm. This fluorescence was observed in samples with antibodies without the MWCNT-QDs modification (Fig. 3C) as well as antibodies with MWCNT-QDs (Fig. 3D). However, the fluorescence was 4 times higher in the case of anti-ssDNA modified with MWCNT-QDs than unmodified antibodies and it increased with the increasing DNA concentration linearly. This difference between the fluorescence of carbon quantum dots and antibodies modified with carbon quantum dots bound to DNA can be probably explained by fluorescence resonance energy transfer between the DNA, antibodies and carbon quantum dots.

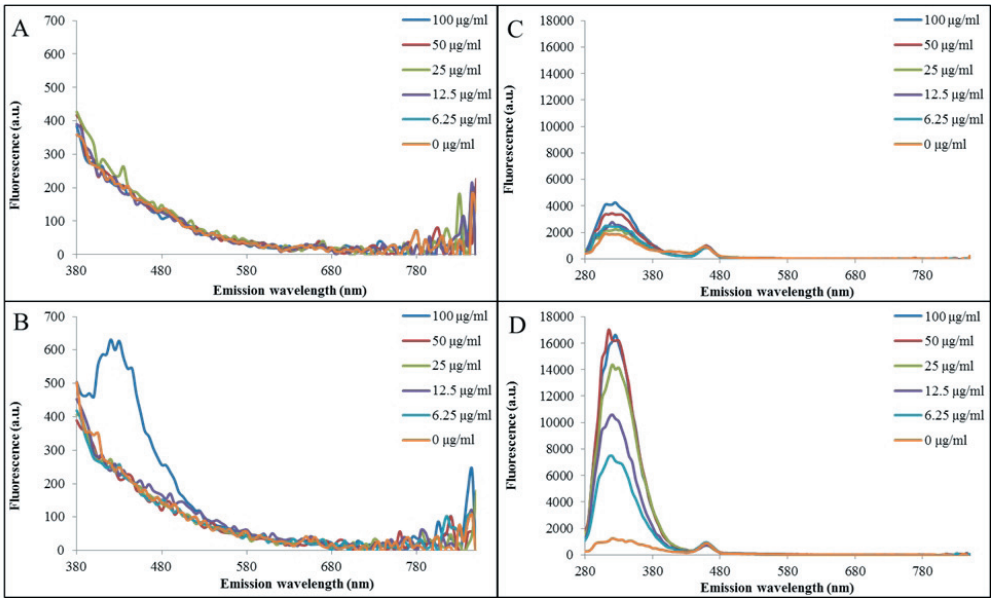

Figure 3: Modification of anti-DNA antibodies with MWCNT-CQDs determined by ELISA-like method with fluorescent detection. (A) Fluorescence spectra (excitation wavelength 330 nm) of microtiter plate wells coated with DNA fragment after incubation with anti-ssDNA antibodies. (B) Fluorescence spectra (excitation wavelength 330 nm) of microtiter plate wells coated with DNA fragment after incubation with anti-ssDNA antibodies modified with MWCNT-CQDs. (C) Fluorescence spectra (excitation wavelength 230 nm) of microtiter plate wells coated with DNA fragment after incubation with anti-ssDNA antibodies. (D) Fluorescence spectra (excitation wavelength 230 nm) of microtiter plate wells coated with DNA fragment after incubation with anti-ssDNA antibodies modified with MWCNT-CQDs.

3. Experimental Section

3.1 Chemicals

All chemicals of ACS purity were obtained from Sigma-Aldrich (St. Louis, MO, USA) unless otherwise stated. Deionized water underwent demineralization by reverse osmosis using the instrument Aqua Osmotic 02 (Aqua Osmotic, Tisnov, Czech Republic) followed by further purification using Millipore RG (Millipore, Billerica, MA, USA, 18 MO)–MiliQ water. The pH was measured using WTW inoLab pH meter (Weilheim, Germany).

3. 2 dsDNA and ssDNA preparation

3 different lengths of DNA were used as samples for evaluation of antibody reactivity – genomic DNA (48502 bp), DNA fragment (498 bp) and oligonucleotides (12 bp). Genomic DNA isolated from bacteriophage λ was purchased from New England Biolabs (Ipswitch, MA, USA). From this DNA, xis gene fragment was amplified using Taq PCR kit purchased from New England Biolabs (Ipswitch, MA, USA) and primers synthesized by Sigma-Aldrich (St. Louis, MO, USA) with the sequence 5´-CCTGCTCTGCCGCTTCACGC-3´ for forward primer and 5´-TCCGGATAAAAACGTCGATGACATTTGC-3´ for reverse primer. The reaction mixture (100 µL) composed of 1× standard Taq reaction buffer; 0.2 µM deoxynucleotide solution; 0.2 µM of each primer; 6.25 U of Taq DNA polymerase and 750 ng DNA. PCR took place in Mastercycler ep realplex4 S (Eppendorf, New Brunswick, Germany) and the cycling conditions were as follows: denaturation for 120 s at 95 °C; 30 cycles of denaturation for 15 s at 95 °C, annealing for 15 s at 64 °C and elongation for 45 s at 72 °C with a final elongation for 5 min at 72 °C. Obtained DNA fragments were purified using MinElute PCR Purification Kit (Qiagen, Hilden, Germany) and their concentration was determined spectrophotometrically (Analytic Jena, Jena, Germany). The oligonucleotide se-

quences were 5´-ATGGAATGCAGG-3´ (O1) and 5´-CCTGCATTCCAT-3´ (O2), respectively and they were synthesized by Sigma-Aldrich (St. Louis, MO, USA).

To produce double stranded oligonucleotides, O1 and O2 were mixed in 1:1 molar ratio, heated at 99 °C for 4 min and slowly cooled to room temperature to enable the formation of double strand. To dissolve double stranded DNA fragment and genomic DNA and produce single stranded DNA, the samples were heated at 99 °C for 4 min, shock-cooled on ice to prevent the re-formation of double stranded DNA and immediately used for subsequent analysis.

3.3 Preparation of antibodies

Chicken anti-DNA antibodies were prepared by HENA (Prague, Czech Republic). Hens were immunized with DNA-mBSA complex and IgY fraction reactive to DNA-mBSA was obtained from egg yolk. The antibodies were stabilized with 0.1% NaN_3 in PBS and protein concentration was 38.8 mg/mL in immunoglobulin fraction for anti-dsDNA, 30.1 mg/mL for anti-ssDNA, 29.2 mg/mL for afi-dsDNA and 22.2 mg/mL for afi-ssDNA. For the analysis, antibodies were diluted with antibody dilution buffer containing 1 mg/mL BSA in PBS (137 mM NaCl, 2.7 mM KCl, 1.4 mM NaH_2PO_4, and 4.3 mM Na_2HPO_4, pH 7.4) to a concentration of 22 µg/mL.

3.4 Dot bot assay

2 µL of the DNA samples (15 nM or 100 µg/mL) were immobilized on a Zeta Probe membrane (Bio-Rad, Hercules, CA, USA) and dried at 37 °C in an incubator Galaxy 14S (Eppendorf, New Brunswick, Germany). The membrane was blocked for 30 min during rotation at 40 rpm (Multi RS-60, Biosan, Riga, Latvia) in a blocking buffer containing 1% milk powder in PBS. The solution was replaced by primary antibodies (anti-dsDNA, afi-dsDNA, anti-ssDNA or afi-ssDNA antibody). The membrane was incubated with antibodies for 1 h at room temperature during rotation and then washed with PBS with 0.05% Tween 20 (PBS-T). The secondary antibodies labeled with horseradish peroxidase (Dako, Glostrup, Denmark) in dilution of 1:1500 in dilution buffer were added to the membrane and incubated for 1 h during rotation. Visualization in chromogenic substrate followed after washing with PBS-T. The membrane was immersed in the solution composed of substrate buffer (0.5 M acetate buffer, pH 5.4), 0.4 mg/mL 3-amino-9-ethylcarbazole and hydrogen peroxide in the ratio 1000:10:1. The assay was performed according to [27]. Mean intensity of the color was quantified by Carestream Molecular Software (Rochester, NY, USA) in each spot and the color of the background was deducted.

3.5 Multiwall carbon nanotubes-based CQDs (MWCNT-CQDs) preparation and characterization

MWCNT (0.1 g) were heated in 3:1 mixture of H_2SO_4 : HNO_3 (10 ml) under reflux at 140 °C for 8 h. After cooling acetone (10 ml) was added. The mixture was left overnight and Na_2CO_3 (10.6 g) in water (80 ml) was added with stirring. Brown oily viscous liquid was collected on the bottom of the tube after centrifugation (25000 rpm, 20 min, 20 °C). Aqueous layer was used for fluorescence measurement. Absorbance and fluorescence spectra were measured using the TECAN microtitration plate reader Infinite 200 PRO (Männedorf, Switzerland) using 100 µL of the sample in the UV transparent 96-well plate. Each absorbance value is an average of 5 measurements.

3.6 Modification of anti-DNA antibodies with MWCNT-CQDs and ELISA-like verification method

25 µL of MWCNT-CQDs was mixed with 5 µL of anti-ssDNA antibodies (1.4 mg/mL) and 75 µL of water and incubated for 2 h at 20 °C during rotation at 60 rpm. 50 µL of DNA fragment (100 µg/mL) was pipetted on microtiter plate well and incubated at 37 °C for 2 h. The rest of the well surface was blocked for 30 min with a blocking buffer containing 1% milk powder in PBS. The solution was replaced by 100 µL of anti-ssDNA antibodies modified with MWCNT--CQDs and incubated at 37 °C for 1 h and then washed three times with water. Visualization was performed by absorbance and fluorescence

spectra measurement using TECAN microtitration plate reader Infinite 200 PRO (Männedorf, Switzerland) in 100 µL of water.

4. Conclusions

In this work, the reactivity of anti-DNA antibodies was evaluated using the dot blot method. The antibodies were subsequently modified with carbon quantum dots and used in an ELISA-like DNA detection method with fluorescent detection. Using this approach it is possible to increase the sensitivity of DNA immuno-based detection and eliminate the need to use secondary antibodies labeled with HRP in these methods. Moreover, using the combination of different anti-DNA antibodies it is possible to determine different DNA structures.

Acknowledgments

Financial support from SIX CZ.1.05/2.1.00/03.0072 is highly acknowledged.

Conflicts of Interest

The authors declare they have no potential conflicts of interests concerning drugs, products, services or another research outputs in this study. The Editorial Board declares that the manuscript met the ICMJE „uniform requirements“ for biomedical papers.

References

1. Durandy, A.; Kracker, S. Immunoglobulin class-switch recombination deficiencies. Arthritis Res. Ther. 2012, 14.
2. Zhao, Y.; Rabbani, H.; Shimizu, A.; Hammarstrom, L. Mapping of the chicken immunoglobulin heavy-chain constant region gene locus reveals an inverted alpha gene upstream of a condensed upsilon gene. Immunology 2000, 101, 348-353.
3. Janu, L.; Stanisavljevic, M.; Krizkova, S.; Sobrova, P.; Vaculovicova, M.; Kizek, R.; Adam, V. Electrophoretic study of peptide-mediated quantum dot-human immunoglobulin bioconjugation. Electrophoresis 2013, 34, 2725-2732.
4. Lin, J.; Wang, R.; Jiao, P.; Li, Y.; Li, Y.; Liao, M.; Yu, Y.; Wang, M. An impedance immunosensor based on low-cost microelectrodes and specific monoclonal antibodies for rapid detection of avian influenza virus h5n1 in chicken swabs. Biosensors & bioelectronics 2015, 67, 546-552.
5. Li, W.; Jiang, X.; Xue, J.; Zhou, Z.; Zhou, J. Antibody modified gold nano-mushroom arrays for rapid detection of alpha-fetoprotein. Biosensors & bioelectronics 2015, 68, 468-474.
6. Weng, C.-I.; Chang, H.-T.; Lin, C.-H.; Shen, Y.-W.; Unnikrishnan, B.; Li, Y.-J.; Huang, C.-C. One-step synthesis of biofunctional carbon quantum dots for bacterial labeling. Biosensors & bioelectronics 2015, 68, 1-6.
7. Krizkova, S.; Nguyen, H.V.; Stanisavljevic, M.; Kopel, P.; Vaculovicova, M.; Adam, V.; Kizek, R. Microchip capillary electrophoresis: Quantum dots and paramagnetic particles for bacteria immunoseparation : Rapid superparamagnetic-beads-based automated immunoseparation of zn-proteins from staphylococcus aureus with nanogram yield. Methods in molecular biology (Clifton, N.J.) 2015, 1274, 67-79.
8. Zitka, O.; Krizkova, S.; Skalickova, S.; Dospivova, D.; Adam, V.; Kizek, R. Microfluidic tool coupled with electrochemical assay for detection of lactoferrin isolated by antibody-modified paramagnetic beads. Electrophoresis 2013, 34, 2120-2128.
9. Krizkova, S.; Ryvolova, M.; Hynek, D.; Eckschlager, T.; Hodek, P.; Masarik, M.; Adam, V.; Kizek, R. Immunoextraction of zinc proteins from human plasma using chicken yolk antibodies immobilized onto paramagnetic particles and their electrophoretic analysis. Electrophoresis 2012, 33, 1824-1832.
10. Ceppellini, R.; Polli, E.; Celada, F. A DNA-reacting factor in serum of s patient with lupus erythematosus diffusus. Proc. Soc. Exp. Biol. Med. 1957, 96, 572-574.
11. Schur, P.H.; Sandson, J. Immunologic factors and clinical activity in systemic lupus erythematosus N. Engl. J. Med. 1968, 278, 533-&.
12. Tojo, T.; Friou, G.J. Lupus nephritis - varying complement-fixing properties od immunoglobulin g antibodies to antigens of cell nuclei Science 1968, 161, 904-&.
13. Stearns, N.A.; Lee, J.; Leong, K.W.; Sullenger, B.A.; Pisetsky, D.S. The inhibition of anti-DNA binding to DNA by nucleic acid binding polymers. PLoS One 2012, 7.
14. Rothfiel.Nf; Stollar, B.D. Relation of immunoglobulin class pattern of antinuclear antibody and complement-fixing antibodies to DNA in sera from patients with systemic lupus erythematosus J. Clin. Invest. 1967, 46, 1785-&.
15. Oka, Y.; Hirabayashi, Y.; Takahashi, R.; Ishii, T.; Sasaki, T. Can viral infection be a trigger of anti-DNA antibody production through endoplasmic reticulum stress? Arthritis Rheum. 2006, 54, S298-S298.
16. Kalsi, J.K.; Martin, A.C.R.; Hirabayashi, Y.; Ehrenstein, M.; Longhurst, C.M.; Ravirajan, C.; Zvelebil, M.; Stollar, B.D.; Thornton, J.M.; Isenberg, D.A. Functional and modelling studies of the binding of human monoclonal anti-DNA antibodies to DNA. Mol. Immunol. 1996, 33, 471-+.
17. Hirose, J.; Inoue, K.; Morimoto, E.; Iwamoto, H.; Yamaguti, Y.; Kitase, M.; Inagaki, K.; Hiromi, K. Characterization of monoclonal antibodies against (1r,2r)-cyclohexanediamine platinum(ii)-DNA adduct. Biol. Pharm. Bull. 1996, 19, 1220-1222.

18. Xia, Y.M.; Janda, A.; Eryilmaz, E.; Casadevall, A.; Putterman, C. The constant region affects antigen binding of antibodies to DNA by altering secondary structure. Mol. Immunol. 2013, 56, 28-37.
19. Stanisavljevic, M.; Chomoucka, J.; Dostalova, S.; Krizkova, S.; Vaculovicova, M.; Adam, V.; Kizek, R. Interactions between cdte quantum dots and DNA revealed by capillary electrophoresis with laser-induced fluorescence detection. Electrophoresis 2014, 35, 2587-2592.
20. Xiao, J.; Liu, P.; Li, L.H.; Yang, G.W. Fluorescence origin of nanodiamonds. J. Phys. Chem. C 2015, 119, 2239-2248.
21. Du, F.Y.; Li, J.A.; Hua, Y.; Zhang, M.M.; Zhou, Z.; Yuan, J.; Wang, J.; Peng, W.X.; Zhang, L.; Xia, S., et al. Multicolor nitrogen-doped carbon dots for live cell imaging. J. Biomed. Nanotechnol. 2015, 11, 780-788.
22. Pandey, N.; Srivastava, R.K.; Singh, M.K.; Singh, J. Optical properties of carbon nanodots synthesized by laser induced fragmentation of graphite powder suspended in water. Mater. Sci. Semicond. Process 2014, 27, 150-153.
23. Soldano, C. Hybrid metal-based carbon nanotubes: Novel platform for multifunctional applications. Prog. Mater. Sci. 2015, 69, 183-212.
24. Hou, J.; Dong, J.; Zhu, H.; Teng, X.; Ai, S.; Mang, M. A simple and sensitive fluorescent sensor for methyl parathion based on l-tyrosine methyl ester functionalized carbon dots. Biosensors & bioelectronics 2015, 68, 20-26.
25. Chen, X.F.; Zhang, W.X.; Wang, Q.J.; Fan, J.Y. C-8-structured carbon quantum dots: Synthesis, blue and green double luminescence, and origins of surface defects. Carbon 2014, 79, 165-173.
26. Milosavljevic, V.; Nguyen, H.V.; Michalek, P.; Moulick, A.; Kopel, P.; Kizek, R.; Adam, V. Synthesis of carbon quantum dots for DNA labeling and its electrochemical, fluorescent and electrophoretic characterization. Chem. Pap. 2015, 69, 192-201.
27. Krizkova, S.; Adam, V.; Eckschlager, T.; Kizek, R. Using of chicken antibodies for metallothionein detection in human blood serum and cadmium-treated tumour cell lines after dot- and electroblotting. Electrophoresis 2009, 30, 3726-3735.

The article is freely distributed under license Creative Commons (BY-NC-ND). But you must include the author and the document can not be modified and used for commercial purposes.

ARTICLE

Fluorescence detection of carbon quantum dots assessed by stratospheric platform

Lukas Nejdl[1,2], Jan Zitka[1], Kristyna Cihalova[1], Vedran Milosavljevic[1], Amitava Moulick[1], Ondrej Zavodsky[3], Zbynek Heger[1,2], Jakub Kapus[3], Libor Lenza[4], Vojtech Adam[1,2] and Rene Kizek[1,2]

[1] Department of Chemistry and Biochemistry, Laboratory of Metallomics and Nanotechnologies, Mendel University in Brno, Zemedelska 1, CZ-613 00 Brno, Czech Republic - European Union; E-Mail: lukasnejdl-mail.com (L.N); zitka12@gmail.com (J.Z.); kriki.cihalova@seznam.cz (K.C.); grizlidripac@gmail.com (V.M.); amitavamoulick@gmail.com (A.M.); heger@mendelu.cz (Z.H.); ilabo@seznam.cz (V.A.); kizek@sci.muni.cz (R.K.)

[2] Central European Institute of Technology, Brno University of Technology, Technicka 3058/10, CZ-616 00 Brno, Czech Republic - European Union

[3] Slovak Organisation for Space Activities, Zamocka 5, 811 03 Bratislava, Slovakia, European Union; E-Mail: zawin@svetelektro.com (O.Z.); jakub.kapus@sosa.sk (J.K.)

[4] Observatory Valasske Mezirici, p. o., Vsetinska 78, 757 01 Valasske Mezirici, Czech Republic, European Union; E-Mails: libor.lenza@astrovm.cz (L.L.)

* Author to whom correspondence should be addressed; E-Mail: kizek@sci.muni.cz;
Tel.: +420-5-4513-3350; Fax: +420-5-4521-2044.

Received:18.6.2015 / Accepted:19.8.2015 / Published:1.10.2015

Using of 3D printing technology (acrylonitrile butadiene styrene as material) stratospheric probe (SP) was developed for the purpose of this experiment. Fluorescent behavior of carbon quantum dots (CQDs) in concentration range 0-32 mg.ml^{-1} was monitored by stratospheric probe and classical fluorescence spectroscopy. Balloon flight lasted 120 minutes. During this time it traveled 90 km. At a height of approximately 40 km there was a rupture of balloon. Thanks to a parachute SP landed in a controlled manner in the wood in the cadastral area of municipality Brusnica (Slovak Republic). It was found that the fluorescence intensity of CQDs changed slightly before and after the flight, however this was caused by the CQDs instability and not by the detector design.

Keywords: 3D printing; Carbon quantum dots (CQDs), Fluorescence; Probe; Stratosphere

1. Introduction

Measurement of molecular fluorescence is one of the most sensitive methods to detect the signal of interest. It can be realized in numerous arrangements including flow-through geometry (i. e. chromatography, capillary electrophoresis) [1,2], imaging and microscopy [3,4], however the most commonly used is the stationary fluorescence spectrometry [5]. The diversity of the detectors is based on several factors such as light source and/or geometry of the detection cell. Currently, the utilization of the light emitting diodes as a light source is a trend enabling miniaturization of the instrumentation [6-8]. The portable devices moreover allow the in situ analyses, which have number of advantages such as obtaining the data in real time, lowering the time of the analysis as well as its costs. Especially in cases where the detection site is difficult to reach, the remote-controlled analyzers are beneficial. Stratosphere is one of these hard-to reach places and therefore stratospheric or space research is a new challenge for these devices [9]. Nowadays, balloons are a main tool for stratospheric in situ research mostly focused on the stratosphere composition. In case that balloon is above the ozone layer, nearly the same radiation as in free space affects

the balloon. This fact is used to test durability of space materials in cheap way [10]. Ghysels et al. used optical sensor carried by balloon to quantify amount of carbonic dioxide in upper parts of troposphere and stratosphere [11]. Photometric quantification was also used to quantify vertical distribution of oxides of bromine [12]. However, to our knowledge, no fluorimetric device has been used in stratospheric conditions so far.

To monitor the behavior of the detector above the ground, carbon quantum dots (CQDs) can be employed. CQDs are new type of nanomaterial. They retain portion of bulk material properties and gain new, which arise from their nanometer diameter. They are biocompatible and possess chemical inertness and low toxicity [13]. The importance of CQDs is reflected in their electronic, mechanical, chemical and optical properties. All of these properties allow using CQDs in different fields of research such as catalysis, sensing, bioimaging, tissue engineering, optoelectronic and electronic devices [14-16]. The fluorescent labeling of DNA using nanoparticles enables DNA to be observable in in vivo or in vitro experiments [17].

The aim of this work was to test the fluorescence analyzer made by 3D printer in stratospheric conditions. For testing of this stratospheric equipment 0-32 $mg.ml^{-1}$ CQDs were used. Testing was performed prior and after the return of stratospheric probe from the stratosphere

2. Results and Discussion

2.1 Miniaturized fluorescence analyzer

The analyzer was composed mostly from parts, fabricated using 3D printing technology, Fig. 1 A. These parts are good heat insulators due to use of fused deposition modeling technology of 3D printing. The other advantages of 3D printing are speed of fabrication, which also enables fast testing of prototypes. The final shape of the probe was cylindrical with diameter 26 cm, high 28 cm and weight 2200 g. Servomotors were used to eject the samples out from the probe. The detection part of the probe includes a light emitting diode (LED) source of radiation of wavelength 245 nm (Fig. 1 B-a), photomultiplier suitable for these measurements with optical filter, Fig. 1 B-c,d. Temperature of this part of the probe is stabilized. Heaters and temperature sensors maintain the proper temperature. The detection is based on irradiation of the sample (Fig. 1 B-e) using luminescent diode and detection of emission intensity ($\lambda = 450$ nm). The stratospheric probe contained two UV cuvettes with solution (1 ml) containing CQDs/DNA conjugate. One cuvette was ejected to outer environment regularly, where it was exposed to UV irradiation. The second reference cuvette stayed within probe. Experimental data were transferred on-line to computer in control center.

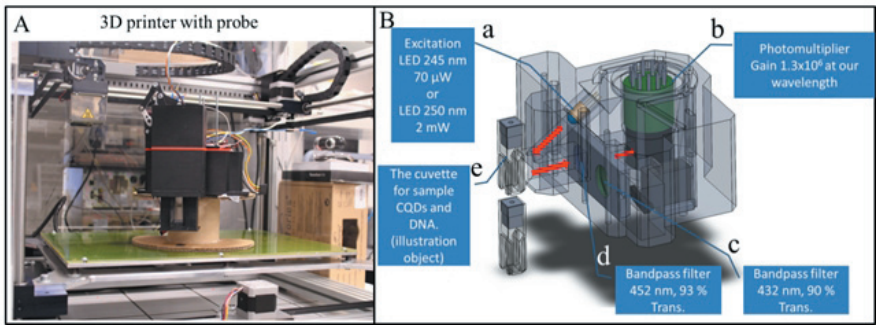

Figure 1: (A) 3D printer with detection part of probe. (B) 3D model of stratospheric probe detection part.

2.2 Flight computer - Julo-X

The board, which is connected with Julo-X (flight computer was developed by SOSA, Fig. 1 A and 1 Aa) included 7 power outputs for heating elements, 10 temperature sensors, high voltage source for powering the photomultiplier tube (PMT), LED current driver for the operating point stabilization, SD card storage for all of data and three current measurements on servo1, servo2 and PMT output. ATmega128 was employed as the micro control unit. For the temperature measurement was chosen because of easy connection to MCU. The power on servos was detected and from this data, the load of devices was derived. Julo-X recorded outside temperature, humidity, pressure, GPS position and altitude and sent them into ground PC. Before stratospheric launch was Julo-X (Fig. 1 A and 1 Aa) connected with miniaturized fluorescence analyzer, Fig. 1B. Finally, the stratospheric probe was wrapped in a thermal protection layer and attached to parachute and balloon.

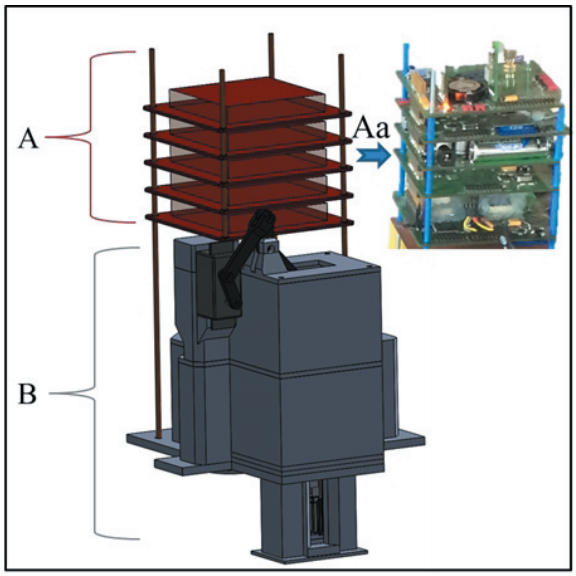

Figure 2: (A) 3D model of flight computer Julo-X and its real photo (Aa). B) Schematic illustration of miniaturized fluorescence analyzer connected with Julo-X.

2.3 Launch of stratospheric probe

The proposed detector was implemented to the platform Julo-X (flight computer) and released to stratosphere using balloon filled with helium. Prior to the launch of stratospheric probe, the last tests of communication between the probe and the control center were done, Fig. 3 A. Subsequently, the stratospheric balloon was filled with helium (Fig. 3 B) from the storage bomb. SP was launched 12. 9. 2014 at 7:30 a.m. from the airport situated in the Spišská Nová Ves (Slovak republic). Balloon flight lasted 120 minutes. During this time, it traveled 90 km. At a height of approximately 40 km there was a rupture of the balloon. Thanks to a parachute SP landed in a controlled manner in the wood in the cadastral area of municipality Brusnica (Slovak Republic). Thanks to radio and GPS module spacecraft was found, Fig. 3 C.

2.4 Verification of fluorescence functionality the stratospheric probes

Water soluble CQDs were prepared according to the general method reported by Wang et al. [18]. Fluorescent activity of 0-32 mg.ml^{-1} CQDs was determined by stratospheric probe. The intensity of fluorescence was recorded before the flight into the stratosphere in field conditions (Fig. 4 A-a) and subsequently after completion of the flight, Fig.4 A-b. It was found that the fluorescent signal of CQDs after completion of the flight was decreased compared to that before the flight. The same analysis was also performed using fluorescence analyzer Infinite M 200 pro, Fig 4 B-a (before the flight in the laboratory conditions) and Fig. 4 B-b (after flight in laboratory conditions). The fluorescent signals of CQDs were also lower. From these results, it can be concluded that the decrease in the fluorescence signals of CQDs was not caused by the construction faults of the fluorescence analyzer, but probably by the instability of CQDs in time. In this way, it was verified that the fluorescent analyzer manufactured by 3D printer could be used in stratospheric environment.

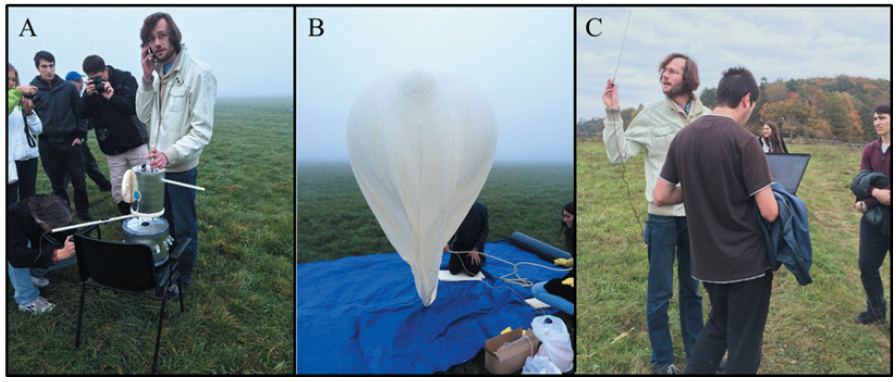

Figure 3: (A) Test of communication between the stratospheric probe and the control center. (B) Filling of latex balloon with helium. (C) Localization of the stratospheric probe by radio signal.

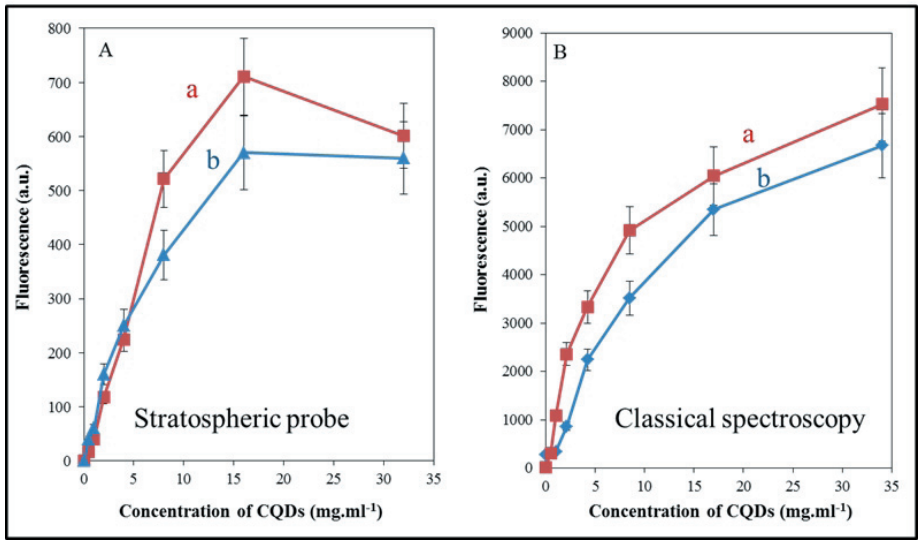

Figure 4: (A) Fluorescent activity of 0-32 mg.ml^{-1} CQDs determined by stratospheric probe a) before launch, b) after landing probe. (B) Fluorescent activity of 0-32 mg.ml^{-1} CQDs determined by fluorescence analyzer a) before launch in the laboratory, b) after landing probe in the laboratory.

3. Experimental Section

3.1 Chemicals and materials

All the reagents were purchased from Sigma-Aldrich (St. Louis, MO, USA) in ACS purity, unless noted otherwise. Deionized water underwent demineralization by reverse osmosis using Aqua Osmotic 02 (Aqua Osmotic, Tisnov, Czech Republic) and was subsequently purified using Millipore RG (MiliQ water, 18 MΩ, Millipore Corp., Billerica, Massachusetts, USA).

3.2 Synthesis and characterization of CQDs

The preparation of water soluble CQDs was carried out following the protocol of Wang et al [19]. The fluorescence of resulting CQDs was measured using multifunctional microplate reader Tecan Infinite 200 PRO (Tecan group Ltd. Männedorf, Switzerland) [20]. The average particle size and size distribution were determined by quasielastic laser light scattering with a Malvern Zetasizer (NANO-ZS, Malvern Instruments Ltd., Worcestershire, U.K.). Nanoparticles/distilled water solution (1 mg.mL^{-1}) was put into a polystyrene latex cell and measured at a detector angle of 173º, a wavelength of 633 nm, a refractive index of 0.30, a real refractive index of 1.59, and a temperature of 25 ºC.

3.3 Construction of miniaturized fluorescence analyzer by 3D printer

Rest of the probe was crafted on Profi 3D maker (3DFactories, Straznice, Czech Republic) by using acrylonitrile butadiene styrene. All parts of the device were changeable. The advantage in 3D printing technology is the short time of production and designing the model in CAD software Solidworks (Dassault Systèmes SolidWorks Corp., a subsidiary of Dassault Systèmes, S. A. (Vélizy, France) where the components were tested for noncollision in final assembly.

3.4 fluorescence spectroscopy

Fluorescence spectra were acquired by multifunctional microplate reader Tecan Infinite 200 PRO (TECAN, Männedorf,Switzerland). Briefly, 50 µL of sample CQDs was placed in a transparent 96 well microplate with flat bottom by Nunc (Thermo Scientific,Waltham, USA). 245 nm was used as an excitation wavelength and the fluorescence scan was measured with the range from 585 to 800 nm per 2-nm steps. Each intensity value was an average of three measurements. The detector gain was set to 100.

4. Conclusions

The developed concept was used to construct of fluorescence detector, which was carried to stratosphere by balloon. The detector was also tested after return to ground. The successful functioning of the SP under stratospheric conditions was verified and the applicability of 3D printing technology for the stratospheric detection devices was confirmed

Acknowledgments

Financial support from the projects PQDNA-STRATO012014 realized as a part of project Joint education for a common Future, which is financed from Operational Programme Cross-border cooperation SR CR 2007-2013, Fond micro-projects.

Conflicts of Interest

The authors have declared no conflict of interest.

References

1. de Kort, B.J.; de Jong, G.J.; Somsen, G.W. Native fluorescence detection of biomolecular and pharmaceutical compounds in capillary electrophoresis: Detector designs, performance and applications: A review. Analytica Chimica Acta 2013, 766, 13-33.
2. Smalley, M.B.; McGown, L.B. Fluorescence detectors in hplc. In Advances in chromatography, vol 37, Brown, P.R.; Grushka, E., Eds. 1997; Vol. 37, pp 29-71.
3. Michalet, X.; Siegmund, O.H.W.; Vallerga, J.V.; Jelinsky, P.; Millaud, J.E.; Weiss, S. Detectors for single-molecule fluorescence imaging and spectroscopy. Journal of Modern Optics 2007, 54, 239-281.
4. Spring, K.R. Detectors for fluorescence microscopy. Scanning Microscopy 1991, 5, 63-69.
5. Agbaria, R.A.; Oldham, P.B.; McCarroll, M.; McGown, L.B.; Warner, I.M. Molecular fluorescence, phosphorescence, and chemiluminescence spectrometry. Analytical Chemistry 2002, 74, 3952-3962.
6. Dasgupta, P.K.; Eom, I.Y.; Morris, K.J.; Li, J.Z. Light emitting diode-based detectors absorbance, fluorescence and spectroelectrochemical measurements in a planar flow-through cell.

Analytica Chimica Acta 2003, 500, 337-364.
7. Hillebrand, S.; Schoffen, J.R.; Mandaji, M.; Termignoni, C.; Grieneisen, H.P.H.; Kist, T.B.L. Performance of an ultraviolet light-emitting diode-induced fluorescence detector in capillary electrophoresis. Electrophoresis 2002, 23, 2445-2448.
8. Yang, B.C.; Guan, Y.F. Light-emitting-diode-induced fluorescence detector for capillary electrophoresis using optical fiber with spherical end. Talanta 2003, 59, 509-514.
9. In European rocket & balloon programmes and related research, Thun, Switzerland, 2013; Thun, Switzerland.
10. Kondyurin, A.; Kondyurina, I.; Bilek, M. Radiation damage of polyethylene exposed in the stratosphere at an altitude of 40 km. Polym. Degrad. Stabil. 2013, 98, 1526-1536.
11. Ghysels, M.; Durry, G.; Amarouche, N. Pressure-broadening and narrowing coefficients and temperature dependence measurements of co2 at 2.68 mu m by laser diode absorption spectroscopy for atmospheric applications. Spectroc. Acta Pt. A-Molec. Biomolec. Spectr. 2013, 107, 55-61.
12. Pundt, I.; Pommereau, J.P.; Chipperfield, M.P.; Van Roozendael, M.; Goutail, F. Climatology of the stratospheric bro vertical distribution by balloon-borne uv-visible spectrometry. J. Geophys. Res.-Atmos. 2002, 107.
13. Qian, Z.; Ma, J.; Shan, X.; Shao, L.; Zhou, J.; Chen, J.; Feng, H. Surface functionalization of graphene quantum dots with small organic molecules from photoluminescence modulation to bioimaging applications: An experimental and theoretical investigation. Rsc Advances 2013, 3, 14571-14579.
14. Bai, W.; Zheng, H.; Long, Y.; Mao, X.; Gao, M.; Zhang, L. A carbon dots-based fluorescence turn-on method for DNA determination. Analytical Sciences 2011, 27, 243-246.
15. Xu, X.; Wang, L.; Xu, H.-Q.; Huang, X.-E.; Qian, Y.-D.; Xiang, J. Clinical comparison between paclitaxel liposome (lipusu (r)) and paclitaxel for treatment of patients with metastatic gastric cancer. Asian Pacific Journal of Cancer Prevention 2013, 14, 2591-2594.
16. Yang, T.; Lu, M.M.; Mao, X.L.; Liu, W.H.; Wan, L.; Miao, S.D.; Xu, J.Z. Synthesis of cds quantum dots (qds) via a hot-bubbling route and co-sensitized solar cells assembly. Chem. Eng. J. 2013, 225, 776-783.
17. Sun, D.; Gang, O. DNA-functionalized quantum dots: Fabrication, structural, and physicochemical properties. Langmuir 2013, 29, 7038-7046.
18. Wang, F.; Pang, S.P.; Wang, L.; Li, Q.; Kreiter, M.; Liu, C.Y. One-step synthesis of highly luminescent carbon dots in noncoordinating solvents. Chem. Mat. 2010, 22, 4528-4530.
19. Wang, F.; Pang, S.; Wang, L.; Li, Q.; Kreiter, M.; Liu, C.-y. One-step synthesis of highly luminescent carbon dots in noncoordinating solvents. Chem. Mat. 2010, 22, 4528-4530.
20. Milosavljevic, V.; Nguyen, H.V.; Michalek, P.; Moulick, A.; Kopel, P.; Kizek, R.; Adam, V. Synthesis of carbon quantum dots for DNA labeling and its electrochemical, fluorescent and electrophoretic characterization. Chemical Papers 2014.

The article is freely distributed under license Creative Commons (BY-NC-ND). But you must include the author and the document can not be modified and used for commercial purposes.